Room Modal Equalisation with Electroacoustic Absorbers

PAR

Etienne Thierry Jean-Luc RIVET

EPFL

ÉCOLE POLYTECHNIQUE
FÉDÉRALE DE LAUSANNE

Suisse
2016

To Camila and Alice…

Acknowledgements

This thesis would not have been possible without the help, supervision, guidance, friendship of many great people.

First of all, I would like to deeply thank my main thesis supervisor, Dr Hervé Lissek, for giving me the possibility of working on the best thesis topic forever! Thank you Hervé for your trust and guidance. Despite the good times bad times these last years, you succeeded in keeping the acoustic group "alive" to the delight of your collaborators. Since then, *nobody calls you Lissek...* I hope that the results of this thesis will push you to continue working on this exciting topic. Also I would like to thank my two successive thesis co-directors: Prof. Juan Mosig and Prof. Pierre Vandergheynst. Thank you Juan for accepting me at the LEMA lab, while trusting Hervé. I wish you a happy retirement. Thank you Pierre for welcoming the acoustic group at the LTS2 lab since 2015.

I sincerely thank the members of my jury, Prof. Marie-Annick Galland, Dr Bruno Fazenda, and Dr Philippe Müllhaupt, who read my manuscript and leaded a fruitful discussion during my thesis defense. Thank you for your insightful questions and comments. A special thanks goes to Dr Jean-Marc Vesin for our many discussions, more about rugby than science.

Also I am very thankful to the INTERACTS project members: Dr Véronique Adam, Torje Nikolai Thorsen, Quentin Berthet, Olivier Schmitt, Alain Roux, Christian Martin, Roger Roschnik, Prof. Antoine Pittet, and David Strobino. I am very delighted to have worked on this project with you and I have learnt a lot during our collaboration. With respect to my work, I want to thank the Swiss Federal Commission for Technology and Education, which has supported the financial and thematic framework of this thesis.

My warmest thanks go to the former and current members of the LEMA, LTS2, ASPG, LTS4, LTS5, and MMSPG labs, for the daily life inside and outside the EPFL. A special thanks goes to my former and current colleagues of the acoustic group: Xavier Falourd, Patrick Marmaroli, Cédric Monchâtre, Lukas Rohr, Gilles Courtois, Baptiste Crettaz, Hussein Esfahlani, Patrick Roe, and Romain Boulandet with whom I have worked on this topic even before starting my PhD thesis. Last but not least, I am very thankful to my office mate, Sami Karkar. Your suggestions and ideas have significantly contributed to the results of this thesis. Also thank you for the good times and your sense of humour. I wish you all the best for your career advancement. Thanks to the students Fabian, Clément, Johannes, Mathilde, Yann, Aymeric, Julien, William, and Romain, I had the pleasure to supervise them during these years. Undoubtedly, many

Abstract

The sound quality in a room is of fundamental importance for both recording and reproducing processes. Because of the room modes, the distributions in space and frequency of the sound field are largely altered. Excessive rise and decay times caused by the resonances might even mask some details at higher frequencies, and these irregularities may be heard as a coloration of the sound. To address this problem, passive absorbers are bulky and too inefficient to significantly improve the listening conditions. On the other hand, the active equalisation methods may be complicated and costly, and the sound field might not be well controlled, because of the added sound energy in the room. Another approach is the active absorption, which consists in varying the impedance of a part of the enclosure boundaries, so as to balance the sound field thanks to the absorbed sound power into the active boundary elements.

The thesis deals with the design and optimisation of electroacoustic absorbers intended to specifically reduce the effect of the unwanted room modes. These active absorbers are closed box electrodynamic loudspeaker systems, whose acoustic impedance at the diaphragms is judiciously adjusted with passive or active components to maximise their absorption performance in the domain in which it is located. Several configurations merging sensor- and shunt-based methods are proposed resulting in an efficient and broadband sound absorption at low frequencies. A multiple degree-of-freedom target impedance that is assigned at the transducer diaphragms is then optimised to lower the modal decay times at best. The performance of the electroacoustic absorbers for the modal equalisation is investigated in actual listening rooms, and their audible effect is subjectively evaluated. The overall combination of concepts and developments proposed in this thesis paves the way towards new active absorbers that may improve the listening experience at low frequencies in rooms.

Key words: active absorption, acoustic impedance control, resonance damping, electrodynamic loudspeaker, multiple degree-of-freedom resonators, shunt loudspeaker, sensorless control.

Résumé

La qualité sonore dans une salle est d'une importance fondamentale lors des enregistrements et reproductions audio. À cause des modes de salle, les répartitions spatiale et fréquentielle du champ sonore sont largement modifiées. Les temps de montée et de décroissance excessifs causés par ces résonances peuvent même masquer certains détails à des fréquences plus élevées, et ces irrégularités peuvent être entendues comme une coloration du son. Pour résoudre ce problème, les absorbeurs passifs sont encombrants et trop inefficaces pour améliorer considérablement les conditions d'écoute. D'autre part, les méthodes d'égalisation active peuvent être compliquées et coûteuses, et le champ acoustique peut ne pas être suffisament bien contrôlé, en raison de l'ajout d'énergie acoustique dans la salle. Une autre approche est l'absorption active, qui consiste à faire varier l'impédance d'une partie des parois de la salle, de manière à égaliser le champ sonore grâce à la puissance acoustique absorbée dans ces éléments actifs.

La thèse traite de la conception et de l'optimisation d'absorbeurs électroacoustiques destinés à réduire spécifiquement l'effet des modes de salle non désirés. Ces absorbeurs actifs sont des haut-parleurs électrodynamiques en enceinte close, dont l'impédance acoustique au niveau des membranes est ajustée judicieusement avec des éléments passifs ou actifs, afin de maximiser les performances d'absorption dans le domaine dans lequel il se trouve. Plusieurs configurations combinant des méthodes de shunt ou comprenant des capteurs sont proposées, ayant pour conséquence une absorption acoustique efficace et large bande aux basses fréquences. Une impédance acoustique cible à plusieurs degrés de liberté affectée aux membranes des transducteurs est alors optimisée pour réduire les temps de décroissance modaux. La performance des absorbeurs électroacoustiques pour l'égalisation modale est étudiée dans des salles d'écoute réelles, et leur effet audible est évalué subjectivement. La combinaison globale des concepts et des développements proposés dans cette thèse ouvre la voie vers de nouveaux absorbeurs actifs, qui peuvent améliorer l'expérience d'écoute aux basses fréquences dans les salles.

Mots clefs : Absorption active, contrôle d'impédance acoustique, amortissement de résonances, haut-parleur électrodynamique, résonateurs à plusieurs degrés de liberté, haut-parleur shunté, contrôle sans capteur.

Contents

Contents

List of Figures

List of Tables

List of Tables

Introduction

Context

The sound quality in a room is of fundamental importance for both recording and reproducing processes. The sound that is heard by a listener is a combination of the direct sound from the source(s) and the indirect reflections, which can be absorbed, reflected, or transmitted, depending on the acoustic properties of the wall surfaces. A right balance between the energy supplied by the source and that absorbed by the boundary may be reached, thanks to an appropriate combination and placement of absorbers and diffusers to control the reverberation time and early reflections respectively. At the low frequencies, the coupling with the room caused by standing waves largely alters the sound quality. These low-frequency resonances occur when reflected waves interfere constructively and destructively with incident waves, resulting in axial, tangential, and oblique modes. Because of these room modes, the distributions in space and frequency of the sound field are largely affected, and the temporal acoustic response is altered resulting in long rise and decay times. Small and medium rooms, such as recording/broadcasting studios or home cinemas, usually suffer from the low-frequency modes, because the natural modes of the room are sparse. Even in a small listening room that is well damped at mid and high frequencies, the frequency response functions, which are usually defined from the volume velocity of the sound source to the sound pressure level at measurement positions, are uneven, as illustrated in Fig. 1. In steady state, some frequencies are emphasised with high sound pressure levels and others are almost inaudible because of low sound pressure levels. As a result, depending on the placement of the listener and loudspeakers in the room, a single tone at a resonance may quickly become audible or inaudible.

The phenomena caused by the low-frequency modes are thus critical for the sound quality with both live music and playback of recorded music in listening rooms. At mid and high frequencies, the resonances are dense and the rise and decay times are fast enough to be imperceptible, because the natural decays of the musical content exceed those of the resonances. However, at low frequencies, the modal density is low and the decay times are obviously perceptible with resonances [2]. Excessive rise and decay times caused by the resonances might even mask some details at higher frequencies, and these irregularities may be heard as a colouration of the sound. The different phases of the room behaviour are illustrated
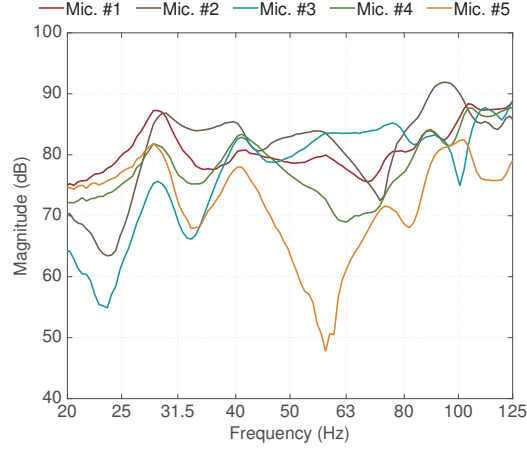
Figure 1 – Frequency response measurements at different locations in a small listening room.

in Fig. 2 for a pure sine tone at a resonance with a given modal decay time (MT_{60}), which corresponds to the time interval during which the decay level drops down by 60 dB during the free response. When a sound source radiates sound power in the room, for example with a pure sine tone whose frequency is close to that of a given mode, this power gives rise to an energy increase inside the room (the sound power increases with a given rise time). At the same time, an amount of energy is absorbed by the boundary surfaces that depends on the sound absorption capabilities of materials, and another is temporarily stored in the reactive components of surfaces. On the other hand, when the sound source is turned off at time t_0, the sound pressure decreases and the energy which was temporarily stored decreases in the room with a given decay time (more details can be found in [3]). The lower the modal decay times, the better the sound reproduction.
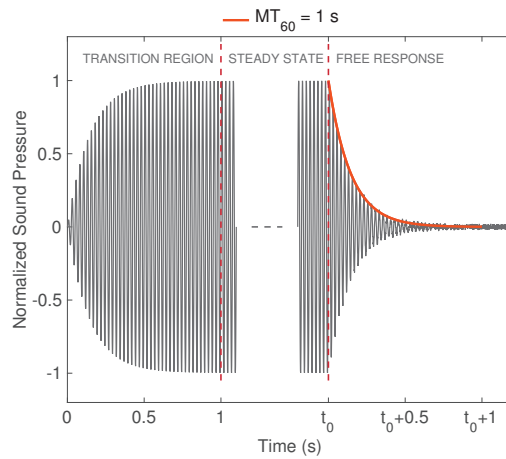
Figure 2 – Sound pressure of a pure sine tone at 40 Hz computed for a given value of modal decay time (in orange).

Motivation

Even when the room dimensions and placement of the sound sources are carefully chosen, the frequency response function at a given location may still be uneven and acoustic treatment is needed to equalise it. Various passive absorbers that are cheap and simple to implement, such as Helmholtz resonators or membrane absorbers, are usually used to treat the most significant modes [4]. However, they are bulky and not efficient enough to significantly improve the sound reproduction at low frequencies (considering a reasonable amount of absorptive surface). An alternative, but expensive solution, is the active equalisation based on the destructive interference principle through one or multiple sources. On the one hand, the local control method consists in reducing the sound pressure at locations defined by the placement of error microphones; on the other hand, the global control method aims at reducing the overall sound power radiated from the primary sources [5]. Nevertheless, the control may be complicated, costly, and long to implement, and the sound field might not be well controlled because of the added energy in the room.

Another approach is the active absorption, which consists in varying the impedance of a part of the enclosure boundaries, so as to balance the sound field thanks to the absorbed sound power into the boundary elements. Turning an electrodynamic loudspeaker into an *electroacoustic absorber* enables the sound power of incident waves to be dissipated. As the transducer impedance is mainly reactive, its absorption capabilities can be improved through different methods. The active absorption can be achieved either through feedback and feedforward techniques by measuring acoustic quantities with sensors, or through shunt-based and self-sensing methods by connecting an appropriate electrical impedance to the transducer terminals. With these methods, the active system alters the acoustic impedance at the transducer diaphragm towards a target value. To increase the absorption surface, resistive materials may also be used in front of the active surface. Several studies validated the performance of active absorption, mainly in lightly damped rooms. In particular, a preliminary experiment evaluated the performance of sensorless electroacoustic absorbers for modal equalisation in a small lightly damped room [6]. Nevertheless, the acoustic impedance at the transducer diaphragms was not necessarily optimised for the room, and the absorption bandwidth was limited because of some control limitations.

The audio industry focused its efforts on the design of the best sound diffusion systems, in view of presenting flat frequency response functions. To address the problem of room modes at low frequencies and thus ensure the highest listening experience, Swiss manufacturers wanted to develop innovative audio solutions. This thesis was carried out in the framework of a research project named *INTERACTS* for "Intelligent low-frequeNcy acousTic Equalisation of Rooms using Active ConTrol Subwoofers". Supported by the Swiss Commission for Technology and Innovation under grant agreement n°14220.1 PFNM-NM, the project was a collaboration between two industrial partners (AudioNetworks S.A. and Relec S.A.), and two academic partners (the Applied Acoustics Laboratory at Haute Ecole du Paysage, d'Ingénieurie et d'Architecture de Genève and the Signal Processing Laboratory LTS2 at Ecole polytechnique

fédérale de Lausanne).

Objectives
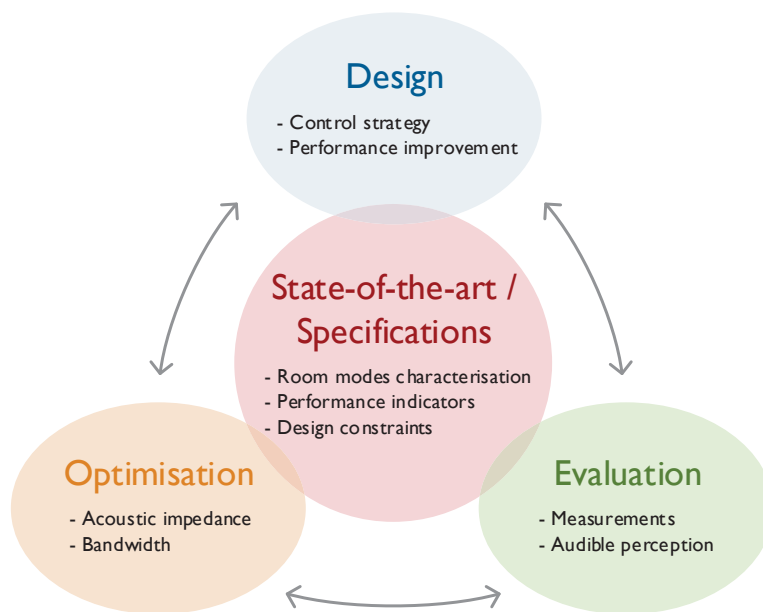
Figure 3 – Objectives of the thesis.

The main objective of this thesis is to improve the sound quality in listening rooms at low frequencies thanks to the electroacoustic absorber concept. The thesis is structured around three topics (design, optimisation, and evaluation) depending on specifications from manufacturers and based on what has been previously studied and developed, as illustrated in Fig. 3. The electroacoustic absorber can be designed through one or several control strategies according to constraints. Ideally, the absorber should be a "plug-and-play" device, and the control should perform whatever the room geometry and damping of the given room with a reasonable number of absorbers. Moreover, the performance should be set so as to be efficient over a large frequency range, stable, and not vulnerable to changes such as room occupancy. Lastly, the electroacoustic absorber should not make any audible sound, which would alter the original sound emitted in the room. At low frequencies, the sound field is not diffuse and the performance of an absorptive surface is not quantifiable through simple statistical laws/equations, such as the conventional sound absorption coefficient. In addition to the characterisation of the room modes, global indicators should thus be defined to evaluate objectively the performance of the electroacoustic absorber. These indicators could also be useful for computations such as for the optimisations of the target impedance and absorption bandwidth. The performance of the developed electroacoustic absorbers for the

modal equalisation should be evaluated in the worst conditions through measurements, and the audible perception of this approach should be investigated through a psychoacoustic study. The following section details the thesis structure and summarises the objectives of each chapter, together with the original contribution.

Outline and original contributions

This section summarises the contents and original contributions of the chapters of this thesis as depicted in Fig 4.
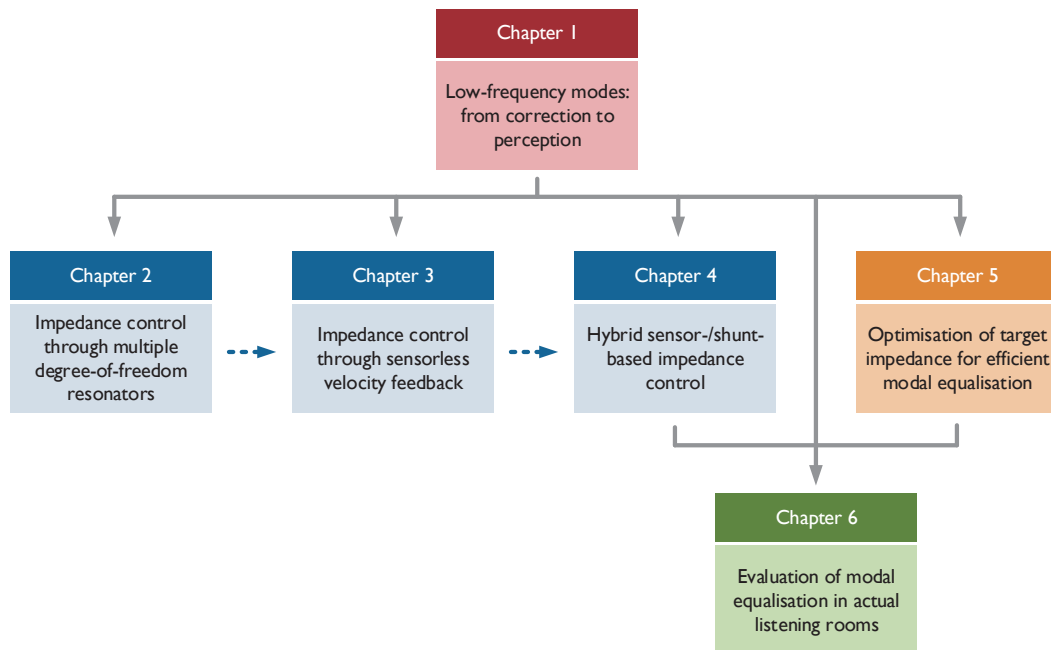
Figure 4 – Outline of the thesis with connections between chapters.

Chapter 1 - Low frequency modes: from correction to perception

Description: The simple modal representation of the sound pressure is briefly recalled, as well as the different methods to characterise the sound field. A state-of-the-art review on the passive and active correction techniques is then provided. This overview serves to justify the development of the active impedance control for modal equalisation. The last part focuses on the perception of the low frequencies in the context of music listening.

Chapter 2 - Impedance control through multiple degree-of-freedom resonators

Description: Different systems of multiple degree-of-freedom electroacoustic absorber through electrical and mechanical resonators constituted of conventional components are developed from the shunt-based methods and a judicious arrangement of several loudspeakers in an enclosure. The specific acoustic impedance of each system is optimised through two objective functions, depending on a target sound absorption coefficient value to take advantage of the system. The different optimised configurations are evaluated experimentally and compared with each other.

Original contributions: Guidelines are provided for the design and practical realisation of multiple degree-of-freedom electroacoustic absorber systems. Performance indicators, such as the bandwidth of efficient absorption, are introduced for the optimisation and evaluation of absorption performance. These passive achievements will also serve as acoustic specifications for the development of strategies of active impedance control for room modal equalisation.

Chapter 3 - Impedance control through sensorless velocity feedback

Description: To simplify the implementation, a self-sensing based method with a dual coil electrodynamic loudspeaker is investigated. The parameters of the transducer are identified before designing the sensorless control combined with a current driving method and depending on a target specific acoustic impedance. Analytical and experimental evaluations are provided and general remarks regarding control limitations are discussed.

Original contributions: Taking advantage of the dual coil of the transducer, the inductance of the voice coils, which limits the absorption performance in sensorless techniques, can be bypassed in the control. With the knowledge of the model parameters, a target specific acoustic impedance that is partly defined from the transducer parameters can be achieved at the diaphragm.

Chapter 4 - Hybrid sensor-/shunt-based impedance control

Description: As the shunt-based and self-sensing methods become limited when it comes to the absorption bandwidth extension, a novel control strategy using only one sensor and taking into account the model parameters enables the target impedance to be imposed at the diaphragm. Stability and absorption performance are studied in the presence of transducer model uncertainties and possible control limitations. The power efficiency of the electroacoustic absorber is investigated as well. Last, an experimental validation of the concept in a waveguide is provided.

Original contributions: A hybrid impedance control merging sensor- and shunt-based methods is proposed, resulting in a broadband and stable low-frequency electroacoustic absorber. This control strategy is simple to implement and the target impedance may accurately be

imposed at the transducer diaphragm. This approach is particularly adapted for modal equalisation applications. The Chapters 2, 3, and 4 show the transition from the shunt-based methods to sensor-based controls, via the self-sensing technologies, by emphasising the advantages and limitations of these different approaches.

Chapter 5 - Optimisation of target impedance for efficient modal equalisation

Description: The optimal value of the target specific acoustic impedance is investigated through simulations in 1D and 3D cases to correlate the effective absorption area and the modal decay times. Then, with a fixed absorption area, the effects of the wall impedance and room geometry are studied as well. The effect of the active sound power dissipated into the absorbers is correlated with the modal decay times. From these results, the target impedance is optimised so that it approaches the optimal resistance value for each mode at best, in order to lower the modal decay times.

Original contributions: Different configurations of absorbers in rooms are simulated to establish some relationship between the parameters and performance of the absorbers. A modified sound absorption coefficient is derived to characterise the performance of the absorbers in rooms. From this coefficient and simulation results, a target multiple degree-of-freedom acoustic impedance is optimised to maximise the possible performance of the absorbers in order to decrease a given set of modal decay times.

Chapter 6 - Evaluation of modal equalisation in actual listening rooms

Description: The performance of the electroacoustic absorbers is investigated in listening rooms that are well damped at mid and high frequencies, in order to highlight the potential of the proposed concept for modal equalisation. The performance is evaluated through frequency response function measurements and estimated modal decay times. Then, their effect is subjectively evaluated from a psychoacoustic perspective.

Original contributions: The control strategy proposed in Chapter 4 is associated to the target multiple degree-of-freedom impedance optimised from the simulation results in Chapter 5, to validate its performance in realistic listening conditions. To highlight the performance of the concept for the modal equalisation, a global curve fitting technique from the frequency response function measurements, which was developed for vibration structures, is applied for the estimation of the modal decay times. The results of the psychoacoustic study are compared with previous studies addressing low-frequency perception in the context of music listening. This evaluation intends to show the advantages of this complementary absorption solution to passive ones at mid and high frequencies, in order to improve the sound quality in any listening room. It also proves the actual performance of such active solution for damping the room modes, and therefore represents a significant milestone in the domain of audible perception studies in the low frequency range.

1 Low-frequency modes: from correction to perception

1.1 Introduction

Modal equalisation aims at flattening the frequency response function at every location in a given enclosure, that is equivalent to getting more uniform distributions in space and frequency of the sound field, resulting in small values of modal decay times. For better understanding of this thesis, an introduction of the modal representation of the sound pressure from the wave equation is firstly given. Then, the existing active and passive procedures for correcting the modal problem are presented. Lastly, the studies, which have investigated the low-frequency perception, are briefly summarised.

1.2 Modes and eigenfrequencies

1.2.1 Modal representation of the sound pressure

Formal solution of the wave equation

Inside an enclosure, the sound pressure field generated by a sound source satisfies the inhomogeneous wave equation. For a time dependence $\exp(j\omega t)$, where ω is the angular frequency, it simplifies to the Helmholtz equation associated to a source function, which is expressed as

$$\Delta p(\mathbf{r}) + k^2 p(\mathbf{r}) = -j\omega\rho q(\mathbf{r}) \tag{1.1}$$

where p is the sound pressure, $k = \omega/c$ is the wavenumber, c is the sound speed and ρ is the density in the medium, q is the volume velocity of the sound source, and $\mathbf{r}$ is the field point represented by the three spatial coordinates. Assuming that the boundaries are locally reacting to the sound field (that is the waves propagating in or behind the walls do not interact with the sound field inside the room), the boundary condition satisfies on

$$\frac{Z}{\rho c}\nabla p(\mathbf{r}) \cdot \mathbf{n} = -jkp(\mathbf{r}) \tag{1.2}$$

where $\mathbf{n}$ is the unit vector normal to the boundary surface area in the direction of the outward normal to the wall, and Z is the acoustic impedance at the boundary [7]. The source function $q(\mathbf{r})$ can be expanded in a series of eigenfunctions Φ_n

$$q(\mathbf{r}) = \sum_n Q_n \Phi_n(\mathbf{r}) \tag{1.3}$$

where

$$Q_n = \frac{1}{K_n} \int \int \int_V \Phi_n(\mathbf{r}) q(\mathbf{r}) dv \tag{1.4}$$

with K_n is a constant expressed in $\mathrm{Pa}^2 \cdot \mathrm{m}^3$ and V is the enclosure volume. The eigenfunctions Φ_n satisfy the orthonormal property given by

$$\int \int \int_V \Phi_m(\mathbf{r}) \Phi_n(\mathbf{r}) dv = K_n \delta_{mn} \tag{1.5}$$

where δ_{mn} is the Kronecker delta function. In the same way, the solution $p_\omega(\mathbf{r})$ can be expressed as

$$p_\omega(\mathbf{r}) = \sum_n P_n \Phi_n(\mathbf{r}) \tag{1.6}$$

where P_n are the unknown coefficients. Every term is related to the corresponding eigenvalue $\lambda_n = -k_n{}^2$ through $\Delta \Phi_n = \lambda_n \Phi_n$. If the sound source is considered as a point source emitting a sine signal with a volume velocity q_0 located at the arbitrary point $\mathbf{r}_0$, that is $q(\mathbf{r}) = q_0 \delta(\mathbf{r} - \mathbf{r}_0)$, the final solution for the sound pressure is written as

$$p_\omega(\mathbf{r}) = j\omega\rho q_0 \sum_n \frac{\Phi_n(\mathbf{r}) \Phi_n(\mathbf{r}_0)}{K_n \left(k_n{}^2 - k^2\right)} \tag{1.7}$$

Expressing the eigenvalues in complex quantities, that is $k_n = (\omega_n + j\delta_n)/c$ with the damping coefficient $\delta_n \ll \omega_n$, Eq. (1.7) becomes

$$p_\omega(\mathbf{r}) = \rho c^2 \omega q_0 \sum_n \frac{\Phi_n(\mathbf{r}) \Phi_n(\mathbf{r}_0)}{K_n \left[2\delta_n \omega_n + j \left(\omega^2 - \omega_n{}^2\right)\right]} \tag{1.8}$$

Modal decay time

Whatever the shape of the enclosure, the modal decay time of a given mode, which is defined as the time interval during which the decay level drops down by 60 dB during the free response, is related to its corresponding damping δ_n or to its eigenfrequency $\omega_n + j\delta_n$ and quality factor Q_n as

$$MT_{60_n} = \frac{3\ln(10)}{\delta_n} = \frac{6\ln(10) Q_n}{\sqrt{\omega_n{}^2 + \delta_n{}^2}} \tag{1.9}$$

The modal decay times can then be lowered by providing additional damping at boundaries for example.

Normal modes in rectangular rooms with rigid boundaries

When the enclosure is rectangular and lightly damped, the eigenfunctions Φ_m are approximated by the mode shape functions determined for rigid boundaries in Cartesian coordinates by

$$\Phi_{n_x n_y n_z}(x, y, z) = \cos\left(\frac{n_x \pi x}{l_x}\right)\cos\left(\frac{n_y \pi y}{l_y}\right)\cos\left(\frac{n_z \pi z}{l_z}\right) \tag{1.10}$$

where the modal indices $(n_x, n_y, n_z) \in \mathbb{N}^3$ are non-simultaneously equal to zero. The corresponding eigenfrequencies are expressed as

$$\omega_{n_x n_y n_z} = \pi c \sqrt{\left(\frac{n_x}{l_x}\right)^2 + \left(\frac{n_y}{l_y}\right)^2 + \left(\frac{n_z}{l_z}\right)^2} \tag{1.11}$$

and $K_n = V/(\epsilon_{n_x}\epsilon_{n_y}\epsilon_{n_z})$ where $\epsilon_{n_s} = 1$ if $n_s = 0$ and $\epsilon_{n_s} = 2$ if $n_s > 0$. Examples of normal modes in a lightly damped rectangular room are illustrated in Fig. 1.1. The general expression of the boundary condition in Eq. (1.2) can only be formulated if the boundaries are locally reacting. If it is not the case, the normal modes may be coupled with the modes outside the boundaries as proposed in [8]. Moreover, the eigenfrequencies in Eq. (1.11) are only valid for enclosures with simple geometry and boundary conditions, with the assumption of a uniform distribution of the impedance on the boundaries. In most of the cases, more complex methods have to be taken into account for the characterisation of the sound field in enclosures.

(a) (b)
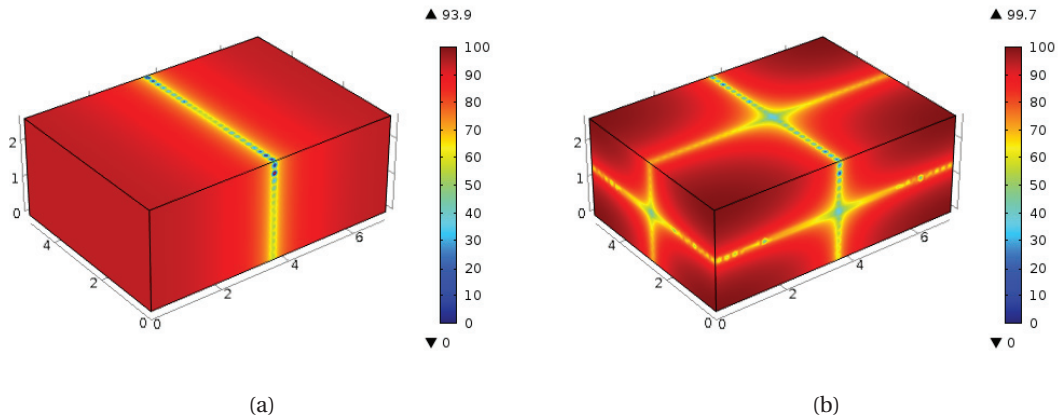
Figure 1.1 – Modes (a) (1,0,0) and (b) (1,1,1) of a lightly damped room.

1.2.2   Sound field characterisation

Methods

The description and characterisation of the sound field in enclosures can be analysed through several perspectives:

- Statistical methods are based on the hypothesis of a diffuse sound field, whose acoustic energy is uniform and travels in all the directions with the same probability [9];

- Diffusion models, which are an extension of the statistical theory to spatially varying reverberant sound fields, are based on the analogy of the sound energy density travelling along straight lines [10];

- Geometric methods are based on the ray tracing method [11, 12] or image source methods [13] among others;

- Wave-based methods are based on the wave equation to describe a complete sound field in enclosures, whose numerical simulations are the boundary element method [14, 15], the finite element method [16–19], and the finite-difference time domain [20, 21];

- Modal expansion methods are based on the expression of the sound field as a linear combination of the modes. The simplest and most widely used modal analysis in the literature is the normal mode analysis described in [22]. However, it is only suitable for enclosures with rigid or very lightly damped boundaries. The classical modal analysis theory based on the Green's theorem was then developed in [23]. Because of large errors in the regions near boundaries for damped enclosures [24], some approaches of exact eigenvalue problem were proposed in [25, 26], where the modes are uncoupled (named exact modes). The previous method being complex and time consuming, the hybrid modal analysis, which combines the free field Green's function with the modal expansion, was developed in [27].

Sound intensity

The sound intensity is very useful to study the energetic properties of a sound field. Statistical properties of the active and reactive intensities in reverberant enclosures subjected to pure-tone excitation were studied in [28, 29]. The behaviour of the scalar and vector characteristics of the steady-state sound field inside coupled and irregular enclosures were analysed in [30] and [31] respectively. Thanks to the modal expansion method, the active and reactive intensities were also determined depending on the eigenfrequencies and modal damping [32].

Modal decay time

The modal decay time is the main parameter that enables the sound quality of the enclosure to be assessed [2, 33]. These modal decay times can easily be derived for the normal modes in a rectangular room [34] or in room of irregular shape [35] with different sound absorption coefficients on room walls. From measurements, the modal decay times can be evaluated from a decay curve defined as the graphical representation of the sound pressure level variation, as a function of time after the cut-off of a continuous sound source according to the International Organization for Standardization [36]. On the other hand, they can be estimated either from the decay function, which can be determined by non-linear polynomial regression from the sound pressure envelope obtained via the discrete Hilbert transform [37], or from the reverse-time integration of the squared room impulse response by the use of the Schroeder integration method [38]. A method taking into account the background noise floor in the measurements was also developed in [39]. Another approach proposed in [40] was the estimation of the modal decay times from measurements, by evaluating the half power bandwidth of the resonance peaks.

Sound field reconstruction

The spatial distribution of the sound field in rooms was investigated, in particular the evolution of the room impulse responses as a function of the microphone positions in the room. Experiments proved that the sound field can be recreated at any spatial position, from the measurements of the sound pressure in a finite number of positions [41]. An optimal sampling pattern for the microphone positions was given to reconstruct accurately the sound field. In another example, the frequency response functions in rooms were interpolated and extrapolated at low frequencies, from a method of estimated residue values and common acoustical poles based on the wave equation [42]. In [43], a method based on the dynamic time warping was used for the interpolation of the early part of the room impulse responses from sparse measurements. To reduce the number of microphones used for the measurements, the method proposed in [44] was adapted to the compress sensing technique to reconstruct the sound field in the low frequency range.

1.3 Correction strategies

Low-frequency room modes can be treated using a number of well-known passive and active strategies. These techniques address the modal problem from different perspectives, resulting in varying advantages and shortcomings.

1.3.1 Passive means

Passive absorbers

Conventional passive techniques based on foam-based absorbers are often used in order to reduce the mid-/high-frequency reflections. Since their size is dictated by the wavelengths in the targeted frequency range, they are not well suited to the low frequencies. As pointed out in [4], the porous absorbers are often set up in the room corners with a view to damping a majority of modes. However, while the sound pressure is maximal at these locations, the particle velocity is almost null, and consequently the absorption is inefficient if the size is well below the quarter of the wavelength of eigenfrequencies. For this reason, resonant absorbers including membrane absorbers (with vibrating panels) or Helmholtz resonators, which consist of small cavities communicating with the sound field through necks, are preferred for the low-frequency sound absorption [45–47]. Nevertheless, even if the parameters of Helmholtz resonators are optimised for a given enclosure [48, 49], the high quality factor causes a narrow frequency band of efficient absorption. Thus, two and three degree-of-freedom Helmholtz resonators, which consist of pairs of cylindrical necks and cavities connected in series, were designed in [50, 51] and [52] respectively, to improve the absorption capabilities. The effect of resonator arrays on the sound field in cavities are evaluated in [53, 54]. These resonators can also be combined with micro-perforated panels constituted of very thin perforations backed by a cavity, which were firstly introduced in [55, 56], so as to improve the absorption performance at higher frequencies [57]. Their performance was then studied in enclosure in [58, 59], as well as a membrane backed by an air cavity in [60]. Recently, an original design constituted of panels arranged with parallel extended tubes, was proposed in [61]. Thanks to high absorption at four different frequencies, this arrangement showed promising experimental results with an efficient absorption from 150 Hz to 440 Hz. However, none of these passive absorbers is efficient below 150 Hz.

Optimal room design

Optimal ratios of room sizing have been suggested over the years to avoid high values of modal decay times. Charts of preferred room ratios were determined by directly averaging the modal spacing [62], while the standard deviation was preferred in [63]. The design of listening rooms depending on the absorption materials and room sizing was studied in [64], pointing out that the axial modes represent the major difficulty in rooms. A criterion was proposed in [65] for the design of listening rooms, based on the fact that the modal density of a given one-third octave band should never be greater than that of the next higher band. A new criterion was derived in [66] to allow a wider range of room proportions from the room height, even though the International Electrotechnical Commission gives slightly different criteria [67]. The Bonello criterion defined in [65] was compared with two other metrics that were chosen to predict the low-frequency performance in rooms, pointing out the limitations of these criteria that were based on simplistic assumptions [68]. Then, an optimised method was developed in [17]

to redistribute some modes within a frequency range by means of geometric modifications of the room walls. However, these modifications appear to be too complicated to realise. Lastly, an iterative algorithm aiming at determining the small room dimensions, including design constraints (one dimension is fixed for example) was proposed in [69], to get the flattest possible frequency response function.

Optimal configurations of sound sources

When it is not possible to modify the enclosure sizing and the passive absorbers are not sufficient at low frequencies, the best location of the sound sources may be optimally placed to get the best listening experience. The optimisation of the location of a single subwoofer in small rooms was firstly studied in [70–72], to get a uniform radiated power without taking into account the listener location. The positions of absorption materials were also studied in addition to that of the sound source in [73], pointing out that the room corner is an optimal location for both the material and loudspeaker to improve the frequency response functions at the listening positions. In a second step, locating the listeners and multiple low-frequency sound sources strategically through numerical optimisations can reduce the audible effects of modes by minimising the energy of the error over the region of control [14, 21, 74, 75]. Such active equalisation techniques are described in the next part.

1.3.2 Active equalisation

Parametric equalisation

Active corrections have received much attention in the last decades for the low-frequency equalisation in listening rooms. The most simple and economical technique involves the parametric equalisation from the source signal at a predefined location. Targeting three to five most problematic room modes with notch filters enables the effect of the standing waves on the sound reproduction to be reduced (see Section 1.4). A psychoacoustic study was proposed, where the signal spectral components coinciding with the most problematic modes are filtered and substituted by a virtual bass system, which adds spectral components at higher frequencies [76]. However, these methods cannot address the modal problems at all the listening locations, and on the other hand, they cannot be used for natural sounds, such as musical instruments for example.

Single input equalisation

The parametric equalisation differs from the single-input single-output (SISO) equalisation, which is based on the active noise cancellation principle developed in [77]. The sound field is generated by a single loudspeaker, and the frequency response function is equalised from the measurement at a single listening position. Either a filter can be designed that compensates the magnitude of the frequency response function, which guarantees the stability (but does not

provide a complete equalisation solution because it discardes the phase), or an optimisation approach, which results in a best-case equalisation solution without risking instability, can be implemented [78–82]. However, this technique is only effective for one pair source/listener, and on the other hand, its effect may even be prejudicial at other listening positions. These effects were discussed through a pole-zero analysis in [83].

Multiple inputs equalisation

The next step is the single input multiple-output (SIMO) equalisation. The effective equalisation area can be extended by measuring the sound pressure at various listening positions and by finding a compromise in the filter, which improves the performance at these positions [84, 85]. With multiple-input multiple-output (MIMO) techniques, relying on the use of multiple microphones and loudspeakers, the equalisation zone can be significantly extended. In this case, the input signals are filtered before being sent to every loudspeaker [86, 87]. To achieve a robust equalisation in large areas, the minimisation of the average potential energy of the sound pressure error was taken into account in [88, 89]. Instead of prescribing both the magnitude and phase in the control, only the magnitude was taken into account with an asymmetric arrangement of loudspeaker in a rectangular room [90]. On the contrary, a robust polynomial-based control system framework including a phase compensator was developed in a simulated acoustic environment using not only the channel inversion but also the sound field superposition, to reach the desired target response of each loudspeaker [91]. Last, the separation of inward and outward wavefronts was also proposed in [92] using a spherical harmonics expansion. This technique was then adapted for the measurement of subwoofers in a slightly damped room [93], and even for applications of active anechoic room [94].

An important issue of such adaptive techniques is the location of microphones and loudspeakers [5, 95]. Because of the standing waves in the room, if the error microphone of an adaptive system is located in minima of sound pressure at certain frequencies, the information is mixed with the measurement noise, resulting in an inefficient control. On the other hand, if the loudspeaker is located in minima of sound pressure at certain frequency, then the required signal computed by the corresponding algorithm cannot efficiently be radiated by the diaphragm into the room, which may force the controller to generate high-level electrical signals until saturation.

Plane wave propagation

For rectangular rooms and symmetric loudspeaker arrangements, the equalisation of the entire room can be achieved at low frequencies in an easier way. Instead of requiring the same sound pressure at all targeted positions, plane waves propagating through the room can be actively absorbed by secondary loudspeakers on the opposite wall with the help of error sensors [96–99]. An algorithm was then developed to optimise the placement of the sound sources in [14]. On the other hand, when using the same type of loudspeakers both

at the front and back walls in a symmetric arrangement, the equalisation only consists of an appropriate delay and gain adjustement [100]. Avoiding the need of digital filtering, this alternative approach has the advantage that it does not require the measurement of frequency response functions. The effect of simple arrangement of the primary and secondary sound sources in irregular enclosures was also investigated in [101, 102]. The main drawback of the plane-wave based methods is that it only relies on the hypothesis of a rectangular room and a symmetric loudspeaker setup, which cannot be always assured in practice.

Impedance-based approach

The impedance-based techniques were largely developed to lower the modal decay times in enclosures. The minimisation of the total power output and active absorption of the sound power were studied in [103]. The optimal surface impedance was addressed in [104–106], where the optimal configuration of absorbers was defined to get the most uniform distributions in space and frequency of the sound field. Since the sound field can be expressed as a modal decomposition as described in Section 1.2, it may be considered as the sum of second-orders functions, which can be implemented as multiple infinite impulse response (IIR) biquad filters. The corresponding filter coefficients were determined from the frequency response functions measured in the given enclosure [107]. Although the method was efficient at the measurement location, the control was much less reliable at the other locations. Above all, it would require the calibration of every room or as soon as the furniture is moved. Two methods of implementing active modal equalisation were also proposed in [108], either by modifying the primary sound sources or by using secondary sound sources to lower the modal decay times. A similar method was attempted in [109] by controlling the specific acoustic impedance at given locations in such a way that the plane wave propagates in a desired direction. It was pointed out the difficulty to measure the particle velocity without requiring a lot of processing. Last, an electronic bass trap was developed in [110], but it requires manual tuning of the device to damp only one or two given modes, and the control may be unstable.

1.3.3 Active absorption through impedance control

Direct impedance control

Strategies including local and global controls based on the principle of destructive interferences, which were described in Section 1.3.2, act directly on the sound field with the help of secondary sources. On the one hand, the local control method consists in reducing the sound pressure at locations defined by the placement of error microphones; on the other hand, the global control method aims at reducing the overall sound power radiated from the primary sources. Another approach is the acoustic impedance control, which consists in varying the impedance of a part of the enclosure boundaries, so as to modify the sound field thanks to the sound power absorbed by the boundary elements. The concept of electronic sound absorber (or *electroacoustic absorber*) was firstly introduced in [111]. An amplified feedback

signal, which is derived from the sound pressure measured with a microphone in front of a closed box loudspeaker diaphragm, was used to control the dynamics of the transducer used as a secondary sound source, thus resulting in a decrease of the sound pressure in the vicinity of the sensor. The absorber was studied in a one-dimensional enclosure with the direct rate feedback approach in [112], and a method with two microphones was developed in [113] to impose a target value of acoustic impedance. The active impedance control was then extended to a 3 x 3 loudspeaker array with the aim of controlling the sound reflection coefficient. Although the two-microphone technique is efficient to derive the sound pressure of incident waves, difficulties were encountered in the 3D case to predict the directivity of these incident waves. Later, the technique was combined with the filtered-X LMS algorithm in the 1D case [114, 115].

Simultaneously, feedback and feedforward techniques for the impedance control were developed in [6, 116–120], by measuring the sound pressure in front of the diaphragm loudspeaker and diaphragm velocity with the help of external sensors. Minimising the error signal enabled the value of the target acoustic impedance at the loudspeaker diaphragm to be matched to the characteristic impedance of the medium in 1D cases. In [121], the direct impedance control was adapted to applications using piezoelectric materials. To improve the active control in 1D cases, different techniques of control, such as proportional–integral–derivative-based controllers [122] and phase compensation [123], were also developed, and possibly combined each other [124]. Active resonators were designed with one sensor to improve the absorption bandwidth for plane waves under normal incidence [125]. Instead of absorbing the plane waves in 1D cases, other applications of direct impedance control were also considered. Thanks to a control based on partial differential equations, the acoustic capabilities of a set of distributed transducers coupled to microphones were also investigated in [126, 127] to modify the reflected or transmitted waves.

Shunt-based methods

Firstly introduced on piezoelectric materials [128–132], using a passive electrical network connected to the transducer terminals enabled the dynamics of the structure to be altered. In the case of the close-box loudspeaker system shunted by a resistor, the absorption bandwidth is relatively small and equivalent to an Helmholtz resonator at low frequencies [133, 134]. An optimal acoustic resistance can be achieved, but only at the resonance frequency of the system. In addition, this straightforward solution is not flexible: the loudspeaker system must be tuned, by adding some mass or by varying the volume of its enclosure for example, so as to absorb perfectly at a desired frequency.

Another technique is the connection of a negative impedance to the transducer terminals, which enables the blocked electrical impedance to be almost offset [135, 136]. As a result, the imaginary part of the acoustic impedance is almost null, but the resulting value of the resistive part is too high to absorb the sound energy of any incident wave. The instability of the system happens if the absolute value of the negative resistance is greater than the electrical resistance

of the transducer.

With parallel RC or RL electrical networks[1], the peak of absorption can be tuned apart from the transducer resonance frequency, below or above respectively, thanks to the reactive components [6]. When properly designed, connecting a series RLC electrical network to the transducer terminals becomes a two degree-of-freedom resonator, resulting in two peaks of absorption. Other techniques, such as a parallel RLC shunt network or a hybrid parallel RLC and series RLC shunt network, were proposed in [137] and [138] respectively.

Lastly, a multiple degree-of-freedom electromechanical Helmholtz resonator was proposed in [139], consisting of a Helmholtz resonator coupled to a shunted piezoelectric at the bottom of the cavity. This way, both the resonance frequencies were tuned thanks to the shunted electrical load. Low frequency sound absorption was also improved thanks to the design of a thin micro-perforated plate coated with a shunted piezoelectric transducer [140].

Self-sensing methods

The design of self-sensing actuators, whose method is different from shunt-based method, was also developed. In [141], an actuator was simultaneously used as a sensor as well, for the control of resonant modes in flexible structures. The methodology was then followed in [142–146] for vibration damping applications. This way, the control was thus equivalent to a synthesised electrical load. More recently, this concept has been applied to electrodynamic loudspeakers. A constant volume velocity source was obtained from the estimation of the diaphragm velocity [147], with a technique similar to the motional feedback initially developed in [148]. This method enabled the instabilities caused by the transducer dynamics to be eliminated. The same design was applied to damp the first resonances in a waveguide [149]. Disturbance-observer-type velocity estimators were also developed in [150, 151]. The technique was then derived to estimate the sound pressure and diaphragm velocity from an impedance model, which incorporated the electrical and mechanical parts of the transducer in addition to the dynamics of the coupled acoustic field [152].

The formulation of feedback-based acoustic impedance control revealed formal analogies with shunt strategies. Thus, a method for synthesising electrical networks with analog components was proposed in [134], bridging the gap between passive and active acoustic impedance control. Later, this shunt impedance was digitally synthesised to extend the frequency bandwidth of absorption of an electroacoustic absorber, thanks to a sensorless control [153]. Since the transfer function of the latter was not proper and could not be implemented into a digital platform, the synthesis of an electrical admittance was preferred to that of an impedance. The control was combined with a driving current method to realise the desired electrical impedance at the loudspeaker terminals.

Lastly, standard synthesis techniques, such as linear quadratic regulator [154] or optimal $\mathcal{H}_2$

---

[1]Resistance, inductance, and capacitance are commonly labelled R, L, and C respectively.

and $\mathcal{H}_\infty$ controllers [133, 155–157], were also investigated. Although the resulting impedances do not have a direct physical interpretation, the design process does not require any detailed knowledge of the transducer or acoustic system. However, it is inherently more complex to implement than electrical shunts or synthetic impedances.

Hybrid passive/active impedance control

The concept of hybrid passive/active impedance was firstly introduced in [111]. The idea is to get a sound pressure as low as possible behind a passive surface, by using the active control system, which has been described in Section 1.3.3. This way, the device, which is then equivalent to a quarter wavelength absorber, can improve the low-frequency absorption of a thin sample of porous material. This method was experimentally investigated in an impedance tube with a secondary microphone in front of the porous surface to satisfy a pressure release condition [158]. From the results, it was pointed out the advantages of this approach compared to the conventional passive methods. The suppression of the reflected wave behind the porous surface was experimented in [159], by imposing an impedance matching condition thanks to a filtered-X LMS algorithm.

The performance of the hybrid impedance control was evaluated with only one microphone behind a porous surface under normal and oblique incidences [119]. Preliminary experiments in 3D enclosures followed in [160]. An experimental study was conducted in [161], which demonstrated the superiority of the impedance-matching technique over the pressure-release approach for applications of hybrid absorption. Then, two layer hybrid absorbing system was experimented in [162] with both approaches (pressure release and impedance matching). It was noticed that the performance was mainly dependent on the properties of the absorbing material. On the one hand, the absorption capabilities are optimal when the flow resistance of the porous layer matches the characteristic impedance of the air; on the other hand, the impedance matching condition might be preferred, when the flow resistance is smaller than about 70 % of the impedance of the air.

An alternative approach was developed in [163] with a smart foam design integrating a distributed piezoelectric actuator between individual layers, to reduce the radiated power from a vibrating surface. The performance of the micro-perforated panels using this type of control was also evaluated in [164, 165]. Another method developed in [166] was the use of a thin circular aluminium plate driven by a piezoelectric patch and glued to a flexible rubber support, resulting in similar absorption capabilities to those obtained with a loudspeaker, but with a more compact design.

The hybrid impedance control was also adapted to diffusers to extend their bandwidth to lower frequencies [167–169]. In [170, 171], the case, where the waves are under grazing incidence in a flow duct, was investigated, pointing out that the optimal impedance should be different from that of the air, and should be frequency dependent. Then, the performance was evaluated with the implementation of the hybrid liner with optimised impedances [172, 173]. In the same

time, the reduction of the noise transmitted out of a 3D enclosure was investigated in [174] with two locations of three cells into the cavity. Finally, a module of active/passive control was studied in [175], showing the feasibility of dealing with both absorption and transmission.

1.4 Low-frequency perception in the context of musical listening

In Section 1.3, multiple correction procedures from the optimal room sizing and optimal configuration of sound sources to the active equalisation, including active absorption, have been discussed. Many approaches showed the effectiveness for alleviating the modal problems in enclosures from defined target responses based on specific metrics. The objective is to get a frequency response function as flat as possible at listening positions, which is, by the way, the same criterion for the evaluation of the loudspeaker systems, and modal decay times as low as possible in rooms. Nevertheless, these objective metrics may not be perceived, resulting in a useless, complex, and costly implementation. How do we perceive the peaks and dips in the frequency response functions? In particular, what is our perception when the ears are in the vicinity of a minimum of sound pressure at certain frequencies? In addition, are we able to make the difference between modal decay times equal to 0.1 s and 0.2 s?

Low-frequency resonances

First investigations evaluated the perceptible irregularities over headphones from music, speech, and white noise test signals, pointing out that peaks in the magnitude response are more audible than dips [176]. At the same time, the results of listening tests showed that resonances with low values of quality factors can be detected more easily than high ones [177]. These remarks were confirmed in [178] and it was also observed that the reverberation time may affect the threshold of resonance detections. Nevertheless, these studies did not focus on the frequencies below 200 Hz. The detection of the low-frequency resonances was thus studied in [179] between 63 Hz and 500 Hz. Whatever the test signal (pulse or pink noise), the threshold with a low resonance value was found independent on the values of eigenfrequencies, although it decreased with medium and high values of resonance as the frequency increased. In addition, for pulse test signals, resonances and anti-resonances were detectable in the same manner. Later, the audible perception was investigated in relation to the value of quality factor [33]. From listening tests over headphones with a music sample, it was found that the low-frequency modes, whose quality factor value was below $Q = 16$ (corresponding to modal decay times equal to 1.10 s, 0.56 s, and 0.28 s at 31.5 Hz, 63 Hz, and 125 Hz respectively), were not perceptible. It was also suggested that the quality factor sensitivity might be affected by masking effects of reverberation at higher frequencies.

Room sizing, modal spacing and density

The possible difference between room ratios was subjectively assessed in [180] from two different ideal room ratios determined in [62, 63] (see Section 1.3.1). It was mentioned that the results were mainly dependent on the frequency content of the test signals. The choice of test signals was discussed in [181] and the synthetic signals were recommended for critical listening tests at low frequencies, although in the end, this type of musical content was not used in the listening tests.

Then, the optimal modal spacing and density were investigating in [182]. The optimal modal spacing was shown to increase with frequency and decrease with quality factor. In addition, there might exist an optimal modal density, where listeners can no longer perceive differences between two rooms. The results suggested that at least 4 modes by octave are necessary in the low frequency range, and 32 modes for the higher frequency bands. However, it was noticed that closely spaced resonances may cause negative effects, such as an overall increase of the modal decay times and a reduction of the audibility threshold.

Last, the effect of the sound source/listener location in rooms was investigating in [183, 184] resulting in significant audible perceptions, as suggested in the different studies described in Section 1.3.1. The low-frequency room acoustic parameters, such as the modal decay time, the room volume and sound source/listener location, were evaluated using descriptive analysis in [185]. The results indicated an increased "articulation" with the decrease of modal decay times, thus suggesting the reduction of this parameter as an ideal means for ameliorating the modal problems.

Modal decay times

Since the modal decay times are an important criterion for the perception of low-frequency problems, different studies investigated the values of perceptual thresholds of these modal decay times. In [33], the same value of quality factor was applied for every mode, resulting in a decrease of modal decay times inversely proportional to the frequency (see Eq. 1.9). Thus, several studies favoured the investigation of the modal decay times rather than the quality factors of the low-frequency modes, so as to validate whether the quality factor is constant in the low frequency range. Single resonances at discrete frequencies were added to the driving signal of a single loudspeaker in a room for listening tests [186]. Results showed that the threshold of modal decay times were equal to 0.3 s at 200 Hz and 0.4 s at 100 Hz. No noticeable difference was found at 50 Hz, even for a synthetic modal decay time of almost 2 s. However, the main issue was caused by the listening room used in the study: the thresholds of the modal decay times found in the experiment could not be below those corresponding to the room.

Later, preliminary listening tests over headphones were carried out from natural and artificial test samples with two replay levels at 70 dB and 85 dB [187]. However, as the authors were faced with several problems, such as the test signals and playback equipment, they later

developed windowed sine bursts including fade-in/-out to remove the masking effects [188]. The listening tests were resumed with the preceding developed methods in [2]. It was noticed that the thresholds of modal decay times were independent on the playback level, except for those obtained with artificial signals below 63 Hz. With artificial signals, which may be considered as the worst case because of the absence of temporal masking, the average thresholds were 0.90 s at 32 Hz, 0.30 s at 63 Hz, 0.27 s at 100 Hz, 0.18 s at 150 Hz, and 0.17 s at 200 Hz. With musical samples, they were equal to 0.51 s at 63 Hz, 0.30 s at 125 Hz, and 0.12 s at 250 Hz. These thresholds are important for the development of an auditory model.

Correction comparison

Numerous electronic room correction devices, which aim at fixing awkwardly the modal problems at the defined listening position (see Section 1.3.2), are available on the market. The performance of equalisers was subjectively evaluated in terms of sound quality [189–192]. The most preferred systems had the flattest rated spectral balances. Different configurations of subwoofer systems depending on their location in the room and signal processing, such as those developed in [74, 100], were compared in [193]. The two preferred configurations had the shortest decay times in the listening room used for the study.

Mono versus stereo reproduction

Several listening tests related to resonances used headphones [2, 179, 180], where the low frequency content was the same for both ears. The mono and stereo channel subwoofer reproductions were compared in [194]. It was noticed that some strong narrow-band interaural differences may exist, especially if the listener ears are close to minima of sound pressure, and on the other hand, the modes of the recording room may have an effect on the sound field of the listening room. However, these differences were not significant in the listening tests with several configurations of loudspeakers [195].

1.5 Conclusion

In this chapter, some fundamental theoretical aspects related to the modes in enclosures have been presented, such as the expression of the modal decay time of a given mode and the eigenfrequencies in lightly damped rectangular rooms. The methods for describing and characterising the sound field in enclosures have been summarised. From these methods, the sound intensity and modal decay times can thus be evaluated and solutions were developed to reconstruct the sound field.

To address the room modes problem, correction strategies have been inspected. The passive means, such as the passive absorbers, the optimal room sizing, or the optimal configuration of sound sources, have shown their limits to improve the sound quality at low frequencies.

Some methods of active equalisation enable the frequency response function at different locations to be flattened, but they require a complex and costly implementation. On the other hand, different approaches of active impedance control have shown the possibility to absorb efficiently the sound at low frequencies in enclosures.

The last part discussed the perception of the resonances and their effects on the room sizing, listening placement, and modal spacing and density. Several studies investigated the estimation of the threshold of the modal decay times, while others evaluated the effectiveness of the proposed corrections. The correction procedures as well as the low-frequency perception presented in this chapter serve as a common base for all the investigations and results presented in the next chapters.

2 Impedance control through multiple degree-of-freedom resonators

2.1   Introduction

The main objective of electroacoustic absorbers is to decrease the sound energy in the domain in which it is located. Although the electroacoustic absorber concept generally encompasses control systems with one or more sensors, this chapter will first investigate sensorless techniques. Taking advantage of the reciprocity of the electrodynamic loudspeaker, external sensors are not necessarily used. To modify the absorption capabilities of the closed-box loudspeaker system, shunt-based methods can be used, whose several systems have been summarised in Section 1.3.3. This way, the active sound power is dissipated through the mechanical and electrical parts of the transducer, as well as through the electrical part of the shunt. Moreover, multiple degree-of-freedom Helmholtz resonators can be designed to increase the absorption bandwidth, as described in Section 1.3.1. Different types of resonators, such as Helmholtz resonators and shunted piezoelectric, can even be combined each other (see Section 1.3.3). The coupling of electrical resonators, such as the series RLC network constituted of a resistance (R), inductance (L), and capacitance (C), with the electroacoustic absorber introduces the idea of using mechanical or mixed electrical/mechanical resonators, so as to mimic or improve the absorption capabilities relative to those obtained with electrical shunts.

The goal of this chapter is to design other systems of electroacoustic absorber with several resonators constituted of conventional electrical and/or mechanical components. First, the concept of electroacoustic absorber in open circuit case is reminded to highlight the "natural" absorption capabilities of a loudspeaker. The model of the electrodynamic loudspeaker in a closed box is introduced, before presenting the absorption performance through the definitions of the specific acoustic impedance, and the reflection and absorption coefficients. Then, different systems of electrical and mechanical resonators coupled to the electroacoustic absorber are studied. The absorption performance of every electroacoustic absorber system is optimised through two objective functions, and the optimal configurations are compared with each other. Finally, an experimental evaluation of the different optimal configurations
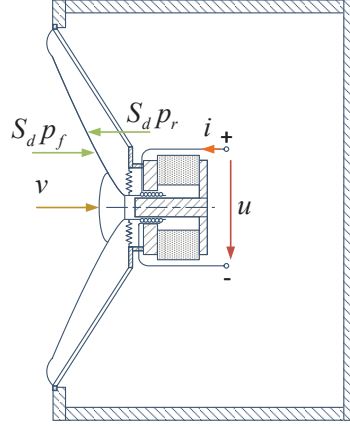
Figure 2.1 – Closed box electrodynamic loudspeaker system.

and a discussion on the corresponding absorption capabilities are given.

2.2 Electroacoustic absorber: concept and formulation

2.2.1 Electrodynamic loudspeaker model

An electrodynamic loudspeaker can be considered as a single degree-of-freedom oscillator, which is mechanically driven by a voice coil within a magnetic field. All forces acting on the transducer, especially those resulting from the sound pressures $p_f(t)$ and $p_r(t)$ at the front and rear faces of the diaphragm, are assumed small enough so that the governing equations should remain linear. The mechanical part is considered as a simple mass – spring - damper system in the low-frequency range, that is the mass M_{ms}, the mechanical compliance C_{ms} accounting for the surround suspension and the spider, and the mechanical resistance R_{ms}, respectively. Denoting S_d as the effective piston area and Bl as the force factor[1] of the moving-coil transducer, the equation of motion of the loudspeaker diaphragm is derived from Newton's second law, which can be written as

$$M_{ms}\frac{dv(t)}{dt} = S_d\left(p_f(t) - p_r(t)\right) - Bl\,i(t) - R_{ms}v(t) - \frac{1}{C_{ms}}\int v(t)\,dt \tag{2.1}$$

where $v(t)$ is the incoming diaphragm velocity and $i(t)$ is the electrical current flowing through the voice coil, as illustrated in Fig. 2.1.

The standard linear governing equation of the electrical dynamics can be written as

$$u(t) = \left(L_e\frac{d}{dt} + R_e\right)i(t) + \varepsilon(t) \tag{2.2}$$

---

[1]where B is the magnetic flux density and l is the length of the voice coil
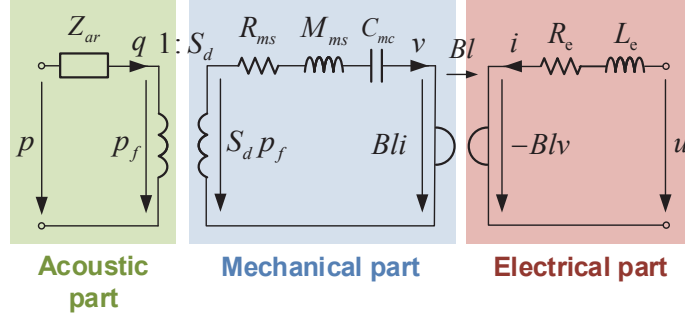
Figure 2.2 – Circuit representation of the closed box electrodynamic loudspeaker system.
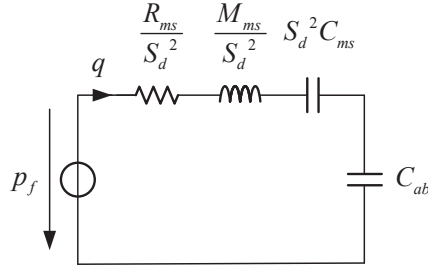
Figure 2.3 – Acoustic equivalent schematic of the closed box loudspeaker in open circuit case.

where $u(t)$ is the input voltage between the electrical terminals, R_e is the DC resistance, L_e is the self inductance of the voice coil, and $\varepsilon(t) = -Bl\, v(t)$ is the electromotive force caused by the movement of the voice coil within the permanent magnetic field.

The loudspeaker is loaded by a rear cabinet of volume V_b (see Fig. 2.1). The sound pressure is considered uniform at the rear face of the diaphragm in the frequency range of interest. The force of the fluid reaction acting on the rear face is usually modelled as

$$S_d p_r(t) = \frac{S_d^2}{C_{ab}} \int v(t)\, dt \tag{2.3}$$

where $C_{ab} = V_b/(\rho c^2)$ represents the acoustic compliance of the enclosure, where ρ is the density of the medium and c is the speed of sound in the air. The acoustic resistance of the box is neglected. Figure 2.2 shows the circuit representation of the electrodynamic loudspeaker, where Z_{ar} is the radiation impedance in front of the diaphragm, and $Q(\omega) = S_d V(\omega)$ is the acoustic volume flow. The acoustic equivalent schematic of the system in open circuit case is given in Fig. 2.3.

Using the Fourier transform where ω is the angular frequency (in rad·s^{-1}), the set of Eqs. (2.1)

and (2.2) is

$$S_d P_f(\omega) = \left(Z_{ms}(\omega) + \frac{S_d{}^2}{j\omega C_{ab}} \right) V(\omega) + Bl\,I(\omega) \tag{2.4}$$

$$U(\omega) = Z_e(\omega)\,I(\omega) - Bl\,V(\omega) \tag{2.5}$$

where $Z_{ms}(\omega) = j\omega M_{ms} + R_{ms} + 1/(j\omega C_{ms})$ is the mechanical impedance of the loudspeaker and $Z_e(\omega) = j\omega L_e + R_e$ is the blocked electrical impedance of the voice coil.

2.2.2 Absorption performance

Acoustic absorption relates to the ability of a given system to dissipate the sound power of an incident wave. Typical examples of passive resonant systems have been summarised in Section 1.3.1. In the case of the electrodynamic loudspeaker, the sound pressure of the reflected wave at the diaphragm should be reduced relative to that of the incident wave. This dissipation is possible thanks to the power losses in the different parts of the transducer. According to the American standard acoustic impedance [196], the specific acoustic impedance $Z_s(\omega)$ describes the dynamic response of the diaphragm to an external acoustic disturbance, characterising the acoustic properties of the surface. This impedance is defined as the complex ratio of the sound pressure $P_f(\omega)$ at the front face of the diaphragm to the diaphragm velocity $V(\omega)$. When the loudspeaker is in open circuit case, that is no electrical current $I(\omega)$ circulates through the voice coil, this quantity is directly derived from Eqs. (2.4) and (2.5), or from the acoustic equivalent schematic illustrated in Fig. 2.3, as

$$Z_s(\omega) = \frac{P_f(\omega)}{V(\omega)} = \frac{Z_{ms}(\omega)}{S_d} + \frac{S_d}{j\omega C_{ab}} \tag{2.6}$$

The corresponding resonance frequency is equal to

$$f_0 = \frac{1}{2\pi\sqrt{M_{ms}\dfrac{C_{ms}C_{ab}}{S_d{}^2 C_{ms} + C_{ab}}}} \tag{2.7}$$

The acoustic properties of a surface are defined by the sound reflection coefficient $r(\omega)$ and corresponding sound absorption coefficient $\alpha(\omega)$. Under normal incidence, these quantities are expressed respectively as

$$r(\omega) = \frac{Z_s(\omega) - Z_c}{Z_s(\omega) + Z_c} \quad \text{and} \quad \alpha(\omega) = 1 - |r(\omega)|^2 = \frac{4Z_c\,\mathrm{Re}\,(Z_s(\omega))}{|Z_s(\omega) + Z_c|^2} \tag{2.8}$$

where $Z_c = \rho c$ is the characteristic impedance of the air. For a completely absorbent system, its specific acoustic impedance is equal to the characteristic impedance of the medium in the frequency range of interest. To highlight the acoustic absorption capabilities of the system, the bandwidth of efficient sound absorption BW is defined as the frequency range over which the total sound intensity in front of the diaphragm is less than twice the total sound intensity

in the ideal case $\alpha(\omega) = 1$ [2]. It is equivalent to $P_f(\omega) \leq \sqrt{2} P_i(\omega)$ where P_i is the sound pressure of the incident wave. This criterion corresponds to a threshold value of minimal efficient absorption $\alpha_{th} = 1 - (\sqrt{2} - 1)^2 \simeq 0.83$. In the ideal case, the total sound intensity is equal to the sound intensity of the incident wave. In the threshold case, the total sound intensity in front of the diaphragm (sound intensity of the sum of incident and reflected waves) is equal to twice the sound intensity of the incident wave alone. The bandwidth of efficient sound absorption BW is found to be

$$BW = \frac{S_d}{2\pi M_{ms}} \sqrt{\frac{(1 - \alpha_{th})\left(\frac{R_{ms}}{S_d} + Z_c\right)^2 - \left(\frac{R_{ms}}{S_d} - Z_c\right)^2}{\alpha_{th}}} \tag{2.9}$$

and only valid for $|R_{ms}/S_d - \sqrt{2} Z_c| \leq Z_c$, that is $R_{ms}/S_d \geq 171\ \text{Pa·s·m}^{-1}$ and $R_{ms}/S_d \leq 997\ \text{Pa·s·m}^{-1}$. Note that the higher the term S_d/M_{ms}, the wider the bandwidth BW.

An electroacoustic absorber is thus a closed box electrodynamic loudspeaker, which is able to absorb, partially or totally, the sound intensity of the incident wave. In the following, different solutions are presented to maximise the sound absorption capabilities, which is equivalent to minimising the sound intensity of the reflected waves.

2.3 Design of multiple degree-of-freedom electroacoustic absorbers

This chapter investigates three different systems of electroacoustic absorber, when the closed box loudspeaker is coupled to an electrical (system A), a mechanical (system B), and an electromechanical (system C) resonators.

2.3.1 With an electrical resonator

Rather than employing sensors to modify the dynamics of the loudspeaker, an appropriate electrical circuit connected to its electrical terminals efficiently enables the dissipation of the sound power at the diaphragm through mechanical and electrical losses, thus modifying its sound absorption capabilities. An electrical load represented by the complex impedance $Z_l(\omega)$ is connected to the transducer terminals. This impedance is added in series to the blocked electrical impedance $Z_e(\omega)$. When the voice coil moves with the velocity $V(\omega)$, the electromotive force generates the current $I(\omega)$ circulating through the closed electrical circuit given by

$$I(\omega) = \frac{Bl}{Z_e(\omega) + Z_l(\omega)} V(\omega) \tag{2.10}$$

---

[2] The bandwidth of efficient absorption BW should not be confused with the bandwidth Δf of a given resonator ($\Delta f = f_0/Q$ where f_0 is the resonant frequency and Q is the quality factor).
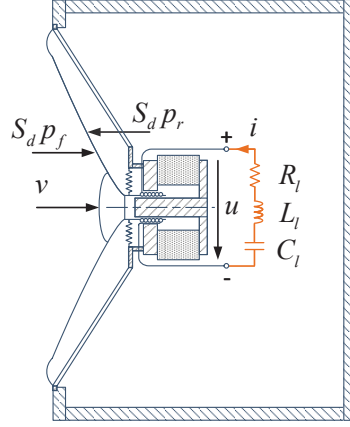
Figure 2.4 – Closed-box loudspeaker connected to an electrical resonator (system A).
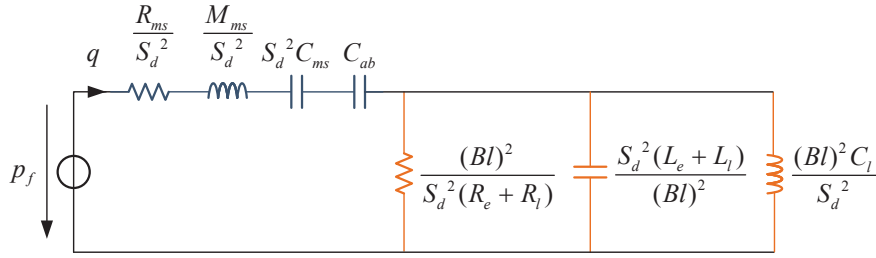
Figure 2.5 – Equivalent acoustic circuit of the system A.

The study focuses on the electrical resonator constituted of the series RLC network, as illustrated in Fig. 2.4. The equivalent acoustic circuit of the closed box loudspeaker connected to this electrical resonator (system A) is illustrated in Fig. 2.5. The electrical impedance of this shunt network is written as

$$Z_l(\omega) = j\omega L_l + R_l + \frac{1}{j\omega C_l} \tag{2.11}$$

 Combining Eq. (2.10) with Eqs. (2.4) and (2.5), or from the equivalent acoustic circuit in Fig. 2.4, gives the expression of the specific acoustic impedance

$$Z_{s_A}(\omega) = \frac{Z_{ms}(\omega)}{S_d} + \frac{S_d}{j\omega C_{ab}} + \frac{Z_{me_A}(\omega)}{S_d} \tag{2.12}$$

where

$$Z_{me_A}(\omega) = \frac{(Bl)^2}{j\omega(L_e + L_l) + R_e + R_l + \frac{1}{j\omega C_l}} \tag{2.13}$$

30

corresponds to the equivalent mechanical impedance of the electrical resonator in series with the electrical impedance of the loudspeaker. The resonance frequency of the electrical resonator is equal to

$$f_{0_A} = \frac{1}{2\pi\sqrt{(L_e + L_l)\,C_l}} \tag{2.14}$$

The poles of the specific acoustic impedance $Z_{s_A}(\omega)$ are the same as those of the equivalent mechanical impedance $Z_{me_A}(\omega)$, but the zeros cannot be expressed analytically in a simple way. The real and imaginary parts of the specific acoustic impedance $Z_{s_A}(\omega)$ can be derived from Eqs. (2.12) and (2.13) as

$$\mathrm{Re}\left(Z_{s_A}(\omega)\right) = \frac{R_{ms}}{S_d} + \frac{(Bl)^2(R_e + R_l)}{S_d\left[(R_e + R_l)^2 + \left(\omega(L_e + L_l) - \dfrac{1}{\omega\,C_l}\right)^2\right]} \tag{2.15}$$

$$\mathrm{Im}\left(Z_{s_A}(\omega)\right) = \frac{1}{S_d}\left[\omega M_{ms} - \frac{1}{\omega}\left(\frac{1}{C_{ms}} + \frac{S_d^{\ 2}}{C_{ab}}\right)\right] - \frac{(Bl)^2\left(\omega(L_e + L_l) - \dfrac{1}{\omega\,C_l}\right)}{S_d\left[(R_e + R_l)^2 + \left(\omega(L_e + L_l) - \dfrac{1}{\omega\,C_l}\right)^2\right]} \tag{2.16}$$

As discussed in Section 1.3.3, if a negative impedance $Z_l(\omega)$ is connected to the transducer electrical terminals, the stability condition is $Z_e(\omega) + Z_l(\omega) \geq 0 \quad \forall \omega$. As a result, the electrical resonator can only add resistance to the whole system. For the reactive part, if the values of inductance L_l and capacitance C_l are judiciously chosen, the electrical resonator can partly decrease both mass and stiffness of the closed box loudspeaker over a certain frequency range.

2.3.2 With a mechanical resonator

The main motivation of the method presented in this chapter is to be able to mimic, and possibly improve, the absorption capabilities of the closed box loudspeaker coupled to the electrical resonator (system A), by means of a mechanical coupling. Thanks to the resonant behaviour of the loudspeaker, several loudspeakers may be arranged behind each other to increase the order of the resonant system, as well as the absorption bandwidth. Shunt resistors are eventually connected to the loudspeakers terminals to adjust the acoustic resistances of the diaphragms. Fig. 2.6 illustrates the system B constituted of two loudspeakers, whose parameters (represented by indices $i = [1, 2]$) are connected to shunt resistors R_{l_1} and R_{l_2} and loaded in closed boxes. The second closed box loudspeaker (in green) is called the mechanical resonator. Within each of the two volumes V_{b_1} and V_{b_2} of the enclosures, the sound pressure is considered uniform in the frequency range of interest. By conservation of the volume flow, the sound pressure $P_{r_1}(\omega)$ at the rear face of the diaphragm #1 and the sound pressure $P_{f_2}(\omega)$
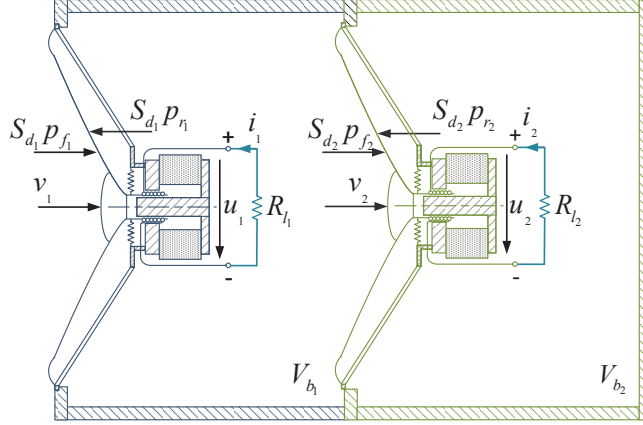
Figure 2.6 – Two loudspeakers connected to shunt resistors and loaded in closed boxes (system B).

at the front face of the diaphragm #2 are expressed as

$$P_{r_1}(\omega) = P_{f_2}(\omega) = \frac{1}{j\omega C_{ab_1}} \left(S_{d_1} V_1(\omega) - S_{d_2} V_2(\omega) \right) \tag{2.17}$$

where $C_{ab_1} = V_{b_1}/(\rho c^2)$. The sound pressure $P_{r_2}(\omega)$ at the rear face of the diaphragm #2 is expressed as

$$P_{r_2}(\omega) = \frac{S_{d_2}}{j\omega C_{ab_2}} V_2(\omega) \tag{2.18}$$

where $C_{ab_2} = V_{b_2}/(\rho c^2)$. The coupled equations of motion of the loudspeaker diaphragms can then be written as [3]

$$\left(Z_{ms_1}(\omega) + \frac{S_{d_1}^2}{j\omega C_{ab_1}} \right) V_1(\omega) - \frac{S_{d_1} S_{d_2}}{j\omega C_{ab_1}} V_2(\omega) = S_{d_1} P_{f_1}(\omega) - Bl_1 I_1(\omega) \tag{2.19}$$

$$\frac{S_{d_1} S_{d_2}}{j\omega C_{ab_1}} V_1(\omega) - \left(Z_{ms_2}(\omega) + \frac{S_{d_2}^2}{j\omega C_{ab_1}} + \frac{S_{d_2}^2}{j\omega C_{ab_2}} \right) V_2(\omega) = Bl_2 I_2(\omega) \tag{2.20}$$

The equivalent acoustic circuit of the system B is illustrated in Fig. 2.7, where $Q_1(\omega) = S_{d_1} V_1(\omega)$ and $Q_2(\omega) = S_{d_2} V_2(\omega)$. Combining Eqs. (2.10), (2.17) and (2.18) with Eqs. (2.19) and (2.20), or from the equivalent acoustic circuit in Fig. 2.7, gives the expression of the specific acoustic impedance

$$Z_{s_B}(\omega) = \frac{Z_{ms_1}(\omega)}{S_{d_1}} + \frac{S_{d_1}}{j\omega C_{ab_1}} + \frac{(Bl_1)^2}{S_{d_1}(Z_{e_1} + R_{l_1})} + \frac{Z_{me_B}(\omega)}{S_{d_1}} \tag{2.21}$$

---

[3] $B_1 l_1$ and $B_2 l_2$ are noted Bl_1 and Bl_2 respectively to avoid numerous subscripts.
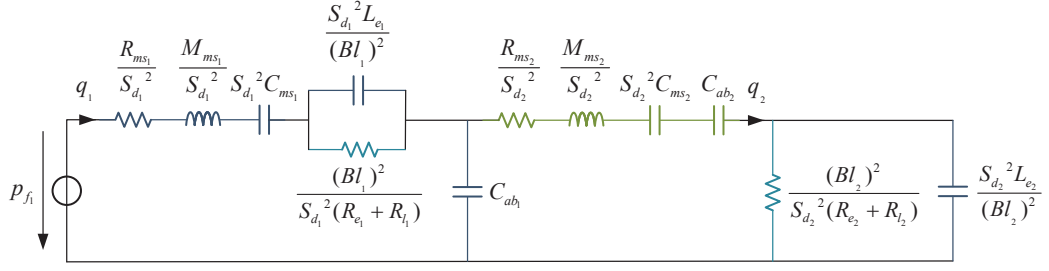
Figure 2.7 – Equivalent acoustic circuit of the system B.

where

$$
Z_{me_B}(\omega) = -\frac{\left(\dfrac{S_{d_1} S_{d_2}}{j\omega\, C_{ab_1}}\right)^2}{Z_{ms_2}(\omega) + \dfrac{S_{d_2}{}^2}{j\omega}\left(\dfrac{1}{C_{ab_1}} + \dfrac{1}{C_{ab_2}}\right) + \dfrac{(Bl_2)^2}{Z_{e_2}(\omega) + R_{l_2}}}
\tag{2.22}
$$

corresponds to the equivalent mechanical impedance of the mechanical resonator. The two poles in zero of this impedance highlight the coupling coefficient $(S_{d_1} S_{d_2}/C_{ab_1})^2$ between both mechanical resonators, showing the great importance of these three values for the absorption performance of the electroacoustic absorber. For this system, it is difficult to analyse the effects of every system model parameter on the resistive and reactive parts of the specific acoustic impedance.

2.3.3 With an electromechanical resonator

The electroacoustic absorber might also be a combination of two (or more) resonators of different type to improve the bandwidth of absorption. Here, the series RLC network substitutes for the shunt resistor connected to the second loudspeaker terminals, as illustrated in Fig. 2.8. This subsystem becomes a two degree-of-freedom electromechanical resonator. The equivalent acoustic circuit of the system C is illustrated in Fig. 2.9. Replacing the electrical resistance R_{l_2} by an electrical impedance Z_{l_2} in Eq. (2.22), or from the equivalent acoustic circuit in Fig. 2.8, gives the expression of the specific acoustic impedance

$$
Z_{s_C}(\omega) = \frac{Z_{ms_1}(\omega)}{S_{d_1}} + \frac{S_{d_1}}{j\omega\, C_{ab_1}} + \frac{(Bl_1)^2}{S_{d_1}(Z_{e_1}(\omega) + R_{l_1})} + \frac{Z_{me_C}(\omega)}{S_{d_1}}
\tag{2.23}
$$

where

$$
Z_{me_C}(\omega) = -\frac{\left(\dfrac{S_{d_1} S_{d_2}}{j\omega\, C_{ab_1}}\right)^2}{Z_{ms_2}(\omega) + \dfrac{S_{d_2}{}^2(C_{ab_1} + C_{ab_2})}{j\omega\, C_{ab_1} C_{ab_2}} + \dfrac{(Bl_2)^2}{Z_{e_2}(\omega) + Z_{l_2}(\omega)}}
\tag{2.24}
$$

33
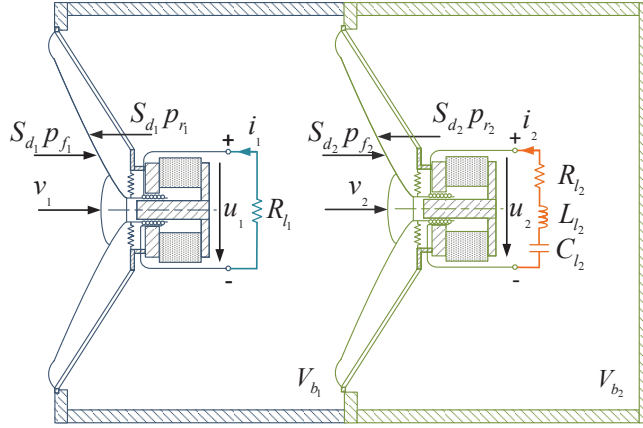
Figure 2.8 – Two loudspeakers loaded in closed boxes, one connected to a shunt resistor, the other connected to a series resistance - inductance - capacitance network (system C).
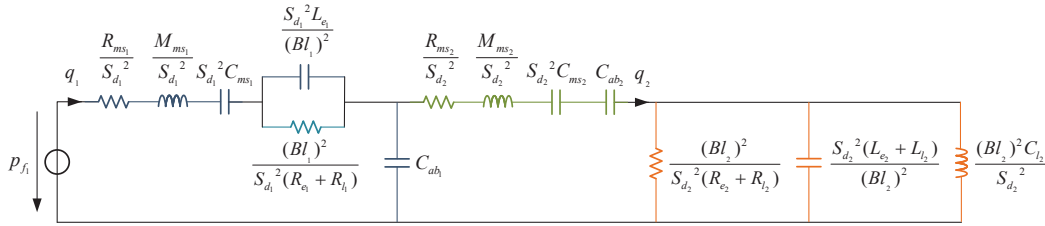
Figure 2.9 – Equivalent acoustic circuit of the system C.

corresponds to the equivalent mechanical impedance of the electromechanical resonator. If the electromechanical resonator is properly designed, the system C should behave like a three degree-of-freedom resonator with three peaks of absorption. Note that an electrical resonator could similarly be connected to the first loudspeaker as well.

2.4 Optimisation of multiple degree-of-freedom electroacoustic absorbers

2.4.1 Strategy

In Section 2.3, the specific acoustic impedance expressions of the systems A, B, and C in Eqs. (2.12), (2.21) and (2.23) respectively show the difficulty to analyse the effect of each system model parameter and to find optimal values for these parameters to maximise the sound absorption coefficient. In this section, parametric optimisations are carried out through two objective functions.

- The weighted bandwidth wBW corresponds to the area delimited by the curve of the

sound absorption coefficient between the bounds of the bandwidth of efficient sound absorption BW defined in Section 2.2.2

$$wBW = \int_{BW} \alpha(f)\,\mathrm{d}f \tag{2.25}$$

This objective function enables the bandwidth of efficient absorption BW to be maximised.

- The area over threshold $\mathcal{A}$ corresponds to the area below the curve of the sound absorption coefficient of Eq. (2.8) and above the threshold of the efficient sound absorption $\alpha_{th} = 1 - (\sqrt{2} - 1)^2$

$$\mathcal{A} = \int \max\big(\alpha(f) - \alpha_{th}, 0\big)\,\mathrm{d}f \tag{2.26}$$

It corresponds to the weighted bandwidth wBW minus the bandwidth of efficient absorption BW weighted by the threshold of efficient absorption α_{th}. Instead of favouring a large bandwidth of efficient absorption with a "low" maximal value of sound absorption coefficient, this objective function enables the absorption coefficient to be maximised (that is near a perfect absorption), over a frequency range as large as possible.

In the following, the bandwidth BW and centre frequency $f_0' = \sqrt{BW^- BW^+}$ of the electroacoustic absorber coupled to one of the three resonators, where BW^- and BW^+ are the lower and upper bounds of BW, are given as additional indicators.

The overall performance is evaluated through two approaches: the comparison of the three optimal configurations through either objective function, and the comparison of both optimal configurations given by the objective functions for a given system. Considering a Visaton AL-170 loudspeaker, its model mechanical parameters were estimated from the measurement of the mechanical impedance of the loudspeaker diaphragm, mounted at the termination of a standing-wave duct, excited by an external sound source with broadband noise. The experimental setup is detailed in Section 2.5.1. The radiation impedance, which depends on the environment in which the loudspeaker is located, was already taken into account in the mechanical impedance $Z_m(\omega)$. The loudspeaker model parameters are reported in Table 2.1. The density of the air at 294 K is $\rho = 1.20\,\mathrm{kg\cdot m^{-3}}$ and the sound speed in the air is $c = 343.86\,\mathrm{m\cdot s^{-1}}$.

Because the model parameters of any electrodynamic loudspeaker are actually limited by physical and technological constraints, some parameters are fixed in advance, and are not taken into account for the optimization. Hence, in the case of the system A where the closed box loudspeaker is coupled with the electrical resonator, the performance is only optimised on the electrical parameters of the series RLC network. In the case of the system B where the closed box loudspeaker is coupled with the mechanical resonator, the total volume $V_{b_1} + V_{b_2}$ is

Table 2.1 – Loudspeaker model parameters of the Visaton AL-170 and Monacor MSH-115.

	Visaton AL-170		Monacor MSH-115		
	Notation	Value	Notation	Value	Unit
Effective piston area	S_{d_1}	133	S_{d_2}	55	cm^2
Moving mass	M_{ms_1}	13.00	M_{ms_2}	5.50	g
Mechanical resistance	R_{ms_1}	0.60	R_{ms_2}	1.14	$N{\cdot}s{\cdot}m^{-1}$
Mechanical compliance	C_{ms_1}	594.85	C_{ms_2}	316.94	$\mu m{\cdot}N^{-1}$
Force factor	Bl_1	6.9	Bl_2	4.8	$N{\cdot}A^{-1}$
Voice coil inductance	L_{e_1}	0.9	L_{e_2}	0.3	mH
DC resistance	R_{e_1}	5.6	R_{e_2}	6.3	Ω

fixed so as to conserve the same volume equal to that of the original loudspeaker enclosure. Thus, the value of the volume V_{b_1} may vary between 0 and $10\,cm^3$, and the volume V_{b_2} is deduced accordingly. The shunt resistances R_{l_1} and R_{l_2} are free to vary without constraint during the optimisation. In the case of the system C where the closed box loudspeaker is coupled with the electromechanical resonator), the total volume $V_{b_1} + V_{b_2}$ is also fixed, as well as the model parameters of the secondary loudspeaker, for which a Monacor MSH-115 was chosen, and whose loudspeaker model parameters are reported in Table 2.1. The electrical shunt parameters L_{l_2} and C_{l_2} may also vary without constraint during the optimisation for the system C.

2.4.2   Comparison of the systems from a given objective function

Table 2.2 summarises the results for the systems A, B, and C after optimisation using either objective function wBW or $\mathcal{A}$. In this table, the optimised parameters and corresponding performance indicators are given for every objective function, that is the centre frequency f_0', bounds of the bandwidth of efficient absorption BW^- and BW^+, weighted bandwidth wBW, and area over threshold $\mathcal{A}$. First, the performance of the three systems are compared from the objective function $\mathcal{A}$. The Bode plot of the resulting specific acoustic impedance is displayed in Fig. 2.10a, and the expected performance in terms of sound absorption coefficient is given in Fig. 2.10b. When the closed box loudspeaker system is in open circuit and is not coupled to any additional resonator (named basic configuration), it behaves as a passive second-order bandpass system. At low frequencies the specific acoustic impedance is controlled by the stiffness, the magnitude decreasing as $1/(f\,S_d C_{mc})$. Then it is controlled by the resistance R_{ms}/S_d, with a minimal magnitude at resonance, and above resonance, it is controlled by the mass, the magnitude increasing as $f\,M_{ms}/S_d$. The phase shift between the total sound pressure at the diaphragm and diaphragm velocity tends to $-\pi/2$ at low frequencies, is equal to zero at resonance, and tends to $\pi/2$ at high frequencies.

Table 2.2 – Values of the optimised system parameters and corresponding absorption performance indicators for both objective functions.

			System A		System B		System C	
			Objective Functions		Objective Functions		Objective Functions	
			wBW	$\mathcal{A}$	wBW	$\mathcal{A}$	wBW	$\mathcal{A}$
Optimised Parameters	V_{b_1}	(L)	10.00	10.00	1.83	2.02	1.87	2.03
	R_{l_1}	(Ω)	-1.84	0.05	∞	∞	∞	∞
	L_{l_1}	(mH)	3.46	8.75	-	-	-	-
	C_{l_1}	(μF)	706.74	321.28	-	-	-	-
	V_{b_2}	(L)	-	-	8.17	7.98	8.13	7.97
	R_{l_2}	(Ω)	-	-	3.18	4.78	1.28	3.51
	L_{l_2}	(mH)	-	-	-	-	14.24	16.00
	C_{l_2}	(μF)	-	-	-	-	99.32	87.44
Perf. Indicators	$f_0{}'$	(Hz)	90.4	90.4	142.1	141.0	137.2	135.7
	BW^-	(Hz)	43.7	52.3	94.9	97.2	84.4	85.8
	BW^+	(Hz)	187.0	156.2	212.9	204.6	223.3	214.6
	wBW	(Hz)	125.83	98.74	107.00	100.40	126.70	119.86
	$\mathcal{A}$	(Hz)	7.15	12.63	9.19	11.44	11.60	13.12

Connecting an electrical resonator to the loudspeaker terminals causes the stiffness and mass of the electroacoustic absorber to be reduced over a relatively narrow frequency band, increasing the sound absorption performance around the resonance frequency. For the systems B and C, the volume V_{b_1} is much smaller than the volume V_{b_2}. Note that the connection of a series RLC network to the terminals of the loudspeaker #1 is useless, since the results of Table–2.2 shows that any additional acoustic resistance is not required for this loudspeaker. This result even suggests that the value R_{ms_1}/S_{d_1} should be as low as possible to maximise the absorption performance. As each loudspeaker is loaded by a smaller volume than for the system A, the centre frequency $f_0{}'$ is inevitably higher. The systems B and C exhibit a bandwidth of efficient absorption BW of the same order of magnitude as that obtained with the system A, but at higher frequencies. If the difference of frequency ranges of efficient absorption between the systems are not considered for the comparison, the system C provides the best absorption performance, in terms of area over threshold $\mathcal{A}$ and weighted bandwidth BW, thanks to the three peaks of resonances.

To understand the effects of the additional resonators on the absorption capabilities, the real and imaginary parts of the specific acoustic impedance of each system, according to the results of the objective function $\mathcal{A}$, are given in Fig. 2.11. For the system A, the real part of the specific acoustic impedance $Z_{me_A}(\omega)/S_{d_1}$ of the electrical resonator prevails over that of the closed-box
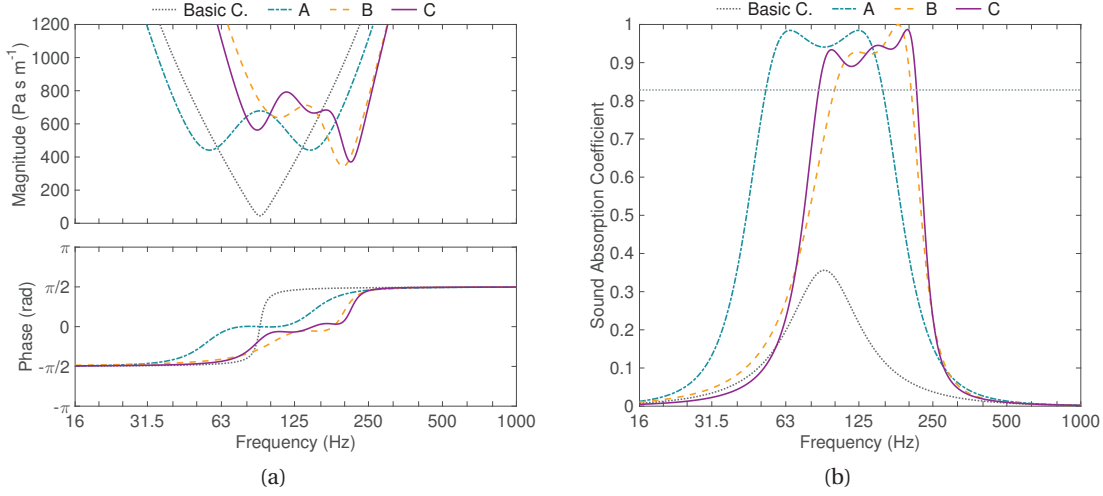
Figure 2.10 – (a) Bode plot of the specific acoustic impedance and (b) corresponding sound absorption coefficient of the electroacoustic absorber computed in the case of systems A, B, and C after optimisation using the objective function $\mathcal{A}$, relative to the basic configuration.

loudspeaker at low frequencies (see Fig. 2.11a). On the other hand, the imaginary part of the electrical resonator has an influence on the electroacoustic absorber impedance only around the resonance frequency. Beyond this range, the closed box loudspeaker reactance prevails. Note that the resonance frequencies of both resonators are equal to maximise the absorption capabilities. As can be seen in Eqs. (2.15) and (2.16), the expression of the equivalent mechanical impedance $Z_{me_A}(\omega)$ of the electrical resonator is equivalent to the inverse of the mechanical impedance of the closed-box loudspeaker. Their behaviours are reversed over the frequency band of interest. This way, the imaginary part of the overall specific acoustic impedance $Z_{s_A}(\omega)$ of the system is closer to zero over a greater frequency range than in the case of the basic configuration (open circuit), thus increasing the absorption capabilities around the resonance frequency. For the system B illustrated in Fig. 2.11b, the real and imaginary parts of the specific acoustic impedance $Z_{me_B}(\omega)/S_{d_1}$ of the mechanical resonator are not symmetrical because of the double pole involving the coupling factor. Nevertheless, the behaviours of the loudspeaker and mechanical resonator are reversed as well, leading to absorption capabilities similar to the first configuration. Finally, for the system C illustrated in Fig. 2.11c, the specific acoustic impedance $Z_{s_C}(\omega)$ is a "mix" of those obtained with the systems A and B. This system is tuned so as to exhibit three resonances, providing the best absorption performance of the three systems.

2.4.3 Comparison of the objective functions from a given system

This section intends to compare both objective functions for a given system to evaluate the differences of absorption capabilities. Considering the three systems, the optimisation results of both objective functions are presented in Table 2.2. The Bode plots of the resulting specific
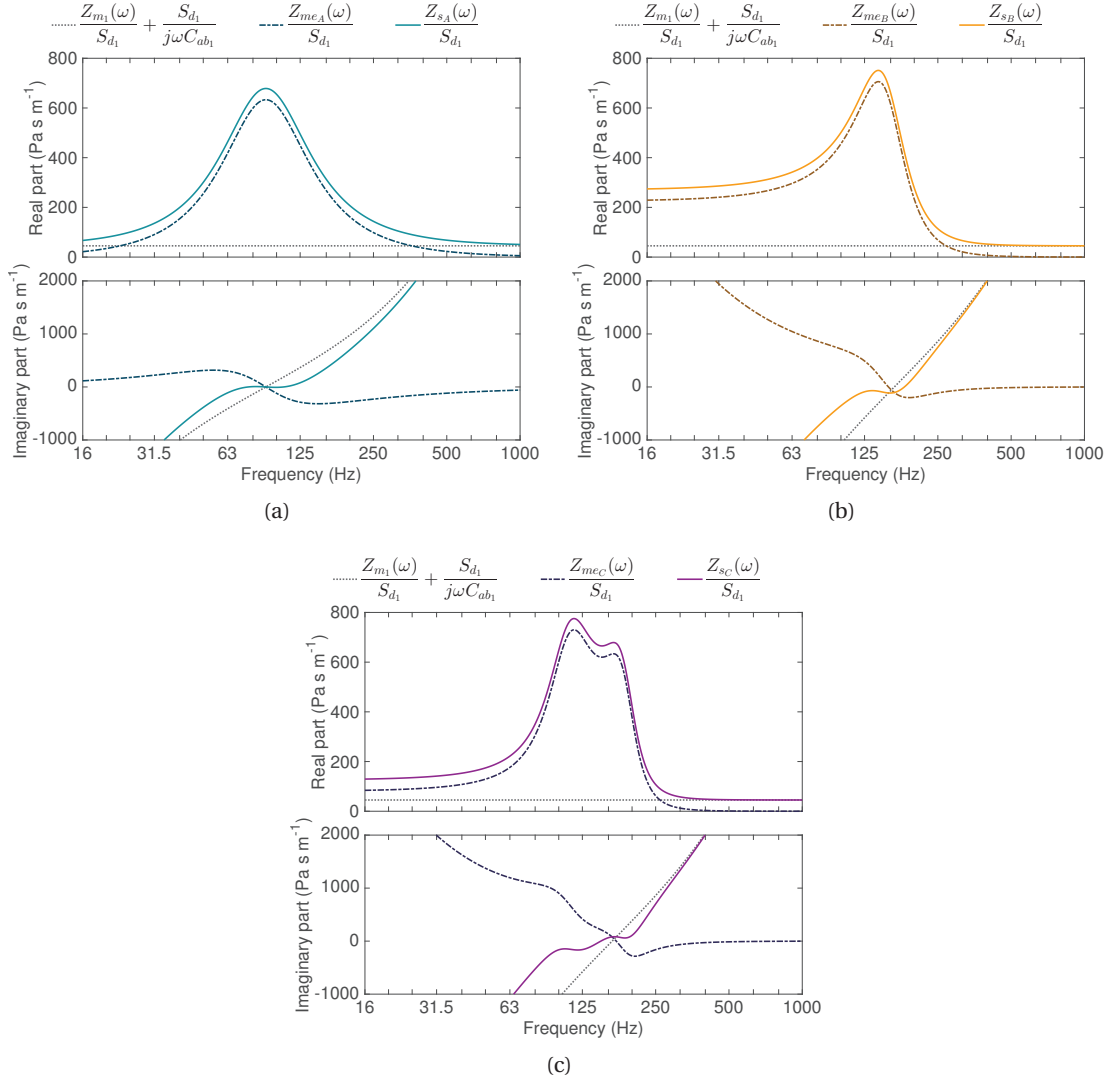
Figure 2.11 – Real and imaginary parts of the specific acoustic impedance of the electroacoustic absorber computed in the case of (a) system A, (b) system B, and (c) system C after optimisation using the objective function $\mathcal{A}$.

acoustic impedance of the systems A, B, and C are displayed in Figs. 2.12a, 2.13a, and 2.14a respectively. The expected performance in terms of sound absorption coefficient is given in Figs. 2.12b, 2.13b, and 2.14b. For the system A, the results are different according to the given objective function. The objective function wBW extends the bandwidth of efficient absorption at its maximum, while the other favours the sound absorption coefficient close to one. Although the absorption performance are rather similar in both configurations involving the mechanical resonator, the performance indicators wBW and $\mathcal{A}$ summarised in Table 2.2 highlight the indicator which is maximised through the given objective function. For the systems B and C, note that the loudspeaker #1 is left open circuit, whatever the chosen

39
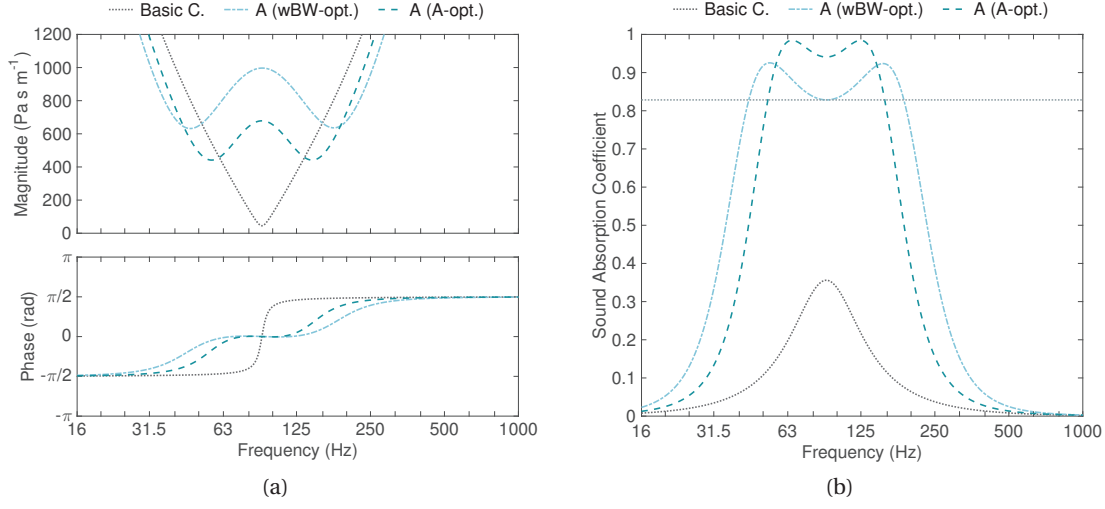
Figure 2.12 – (a) Bode plot of the specific acoustic impedance and (b) sound absorption coefficient of the system A depending on the objective function, relative to the basic configuration.
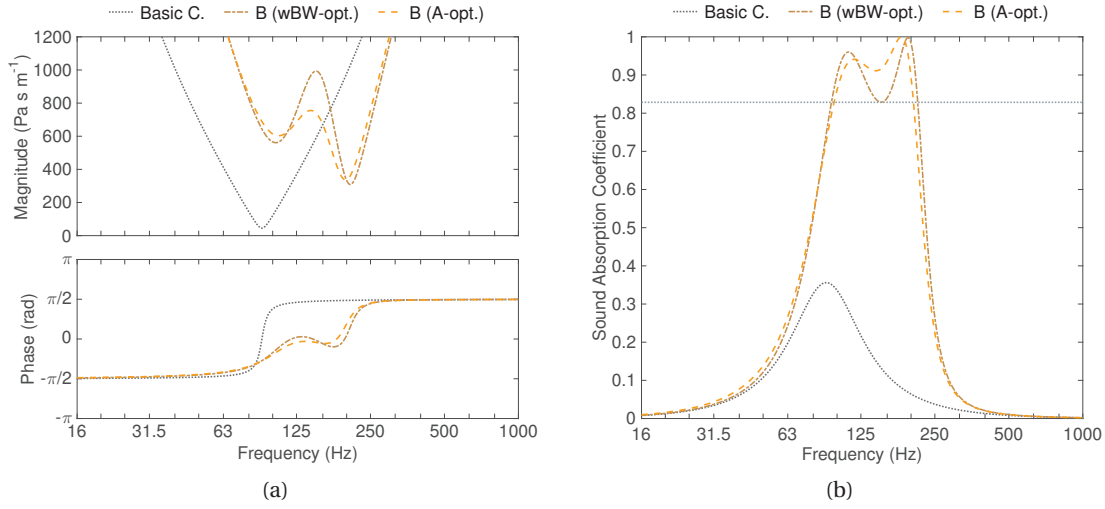
Figure 2.13 – (a) Bode plot of the specific acoustic impedance and (b) sound absorption coefficient of the system B depending on the objective function, relative to the basic configuration.

objective function. Interestingly, the results point out that there are several combinations of parameters values for the mechanical and electromechanical resonators to get similar absorption capabilities. Thus, it allows to have some flexibility over the volumes V_{b_1} and V_{b_2} for the realisation of the electroacoustic absorber. Then, the shunt resistor R_{l_2} can tune the acoustic resistance of the additional resonator to maximise the absorption performance. Depending on given specifications for a practical implementation, one strategy can thus be favoured over the other.
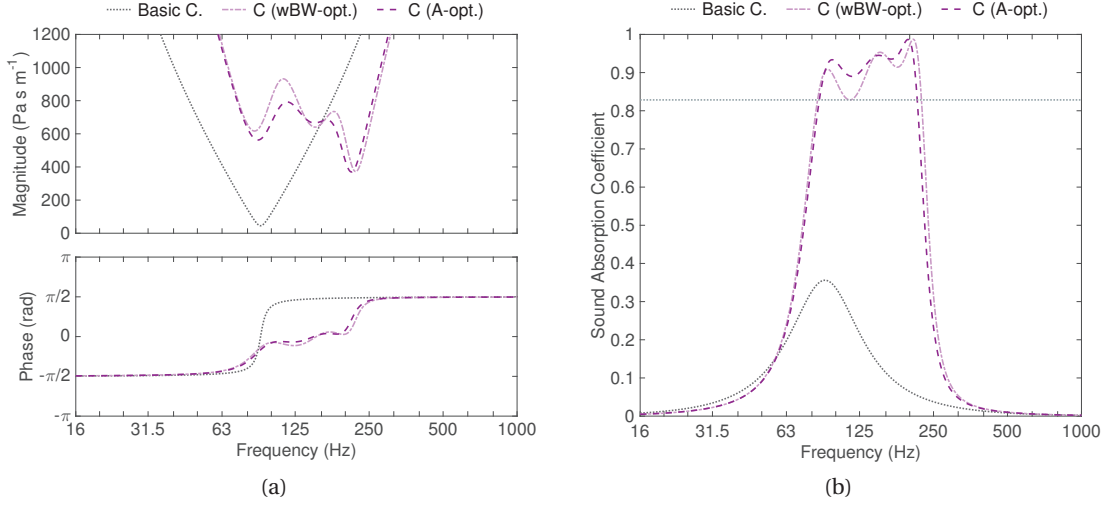
Figure 2.14 – (a) Bode plot of the specific acoustic impedance and (b) sound absorption coefficient of the system C depending on the objective function, relative to the basic configuration.
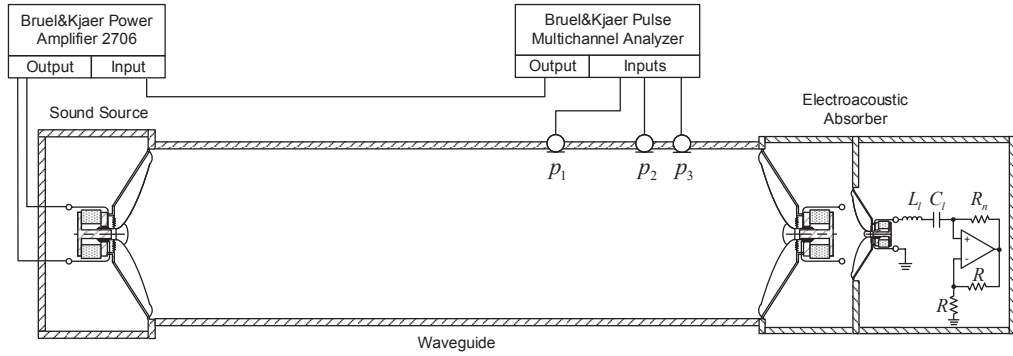
Figure 2.15 – Schematic of the experimental setup for the system C.

2.5 Performance evaluation

2.5.1 Experimental setup

To experimentally validate the results in Section 2.4, a waveguide was designed (length $L = 1.97$ m and internal diameter $\phi = 150$ mm) as depicted in Fig. 2.15. One termination was closed by the electroacoustic absorber and the other one was closed by a closed-box electrodynamic loudspeaker, delivering a band-limited pink noise of bandwidth [2 Hz - 2 kHz]. The specific acoustic impedance and corresponding sound absorption coefficient were evaluated according to ISO 10534-2 standard [197]. Three 1/4" 130D20 microphones were wall-mounted at positions $x_1 = 1.02$ m, $x_2 = 1.51$ m, and $x_3 = 1.62$ m from the sound source, measuring the sound pressures $p_1 = p(x_1, t)$, $p_2 = p(x_2, t)$, and $p_3 = p(x_3, t)$. The frequency response functions $H_{13} = p_3/p_1$ and $H_{23} = p_3/p_2$ were processed through a Brüel and Kjær Pulse multi-

Table 2.3 – Measured values of the additional resonators parameters and corresponding absorption performance indicators, from the optimisation results with the objective function $\mathcal{A}$

			Objective function $\mathcal{A}$		
			System A	System B	System C
Optimised Parameters	V_{b_1}	(L)	10.0	2.0	2.0
	R_{l_1}	(Ω)	-3.3	-	-
	L_{l_1}	(mH)	8.5	-	-
	C_{l_1}	(μF)	307.2	-	-
	V_{b_2}	(L)	-	8.0	8.0
	R_{l_2}	(Ω)	-	7.3	0.4
	L_{l_2}	(mH)	-	-	15.7
	C_{l_2}	(μF)	-	-	76.9
Perf. Indic.	f_0'	(Hz)	99.8	149.4	150.2
	BW	(Hz)	$[55.9\,;143.7]$	$[96.2\,;202.6]$	$[85.4\,;215.0]$
	wBW	(Hz)	84.24	100.40	118.26
	$\mathcal{A}$	(Hz)	11.50	12.27	10.93

channel analyser. This experimental setup has allowed the evaluation of the electroacoustic absorber performance with plane waves under normal incidence, over a frequency range between 44 Hz and 1340 Hz. The displayed frequency range was reduced to 1 kHz to focus the analysis on the bandwidth over which the absorption was supposed to be efficient.

For the purpose of the experimental evaluation, the experimental study was limited to the comparison of the three systems through the objective function $\mathcal{A}$. The three systems were made, according to the optimal parameters found from the objective function $\mathcal{A}$ given in Table 2.2, and measured. Since the target parameter values given in Table 2.2 were not exactly realised in practice, the measured values of the actual parameters of the experimental systems are given in Table 2.3.

Note that the volumes of the loudspeakers in the boxes were taken into account in the design of the prototype, to get equivalent volumes very close to the values reported in Table 2.2. For the series RLC networks, as the resistive parts of inductances and capacitances have non-zero values, a current inversion negative impedance converter, including two resistors R and a resistor R_n, was used to adjust the resistive value of the networks to the ones of the optimised resistances R_{l_1} and R_{l_2}. The equivalent resistance of the series RLC networks was then equal to $R_{l_i} = \text{Re}(j\omega L_{l_i} + 1/(j\omega C_{l_i})) - R_{n_i}$. Figure 2.16 illustrates the overview of the prototype, when the electroacoustic absorber is coupled to the mechanical resonator (the electrical shunt is not connected).

Figure 2.16 – Overviews of the prototype.

(a)

(b)
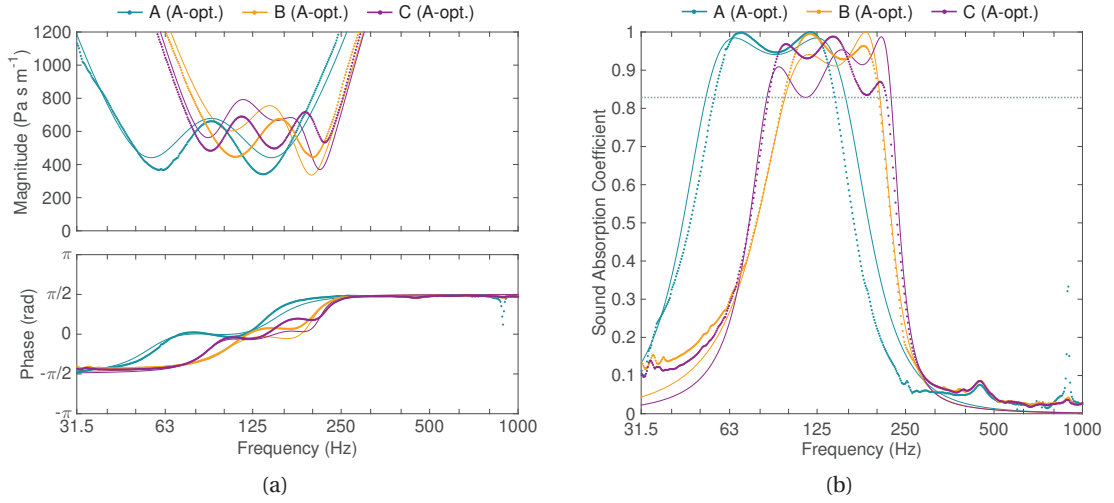
Figure 2.17 – (a) Bode plot of the measured specific acoustic impedance and (b) sound absorption coefficient for the experimental realisation of the systems A, B, and C, based on the optimisation results with the objective function $\mathcal{A}$.

2.5.2 Sound absorption measurements

Figure 2.17 illustrates the performance of the electroacoustic absorber in the three configurations in terms of measured specific acoustic impedance and sound absorption coefficient. Thanks to the coupling, both the acoustic resistance and reactance of the electroacoustic absorber are changed relative to the baseline configuration, to reach the desired effect according to the optimisation results. The dynamics of the closed box loudspeaker are noticeably modified, and two (respectively three) resonances are visible, when it is coupled to a single (respectively double) degree-of-freedom resonator. For the system A, the performance indicators are below the expectations. Note that the first mode of the enclosure causes the resonance at 894 Hz.

For the system B, the measured specific acoustic impedance is slightly different between

both resonances, which causes the asymmetry of the sound absorption coefficient. Although the value of the resistance R_{l_2} is slightly different from the one found in the simulation, the weighted bandwidth is exactly as expected and the area over threshold is even better than the optimisation results.

Finally, for the system C, the measured specific acoustic impedance and sound absorption coefficient are different from what was expected, and illustrated in Figs. 2.10a and 2.10b. The measured weighted bandwidth BW is similar to that obtained by simulation and given in Table 2.2, but the value of area over threshold $\mathcal{A}$ is below the expectation. Every configuration provides at least one octave in the bandwidth of efficient absorption in the low-frequency range.

2.5.3   Discussion

Slight differences are observed on the specific acoustic impedance and sound absorption coefficient for the three configurations. These differences can be attributed to imperfections in the model parameter of both loudspeakers and to the approximation of the equivalent closed boxes volumes. Nevertheless, the general trend is confirmed and these slight discrepancies do not contradict the results presented in this chapter.

When the closed box loudspeaker is coupled to the electrical resonator, the absorption performance is improved relative to the basic configuration. Since the measured values of the inductances and capacitances are different from the ones indicated by the manufacturers, it was difficult to get exactly the same values as those reported in Table 2.2. However, connecting either a series RLC network, a shunt resistor, or a negative impedance does not enable the specific acoustic resistance at the primary diaphragm to be reduced.

Because of the strong interaction effects of the parameters on the specific acoustic impedance of the systems B and C as seen in Eqs. (2.21,2.22) and (2.23,2.24) respectively, the mechanical and electromechanical resonators are more difficult to tune without an optimisation process. When one parameter value is modified, the absorption performance of the systems B and C is less predictable than for the system A where the loudspeaker is coupled with the electrical resonator. The coupling coefficient in Eq. (2.24), depending on both effective diaphragm areas and volume between the loudspeakers, plays a crucial part for the absorption capabilities. Note that even though the volumes V_{b_1} and V_{b_2} are not exactly equal to the ones found in the optimisation, the specific acoustic impedance $Z_{s_m}(\omega)$ can be tuned through the shunt resistance R_{l_2}, so as to maximise the absorption performance. Moreover, because the total volume is the same for the three systems, the frequency range of absorption is higher for the systems B and C relative to the system A. Although the system C exhibits three resonances on the sound absorption curve, the measurements show that it does not necessarily outperform the system B in terms of area over threshold $\mathcal{A}$.

In this study, commercial loudspeakers were chosen for the sake of simplicity. As their parame-

ters are limited by physical and technological constraints, and are initially designed for sound generation, the study was only focused on the optimisation of the volumes of enclosures and electrical shunt networks. As discussed in Section 2.4.1, a further stage of optimisation could consist in designing specific transducers adapted for sound absorption applications. Moreover, the main criterion of both objective functions was based on the threshold value of minimal efficient absorption, the ideal case being the matching of the specific acoustic resistance at the primary diaphragm with that of the air. If this target resistance is less than the characteristic impedance of the air as the case in rooms (see Chapter 5), the optimisation leads to a smaller bandwidth of efficient absorption. With this approach of multiple degree-of-freedom electroacoustic absorbers, the target resistance cannot be smaller than that of the loudspeaker in open circuit coupled to the acoustic domain.

The negative impedance converter was used to compensate the resistive part of inductances and capacitances. Because of the negative value of the resistance R_{l_1} in the experimental realisation of the system A, this type of electroacoustic absorber cannot be considered as purely passive, since external electrical power is required to operate.

2.6 Conclusion

In this chapter, the concept of electroacoustic absorber has been defined with some fundamental definitions to determine the acoustic properties of a given surface. A performance indicator on the bandwidth has also been defined to quantify the absorption capabilities of the system. The resonant behaviour of the closed box loudspeaker system enables a small amount of sound intensity of the incident wave to be dissipated through mechanical and electrical losses. To improve the absorption capabilities of the system, an appropriate electrical network can be connected to the loudspeaker terminals. The study has only focused on the loudspeaker coupled to series resistance - inductance - capacitance network, which becomes a two degree-of-freedom resonator. Mechanical resonators based on the arrangement of loudspeakers behind each other have pointed out that the order of the system increases in the same manner. From the previous systems, the main loudspeaker can eventually be coupled to a combination of two (or more) resonators resulting in a (at least) three degree-of-freedom resonator.

Parametric optimisations have been carried out through two objective functions: the one enabling the bandwidth of efficient absorption to be maximised, and the other enabling the absorption capabilities to be maximised, over a frequency range as large as possible. The three systems that were designed with conventional components were compared with each other depending on the strategy of optimisation. Lastly, an experimental evaluation of these systems from the optimisation results was carried out. Few differences were observed between the measurements and corresponding simulations.

An improvement in the performance of the electroacoustic absorber would be to add perforated panels or multi-layered elements, so as to absorb at mid and high frequencies as

well. Other coupled resonators could also be added to increase the absorption performance. In this case, given the difficulty of implementing several electrical or mechanical networks with physical components, an alternative would be the digital implementation of multiple degree-of-freedom resonators by synthesising a shunt electrical impedance/admittance as in [153, 198]. As this approach is limited by the bandwidth of efficient absorption in the case where the target specific acoustic resistance is low (see Chapter 5), the design of a self-sensing method with a dual coil electrodynamic loudspeaker will be investigated in Chapter 3.

3 Impedance control through sensorless velocity feedback

3.1 Introduction

Coupling an electroacoustic absorber with additional resonators is an interesting approach for a practical implementation, because it only involves conventional electrical and mechanical components. Nevertheless, even if it is quite easy to get two or three narrow peaks of absorption, it might be more difficult to properly tune the parameters of the resonators, so as to achieve a broadband bandwidth of absorption. Various control systems have been developed to modify the dynamics of transducers, including the self-sensing methods (see Section 1.3.3). Among the different approaches, a shunt impedance was synthesised to further extend the frequency bandwidth of absorption of the electroacoustic absorber, whereas achieving sound absorption in the low frequency range, thanks to a sensorless control loop [153]. The control required to neutralise the blocked electrical impedance of the voice coil for a significant sound absorption performance, as described in Section 1.3.3. Several improved models taking into account the semi-inductive behaviour were proposed, but cannot be perfectly represented by equivalent electrical circuits or digitally implemented [199–201]. Using a simplified model of the blocked electrical impedance of the voice coil in the synthesised impedance limited the sound absorption capabilities, especially above the loudspeaker resonance frequency.

Another approach is the use of a dual coil electrodynamic loudspeaker, which is a reversible transducer consisting of primary and secondary voice coils subjected to the same magnetic field. This configuration enables the diaphragm to reproduce an acoustic signal in response to an electrical signal connected to one or both electrical terminals. This type of loudspeaker offers a greater flexibility of connection of electrical inputs to the amplifier, thereby providing an increase of the transducer power or an improvement of the sound quality [202]. If an electrical current flows through the primary voice coil, it provides an electromagnetic force to the diaphragm by the reaction of the magnetic field induced by a permanent magnet of the current flowing through it. The voltage across the secondary voice coil is then induced by both the diaphragm velocity in the electromagnetic field (motional electromotive force) and mutual inductance between the primary and secondary windings. Feedback compensation

using a proportional controller was designed to minimise magnitude and phase variations of the loudspeaker response in [203]. The distortions may be reduced and the low frequency response of a dual coil loudspeaker may be extended as well [204]. The diaphragm velocity was derived from the induced voltage at the secondary coil after compensating the mutual inductance effect between both coils. In addition, an adaptive feedforward controller based on a modified, filtered-X, recursive-least-square algorithm with the use of a dual coil loudspeaker has been designed in [205]. A similar approach was proposed in [206] with a dual piezoelectric transducer to measure the electromechanical impedance from large-scale structures. This type of transducer could then be used to assign a desired specific acoustic impedance at the diaphragm from a velocity feedback control.

The goal of this chapter is to provide a solution for designing a sensorless electroacoustic absorber. First, the model of the dual coil electrodynamic loudspeaker in a closed box is introduced. The parameters of the model are identified before presenting the sensorless velocity feedback control. Then, a target specific acoustic impedance is defined for the control, and the absorption capabilities are analysed. Finally, the sensorless electroacoustic absorber is experimentally evaluated and general remarks regarding limitations of the control are discussed.

3.2   Design of the sensorless electroacoustic absorber

3.2.1   Dual coil electrodynamic loudspeaker model

The model of the dual coil electrodynamic loudspeaker, whose schematic is displayed in Fig. 3.1, is introduced. Because of the secondary coil, the electrical part is different from a usual loudspeaker as seen in Chapter 2. The governing equations of the electrical dynamics can be written as

$$U_1(\omega) = Z_{e1}(\omega) I_1(\omega) + Z_{ep}(\omega) I_2(\omega) - Bl_1 V(\omega) \tag{3.1}$$

$$U_2(\omega) = Z_{es}(\omega) I_1(\omega) + Z_{e2}(\omega) I_2(\omega) - Bl_2 V(\omega) \tag{3.2}$$

where $U_1(\omega)$ and $U_2(\omega)$ are the input voltages applied to the electrical terminals of the primary and secondary coils respectively, $I_1(\omega)$ and $I_2(\omega)$ are the electrical currents flowing through these coils, the force factors are denoted as Bl_1 and Bl_2 respectively, and $V(\omega)$ is the diaphragm velocity. The self inductances are expressed from the model described in [199, 207], and enhanced with a second RL-parallel stage. The blocked electrical impedances $Z_{ek}(\omega)$ represented by indices $k = [1, 2]$ are then written as

$$Z_{ek}(\omega) = R_{ek} + j\omega L_{ek} + \frac{j\omega L_{2k} R_{2k}}{R_{2k} + j\omega L_{2k}} + \frac{j\omega L_{2k+1} R_{2k+1}}{R_{2k+1} + j\omega L_{2k+1}} \tag{3.3}$$

where R_{e1} and L_{e1} are the DC resistance and the self inductance of the primary coil respectively, R_2 and R_3 are the resistances representing the eddy currents at mid and high frequencies
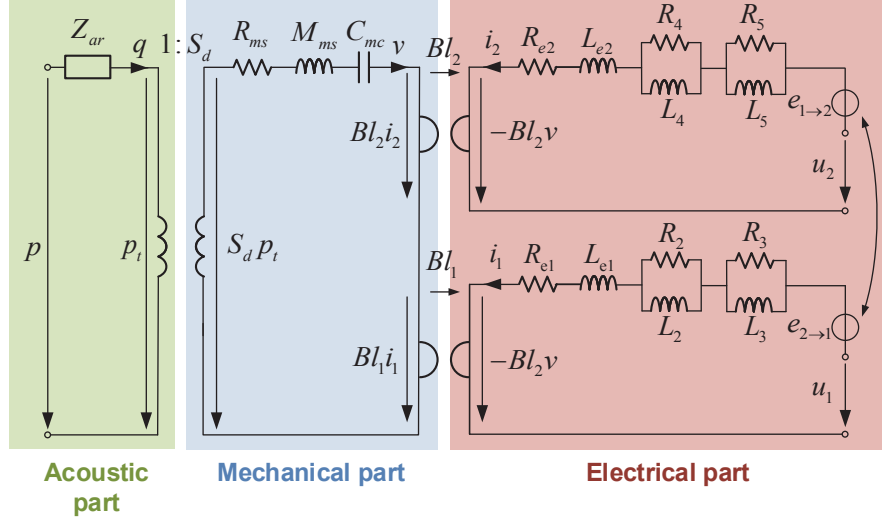
Figure 3.1 – Schematic of the dual coil electrodynamic loudspeaker.

respectively, and L_2 and L_3 are the para-inductances of the primary coil at at mid and high frequencies respectively. The secondary coil is modelled in the same way by the terms R_{e2}, L_{e2}, R_4, R_5, L_4 and L_5. The terms $e_{2\to1}(\omega) = Z_{ep}(\omega)\,I_2(\omega)$ and $e_{1\to2}(\omega) = Z_{es}(\omega)\,I_1(\omega)$ represent the mutual effects of the coils, whose mutual impedance is expressed with the same type of model as

$$Z_{ep}(\omega) = Z_{es}(\omega) = j\omega M + \frac{j\omega L_{m1} R_{m1}}{R_{m1} + j\omega L_{m1}} + \frac{j\omega L_{m2} R_{m2}}{R_{m2} + j\omega L_{m2}} \tag{3.4}$$

where M is the mutual inductance between the coils, R_{m1}, L_{m1}, R_{m2} and L_{m2} are the mutual terms of resistances and para-inductances defined by analogy with the model for the self inductances. If a high impedance device is used to measure the voltage $U_2(\omega)$ at the secondary coil terminals, the current $I_2(\omega)$ is null. In this special case, the Eqs. (3.1) and (3.2) become

$$U_1(\omega) = Z_{e1}(\omega)\,I_1(\omega) - Bl_1\,V(\omega) \tag{3.5}$$

$$U_2(\omega) = Z_{es}(\omega)\,I_1(\omega) - Bl_2\,V(\omega) \tag{3.6}$$

Denoting S_d as the effective piston area, M_{ms} and R_{ms} as the mass and mechanical resistance respectively, and C_{ms} as the mechanical compliance, as it is written in Section 2.2.1, for small displacements and below the first resonance frequency of the diaphragm, the equation of motion of the closed box loudspeaker diaphragm can be written as

$$S_d P_t(\omega) = \left(j\omega M_{ms} + R_{ms} + \frac{1}{j\omega C_{ms}} + \frac{\rho c^2 S_d^2}{j\omega V_b} \right) V(\omega) + Bl_1\,I_1(\omega) + Bl_2\,I_2(\omega) \tag{3.7}$$

where $P_t(\omega)$ is the total sound pressure at the front of the diaphragm. The last term of

the mechanical impedance $Z_m(\omega)$ in Eq. (3.7) can be represented by the total mechanical compliance $C_{mc} = (C_{ms}C_{mb})/(C_{ms} + C_{mb})$. In this configuration, the model of the dual coil loudspeaker finally comes down to the system of Eqs. (3.5), (3.6), and (3.7).

3.2.2 Identification of loudspeaker parameters

Before introducing the formulation of the control, the identification of parameters of the dual coil loudspeaker model is necessary. The parameters were identified by following the method proposed in [207] and adapted for the model expressed in Section 3.2.1. Considering a Monacor SPH-300TC dual coil electrodynamic loudspeaker loaded by an enclosure of volume $V_b = 23\,\text{dm}^3$, the resulting electroacoustic absorber, which was open circuit, was located in an anechoic room (free field condition) at 1 m of a broadband sound source. The diaphragm velocity $V(\omega)$ and total sound pressure $P_t(\omega)$ at the electroacoustic absorber diaphragm were measured at the center of the diaphragm with the help of a Polytec OFV-525 vibrometer sensor head and its OFV-5000 controller, a PCB 130D20 microphone, and a Brüel and Kjaer 3160 Pulse multichannel analyser. This way, the parameters of the mechanical impedance $Z_m(\omega)$, that is the mass M_{ms} and mechanical resistance R_{ms} including the radiation mass and resistance respectively, and mechanical compliance C_{mc}, were directly estimated from the measurement of the specific acoustic impedance $Z_s(\omega) = Z_m(\omega)/S_d$ in open circuit case and manufacturer's data for the effective piston area S_d. Then, after removing the sound source from the room, a broadband white noise of small magnitude was sent to the primary coil terminals through a Brüel and Kjær 2706 power amplifier. The primary coil current $I_1(\omega)$ and the voltages $U_1(\omega)$ and $U_2(\omega)$ at the terminals of the primary and secondary coils respectively were measured with current and voltage sensors. The parameters of the blocked electrical impedance $Z_{e1}(\omega)$, the mutual impedance $Z_{es}(\omega)$ of the secondary coil, and the force factors Bl_1 and Bl_2 were estimated by adjusting the measurements of three frequency response functions to a linear model of the transducer described in Section 3.2.1, through a method of least-squares:

- Figure 3.2a shows the estimated input impedance of the transducer at the primary coil terminals, which is expressed as

$$Z_{in1}(\omega) = \frac{U_1(\omega)}{I_1(\omega)} = Z_{e1}(\omega) + \frac{(Bl_1)^2}{Z_m(\omega)} \tag{3.8}$$

- Figure 3.2b shows the estimated frequency response function from primary coil current to the open circuit secondary coil voltage, which is expressed as

$$\frac{U_2(\omega)}{I_1(\omega)} = Z_{es}(\omega) + \frac{Bl_1 Bl_2}{Z_m(\omega)} \tag{3.9}$$

- Figure 3.2c shows the estimated frequency response function from the primary coil voltage to the open circuit secondary coil voltage primary coil voltage to the open circuit
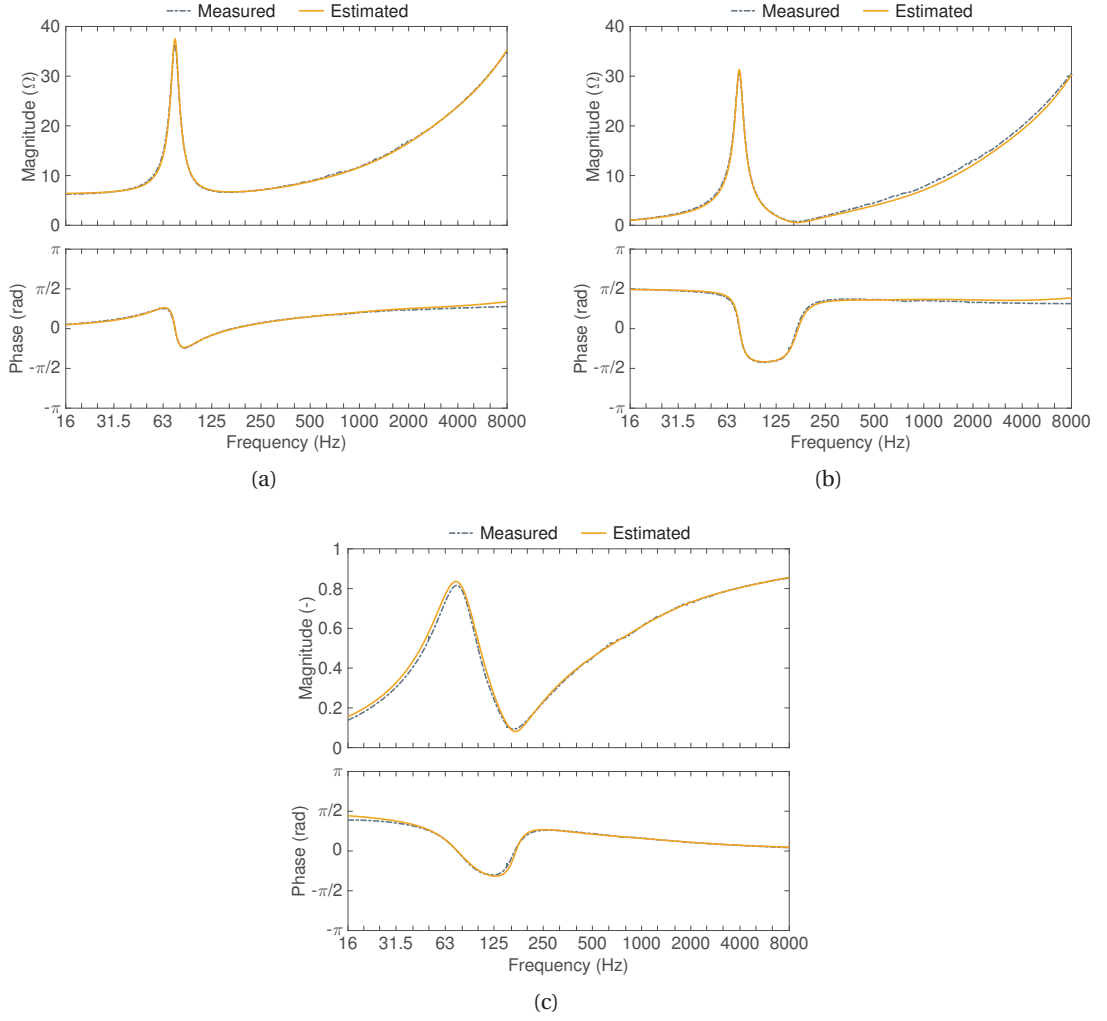
Figure 3.2 – Frequency responses computed (dash-dot line) and estimated (solid line) from (a) the primary coil current to the primary coil voltage, (b) the primary coil current to the open circuit secondary coil voltage, and (c) the primary coil voltage to the open circuit secondary coil voltage, when the loudspeaker is in free field.

secondary coil voltage, which is expressed as

$$\frac{U_2(\omega)}{U_1(\omega)} = \frac{Z_{es}(\omega)Z_m(\omega) + Bl_1 Bl_2}{Z_{e1}(\omega)Z_m(\omega) + (Bl_1)^2} \tag{3.10}$$

The estimated values of the linear model are summarised in Table 3.1. Note that the force factors Bl_1 and Bl_2 were quite equal, highlighting that both coils were of equal length. Moreover, the mutual inductance M was almost equal to the self inductance L_{e1}. Whereas the linear model assumes that all parameters are constant, the model for large signals may consider

Table 3.1 – Small signal parameters of the Monacor SPH-300TC dual coil loudspeaker in a closed box in a closed box of volume $V_b = 23\,\mathrm{dm}^3$.

Parameter	Notation	Value	Unit
DC resistance (coil #1)	R_{e1}	6.30	Ω
Self inductance (coil #1)	L_{e1}	0.55	mH
Resistance caused by eddy currents at mid f. (coil #1)	R_2	2.37	Ω
Para-inductance at mid f. (coil #1)	L_2	0.79	mH
Resistance caused by eddy currents at high f. (coil #1)	R_3	9.70	Ω
Para-inductance at high f. (coil #1)	L_3	0.53	mH
Mutual inductance	M	0.50	mH
Mutual resistance caused by eddy currents at mid f.	R_{m1}	2.13	Ω
Mutual para-inductance at mid f.	L_{m1}	0.94	mH
Mutual resistance caused by eddy currents at high f.	R_{m2}	9.67	Ω
Mutual para-inductance at high f.	L_{m2}	0.52	mH
Force factor (coil #1)	Bl_1	11.94	$\mathrm{N{\cdot}A}^{-1}$
Force factor (coil #2)	Bl_2	11.96	$\mathrm{N{\cdot}A}^{-1}$
Moving mass	M_{ms}	85.68	g
Mechanical resistance	R_{ms}	4.58	$\mathrm{N{\cdot}s{\cdot}m}^{-1}$
Mechanical compliance	C_{mc}	53.20	$\mathrm{\mu m{\cdot}N}^{-1}$
Effective piston area	S_d	495	cm^2
Resonance frequency	f_c	76	Hz

the dependence of other variables such as the temperature and displacement of the coils. Nevertheless, the impedance control is designed in such a way that the transducer behaviour remains linear. The parameters that are involved in the mechanical impedance $Z_m(\omega)$, the blocked electrical impedance $Z_{e1}(\omega)$ of the primary coil, and the mutual impedance $Z_{es}(\omega)$ of the secondary coil, are necessary for the design of the impedance control.

3.2.3 Sensorless velocity feedback control

After identifying the parameters of the model, it is shown how the dual coil loudspeaker can be used to derive the diaphragm velocity, while being able to interact with the sound field. From the linear model of the dual coil loudspeaker introduced in Section 3.2.1, the diaphragm velocity $V(\omega)$ can be expressed from the voltage $U_2(\omega)$ at the secondary coil terminals as

$$V(\omega) = -\frac{Bl_1}{Z_{es}(\omega)Z_m(\omega) + Bl_1 Bl_2} U_2(\omega) \tag{3.11}$$
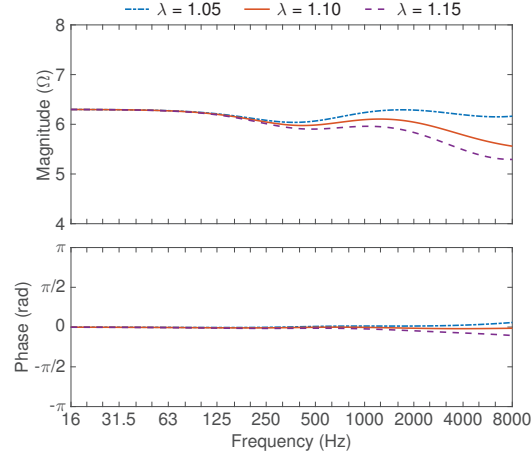
Figure 3.3 – Bode plot of the linear combination $Z_{e1}(\omega) - \lambda Z_{es}(\omega)$.

The implementation of the transfer function expressed in Eq. (3.11) was implemented in [203, 204] to extract the value of the diaphragm velocity from the motional electromotive force. This method required an accurate identification of the mutual impedance $Z_{es}(\omega)$, so as to design an efficient velocity feedback system. Alternatively, the diaphragm velocity may be derived from a linear combination of both coil voltages [208]. As both coils are immersed in the same magnetic field, the inventors have assumed that the mutual inductance and both self inductances were equal, as well as the force factors to $Bl = Bl_1 = Bl_2$. Adding a third inductance L in series with the primary coil and taking the difference of the two voltages, whose voltage $U_2(\omega)$ was multiplied by a given factor λ gives

$$U_1(\omega) - \lambda U_2(\omega) = R_{e1} I_1(\omega) + j\omega(L_{e1} + L - \lambda M) I_1(\omega) + (\lambda - 1) Bl V(\omega) \tag{3.12}$$

without considering the para-inductances. Choosing $\lambda = (L_{e1} + L)/M$, the inductances can balance in the circuit, while knowing the value of the diaphragm velocity $V(\omega)$. However, the para-inductances cannot necessarily be neglected; on the other hand, the values of the mutual inductance M and self inductance L_{e1} of the primary coil summarised in Table 3.1 are slightly different, at least for this model of transducer. As a result, adding a third inductance in series with that of the primary coil is not necessary. This way, the linear combination is written as

$$U_1(\omega) - \lambda U_2(\omega) = (Z_{e1}(\omega) - \alpha Z_{es}(\omega)) I_1(\omega) + (\lambda Bl_2 - Bl_1) V(\omega) \tag{3.13}$$

The parameter λ is then defined in such a way that $Z_{e1}(\omega) - \lambda Z_{es}(\omega)$ would be a real, and Eq. (3.13) becomes

$$U_1(\omega) - \lambda U_2(\omega) = K_e I_1(\omega) + (\lambda Bl_2 - Bl_1) V(\omega) \tag{3.14}$$

where $K_e \in \mathbb{R}$. Figure 3.3 shows the Bode plot of the linear combination $Z_{e1}(\omega) - \lambda Z_{es}(\omega)$, which takes into account the para-inductances, computed for three values of coefficient λ. Note that for $\alpha = L_{e1}/M = 1.10$, the self and mutual inductances cancel each other out and

Figure 3.4 – Block diagram of the dual coil electrodynamic loudspeaker system under control from the linear combination $Z_e(\omega) - \lambda\, Z_{es}(\omega)$.

the linear combination $Z_{e1}(\omega) - \lambda\, Z_{es}(\omega)$ is real over the whole frequency range of interest. Besides, $K_e \simeq R_{e1}$ at low frequencies; however it is not the case at higher frequencies as pointed out in Fig. 3.3.
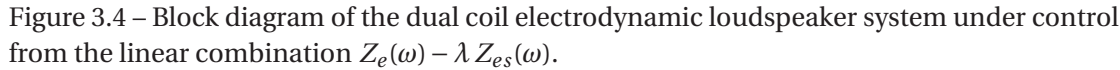
The control strategy intends to match the specific acoustic impedance of the diaphragm to a target specific acoustic impedance Z_{st}, expressed in Pa·s·m^{-1}, without using any external sensor. The idea is to take advantage of the transducer reciprocity thanks to a current driving method, which modifies the dynamics of the loudspeaker to get the desired impedance at the diaphragm. Assuming that the target specific acoustic impedance $Z_{st}(s)$ is realised at the diaphragm, the transfer function from the linear combination of both voltages $U_1(s) - \lambda\, U_2(s)$ to the electrical current $I_1(s)$ flowing through the primary coil, expressed in Ω^{-1}, can be derived from Eqs. (3.7) and (3.14) as

$$H(s) = \frac{I_1(s)}{U_1(s) - \lambda\, U_2(s)} = \frac{Z_m(s) - S_d\, Z_{st}(s)}{K_e\,(Z_m(s) - S_d\, Z_{st}(s)) + Bl_1\,(Bl_1 - \lambda Bl_2)} \tag{3.15}$$

which is equivalent to an electrical admittance. The expression of the specific acoustic impedance then becomes

$$Z_s(s) = \frac{Z_m(s)}{S_d} + \frac{Bl_1\,(Bl_1 - \lambda Bl_2)}{S_d\left(Z_{e1}(s) - \lambda Z_{es}(s) - \dfrac{1}{H(s)}\right)} \tag{3.16}$$

Equation (3.16) points out how the transfer function $H(s)$ can modify the specific acoustic impedance at the diaphragm. Figure 3.4 shows the block diagram of the dual coil electrodynamic loudspeaker with the sensorless control.

3.2.4 Target impedance for the diaphragm

To achieve maximal sound absorption under normal incidence, the specific acoustic impedance $Z_s(s)$ should be set to a target specific acoustic resistance R_{st} equal to the characteristic specific acoustic impedance of the medium $Z_c = \rho c$ (corresponding to the impedance matching case). This condition implies that the phase between the total sound pressure $P_t(s)$ at the diaphragm and diaphragm velocity $V(s)$ should be negligible over the whole frequency range. However, the specific acoustic impedance $Z_s(s)$ in Eq. (3.16) includes reactive terms caused by the compliance C_{mc} and mass M_{ms} of the diaphragm, which invariably induces a mismatch with the desired specific acoustic resistance R_{st} away from the resonance frequency. As neither the mass nor the compliance can be completely cancelled (or physically reduced to the zero value), a practical solution is to define a complex, frequency-dependent target specific acoustic impedance by the following parametric model:

$$Z_{st}(s) = s\frac{\mu M_{ms}}{S_d} + R_{st} + \frac{\mu}{sS_dC_{mc}} \tag{3.17}$$

where $0 < \mu < 1$ is a parameter that decreases simultaneously the effective mass and stiffness, in order to extend the bandwidth of maximal sound absorption. The corresponding resonance frequency is equal to

$$f_0{}' = \frac{1}{2\pi\sqrt{M_{ms}C_{mc}}} \tag{3.18}$$

In this configuration, the bandwidth of efficient sound absorption is found to be

$$BW = \frac{S_d}{2\pi\mu M_{ms}}\sqrt{\frac{(\sqrt{2}-1)^2(R_{st}+Z_c)^2 - (R_{st}-Z_c)^2}{\alpha_{th}}} \tag{3.19}$$

where $\alpha_{th} = 1 - (\sqrt{2}-1)^2$; it is only valid for $|R_{st} - \sqrt{2}Z_c| \leq Z_c$, that is $R_{st} \geq 171\,\text{Pa·s·m}^{-1}$ and $R_{st} \leq 997\,\text{Pa·s·m}^{-1}$. Note that the higher the term $S_d/(\mu M_{ms})$, the wider the bandwidth of efficient absorption BW. Moreover, the compliance C_{mc} is not involved in Eq. (3.19), but makes it possible to adjust passively the desired centre frequency $f_0{}'$ of the electroacoustic absorber, through the cabinet volume V_b as can be seen in Eq. (3.18). Thanks to the parameter μ, the bandwidth of efficient sound absorption can be extended around this centre frequency $f_0{}'$. It is also conceivable to apply two different parameters μ_M for the mass and μ_C for the stiffness in Eq. (3.17), to shift the centre frequency $f_0{}'$ without modifying the cabinet volume V_b.

3.2.5 Absorption capabilities

The performance of the electroacoustic absorber is first estimated by computing the equations presented in Section 3.2. Table 3.2 presents four simulation cases (labelled A–D) corresponding to four sets of values for the target specific acoustic impedance parameters (μ and R_{st}).

Table 3.2 – Settings and corresponding computed control results.

Case	Settings		Control results	
	Factor	Target resistance	Centre frequency	Bandwidth
	μ	R_{st} (Pa·s·m^{-1})	$f_0^{'}$ (Hz)	BW (Hz)
A	1	R_{ms}/S_d	74.5	-
B	1	200	74.5	15.4
C	1	300	74.5	28.4
D	1	ρc	74.5	34.6

The last two columns of Table 3.2 present the achieved control performance in terms of centre frequency $f_0^{'}$ and bandwidth of efficient absorption BW. The basic configuration A corresponds to the passive mechanical resonator situation, where the loudspeaker is in open circuit (no electrical current flowing through the voice coil). Configurations B, C, and D correspond to control settings assigning the target specific acoustic resistances to $\rho c/2$, $3\rho c/4$, and ρc (expressed in Pa·s·m^{-1}). For the configurations B, C, and D, the transfer function $H(s)$ in Eq. (3.15) is thus equivalent to a gain, which can be expressed as

$$ G = \frac{R_{ms} - S_d R_{st}}{K_e (R_{ms} - S_d R_{st}) + Bl_1 (Bl_1 - \lambda Bl_2)} \tag{3.20}$$

Although the proposed control strategy enables the imaginary part of the specific acoustic impedance $Z_s(\omega)$ to be modified, all simulated cases have the same imaginary part and centre frequency $f_0^{'}$ as the loudspeaker in open circuit (case A). It is first intended to prove the concept with simple cases. Note that the bandwidth of efficient absorption BW decreases with the specific acoustic resistance R_{st}. Figure 3.5a illustrates the Bode plot of the specific acoustic impedance computed from the control setting values listed in Table 3.2. The expected performance in terms of sound absorption coefficient is given in Fig. 3.5b. Because of the choice of the values for the target impedance parameters, the peak of absorption is narrow. Nevertheless, a specific acoustic resistance different from that of the closed-box loudspeaker system may be easily imposed at the diaphragm with the proposed method.

3.3 Performance evaluation

3.3.1 Experimental setup and control system implementation

To experimentally validate the results presented in Section 3.2.5, a waveguide was designed (length $L = 3.00$ m and internal diameter $\phi = 0.29$ m) as depicted in Fig. 3.6. A sound source at the left termination delivered a band-limited pink noise of bandwidth [20 Hz - 2 kHz]. The specific acoustic impedance and sound absorption coefficient were evaluated according to ISO 10534-2 standard [197]. Three 1/4" 130D20 ICP microphones were wall-mounted at positions

(a)   (b)
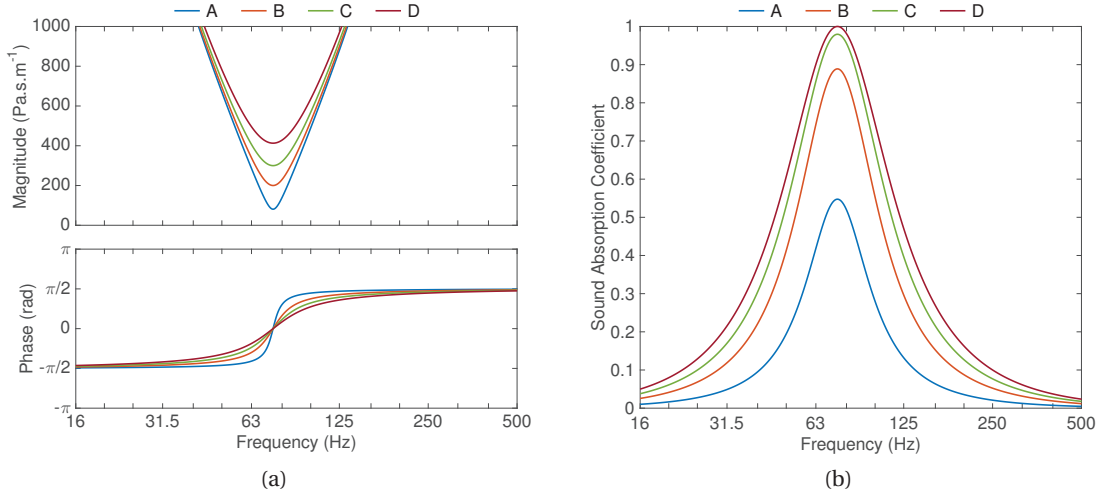
Figure 3.5 – (a) Bode plot of the specific acoustic impedance and (b) corresponding sound absorption coefficient of the electroacoustic absorber computed in open circuit (case A) and under control (cases B, C, and D).
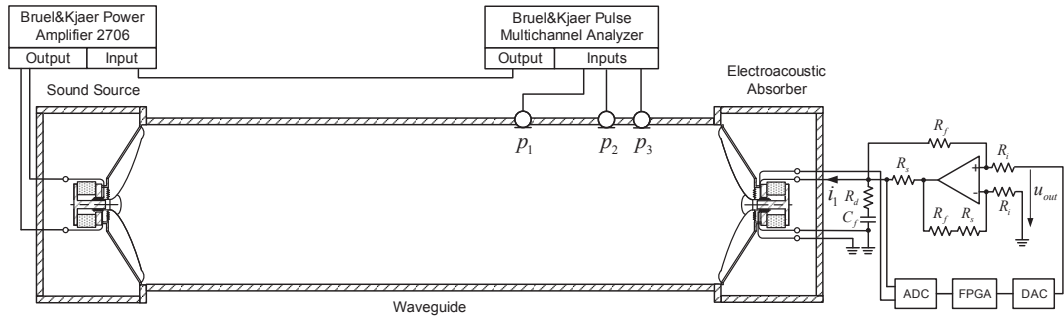
Figure 3.6 – Schematic of the experimental setup.

$x_1 = 0.7\,\mathrm{m}$, $x_2 = 0.9\,\mathrm{m}$, and $x_3 = 1.3\,\mathrm{m}$ from the sound source, measuring the sound pressures $p_1 = p(x_1, t)$, $p_2 = p(x_2, t)$, and $p_3 = p(x_3, t)$. The frequency response functions $H_{13} = p_3/p_1$ and $H_{23} = p_3/p_2$ were processed through a Brüel and Kjær Pulse multichannel analyser. This experimental setup enabled the electroacoustic absorber performance to be evaluated with plane waves under normal incidence for frequencies below 693 Hz. The displayed frequency range was reduced to 500 Hz to focus the analysis on the bandwidth over which the absorption was supposed to be efficient, according to Table 3.2.

The voltages of both coils were measured and digitally converted with a NI 9215 module (no anti-aliasing filter was used). The gain of the difference of both signals was adjusted via a real-time National Instruments CompactRIO platform supporting field-programmable gate array (FPGA) technology. The output signal u_{out} was delivered by a NI 9263 module to a voltage controlled current source that drove the voice coil loudspeaker. Note that this implementation
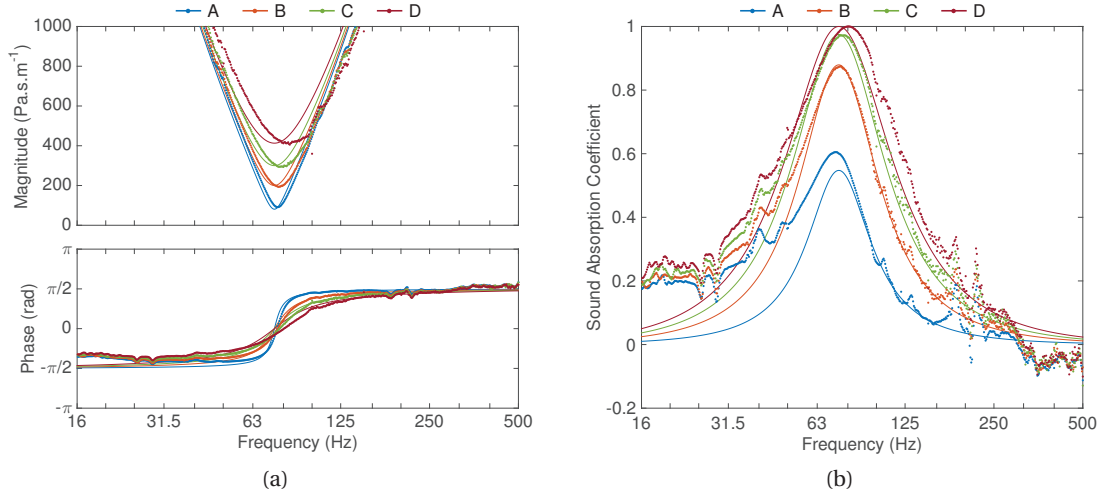
Figure 3.7 – (a) Bode plot of the specific acoustic impedance and (b) corresponding sound absorption coefficient of the electroacoustic absorber measured (dotted lines) and simulated (solid lines) in open circuit (case A) and under control (cases B and C).

could have been done with a purely analog circuit. As illustrated on the right-hand side in Fig. 4.24, the voltage controlled current source was an op-amp based "improved" Howland current pump circuit [209], including an operational amplifier, two input resistors R_i, two feedback resistors R_f, a current sense resistor R_s. As the load was reactive, a compensation circuit supplied by a resistance R_d and capacitance C_f was added to ensure stability with the grounded load [210].

3.3.2 Sound absorption measurements

The settings used for the measurements were the same as those used for the performance analysis in Section 3.2.5, and are summarised in Table 3.2. Figure 3.7 illustrates the performance of the electroacoustic absorber in terms of sound absorption, through the measured frequency response functions of the specific acoustic impedance and corresponding sound absorption coefficient. The results show the effectiveness of this technique to reach the desired specific acoustic resistance. Nevertheless, the measurements point out a slight variation of the centre frequency, which increases with the value of the target specific acoustic resistance R_{st}. The measured bandwidth BW of efficient absorption is equal to 14.0 Hz, 30.6 Hz, and 37.7 Hz for the cases B, C, and D respectively, which is slightly better than the expectations. Note that for every case, even when the loudspeaker is in open circuit (case A), the value of the sound absorption coefficient is slightly below zero above 300 Hz caused by mismatches in the model of the loudspeaker and not the control. In addition, the measured resonance frequency is slightly higher than that in the model, because the radiation impedance in the duct is different from the one in free field corresponding to the conditions for the identification of the loudspeaker parameters (see Section 3.2.2).

3.3.3 Discussion

The specific acoustic impedance at the diaphragm of a dual coil electroacoustic absorber can be modified by imposing an electrical current corresponding to the linear combination of the voltages across both coils amplified by a fixed real gain. This approach is similar to the one proposed in [153], where a synthetic electrical admittance connected to a single coil loudspeaker was designed from the transducer model, to realise the target specific acoustic impedance at the diaphragm. Its overall absorption performance was greater than what can be obtained with a simple shunt resistor. Nevertheless, the method was limited by the model uncertainties of the loudspeaker system and especially stability. One of the limiting factors to higher frequencies than the frequency range of absorption was the frequency dependent variations of some transducer parameters, which were not taken into account in the shunt admittance [211–213]. The stability was also highly sensitive to the discrepancies between the lumped parameter model and actual electrodynamic transducer, which have been described in [199, 214, 215]. The derivation of the synthetic electrical load means that the voice coil needed to be ideally offset, which is hardly achievable in practice [134, 216]. Note that eddy currents might modify the blocked electrical impedance. Even taking into account a lossy-inductance model, it was difficult to offset this impedance, thus limiting the performance of the control.

In the case of the sensorless velocity feedback control, the performance is also limited by uncertainties and stability as for the sensorless impedance control in [153]. The main limitation is caused by the voice coils as well. Although the blocked electrical impedances of the primary coil and mutual impedance are not modelled in the transfer function expressed in Eq. (3.15), the control requires to perfectly match the linear combination of both impedances by a constant value, so as to obtain the desired specific acoustic impedance at the diaphragm. Even if this value might be strictly real for a given value of the parameter λ, it is unlikely that this value will be constant over the whole frequency range. Even if the reactive part of the linear combination of both electrical impedances is small, this affects the specific acoustic impedance with a slight variation of the central frequency absorption relative to the simulation, increasing with the value of the target specific acoustic resistance. For a target specific acoustic impedance with a factor $\mu < 1$ relative to $\mu = 1$, the alterations on the specific acoustic impedance might be more important. On the other hand, the linear combination of both electrical impedances could be taken into account in the expression of the transfer function. In this case, it would be equivalent to the method of the sensorless impedance control proposed in [153]. The interest of the use of the dual coil loudspeaker is that, ideally, the inductances should cancel each other out with the control. In practice, it is not perfectly the case.

In addition, although a digital implementation presents more flexibility to make the system less sensitive to mismatches relative to analog circuits [134], it adds a latency in the control, which cannot be perfectly compensated. As a result, any modification on the controller to improve the stability inevitably alter the absorption capabilities. Limitations, uncertainties and stability of control systems will be studied in details in Chapter 4. Moreover, as the dual coil

loudspeaker is heavier than a single coil loudspeaker, the bandwidth of efficient absorption, which is proportional to the ratio S_d/M_{ms}, is lower for a same effective area. Experimental results have shown the ease and accuracy of this technique to impose a desired specific acoustic resistance, because it is not necessary to know the values of the model parameters. Nevertheless, modifying only the acoustic resistance through the sensorless velocity feedback control is equivalent to connecting a shunt resistance to the loudspeaker terminals. As a result, although the proposed method is original, its advantages and limitations are similar to the sensorless impedance control with a conventional single coil loudspeaker, when it comes to enlarge the bandwidth of efficient absorption.

3.4 Conclusion

In this chapter, the use of a dual coil electrodynamic loudspeaker to assign a desired specific acoustic impedance at its diaphragm from a sensorless control has been presented. The model of this type of transducer was firstly introduced before presenting the identification method of the lumped element parameters. The diaphragm velocity can be derived using a linear combination of the voltages at the primary and secondary coils. A synthetic electrical admittance can be designed from the linear combination of both voltages to the electrical current, so as to correctly assign a target specific acoustic impedance at the diaphragm. This control strategy is possible thanks to the transducer reciprocity on the one hand, and to the use of the dual coil on the other hand, although it has not been designed for this purpose.

For a proof of concept, only the specific acoustic resistance at the diaphragm has been modified by imposing an electrical current corresponding to the linear combination of the voltages across both coils amplified by a fixed real gain. The absorption capabilities of the loudspeaker were enhanced with the ability to achieve a desired acoustic resistance without the use of any external sensor. Although this technique is easy to implement in this simple case, the performance is equivalent to a shunt resistance. The absorption capabilities may be improved by reducing the mass and stiffness of the transducer thanks to the control. Similar methods previously pointed out that this type of sensorless impedance control can reach one octave of bandwidth of efficient absorption. However, the absorption capabilities are still limited because of the use of the "internal" sensor of the transducer. In Chapter 4, an impedance control strategy with the use of an external sensor will be presented.

4 Hybrid sensor-/shunt-based impedance control

4.1 Introduction

To impose a desired specific acoustic impedance at the electroacoustic absorber diaphragm, the sensorless methods are appropriate solutions. Nevertheless, the parameters of additional electrical/mechanical resonators that have been developed in Chapter 2 might be difficult to tune, so as to achieve a broadband bandwidth of absorption. On the other hand, the performance of self-sensing techniques, such as the approach presented in Chapter 3 with the use of a dual coil electrodynamic loudspeaker, is limited by transducer model uncertainties and stability. Alternatively, the direct impedance control techniques present absorption capabilities over a broader bandwidth. As described in Section 1.3.3, these techniques either require two external sensors, but are difficult to use for room applications, or one sensor but requires the design of a constant velocity sound source or the use of a velocity estimator. In addition, these techniques are usually based on the voltage driving method, involving the voice-coil inductance in the control, which as a consequence limits the sound absorption performance at higher frequencies. On the contrary, the current driving method enables the effect of the voice coil to be minimised. Instead of measuring the voltage(s) at the single coil or dual coil loudspeaker terminals, an external sensor, measuring the sound pressure or diaphragm velocity, appears to be an interesting direction to improve the control stability.

The motivation of this chapter is the development of a hybrid control concept that merges sensor- and shunt-based impedance control, leading to broadband low-frequency electroacoustic absorbers. The first part presents the control design by using only one sensor and taking into account the loudspeaker model, so as to impose a desired specific acoustic impedance at the diaphragm of the current-driven loudspeaker. The performance of the electroacoustic absorber is studied in 1D cases according to when the sound source is either at the end or along the wall of the duct. Then, the stability and absorption performance are investigated in the presence of model uncertainties and possible control limitations, before studying the power balance and power efficiency of the electroacoustic absorber. Finally, an experimental validation of the concept in a waveguide is provided.

4.2 Control design

Assuming that a target specific acoustic impedance $Z_{st}(s)$ is realised at the diaphragm, two approaches are presented in the following, depending on whether a sound pressure or diaphragm velocity sensor is used.

Sound pressure sensor

The transfer function $\Theta(s)$ from the total sound pressure $P_t(s)$ at the diaphragm to the electrical current $I(s)$ can be derived from Eq. (2.4) as

$$\Theta(s) = \frac{I(s)}{P_t(s)} = \frac{S_d Z_{st}(s) - Z_m(s)}{Bl\, Z_{st}(s)} \tag{4.1}$$

The expression of the specific acoustic impedance then becomes

$$Z_s(s) = \frac{Z_m(s)}{S_d - Bl\,\Theta(s)} \tag{4.2}$$

Figure 4.1 shows the block diagram of the controlled loudspeaker by measuring the total sound pressure at the diaphragm. Note that the blocked electrical impedance Z_e of the loudspeaker is absent from the control. Nevertheless, this strategy still requires an accurate evaluation of the loudspeaker mechanical parameters, such as the effective piston area S_d, the force factor Bl, and the mechanical impedance (that is the mass M_{ms}, resistance R_{ms}, and compliance C_{mc}).

Diaphragm velocity sensor

A similar approach can be followed by measuring the diaphragm velocity instead of the total sound pressure. The transfer function $\Gamma(s)$ from the diaphragm velocity $V(s)$ to the electrical current $I(s)$ can be derived from Eq. (2.4) as

$$\Gamma(s) = \frac{I(s)}{V(s)} = \frac{S_d Z_{st}(s) - Z_m(s)}{Bl} \tag{4.3}$$

The expression of the specific acoustic impedance then becomes

$$Z_s(s) = \frac{Z_m(s) + Bl\,\Gamma(s)}{S_d} \tag{4.4}$$

Figure 4.2 shows the block diagram of the controlled loudspeaker by measuring the diaphragm velocity, thus taking the form of a feedback control architecture.
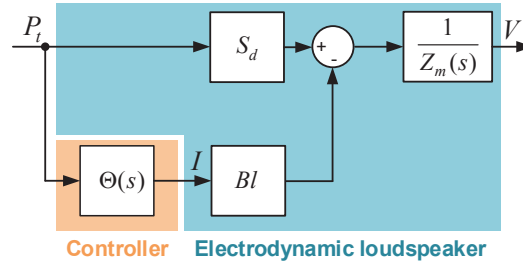
Figure 4.1 – Block diagram of the electrodynamic loudspeaker system under control by measuring the total sound pressure at the diaphragm.
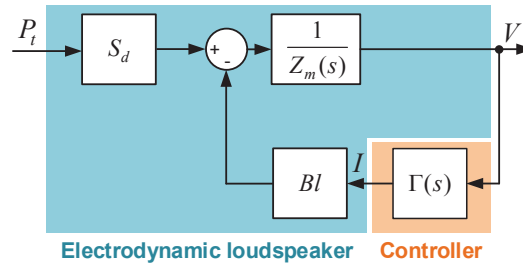
Figure 4.2 – Block diagram of the electrodynamic loudspeaker system under control by measuring the diaphragm velocity.

Strategy

Even if both the transfer functions $\Theta(s)$ and $\Gamma(s)$ in Eqs. 4.2 and 4.4 are similar, one approach can be more appropriate than the other. In the case of a digital implementation of the proposed control, if the target impedance $Z_{st}(s)$ is expressed as in Eq. (3.17) [1], only the transfer function $\Theta(s)$ is causal. In addition, as the use of a sound pressure sensor is less expensive and easier to implement than a velocity sensor, the implementation of the transfer function $\Theta(s)$ is preferred to that of $\Gamma(s)$ in the following.

Discarding the electrical part of the loudspeaker and using the signal received from a sensor thus allows for a simple way to assign a desired impedance at the electroacoustic absorber diaphragm.

---

[1] $Z_{st}(s) = s\mu M_{ms}/S_d + R_{st} + \mu/(sS_d C_{mc})$

4.3 Performance analysis

4.3.1 Absorption capabilities

The performance of the electroacoustic absorber is first estimated by computing the equations presented in Section 4.2, considering a Peerless SDS-P830657 loudspeaker mounted in a closed-box of volume $V_b = 10\,\text{dm}^3$. When it comes to a practical implementation of the control, the acoustic coupling between the sensor and loudspeaker should be taken into account in the control [125]. Actually, in the case of the impedance control from the sound pressure, the microphone measures the total sound pressure of the acoustic field in the vicinity of the transducer diaphragm including its acoustic radiation impedance Z_{ar}, as illustrated in Fig. 2.2.

The mechanical parameters of the loudspeaker were estimated from the measurement of the specific acoustic impedance at the diaphragm, when the open circuit loudspeaker, mounted at the termination of a standing-wave duct, was excited by an external sound source with broadband noise. The experimental setup is further detailed in Section 4.6. The frequency response from the diaphragm velocity of the sound source to the sound pressure was measured with a Polytec OFV-525 vibrometer sensor head and its OFV-5000 controller, and with a PCB 130D20 microphone located at a distance $d = 1\,\text{cm}$ from the diaphragm. This way, the acoustic radiation impedance, which depends on the environment in which the loudspeaker is located and on the sensor position, was already taken into account in the mechanical impedance $Z_m(\omega)$ through the expression

$$Z_s(\omega) = \cos(kd)\frac{Z_m(\omega)}{S_d} + j\,\rho c \sin(kd) \tag{4.5}$$

where k is the wavenumber. Note that the longer the distance d, the more important the effect of the acoustic radiation impedance on the impedance control. To avoid numerous annotations, the estimated mechanical impedance components (M_{ms}, R_{ms}, and C_{mc}) account for the measured impedance $\cos(kd)\,Z_m(\omega) + j\,S_d\rho c \sin(kd)$ in the following. The measured values of the model parameters are reported in Table 4.1.

Table 4.2 presents three simulation cases (labelled A–C) corresponding to three sets of values of the parameters μ and R_{st} for the target specific acoustic impedance $Z_{st}(s)$, which was defined in Section 3.2.4. Although the proposed control enables the centre frequency of the electroacoustic absorber to be changed, all simulated cases are set so as to preserve the same centre frequency $f_0{'}$ (equal to the resonance frequency of the closed-box loudspeaker system). The last two columns of Table 4.2 present the achieved control performance in terms of desired centre frequency $f_0{'}$ and bandwidth of efficient absorption BW [2]. The baseline case A corresponds to the passive mechanical resonator situation, where the loudspeaker is in open circuit (that is no electrical current flowing through the voice coil). Cases B and

---

[2] $f_0{'} = 1/(2\pi\sqrt{M_{ms}C_{mc}})$ and $BW = [S_d/(2\pi\mu M_{ms})]\sqrt{[(1-\alpha_{th})(R_{st}+Z_c)^2-(R_{st}-Z_c)^2]/\alpha_{th}}$

Table 4.1 – Small signal parameters of the Peerless SDS-P830657 loudspeaker in a closed box of volume $V_b = 10\,\mathrm{dm}^3$.

Parameter	Notation	Value	Unit
Effective piston area	S_d	151	cm^2
Moving mass	M_{ms}	14.67	g
Mechanical resistance	R_{ms}	1.31	N·s·m^{-1}
Mechanical compliance	C_{mc}	242.35	μm·N^{-1}
Force factor	Bl	5.98	N·A^{-1}
Density of the air at 294 K	ρ	1.2	kg·m^{-3}
Sound speed in the air at 294 K	c	343.86	m·s^{-1}

Table 4.2 – Settings and corresponding computed control results.

Case	Settings		Control results	
	Factor	Target resistance	Centre frequency	Bandwidth
	μ	R_{st} (Pa·s·m^{-1})	f_0' (Hz)	BW (Hz)
A	1	R_{ms}/S_d	84.4	-
B	0.15	$\rho c/8$	84.4	-
C	0.15	ρc	84.4	410.6

C correspond to control settings achieving the same diminution of 85 % of the loudspeaker effective mass and stiffness, and assigning the target specific acoustic resistance R_{st} to $\rho c/8$ and ρc respectively.

Figure 4.3a illustrates the Bode plot of the specific acoustic impedance computed from the control setting values listed in Table 4.2. The expected performance in terms of sound absorption coefficient is given in Fig. 4.3b. Case C in Fig. 4.3a shows that the specific acoustic impedance of the diaphragm can be matched to the characteristic impedance of the medium ρc over a large frequency range, whereas the mass and stiffness decrease by 85 % relative to those presented by the passive loudspeaker diaphragm, thus extending the control bandwidth. In case B, the target acoustic resistance value is chosen so as to be smaller than the one obtained with the passive loudspeaker diaphragm, to illustrate the possibility to assign small values of acoustic resistance with this control strategy. As shown in Fig. 4.4, the transfer function $\Theta(s)$ computed for cases B and C have different quality factors, according to the desired specific acoustic resistance R_{st}. The phase of the transfer function also changes around the centre frequency depending on the sign of $S_d R_{st} - R_{ms}$.
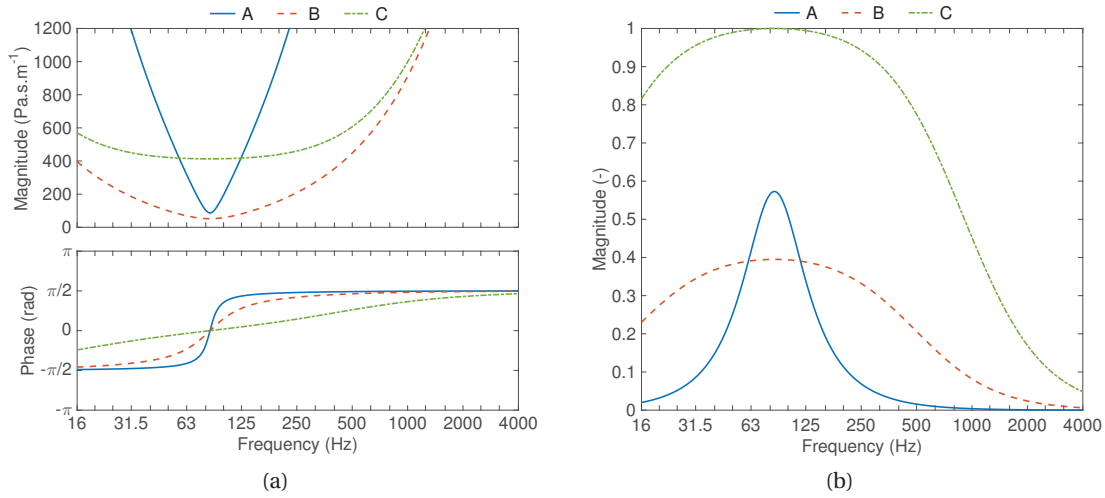
Figure 4.3 – (a) Bode plot of the specific acoustic impedance and (b) corresponding sound absorption coefficient of the electroacoustic absorber computed in open circuit (case A) and under control (cases B and C).
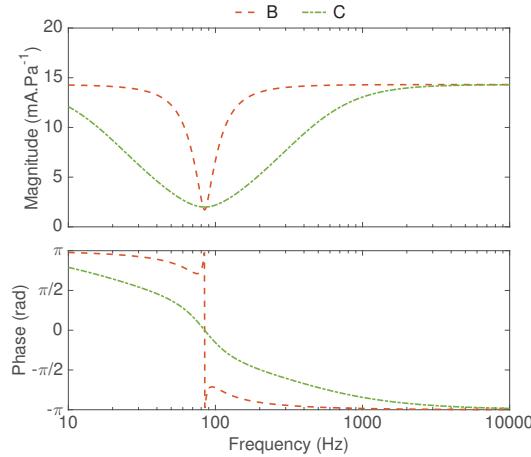
Figure 4.4 – Bode plot of the transfer function from the total sound pressure at the diaphragm to the current flowing through the voice coil computed for the cases B and C.

4.3.2 Modal equalisation in 1D application

To illustrate the capability of the broadband electroacoustic absorber to damp low-frequency resonances in a waveguide, frequency responses from the driving voltage of the sound source to the sound pressure level are processed along the duct, for different absorbing conditions at the termination of the duct. The sound pressure levels with the hard-wall condition are compared to the cases where an electroacoustic absorber terminates the duct, either in open-circuit (case A) or controlled (case C). Through the simulation, it is intended to show the effect of the active impedance control, both in terms of sound absorption performance and attenuation of duct modes. The length of the duct is $L = 1.97$ m (the parameter was adjusted

Table 4.3 – Small signal parameters of the Peerless SDS-P830657 loudspeaker of the sound source in a closed box of volume $V_b = 10\,\text{dm}^3$.

Parameter	Notation	Value	Unit
Effective piston area	S_{d_s}	151	cm^2
Moving mass	M_{ms_s}	12.90	g
Mechanical resistance	R_{ms_s}	1.23	N·s·m^{-1}
Mechanical compliance	C_{mc_s}	260.79	$\mu\text{m·N}^{-1}$
Force factor	Bl_s	5.98	N·A^{-1}
Voice coil inductance	L_{e_s}	0.38	mH
DC resistance	R_{e_s}	6	Ω

to be in agreement with the experimental setup presented in Section 4.6). The sound source consists of a voltage-driven loudspeaker in a closed-box of volume $V_b = 10\,\text{dm}^3$ with physical parameters summarised in Table 4.3. The mechanical parameters of the loudspeaker were estimated from the measurement of the mechanical impedance, as explained in Section 4.3.1, and its electrical parameters were simply retrieved from the manufacturer's data. The blocked electrical impedance and mechanical impedance of the sound source are denoted by $Z_{e_s}(\omega)$ and $Z_{m_s}(\omega)$ respectively.

The assumptions are: (i) plane wave field is considered (where the frequency range is dependent on the dimensions of the waveguide); (ii) both the sound source and electroacoustic absorber diaphragms behave as rigid pistons; (iii) only viscothermal losses are considered in the waveguide (rigid walls); (iv) other electroacoustic components (such as the sensor or current amplifier) are not taken into account. The duct section S is chosen equal to the effective piston area S_d of the electroacoustic absorber and to that of the sound source loudspeaker, to simplify the analytical study. If the absorber area is substantially smaller than the cross-section of the waveguide, the assumption of a uniform pressure at the boundary would not be valid any more. The analytical approach would require the total decomposed field on transverse modes [217], whereas a practical approach could be done with the help of a Finite Element Method software as shown in Section 4.4.2. A surface impedance condition is imposed at the right end of the waveguide. In one configuration, to simulate the rigid termination, the impedance is only resistive on the whole frequency range and is equal to $16\,\text{kPa·s·m}^{-1}$, which amounts to a sound absorption coefficient $\alpha \simeq 0.1$. In the two other configurations, the specific acoustic impedance corresponds to Eq. (3.17) with settings of cases A (open circuit) and C (with control) listed in Table 4.2.

Sound source at one end of the duct

The sound source is located at the left end of the duct (location $x = 0$). Given a surface impedance $Z_{s_L}(\omega)$ at location $x = L$, the sound pressure, satisfying the Helmholtz equation in

the frequency domain, can be expressed as

$$P_{t_x}(\omega) = A(\omega)\left(e^{-jkx} + R_L(\omega)e^{jk(x-2L)}\right) \tag{4.6}$$

where $k = 2\pi f/c + [(1+j)/j]\,3e^{-5}\sqrt{\pi f/S}$ is the wavenumber with the modelling of the viscothermal losses in a cylindrical duct [218], and $R_L(\omega) = \left(Z_{s_L}(\omega) - \rho c\right)/\left(Z_{s_L}(\omega) + \rho c\right)$ is the reflection coefficient at location $x = L$. The convention is chosen in such a way that the incident sound pressure $P_{i_L}(\omega)$ at $x = L$ and reflected sound pressure $P_{R_0}(\omega)$ at $x = 0$ are in the same direction; the reflected sound pressure P_{R_L} and incident sound pressure P_{i_0} are in the same other direction. The incident and reflected sound pressures at both terminations of the waveguide are related by the scattering matrix through the expression

$$\begin{pmatrix} P_{R_0}(\omega) \\ P_{R_L}(\omega) \end{pmatrix} = \begin{pmatrix} 0 & e^{jkL} \\ e^{jkL} & 0 \end{pmatrix} \begin{pmatrix} P_{i_0}(\omega) \\ P_{i_L}(\omega) \end{pmatrix} \tag{4.7}$$

The total sound pressure $P_t(\omega)$ and normal acoustic velocity $V(\omega)$ at both terminations of the waveguide are related through the transfer matrix through the expression

$$\begin{pmatrix} P_{t_L}(\omega) \\ V_L(\omega) \end{pmatrix} = \begin{pmatrix} \cos(kL) & -j\rho c\,\sin(kL) \\ -j\dfrac{\sin(kL)}{\rho c} & \cos(kL) \end{pmatrix} \begin{pmatrix} P_{t_0}(\omega) \\ V_0(\omega) \end{pmatrix} \tag{4.8}$$

The equations of the sound source at the left end of the duct are

$$S_{d_s}P_{t_0}(\omega) = Z_{m_s}(\omega)\,V_0(\omega) + Bl_s\,I_s(\omega) \tag{4.9}$$

$$U_s(\omega) = Z_{e_s}(\omega)\,I_s(\omega) - Bl_s\,V_0(\omega) \tag{4.10}$$

The coefficient $A(\omega)$ can then be derived as

$$A(\omega) = \frac{\rho c}{S_{d_s}\rho c\left(1 + R_L(\omega)e^{-2jkL}\right) + Z_{m_{eq}}(\omega)\left(1 - R_L(\omega)e^{-2jkL}\right)}\frac{(Bl_s)^2}{Z_{e_s}(\omega)}U_s(\omega) \tag{4.11}$$

where $Z_{m_{eq}}(\omega) = Z_{m_s}(\omega) + (Bl_s)^2/Z_{e_s}(\omega)$ is the equivalent mechanical impedance of the sound source. Figure 4.5 illustrates the electrodynamic loudspeaker system under control coupled to the waveguide and sound source.

In the case of a hard-wall termination, the resonance frequencies are

$$f_{r_n} = n\frac{c}{2L} \tag{4.12}$$

where $n \in \mathbb{N}^*$ (see Section 5.2.1). The anti-resonance frequencies f_{ar_n} can be computed from Eq. (4.6) when $P_{t_0}(\omega) = 0$. Simplifying $(Z_{s_L}(\omega) - \rho c)/(Z_{s_L}(\omega) + \rho c) = 1$ at any frequency, nulls of sound pressure occur at locations

$$x_{ar_n}(f) = L - (2n-1)\frac{c}{4f} \tag{4.13}$$
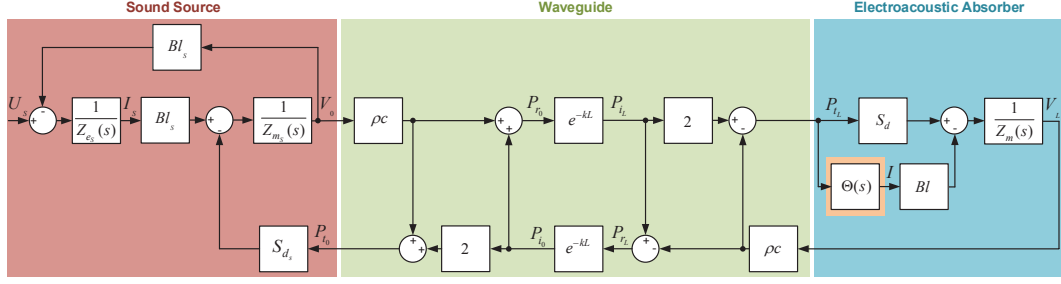
Figure 4.5 – Block diagram of the electrodynamic loudspeaker system under control coupled to the waveguide. At the other end is located the sound source.

Anti-resonance frequencies are thus found inverting Eq. (4.13) for $x_{ar_n} = 0$

$$f_{ar_n} = (2n-1)\frac{c}{4L} \tag{4.14}$$

Figures 4.6a, 4.6c, and 4.6e illustrate the frequency responses from the driving voltage of the sound source to the sound pressure level (expressed in dB re. $20\,\mu\text{Pa·V}^{-1}$) in a space–frequency representation, when the right end is closed either by a hard-wall or an electroacoustic absorber (case C). Figures 4.6b, 4.6d, and 4.6f show the projection of these frequency responses on the frequency axis. As can be seen in these figures, the sound field is characterised by an uneven distribution of the sound field at low frequencies, when the waveguide is closed by a hard wall surface. The strong resonances (in yellow) appear at fixed frequencies whatever the location in the waveguide, whereas the nulls (in blue) are shifted as the observation position moves away from the sound source as indicated in Eq. (4.13). The sound pressure globally decreases when the frequency increases, because of the mechanical impedance of the source loudspeaker as indicated in Eq. (4.11). When the electroacoustic absorber in open circuit (case A) substitutes for the hard wall surface in Figs. 4.6c and 4.6d, both peaks (resonances) and dips (nulls) are attenuated around the resonance frequency of the electroacoustic absorber. However, the dynamics of sound pressure levels in the waveguide is worse than in the rigid case outside this frequency band, because of the cumulative effect of the mechanical impedances of both loudspeakers. Finally, when the electroacoustic absorber is controlled (case C) in Figs. 4.6e and 4.6f, both peaks and dips in frequency spectra are significantly attenuated at low frequencies, which is characterised by a thinner area filled by the whole frequency responses.

Sound source along the duct wall

The sound source is now wall-mounted at the location $x = X_s$ from the left end of the duct. In this case, the solution of the Helmholtz equation is written as

$$\Delta P_{t_x}(\omega) + k^2 P_{t_x}(\omega) = -jk\rho c \frac{S_{d_s} V_{X_s}(\omega)}{S}\delta(x - X_s) \tag{4.15}$$
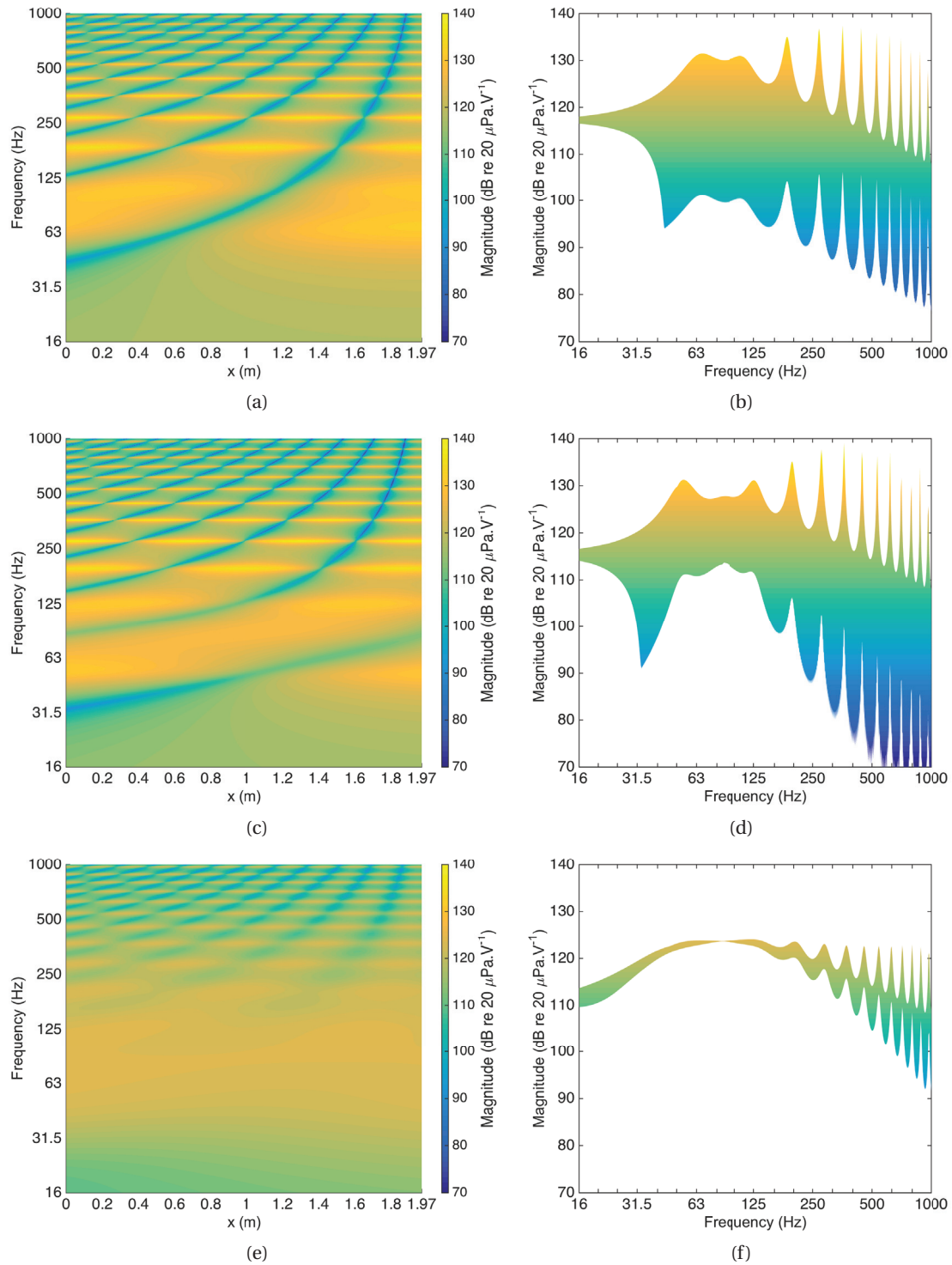
Figure 4.6 – (left column) Space – frequency maps of frequency responses and (right column) dynamic range of all the frequency responses from the driving voltage of the sound source located at the left end of the waveguide to the sound pressure level. At the right end, (a & b) a hard wall surface, or (c & d) and (e & f) an electroacoustic absorber with the control settings of cases A and C is imposed.

where V_{X_s} is the acoustic velocity at location $x = X_S$. Given surface impedances $Z_{S_0}(\omega)$ and $Z_{S_L}(\omega)$ at locations $x = 0$ and $x = L$ respectively, the sound pressures at the left and right of the sound source denoted $P_{l_x}(\omega)$ and $P_{r_x}(\omega)$ respectively and satisfying the Eq. 4.15, are expressed as

$$P_{l_x}(\omega) = B(\omega)\left(R_0(\omega)e^{-jk(x+X_s)} + e^{jk(x-X_s)}\right) \qquad \text{for } x \le X_s \qquad (4.16)$$

$$P_{r_x}(\omega) = C(\omega)\left(e^{-jk(x-X_s)} + R_L(\omega)e^{jk(x+X_s-2L)}\right) \qquad \text{for } x \ge X_s \qquad (4.17)$$

where $R_0(\omega) = \left(Z_{S_0}(\omega) - \rho c\right)/\left(Z_{S_0}(\omega) + \rho c\right)$ is the reflection coefficient at location $x = 0$. The total sound pressure is continuous at the location of the sound source: $P_{l_{X_s}}(\omega) = P_{r_{X_s}}(\omega)$. Then, the jump of the derivative of the sound pressure at location $x = X_S$ is written as

$$\frac{\mathrm{d}}{\mathrm{d}x}\left(P_{l_{X_s}}(\omega) - P_{r_{X_s}}(\omega)\right) = -jk\rho c\frac{S_{d_s}V_{X_s}(\omega)}{S} \qquad (4.18)$$

Lastly, in addition to the relation $Z_{m_{eq}}(\omega)V_{X_s}(\omega) = Bl_s\,U_s(\omega)/Z_{e_s}(\omega) - S_{d_s}P_{l_{X_s}}(\omega)$, the coefficients $B(\omega)$ and $C(\omega)$ can thus be expressed as

$$B(\omega) = \frac{\rho c\left(1 + R_L(\omega)e^{2jk(X_s-L)}\right)}{\dfrac{S_{d_s}^2}{S}\rho c\,DEN(\omega) + 2Z_{m_{eq}}(\omega)\left(R_0(\omega)R_L(\omega)e^{-2jkL} - 1\right)}\frac{(Bl_s)^2}{Z_{e_s}(\omega)}U_s(\omega) \qquad (4.19)$$

$$C(\omega) = \frac{\rho c\left(1 - R_0(\omega)e^{-2jkX_s}\right)}{\dfrac{S_{d_s}^2}{S}\rho c\,DEN(\omega) + 2Z_{m_{eq}}(\omega)\left(R_0(\omega)R_L(\omega)e^{-2jkL} - 1\right)}\frac{(Bl_s)^2}{Z_{e_s}(\omega)}U_s(\omega) \qquad (4.20)$$

where $DEN(\omega) = 1 + R_0(\omega)e^{-2jkX_s} + R_L(\omega)e^{2jk(X_s-L)} + R_0(\omega)R_L(\omega)e^{-2jkL}$.

For the first configuration, hard wall surfaces are imposed at both terminations of the waveguide and the sound source is at location $x = X_s = 0.5\,\mathrm{m}$. Then, the electroacoustic absorber with the control settings of case C substitutes for the hard-wall at the right termination, and also at the left termination for the third configuration. Figures 4.7a, 4.7c, and 4.7e illustrate the frequency responses from the driving voltage of the sound source (located along the wall at location $x = X_s$) to the sound pressure level in a space–frequency representation for the three configurations. The jump of the sound pressure at location $x = X_S$ that is caused by the sound source is visible on the three figures. Figures 4.7b, 4.7d, and 4.7f show the projection of these frequency responses on the frequency axis. As for the study with the sound source located at the left termination of the waveguide, strong resonances appear at fixed frequencies for the first configuration (that is hard wall surfaces at both terminations) in Figs. 4.7a and 4.7b, whereas the nulls of sound pressure are shifted as the observation moves away on both sides of the sound source location. When the electroacoustic absorber in case C substitutes for the hard wall surface at the right end in Figs. 4.7c and 4.7d, the resonances are attenuated along the waveguide in the low frequency range. However, because of the hard wall surface at the left end, only half of the dips are attenuated. Lastly, when two electroacoustic absorbers are at both terminations, the peaks are reduced, and above all, the overall of the dips are increased.
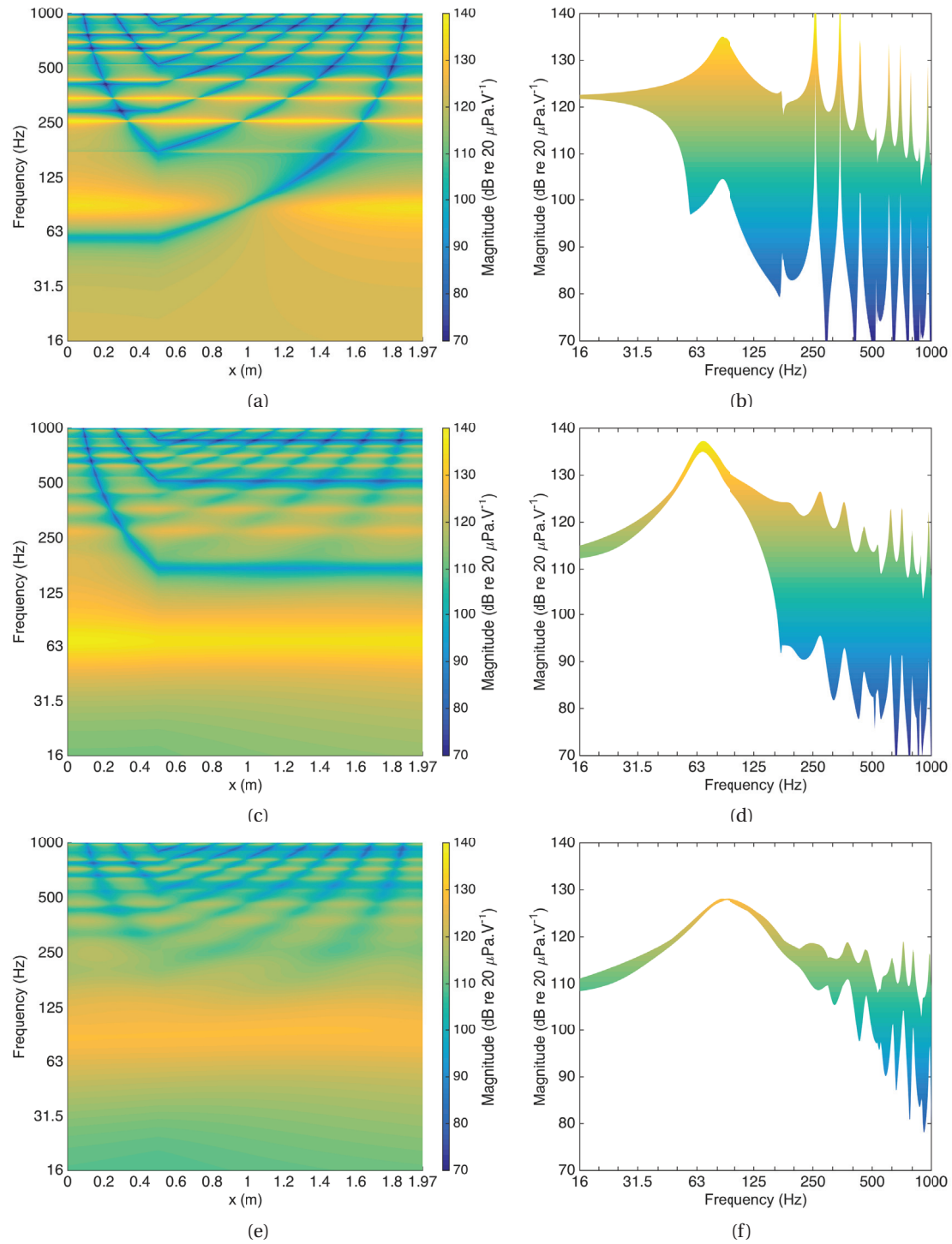
Figure 4.7 – (left column) Space – frequency maps of frequency responses and (right column) dynamic range of all the frequency responses from the driving voltage of the sound source located along the wall at 0.5 m of the left end of the waveguide to the sound pressure level. At the left end is imposed (a, b, c & d) a hard-wall, or (e & f) an electroacoustic absorber with the control settings of case C. At the right end, (a & b) a hard-wall, or (c, d, e & f) an electroacoustic absorber with the control settings of case C is imposed.

As a result, the use of an electroacoustic absorber at one end is not as efficient as the previous configuration with the sound source at the end of the waveguide for equalising the sound pressure.

To summarise, these analytical studies reveal the great performance of the electroacoustic absorber for the modal equalisation in 1D applications over a certain frequency bandwidth.

4.4 Control design issues

As the control modifies the dynamics of the loudspeaker, the stability of the electroacoustic absorber should be considered. Moreover, measuring the sound pressure at the diaphragm as reference for the control actually causes an acoustic feedback path, which is likely to make the active control unstable. In the following, the stability and control limitations of the electroacoustic absorber in the waveguide are studied with the sound source at the left end (see Fig. 4.5), which may be considered as a worst case application for the electroacoustic absorber. Even in the presence of uncertainty, the aim is to study if the stability and absorption performance of the control are still guaranteed.

4.4.1 Limitations and uncertainties

As no mathematical system can accurately model the physical system, some errors must be taken into account, because they might adversely affect the performance of the control system [219]. It is worth investigating the effects of the transducer model uncertainties, measurement noise, sensor location, and time delay on the absorption performance, before analysing the stability of the electroacoustic absorber.

Transducer model

One of the performance limitations is caused by the inadequate fidelity in the model used as the basis of control system design. Ideally, the resultant performance should be insensitive to the difference between the true and estimated models. This characteristic is usually referred to as robustness (or robust control). For a same model of commercial loudspeakers, it is common to measure some variations in the lumped element model of the transducer. First, to characterise the uncertainty on the mechanical impedance, a multiplicative modelling error $\Delta_{Z_m}(s)$ corresponding to the normalised mechanical impedance perturbation away from 1 is expressed as

$$\Delta_{Z_m}(s) = \frac{\tilde{Z}_m(s)}{Z_m(s)} - 1 \tag{4.21}$$

where $\tilde{Z}_m(s)$ is the perturbed mechanical impedance. If the components M_{ms}, R_{ms}, and C_{mc} of the mechanical impedance are estimated from the value of the effective surface area S_d and
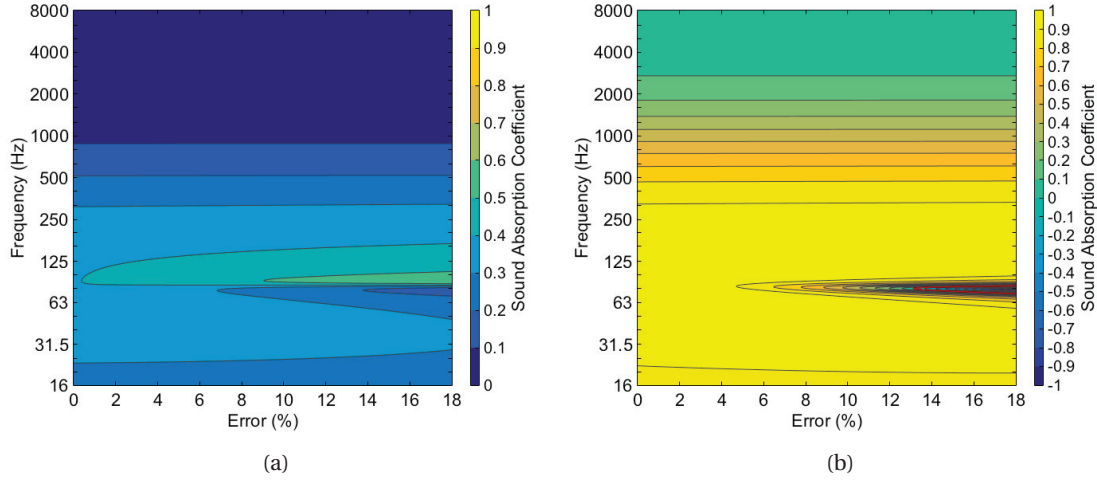
Figure 4.8 – Error – frequency maps of the sound absorption coefficient of the electroacoustic absorber computed in cases (a) B and (b) C depending on the percentage error of the mechanical impedance uncertainty.

the measurement of the specific acoustic impedance of the loudspeaker in open circuit, an uncertainty on the effective piston area S_d is eventually equivalent to an uncertainty on the mechanical impedance. Moreover, the perturbed force factor Bl is expressed as $\tilde{Bl} = (1 + \Delta)Bl$, where Δ is the multiplicative modelling error. When these uncertainties are considered together, the specific acoustic impedance thus becomes

$$Z_s(s) = \frac{\tilde{Z}_m(s)}{S_d - \tilde{Bl}\,\Theta(s)} = \frac{\left(1 + \Delta_{Z_m}(s)\right)Z_m(s)Z_{st}(s)}{(1 + \Delta)\,Z_m(s) - \Delta\,S_d\,Z_{st}(s)} \tag{4.22}$$

To investigate the overall effect of the model uncertainties on the absorption capabilities, the transfer function $\Delta_{Z_m}(s)$ is expressed as

$$\Delta_{Z_m}(s) = \frac{sM_{ms}\Delta + R_{ms}\Delta - \dfrac{\Delta}{s(\Delta + 1)C_{mc}}}{sM_{ms} + R_{ms} + \dfrac{1}{sC_{mc}}} \tag{4.23}$$

This way, the perturbed mechanical impedance $\tilde{Z}_m(s)$ is equivalent to errors in the mechanical resistance and resonance frequency equal to the same percentage error Δ as well as for the force factor Bl. Nevertheless, the effect of each uncertainty on the absorption capabilities could be considered one after another as well. Figure 4.8 shows model uncertainty – frequency maps of the sound absorption coefficient of the electroacoustic absorber computed in cases B and C, depending on the percentage error Δ of the mechanical impedance uncertainty. The consequence of a transducer model uncertainty is mainly a decrease of the sound absorption coefficient around the resonance frequency. This coefficient can even be negative when relative errors are higher than 13 %. Note that it is likely that the uncertainty on the resonance
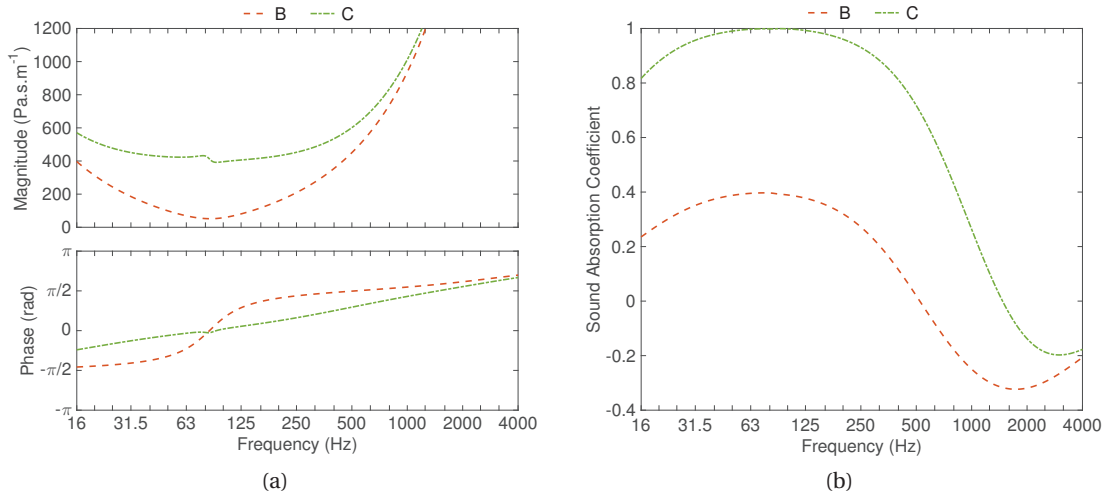
Figure 4.9 – (a) Bode plot of the specific acoustic impedance and (b) the corresponding sound absorption coefficient of the electroacoustic absorber computed in cases B and C, where a low-pass filter ($f_c = 4$ kHz) is applied to the control.

frequency of a given electrodynamic loudspeaker is equal to 15 %. Because of the acoustic compliance C_{ab} of the enclosure, when several Peerless SDS-P830657 loudspeakers are in the same enclosure of volume $V_b = 10$ dm³, experimental tests showed that the error is closer to 5 %. Finally, the uncertainties of other elements of the electroacoustic absorber, such as the sensor or electrical components of the controller, could be included in the study as well.

Measurement noise

When sensors are used, they represent a crucial part of any control system, since they provide the necessary information upon which the controller action is based. A common problem is the electrical noise of the sensor, which may increase by almost 3 dB around 5 kHz in the frequency response of an electret microphone. Note that the lower the factor μ defined in Eq. (3.17), the higher the magnitude of the transfer function $\Theta(s)$, and therefore the higher the noise level delivered by the electroacoustic absorber. Although the magnitude of the transfer function $\Theta(s)$ does not decrease at high frequencies as illustrated in Fig. 4.4, this limitation may be eliminated via a suitable low-pass filter for example. Figure 4.9 illustrates the absorption capabilities, through the specific acoustic impedance and corresponding sound absorption coefficient, when a low-pass filter with a cut-off frequency of 4 kHz is used in addition to the transfer function $\Theta(s)$. The sound pressure and velocity diaphragm are out of phase from around 510 Hz and 1470 Hz in cases B and C respectively. The sound absorption coefficient is thus negative above these frequencies, which means that the electroacoustic absorber fails to absorb, but gives back more than the totality of the sound intensity of the incident wave in the domain in which it is located. Because of the acoustic feedback path of the diaphragm velocity with the medium, any modification on the control for reducing the damaging effects of the
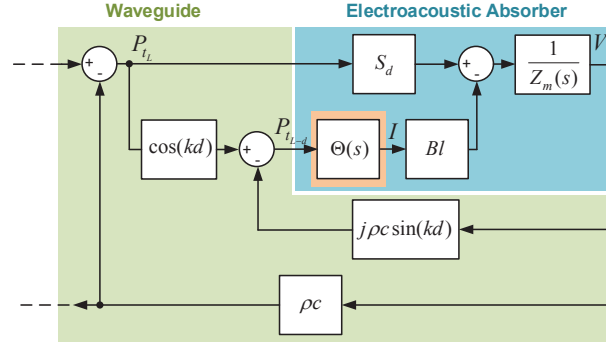
Figure 4.10 – Block diagram of the electrodynamic loudspeaker system under control by measuring the total sound pressure at the distance d of the diaphragm.

measurement system may thus have a negative impact on the absorption performance. The difficulty is thus to reach the right compromise between absorption performance and control stability.

Sensor location

When it comes to practical implementation, the sensor cannot measure the exact value of the sound pressure at the diaphragm, because of its small displaced location relative to the diaphragm along the waveguide axis. This alteration may have some impact on the acoustic performance and stability control. It is therefore worth studying the effect of the microphone location at a distance d from the diaphragm. The expression of the sound pressure at location $x = L - d$ can be derived as

$$P_{t_{L-d}}(\omega) = A(\omega) \left(e^{-jk(L-d)} + R_L(\omega)\, e^{-jkd} \right)$$
$$= \cos(kd)\, P_{t_L}(\omega) + j\, \sin(kd)\, \rho c\, V_L(\omega) \tag{4.24}$$

In that case, the sound pressure $P_{t_{L-d}}$ is not only dependent on the sound pressure P_{t_L} at the diaphragm, but also on the diaphragm velocity V_L. Figure 4.10 highlights the modifications of the coupling between the waveguide and electrodynamic loudspeaker system under control by measuring the total sound pressure at the location $x = L - d$. In this configuration, the specific acoustic impedance of the diaphragm becomes

$$Z_s(\omega) = \frac{Z_m(\omega) + j\, \sin(kd)\, Bl\, \Theta(\omega)}{S_d - \cos(kd)\, Bl\, \Theta(\omega)} \tag{4.25}$$

The distance – frequency maps of the corresponding sound absorption in cases B and C are illustrated in Fig. 4.11. Picking up the sound pressure at a certain distance from the diaphragm has a negative effect on the resulting sound absorption coefficient in both cases. From a distance of a few centimetres, the electroacoustic absorber adds sound intensity in the
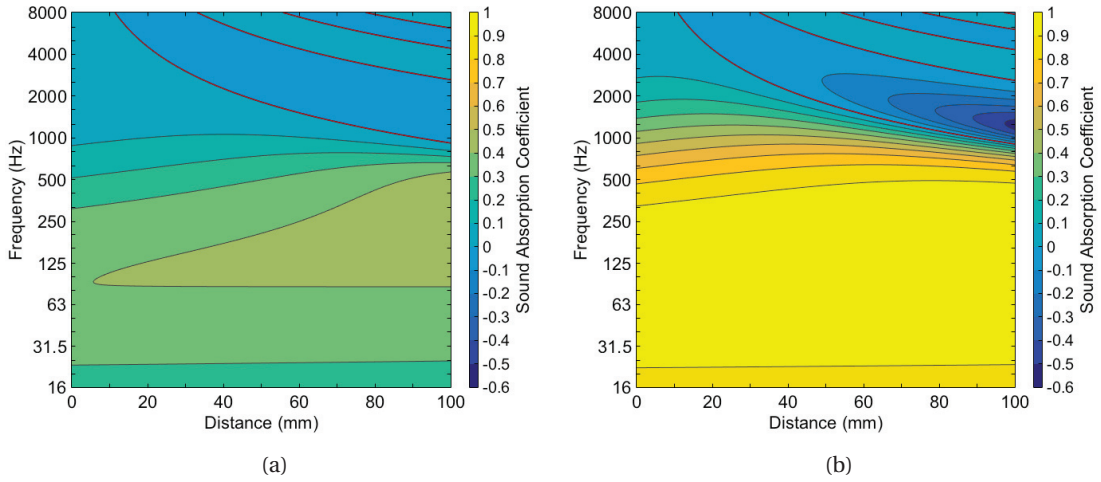
Figure 4.11 – Distance – frequency maps of the sound absorption coefficient of the electroacoustic absorber computed in cases (a) B and (b) C depending on the location of the microphone relative to the diaphragm.

waveguide for frequencies higher than 1 or 2 kHz. This acoustic instability can be reduced, with the addition of passive absorbers close to the diaphragm or located in the closed space for example. Note that these results are only available for the hypothesis of plane waves, that is the transverse modes are not taken into account in this part. The effect of the location of the sensor along the radial axis on the performance and stability will be discussed in Section 4.4.2.

Time delay

In the case of a digital implementation of the transfer function $\Theta(s)$, one of its main advantages is the modification of parameters with ease and accuracy. However, its primary weakness is the increased delay in the control loop. The delay incurred from sampling at regular intervals adds phase lag in the control, thus limiting loop gains and ultimately reducing the responsiveness of the system for real-time applications. The processing time adds a delay from the independent processes of sample-and-hold (depending on the sampling frequency and calculation time), which is specific to the technology of the controller [220]. The time delay factor $e^{-s\tau}$, which is not a rational but analytical function, is treated as a multiplicative pertubation of the controller $\Theta(s)$. Its characteristics are a unit gain and an additional phase lag $\omega\tau$ increasing linearly with frequency. The time delay – frequency maps of the sound absorption coefficient of the electroacoustic absorber computed in cases B and C depending on the time delay factor of the controller are illustrated in Fig. 4.12. The time delay has similar effects to those of the sensor location as shown in Fig. 4.11. The electroacoustic absorber adds sound intensity in the waveguide with real time delays (that is $\tau > 5\,\mu$s) for frequencies higher than a few kHz (depending on the chosen target specific acoustic resistance R_{st}). Direct analog-to-digital converters may be preferred to sigma-delta converters as they have a lower latency. A high
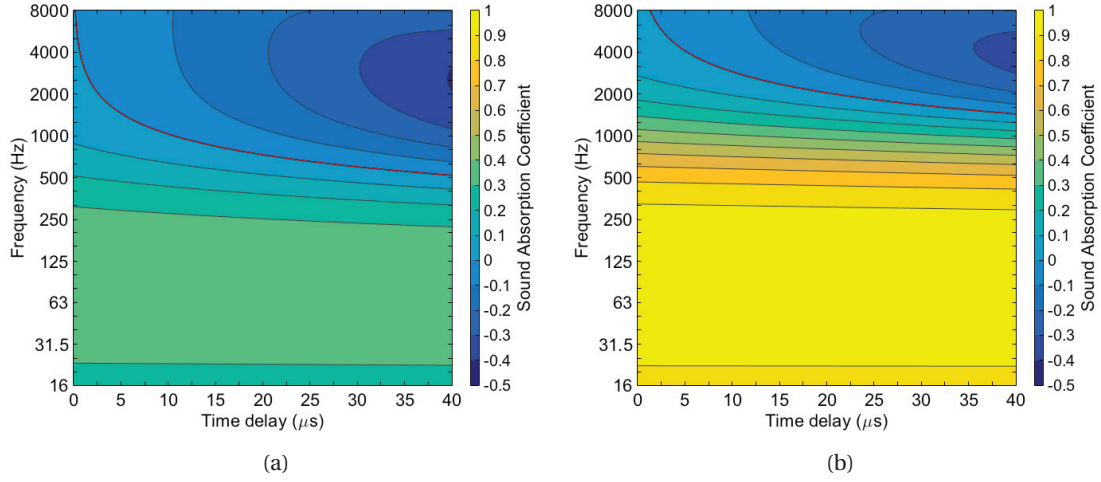
Figure 4.12 – Time delay – frequency maps of the sound absorption coefficient of the electroacoustic absorber computed in cases (a) B and (b) C depending on the time delay factor of the controller.

sampling rate can be advantageous in terms of latency, but it also means that high-frequency noise is more likely to be present in the signal. Nevertheless, this limitation is less disturbing for the absorption capabilities in the frequency band of interest [20 Hz - 500 Hz] than that of the sensor location.

4.4.2 Stability

The aim is now to study if the stability is guaranteed with the limitations and uncertainties previously studied. Because the acoustic impedance condition of the electroacoustic absorber is altered if the control loop is open (between the controller and the loudspeaker for example), the frequency response of the open loop cannot be measured. The stability is therefore studied under plane waves assumption, before integrating the transverse modes through simulation.

Plane waves assumption

First, the frequency response of the open loop is computed under the same hypotheses described in Section 4.3.2 (that is only plane waves in the waveguide). Here the frequency range of study is limited to [16 Hz - 1600 Hz][3]. In the case where the sound source is open circuit (that is $i_0 = 0$), the specific acoustic impedance at the left termination is equal to Z_{m_s}/S_d. To simplify the system illustrated in Fig. 4.5, the specific acoustic impedance ratio at location

---

[3]For a circular cross-section tube of the same section as the effective piston area S_d, the upper frequency limit is $0.586\,c/(2\sqrt{S_d/\pi})$=1436 Hz.

Electroacoustic Absorber

Impedance seen by the
Electroacoustic Absorber
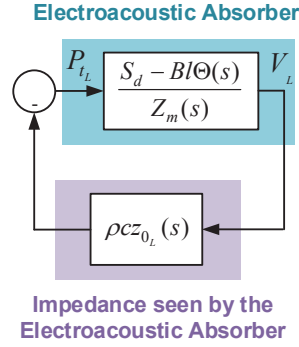
Figure 4.13 – Equivalent system for study of closed-loop stability of the electroacoustic absorber under control, when the sound source is open circuit (case A).

$x = 0$ can be expressed at location $x = L$ via the propagation medium in the waveguide, as

$$z_{0_L}(\omega) = \frac{\dfrac{Z_{m_s}(\omega)}{S_d \rho c} + j \tan(kL)}{1 + j \dfrac{Z_{m_s}(\omega)}{S_d \rho c} \tan(kL)} \tag{4.26}$$

This way, the sound pressure $P_{t_L}(\omega)$ and the diaphragm velocity $V_L(\omega)$ are related by

$$P_{t_L}(\omega) = -\rho c z_{0_L}(\omega) V_L(\omega) \tag{4.27}$$

and the impedance $-\rho c z_{0_L}(\omega)$ corresponds to the impedance "seen" by the electroacoustic absorber in the waveguide. Figure 4.13 shows the equivalent system of the electroacoustic absorber coupled to the waveguide, when the sound source is open circuit (case A). The frequency response of the open loop is thus equal to

$$G_{OL}(\omega) = \frac{\rho c z_{0_L}(\omega)}{Z_s(\omega)} \tag{4.28}$$

Figure 4.14 illustrates the Bode plot and Nyquist diagram of the open loop of the system in cases B and C. Gain and phase margins of stability that describe the stability and robustness of the control to perturbations in the waveguide are summarised in Table 4.4 for the cases B and C, with additional special cases of limitations described in Section 4.4.1, that is the transducer model with an uncertainty of $\Delta = 5\%$, the microphone at a distance $d = 2\,\mathrm{mm}$ from the diaphragm, and a time delay $\tau = 20\,\mu s$. According to the Nyquist stability criterion, the electroacoustic absorber in cases B and C is stable under the assumptions described above and without taking into account any limitation or error. Nevertheless, the case B shows the limits of stability because of the small values of phase margins. When uncertainties are added to the transducer model, the phase margins are slightly higher, because the resonance frequency is 5 % lower than the case B without uncertainty. Note that the time delay causes the
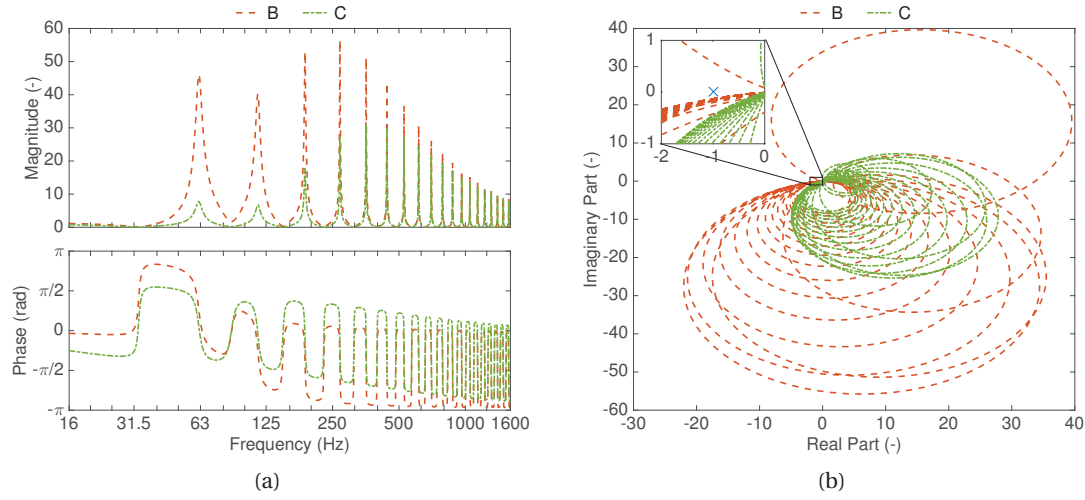
Figure 4.14 – (a) Bode plot and (b) Nyquist diagram of the open loop of the electroacoustic absorber coupled to the waveguide computed for the cases B and C.

Table 4.4 – Gain and phase margins of stability computed from the open loop in the waveguide for the cases B and C with limitations.

Case	Gain margin	Phase margin
B	∞	7.3°
B with uncertainty $\Delta = 5\%$ on transducer model	∞	7.4°
B with microphone at distance $d = 2\,\mathrm{mm}$	∞	7.7°
B with time delay $\tau = 20\,\mu s$	-0.3 dB	-0.2°
C	∞	23.7°
C with uncertainty $\Delta = 5\%$ on transducer model	∞	23.9°
C with microphone at distance $d = 2\,\mathrm{mm}$	∞	26.1°
C with time delay $\tau = 20\,\mu s$	∞	14.0°

main critical limitation of the control stability. If the chosen frequency sample of the digital controller corresponds to a time delay equal to $20\,\mu$s, the electroacoustic absorber in case B should be unstable. The study of stability could be improved by adding other elements, like a finite acoustic impedance to the walls, or modifying the hypotheses to make the model more accurate. Several techniques have been developed with the scope of identifying the loudspeaker diaphragm resonances [221, 222], and incorporating additional lumped elements in the loudspeaker model [223, 224]. These additional elements could also be included in the transfer function $\Theta(s)$ to improve the absorption performance.
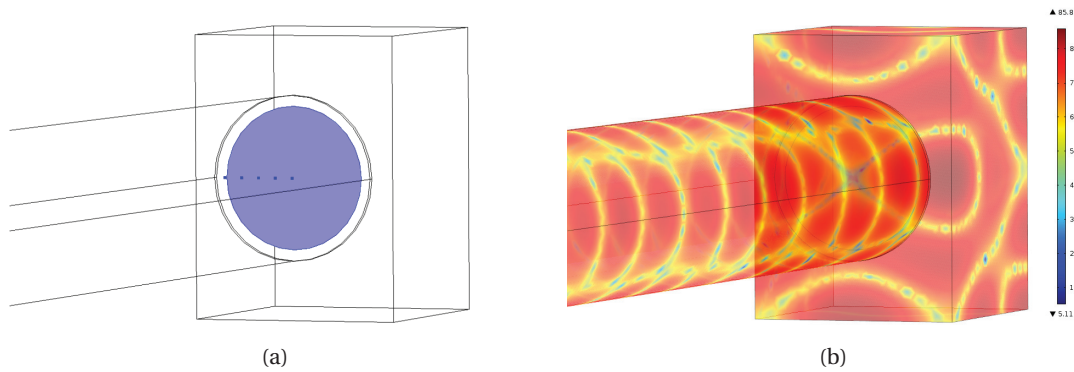
Figure 4.15 – (a) Geometry of the waveguide terminated by a diaphragm (in blue) with five locations for measuring the sound pressure; (b) Sound pressure level computed at 2821 Hz in the waveguide terminated by the electroacoustic absorber.

With transverse modes

When the waves are not plane any more, the transverse modes can have an effect on the stability of the control at higher frequencies. The electroacoustic absorber in the waveguide was simulated with a simple geometry of the diaphragm with the help of a finite element method software (Comsol Multiphysics) (see Fig. 4.15a). As illustrated in Fig. 4.15b, the sound pressure level at the loudspeaker diaphragm at the end of the waveguide is not uniform because of a radial mode at 2821 Hz. In Fig. 4.15a are illustrated five positions of microphone located at 5 mm from the diaphragm (in blue) for measuring the sound pressure for the control: at the center and at the edge of the diaphragm, at one quarter, at half, and at third quarter of the diaphragm radius. The resulting specific acoustic impedance and required electrical current computed from five locations of microphone for the electroacoustic absorber in case C relative to the global pressure at the diaphragm are illustrated in Figs. 4.16a and 4.16b respectively. If the microphone is located in a maximum of sound pressure at a given frequency, the sound pressure level measured by the microphone is higher than the global sound pressure at the diaphragm, resulting in high levels of current for driving the electroacoustic absorber. As a consequence, the location of the microphone measuring the sound pressure has an effect on the stability of the control.

Nevertheless, neither the analytical study under plane waves hypothesis nor simulation taking into account the transverse modes in the waveguide can accurately predict the margins of the electroacoustic absorber in a given configuration.

4.5 Power balance

The hybrid impedance control presented in this chapter was designed so as to assign a desired specific acoustic impedance at the diaphragm, without examining the power balance of
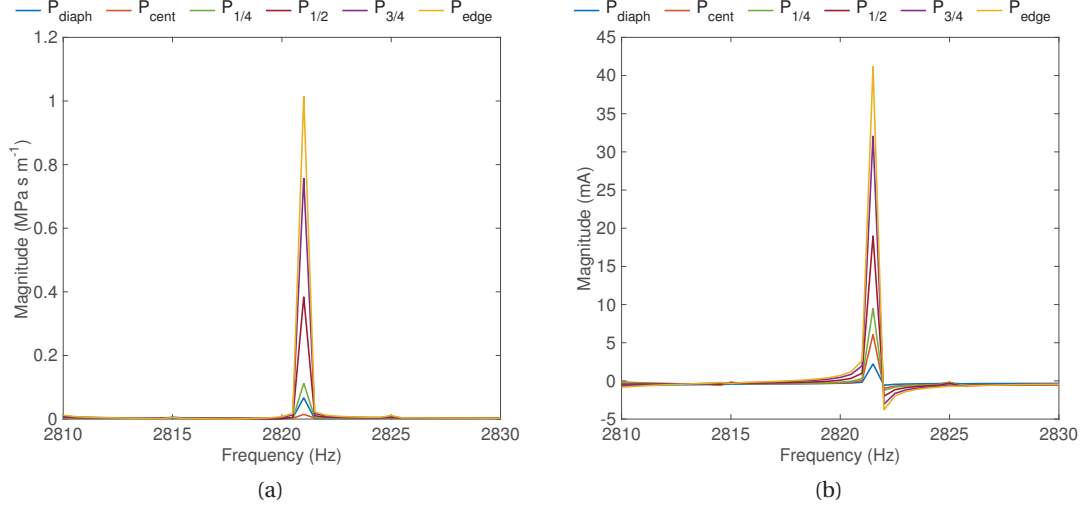
Figure 4.16 – Magnitudes of (a) specific acoustic impedance and (b) required electrical current of the electroacoustic absorber computed in case C depending on the sound pressure which is measured at five locations in front of the diaphragm, relative to the global sound pressure at the diaphragm.

the system yet. Does the transducer always need a supply of energy or can it work as an energy harvester? Although the definition of electrical passivity can vary between authors, an electrical shunt impedance is considered as passive if and only if it does not supply power to the system, that is with the convention taken for the electroacoustic absorber: $\text{Re}\,(U(\omega)\,I^*(\omega)) \leq 0$ $\forall \omega$. Although the hybrid impedance control is implemented through active components, if the active electrical power satisfies this condition, the control is referred to as passive. As shown in Fig. 4.4, the electroacoustic absorber needs some additional power, except around the resonance frequency when the target specific acoustic resistance R_{st} is below the acoustic resistance R_{ms}/S_d (when the loudspeaker is open circuit). In this part, the magnitudes of acoustic and electrical quantities are considered as root mean square values (rms). As active and reactive powers function independently of each other, they can be treated as separate quantities. The complex power $\mathcal{S}(\omega) = \mathcal{P}(\omega) + j\mathcal{Q}(\omega)$ is expressed in VA, the active power $\mathcal{P}(\omega)$ in W, and the reactive power $\mathcal{Q}(\omega)$ in VAR.

First, the complex powers from the characteristic equations of the loudspeaker are expressed as

$$S_d\,P_t(\omega)\,V^*(\omega) = Z_m(\omega)\,|V(\omega)|^2 + Bl\,I(\omega)\,V^*(\omega) \tag{4.29}$$

$$U(\omega)\,I^*(\omega) = Z_e(\omega)\,|I(\omega)|^2 - Bl\,I^*(\omega)\,V(\omega) \tag{4.30}$$

The complex powers are then written as a function of the total sound pressure $P_t(\omega)$ and target specific acoustic impedance $Z_{st}(\omega)$ with the help of Eq. (4.1). Assuming that this target impedance is ideally achieved at the diaphragm, the complex sound power $\mathcal{S}_{s\to m}(\omega)$ absorbed
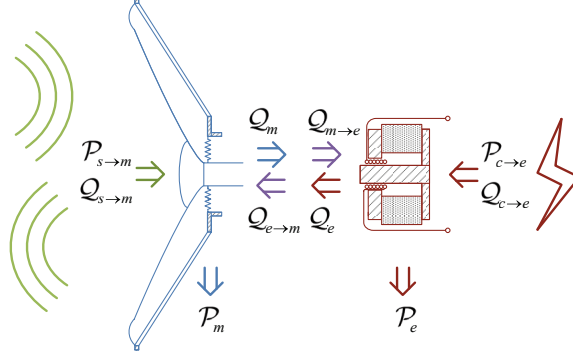
Figure 4.17 – Schematic of the power balance of the electroacoustic absorber.

by the device, the complex power $\mathcal{S}_m(\omega)$ of the mechanical part, the complex powers $\mathcal{S}_{m \to e}(\omega)$ and $\mathcal{S}_{e \to m}(\omega)$ of the electromechanical coupling, and the complex power $\mathcal{S}_e(\omega)$ of the electrical part are respectively

$$\mathcal{S}_{s \to m}(\omega) = S_d\, P_t(\omega)\, V^*(\omega) = \frac{S_d\, Z_{st}(\omega)}{|Z_{st}(\omega)|^2}\, |P_t(\omega)|^2 \tag{4.31}$$

$$\mathcal{S}_m(\omega) = Z_m(\omega)\, |V(\omega)|^2 = \frac{Z_m(\omega)}{|Z_{st}(\omega)|^2}\, |P_t(\omega)|^2 \tag{4.32}$$

$$\mathcal{S}_{m \to e}(\omega) = Bl\left(I(\omega)\, V^*(\omega)\right) = -\mathcal{S}_{e \to m}{}^*(\omega) = Bl\left(I^*(\omega)\, V(\omega)\right)^* \tag{4.33}$$

$$\mathcal{S}_e(\omega) = Z_e(\omega)\, |I(\omega)|^2 = Z_e(\omega)\left|\frac{S_d\, Z_{st}(\omega) - Z_m(\omega)}{Bl\, Z_{st}(\omega)}\right|^2\, |P_t(\omega)|^2 \tag{4.34}$$

From these equations, the complex power $S_{c \to e}(\omega)$ from the electronic circuit of the controller required by the electroacoustic absorber can be derived as

$$\begin{aligned}
\mathcal{S}_{c \to e}(\omega) &= \mathcal{S}_e(\omega) + \mathcal{S}_{e \to m}(\omega) = U(\omega)\, I^*(\omega) \\
&= \left[Z_e(\omega)\left|\frac{S_d\, Z_{st}(\omega) - Z_m(\omega)}{Bl\, Z_{st}(\omega)}\right|^2 - \frac{S_d\, Z_{st}^*(\omega) - Z_m^*(\omega)}{|Z_{st}(\omega)|^2} \right] |P_t(\omega)|^2
\end{aligned} \tag{4.35}$$

The power balance of the system is illustrated in Fig. 4.17. The frequency responses from the absolute square of the total sound pressure $P_t(\omega)$ at the diaphragm to the active and reactive sound powers $\mathcal{P}_{a \to m}(\omega)$ and $\mathcal{Q}_{a \to m}(\omega)$ received by the electroacoustic absorber in case A (open circuit) are presented in Fig. 4.18. These frequency responses are compared to the special case where the electroacoustic absorber is under control with the reduction factor being equal to $\mu = 0.15$ and the specific acoustic resistance R_{st} being variable. These frequency responses are displayed in Figure 4.19. Note that the amount of complex sound power is higher when the electroacoustic absorber is under control relative to the open circuit case.

The active mechanical power $\mathcal{P}_m(\omega)$ mainly caused by friction losses in the suspension and the active electrical power $\mathcal{P}_e(\omega)$ resulting in Joule heating through the voice coil are the only
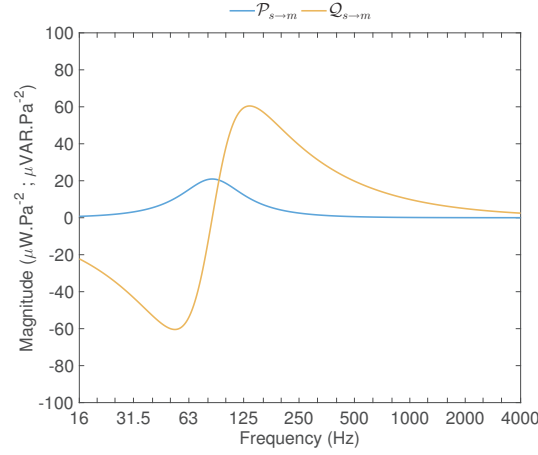
Figure 4.18 – Frequency responses from the absolute square of the total sound pressure at the diaphragm to the active and reactive sound powers received by the electroacoustic absorber with the control settings of case A.

(a)   (b)
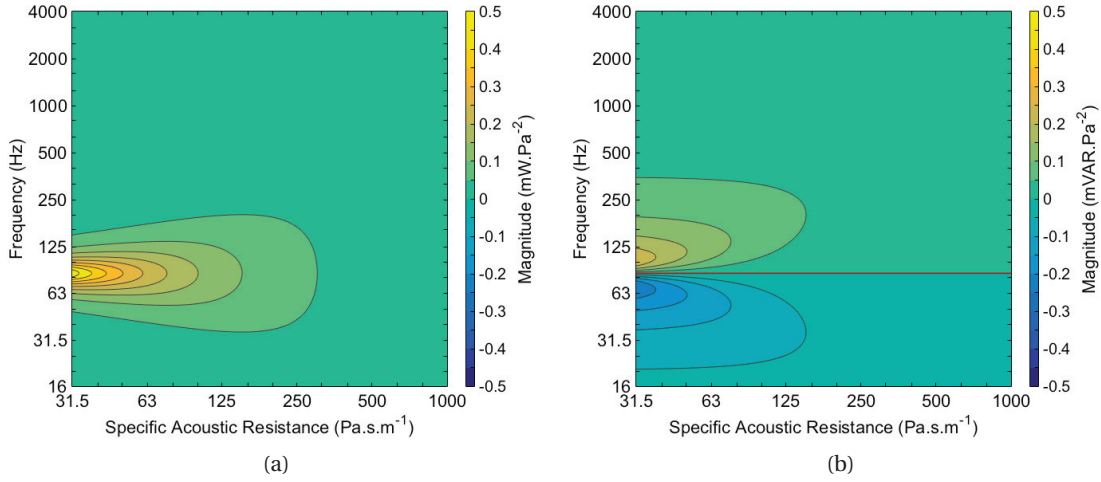
Figure 4.19 – Specific acoustic resistance – frequency maps of the frequency responses from the absolute square of the total sound pressure at the diaphragm to (a) the active sound power and (b) reactive sound power received by the electroacoustic absorber with the reduction factor $\mu = 0.15$.

energy dissipation in the system. Conversely, the reactive elements of the transducer can only store energy and not dissipate it. Therefore, as the reactive power does not contribute to any power dissipation in the electroacoustic absorber, it has an adverse effect on power consumption, because it contributes to increasing the electrical current flowing in the circuit. To confirm this, the active and reactive electrical powers $\mathcal{P}_{c \to e}(\omega)$ and $\mathcal{Q}_{c \to e}(\omega)$ required by the electroacoustic absorber are displayed in Fig. 4.20. Note that the inductance of the voice coil causes an asymmetry of the reactive power (see Fig. 4.20b). Moreover, the required electrical powers are higher than the sound powers. As predicted by the transfer function $\Theta(s)$ in Eq. (4.1),
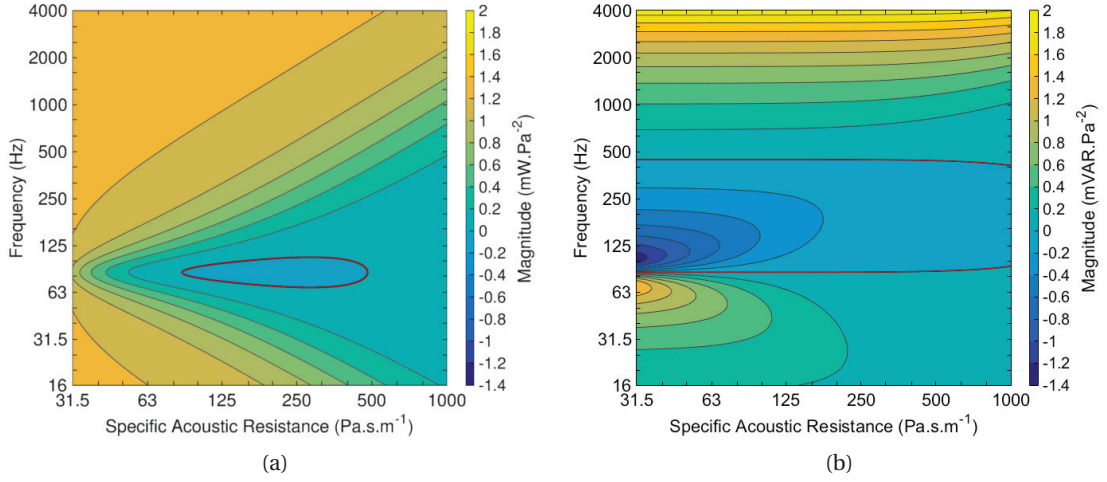
Figure 4.20 – Specific acoustic resistance – frequency maps of the frequency responses from the absolute square of the total sound pressure at the diaphragm to (a) the active electrical power and (b) reactive electrical power required by the electroacoustic absorber with the reduction factor $\mu = 0.15$.

the electroacoustic absorber does not need additional power around the centre frequency f_o', when the target specific acoustic resistance R_{st} is above the acoustic resistance R_{ms}/S_d. The DC resistance R_e is even insufficient to dissipate all this power. The remaining power is thus dissipated through the resistive parts of the electronic circuit of the controller. These electrical requirements are compared to the active powers $\mathcal{P}_m(\omega)$ and $\mathcal{P}_e(\omega)$ dissipated in the mechanical and electrical parts of the system (see Fig.4.21).

Power efficiency

When the loudspeaker is used as a sound diffusing system, its efficiency is defined as the sound power output divided by the electrical power input. Most loudspeakers present very low efficiencies are inefficient transducers: only about 0.5 % of the electrical energy sent by an amplifier to a Peerless SDS-P830657 loudspeaker is converted into sound energy. The remainder is converted to heat, mostly in the resistance of the voice coil. In the case of sound absorption, the power efficiency may be defined as the ratio from the active sound power of the incident wave to the electrical power

$$\eta(\omega) = \frac{\mathcal{P}_{c \to e}(\omega)}{\mathcal{P}_{S_{inc} \to m}(\omega)} = \alpha(\omega) \frac{\mathcal{P}_{c \to e}(\omega)}{\mathcal{P}_{s \to m}(\omega)} \tag{4.36}$$

Figure 4.22 shows the specific acoustic resistance – frequency map of the efficiency of the system. As for a conventional use of the loudspeaker, the electroacoustic absorber needs a significant supply of electrical power to increase its absorption capabilities. However, the efficiency can almost reach 40 % at the centre frequency. Note that the figures were displayed
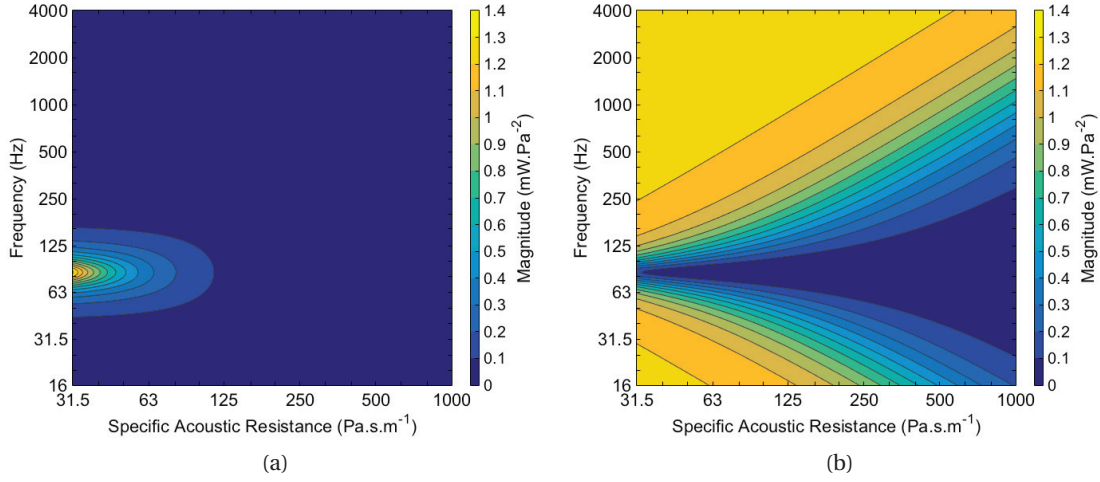
Figure 4.21 – Specific acoustic resistance – frequency maps of the frequency responses from the absolute square of the total sound pressure at the diaphragm to the active powers dissipated in (a) the mechanical part and (b) electrical part of the electroacoustic absorber with the reduction factor $\mu = 0.15$.
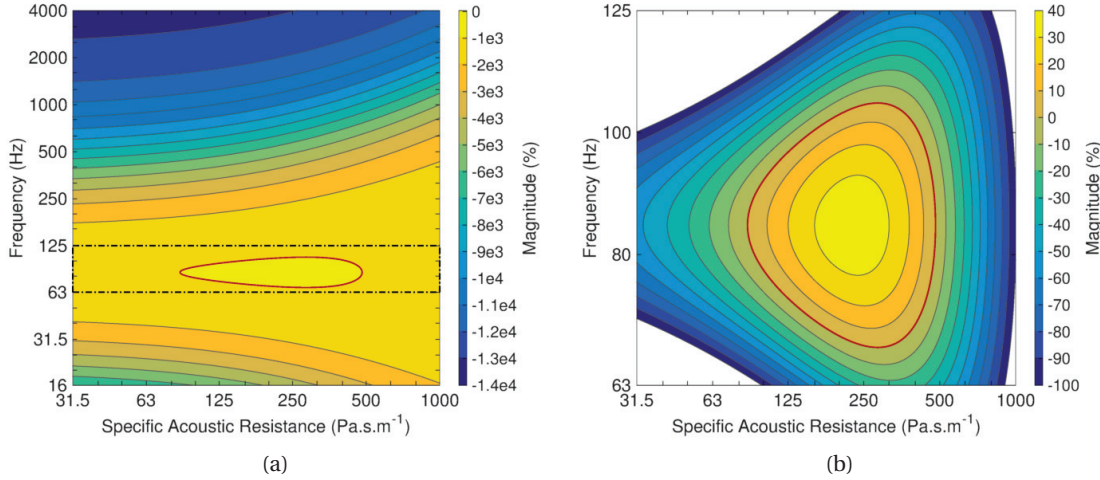
Figure 4.22 – Specific acoustic resistance – frequency maps of the efficiency of the electroacoustic absorber with the reduction factor $\mu = 0.15$ ((a) normal view with the dash-dot lines corresponding to the (b) zoom view between 63 Hz and 125 Hz).

for a special case with a given value of the reduction factor μ. With a view to assessing the effect of the control, the power efficiency is displayed in the case where the reduction factor $\mu = 1$ in Fig. 4.23. As the mass and stiffness are not decreased, the negatives values of efficiency are smaller than in the previous case. With this loudspeaker model, the maximum of efficiency is obtained at the resonance frequency with a specific acoustic resistance equal to almost $\rho c / \sqrt{2}$. Results differ with other loudspeakers or by applying two different reduction factors

86
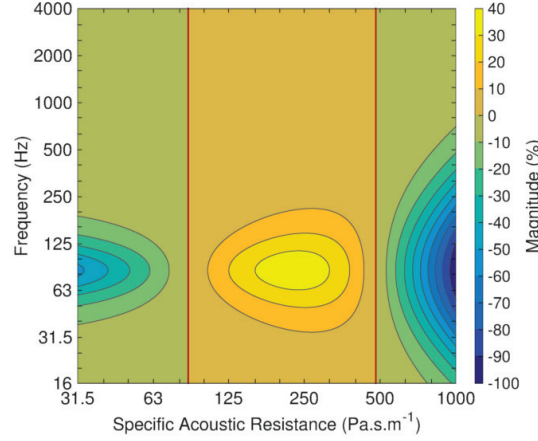
Figure 4.23 – Specific acoustic resistance – frequency map of the efficiency of the electroacoustic absorber with the reduction factor $\mu = 1$.

μ_M and μ_C for the mass and stiffness respectively.

As soon as the mass and stiffness of the electroacoustic absorber are decreased, the device almost always needs extra power, much of which is dissipated by Joule effect in the resistance of the voice coil. Nevertheless, such a system may be considered as energy harvester for stationary noise, provided the spectral centroid is close to the centre frequency of the electroacoustic absorber. An application of shunt damper has been studied in [225], but without taking into account the acoustic domain. Another application has been proposed using non-linear electronic components to compensate the decay voltage of an electrochemical double layer capacitors with the use of a loudspeaker as harvesting system [226].

4.6 Performance evaluation

4.6.1 Experimental setup and control system implementation

To experimentally validate the results presented in Section 4.3, the experimental setup as depicted in Fig. 4.24 was the same as the one used in Section 2.5.1. The pressure used in the control was measured with a 130D20 ICP microphone, located at 1 cm from the electroacoustic absorber diaphragm and close to the lateral duct wall as depicted in Fig. 4.24. The transfer function $\Theta(s)$ given by Eq. (4.1) was first discretised in a discrete-time recursive filter, and then was implemented onto a real-time National Instruments CompactRIO platform supporting field-programmable gate array (FPGA) technology. The microphone sensitivity and gain of the voltage controlled current source were included in the transfer function $\Theta(s)$. The voltage signal from the microphone was digitally converted at 80 kHz via a NI 9215 module (no anti-aliasing filter was used). The output filtered signal u_{out} was delivered by a NI 9263 module to a voltage controlled current source that drove the voice coil loudspeaker. As illustrated on the right-hand side in Fig. 4.24, the voltage controlled current source was the same op-amp based

87
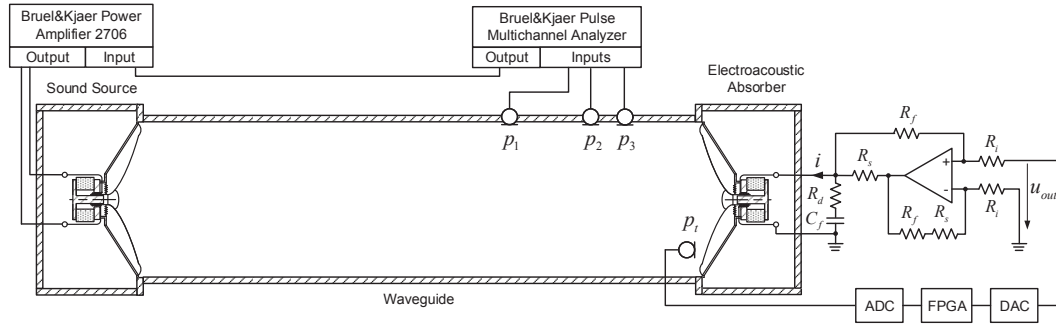
Figure 4.24 – Schematic of the experimental setup. The control implementation is depicted in the right-hand side including the microphone, the digital controller and the transconductance amplifier.
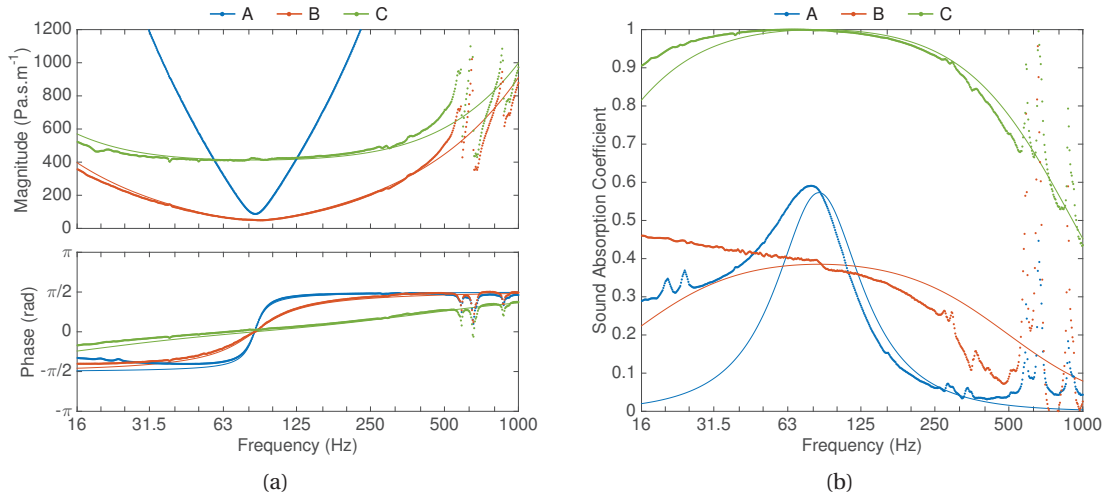
Figure 4.25 – (a) Bode plot of the specific acoustic impedance and (b) sound absorption coefficient of the electroacoustic absorber measured (dotted lines) and simulated (solid lines) in open circuit (case A) and under control (cases B and C).

"improved" Howland current pump circuit described in Section 3.3.1.

4.6.2 Sound absorption measurements

The settings used for the measurements were the same as those used for running the simulation in Section 4.3, and are summarised in Table 4.2. Figure 4.25 illustrates the performance of the electroacoustic absorber in terms of sound absorption, through the measured specific acoustic impedance and sound absorption coefficient. The results show that the measurements are satisfactorily consistent with the corresponding simulation. As expected, a perfect acoustic absorption is obtained over a broad frequency range around the natural resonance of the loudspeaker. The first modes of the electroacoustic absorber enclosure caused the

resonances at 587 Hz and 655 Hz. The upper bound of the bandwidth of efficient absorption is equal to 385 Hz, and is slightly below the expectations ($BW = 410$ Hz), partly because of the resonances of the enclosure modes. With this control strategy, both the acoustic resistance and reactance of the diaphragm are modified, to reach as close as possible the desired specific acoustic impedance Z_{st}.

The slight differences can be attributed to imperfections in the lumped parameter model and to the frequency responses of the microphone and current source used in the control loop, which was not taken into account in the control. As discussed in Section 4.2, it seems obvious that the target specific acoustic impedance cannot be reduced to a constant resistive value, due to the reactive terms of the diaphragm. As discussed in Section 4.4.2, the value of the reduction factor μ is limited by the stability of the closed loop system, between the electroacoustic absorber and the environment in which it is set up. The control settings were chosen close to the limit of stability. Even if the case B was supposed to be unstable according to the simulation, some imperfections and other factors enabled the control to remain stable.

4.6.3 Modal equalisation in a waveguide

The performance for damping low-frequency modal resonances was evaluated in the waveguide. Figure 4.26 shows the measured frequency responses from the driving voltage of the sound source located at the left end of the waveguide to the sound pressure level, expressed in dB re. $20\,\mu$Pa·V^{-1}, at four locations when the duct was ended by a hard wall and by the electroacoustic absorber in cases A and C. The measurements are in good agreement with the corresponding simulation. The study focuses on the global acoustic benefit at low frequencies. In the bandwidth of efficient absorption between 16 Hz and 385 Hz, the difference of sound pressure level between the peaks and dips is 54.1 dB for the rigid termination, 39.5 dB for the open circuit loudspeaker system (case A), and 16.2 dB for the active electroacoustic absorber (case C). Reducing the sound pressure level dynamics by a ratio of more than 3 to 1, these results reveal the modal damping efficiency of the electroacoustic absorber in the low-frequency range. The magnitudes of resonances and anti-resonances are therefore minimised thanks to the active electroacoustic absorber, thereby equalising the distribution of the sound field along the waveguide and the frequency response at any location.

4.7 Conclusion

In this chapter, a hybrid impedance control design has been presented to achieve broadband low-frequency sound absorption. The technique results in a sensor-/shunt-based acoustic impedance control, combined with a current driving method in a similar fashion as the synthetic impedance approach. The main advantage of driving the electroacoustic absorber with a prescribed electrical current is to minimise the negative effects of the voice coil on the control stability above the resonance frequency. Measuring the sound pressure at the diaphragm (or the diaphragm velocity) of the electroacoustic absorber and taking into ac-
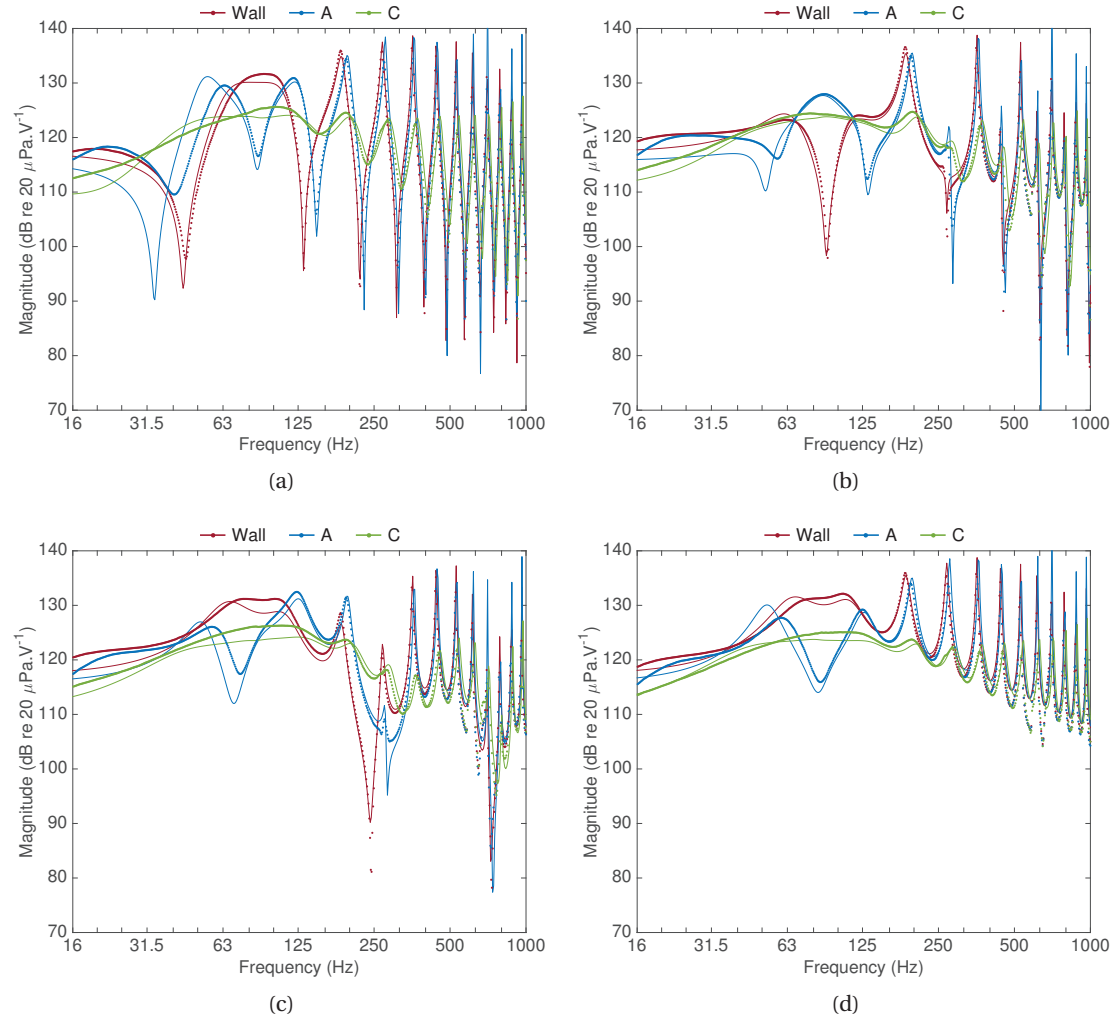
Figure 4.26 – Frequency responses from the driving voltage of the sound source located at the left end of the waveguide to the sound pressure level, measured (points) and simulated (solid lines), at locations (a) $x_0 = 0.01$ m, (b) $x_1 = 1.02$ m, (c) $x_3 = 1.62$ m, and (d) $x_L = 1.96$ m from the sound source. At the right end, a hard-wall termination or an electroacoustic absorber in cases A or C was imposed.

count the transducer model in the control appears an interesting solution between the direct impedance control and self-sensing methods, to assign a desired acoustic impedance at the diaphragm. The technique stands out for its low sensitivity to the voice coil inductance, which can limit the performance of conventional techniques, as well as the sensorless impedance control technique presented in Chapter 3. Numerical analysis and experimental evaluation confirmed the performance improvement compared to the impedance control techniques reported so far, especially in terms of bandwidth of efficient absorption.

The stability has also been investigated. Since the acoustic impedance of the electroacoustic absorber is significantly altered in a lightly damped enclosure when the control loop is open,

the frequency response of the open loop cannot be measured. Nevertheless, the numerical study has shown that the control is relatively stable in the presence of transducer model uncertainties and other factors limiting the control performance, such as the measurement noise, the sensor location, and the time delay (in the case of a digital implementation).

The study of power balance of the electroacoustic absorber has shown that the required electrical power is much higher than the sound power received by the system, so as to absorb over a broad frequency range (the power efficiency is negative). Nevertheless, the system does not need additional power around the centre frequency of the electroacoustic absorber, provided that the target specific acoustic resistance is above that of the system in open circuit (the power efficiency can almost reach 40 % at the centre frequency).

Finally, an application to duct mode damping over a significantly broad frequency range has confirmed the efficiency of the electroacoustic absorber to equalise the acoustic response in cavities. This hybrid sensor-/shunt-based impedance control will be investigated in actual listening rooms in Chapter 6, and should confirm the efficiency of the concept to damp the low-frequency resonances and decrease the modal decay times. As the total absorbing area should be relatively small compared to the total reflecting area of the room for practical reasons, the target specific acoustic impedance, which might be different from that of the air, will be investigated and optimised in Chapter 5.

5 Optimisation of target impedance for efficient modal equalisation

5.1 Introduction

Several impedance control strategies, whose aim is to assign a target impedance at the electroacoustic absorber diaphragm, were presented in the previous chapters. The objective is to standardise the distribution of the sound field and to lower the modal decay times in the domain in which the electroacoustic absorber is located, by increasing the damping of low-frequency modes. With plane waves under normal incidence, the low-frequency absorption is maximal and total, when the specific acoustic impedance at the diaphragm is purely resistive and equals the characteristic impedance of the medium. This condition may only be achievable on a narrow frequency band around the resonance frequency of the electroacoustic absorber. Nevertheless, by imposing the reactive part of the specific acoustic impedance as low as possible relative to the resistive part, the bandwidth of efficient absorption can be increased. If the impedance is too reactive, the energy cannot be dissipated, as shown in Section 4.5. Experiments in a waveguide were in good agreement with the simulation, and confirmed the validity of the model (see Section 4.6).

The working principle of absorption in a 3D domain is somewhat different. It is obviously not realistic to cover the overall wall surface areas of a room with electroacoustic absorbers. These absorbers should have a physical effective absorption surface much smaller than the total surface area of the walls. They should thus provide more damping than in 1D configurations to every eigenmode in the targeted bandwidth, so as to maximise the performance for modal equalisation. This way, depending on the location and effective absorption area of the absorber relative to the total surface area of the domain, the target specific acoustic impedance value may differ from the characteristic impedance of the medium. Extending the 1D results to 3D cases brings up several challenges, such as dealing with non trivial geometries of the domain, the finite size of the absorption area of the device, as well as the absence of simple formulae to determine the eigenmodes and their damping factors in a relatively general framework. In [227], the optimisation of the locations of a limited number of surface impedances on the cavity walls was investigated. Analysing the sound field distribution in rooms with a

given geometry makes it already possible to know where to place the absorbers for maximal performance (preferably in corners for rectangular rooms for example).

The target specific acoustic impedance should be found from a representative criterion for maximising the performance for modal equalisation. A quantity could be derived representing the minimisation of the dynamics of the sound pressure level or the flattening of the frequency responses at different locations. However, with a reasonable number of frequency responses, which are dependent on the location of the source and listener/microphone, it will only give an approximate value of the dynamics of the sound pressure level, as pointed out in Section 4.6.3. Since the modal decay times are critical for the perception of low-frequency problems as discussed in Section 1.4, these quantities can also be used as criterion. The main advantage is that each modal decay time is related to the corresponding damping and eigenfrequency (see Section 1.2.1). It is also independent on the location of the source and listener in the room, and it is easily derived from simulations. The minimisation of the modal decay times is representative of the performance for modal equalisation, and this criterion will be used in the following, in order to find the target specific acoustic impedance at the electroacoustic absorber diaphragms.

To define the target specific acoustic impedance values of one or several absorbers in actual situations, and to analyse the effect of different parameters on the modal decay times, the study is divided into several parts. A first part investigates the optimal value of the target specific acoustic impedance in:

- A first 1D case under normal incidence where an absorber is located at the termination of a cross-section duct of finite length, whose effective absorption area smaller than the cross-section can vary;

- A second 1D case where an absorber is located along the wall of the duct near one of both terminations under grazing incidence;

- A 3D case where four absorbers are located in the bottom corners in a rectangular room with a given orientation and a variable effective absorption area, so as to keep a symmetric distribution of the sound field.

From these results, a design of electroacoustic absorber constituted of several diaphragms with a fixed absorption area is proposed for the next 3D cases. With this configuration, the effect of the resistive wall impedance and room geometry with varying dimensions on the modal equalisation are also studied in the next parts. The simulation is limited to three different values of wall impedance and three sizes of room. The active sound power dissipated into the absorbers is also investigated in the rooms and compared to the results obtained from the modal decay times. Finally, from these simulation results, the target impedance of the diaphragms is optimised from a global criterion, so that this impedance approaches the different optimal resistance values of the low-frequency modes at best.

5.2 Target impedance versus effective absorption area

In this section, the effect of the effective area of the absorber on the value of the target specific acoustic impedance is studied in two 1D cases and one 3D case. In the following, the air is considered as a lossless medium of propagation.

5.2.1 1D case: absorber under normal incidence

Ideal case

If a duct has a perfectly rigid termination at one end and an absorber with a specific acoustic impedance $Z_{s_{abs}}$ and same cross-section area at other end, the complex eigenfrequencies f_{0_n} are the critical values of the input impedance computed at the rigid end, which is expressed as

$$Z_{s_{in}}(\omega) = \rho c \frac{\dfrac{Z_{s_{abs}}}{\rho c} + j\tan(kL)}{1 + j\dfrac{Z_{s_{abs}}}{\rho c}\tan(kL)} = j\rho c \tan(kL + \eta) \tag{5.1}$$

where η is defined such that $j\tan(\eta) = Z_{s_{abs}}/(\rho c)$. The eigenfrequencies f_{0_n} are then

$$f_{0_n} = (2n-1)\frac{c}{4L} - \eta\frac{c}{2\pi L} \tag{5.2}$$

where $n \in \mathbb{N}^*$. In the case where the specific acoustic impedance of the absorber is purely resistive ($Z_{abs} = R_s$), η is purely imaginary and defines the imaginary part of the given eigenfrequency. This term η represents the damping of the corresponding eigenmode: the larger the imaginary part of the eigenfrequency, the larger the damping. Note that a rigid boundary yields $\eta = n\pi/2$ and the above formula gives the classical (multiples of) half-wavelength series of a duct closed at both terminations $f_{0_n} = nc/(2L)$. On the other hand, a free boundary is equivalent to $\eta = 2n\pi$ and the (odd multiples of) quarter-wavelength series of an open-closed duct are $f_{0_n} = (2n-1)c/(4L)$.

The modal decay time MT_{60_n} of the eigenmode n, which is the time needed for a decrease of 60 dB of the magnitude of the sound pressure level during the free response of a given mode, is related to the imaginary part of the eigenfrequency f_{0_n} as

$$MT_{60_n} = \frac{3\ln(10)}{2\pi\,\mathrm{Im}(f_{0_n})} \tag{5.3}$$

As shown in Fig. 5.1 for a duct of length $L = 1.70\,\mathrm{m}$, the modal decay time of a given mode decreases and becomes nearly equal to 0, when the specific acoustic resistance R_s tends to the characteristic impedance of the air $Z_c = \rho c$ (exactly 0.01 s when $R_s = Z_c$).
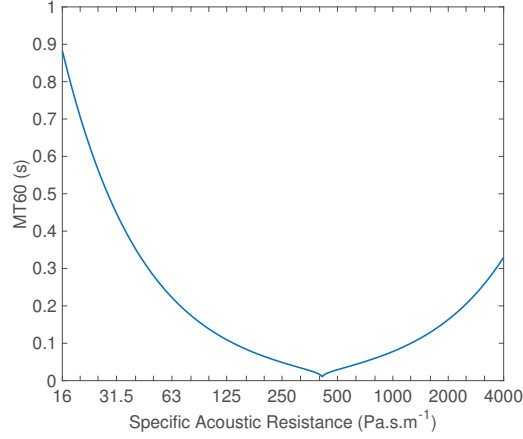
Figure 5.1 – Modal decay time of a given mode in the 1D ideal case depending on the specific acoustic resistance.

Non-uniform boundary conditions

If the cross-section area of the absorber S_{abs} is smaller than that of the duct S and is still surrounded by a hard wall surface area, the boundary condition at this end is non uniform, thus locally, the field is not uniform near this termination. When $S_{abs} \lesssim S$, the hypothesis of an almost uniform sound pressure seems reasonable. However, the particle velocity is equal to that of the absorber v_{abs} on the diaphragm, and equal to zero on the surrounding wall surface area. By conservation of the volume flow, this termination has an approximate effective impedance $Z_{eff} = (S/S_{abs})Z_{abs}$, which differs from the previous case by a factor corresponding to the ratio of the absorber area to the duct cross-section area. On the other hand, if the absorber area S_{abs} is substantially smaller than the cross-section area S of the duct, the approximation no longer holds and an analytical approach may be required to decompose the sound field on the transverse modes, as proposed in [217, 228]. This semi-analytical approach still requires numerical computations to approximate some integrals, and finally leads to a complex nonlinear problem of size $n >> 1$, caused by the contribution of numerous transverse modes, to solve the sharp boundary between the absorber diaphragm and surrounding hard wall surface area.

The longitudinal eigenmodes and corresponding eigenfrequencies of the resonator, that are dependent on the effective area S_{abs} of the absorber, can be determined with a practical approach, which can be more easily generalised to different geometries. The configuration $S_{abs} \neq S$ was simulated with the help of the Comsol Multiphysics commercial finite element analysis, as illustrated in Fig. 5.2. The dimensions of the duct are summarised in Table 5.1. The absorber was modelled by a disk (in red) centred on the termination. The effective absorption area S_{abs} of the absorber varied from $3.14\,\text{cm}^2$ to $314\,\text{cm}^2$ (that is for the radius, from 1 cm to 10 cm). To identify the optimal resistance for every mode in the given configuration, the specific acoustic impedance of the absorber was assumed purely resistive and constant
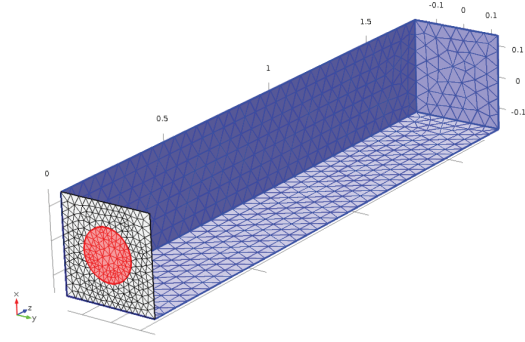
Figure 5.2 – Geometry and mesh of the finite element model of the 1D waveguide terminated by an absorber, whose radius is $r_{abs} = 8$ cm, under normal incidence.

Table 5.1 – Dimensions of the duct and small and medium rooms.

	Length (m)	Width (m)	Height (m)	Floor area (m^2)	Total surface area (m^2)	Volume (m^3)
Duct (D)	1.70	0.30	0.30	0.51	2.22	0.15
Small room (S)	5.33	3.76	2.13	20.04	78.80	42.69
Medium room (M1)	7.02	5.10	2.70	35.80	137.05	96.66
Medium room (M2)	7.87	6.36	3.48	50.05	199.15	174.18

($Z_s = R_s$). The specific acoustic resistance R_s on the disk varied from $0.1\rho c$ to $2.5\rho c$. The configuration was meshed with quadratic elements of minimal size of 0.05 cm and maximal size of 5 cm.

The results for the three first modes are presented in Fig. 5.3. The modal decay times MT_{60}, expressed in s, are displayed depending on the specific acoustic resistance R_s and effective absorption area S_{abs} of the absorber. The almost reflective case leads to modal decay times MT_{60} of about 24 s (see the bottom right corner of the color maps in Fig. 5.3).

For absorbers of sufficient size, there exists an optimal value of impedance resulting in a maximal modal damping. For example, if the absorber covers about 35 % of the termination area, the target impedance should be set to 160 Pa·s·m^{-1}. Note that this target impedance value decreases with the effective absorption area. For the first mode, a 6.5" loudspeaker of effective piston area of 150 cm^2, whose specific acoustic resistance R_s at the diaphragm matches the characteristic impedance of air, has the same performance on the modal decay times than a speaker of effective area 50 cm^2 with $R_s = \rho c/2$, or a speaker of effective area 20 cm^2 with $R_s = \rho c/4$, or even a speaker of effective area 10 cm^2 with $R_s = \rho c/8$. Compared to the ideal case where the absorber diaphragm covers the whole termination, the values of modal decay times are larger for non-uniform boundary conditions.

(a)

(b)

(c)
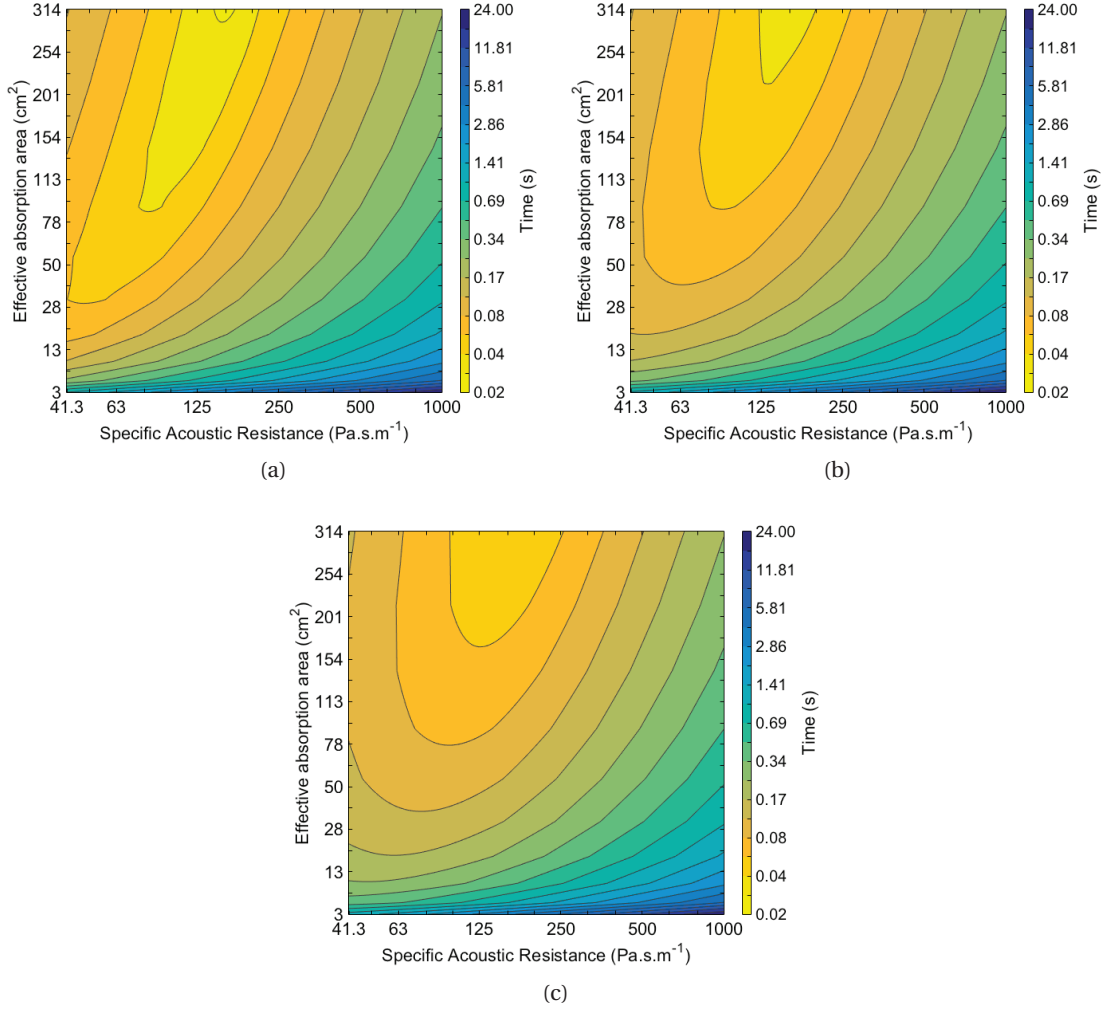
Figure 5.3 – Specific acoustic resistance – effective absorption area maps of the modal decay times of the (a) mode 1, (b) mode 2, and (c) mode 3 computed for an absorber under normal incidence in a 1D waveguide.

5.2.2 1D case: absorber under grazing incidence

In the more general case of sound waves, whose angle of incidence θ may vary between 0 and 90°, the reflection coefficient is expressed as $R(\omega) = (Z_{abs}(\omega)cos\theta - \rho c)/(Z_{abs}(\omega)cos\theta + \rho c)$. Under grazing incidence (that is $\theta = 90°$), the sound absorption coefficient should thus be close to zero. An analytic expression for the optimal impedance of an absorptive surface covering one wall of an infinitely long rectangular duct was found in [229]. The analytical study gives an optimal impedance equal to $Z_{s_{opt}} = (0.91 - j0.76)\rho ckh/\pi$ (h being the height of the duct), which only depends on frequency and height of the duct. On the other hand, a duct of finite length inevitably involves reflections at both ends and may give other values. Starting from the previous model, another configuration was simulated where the absorber
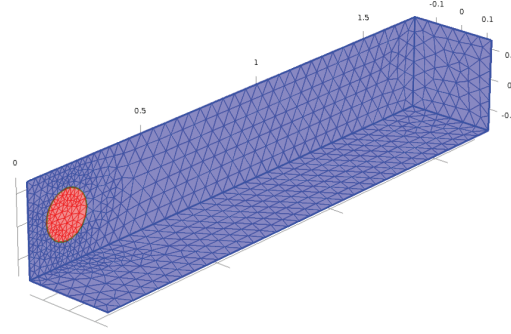
Figure 5.4 – Geometry and mesh of the finite element model of the 1D waveguide with an absorber along the waveguide wall and near one termination under grazing incidence.

was located along the wall of the duct near the termination, whose center was at 15 cm from the duct end, so as to stay close to high sound pressure levels for the first modes. Figure 5.4 illustrates the configuration, where both ends have perfectly rigid wall surface areas. Meshing and parameters were the same as in the previous case.

The results for the first three modes are presented in Fig. 5.5. The modal decay times MT_{60} are also displayed depending on the specific acoustic resistance R_s and effective absorption area S_{abs} of the absorber. Unlike what could be thought, the absorber does actually damp the first modes. Its effect on the modal decay times is even better for the first mode than in the previous case, it is almost the same effect for the second mode, but it is lower for the third mode.

To understand these results, sound pressure isosurfaces are displayed for the first mode in the case of a large effective area $S_{abs} = 314 \, \text{cm}^2$ and a small specific acoustic resistance $R_s = \rho c/4$. Note that the wave fronts are locally deformed by the presence of the absorber and bend toward its surface. The particle velocity is thus locally almost normal to the absorber diaphragm, instead of the expected grazing incidence. Same remarks were made from experimental results in a linear with grazing flow at mid frequencies [173]. These results suggest that the absorber orientation has a small influence on the absorption of a mode with a given spatial structure, as long as it remains sufficiently close to a maximum of sound pressure level for this mode.

5.2.3   3D case: 4 absorbers in a medium room

To investigate the performance of the absorber depending on their effective absorption area in 3D case, a medium room (denoted M1), whose dimensions are summarised in Table 5.1, is also studied. The present study aims at evaluating the worst case in terms of temporal behaviour in the low frequency range. This case is actually not valid for listening rooms, but it might be for a reverberant room. For the simulation, a specific acoustic resistance equal to $100 \, \text{kPa·s·m}^{-1}$, corresponding to a sound absorption coefficient (under normal incidence) $\alpha = 0.016$, was assigned for every wall surface area to simulate hard boundary conditions. Four absorbers,

(a)

(b)

(c)
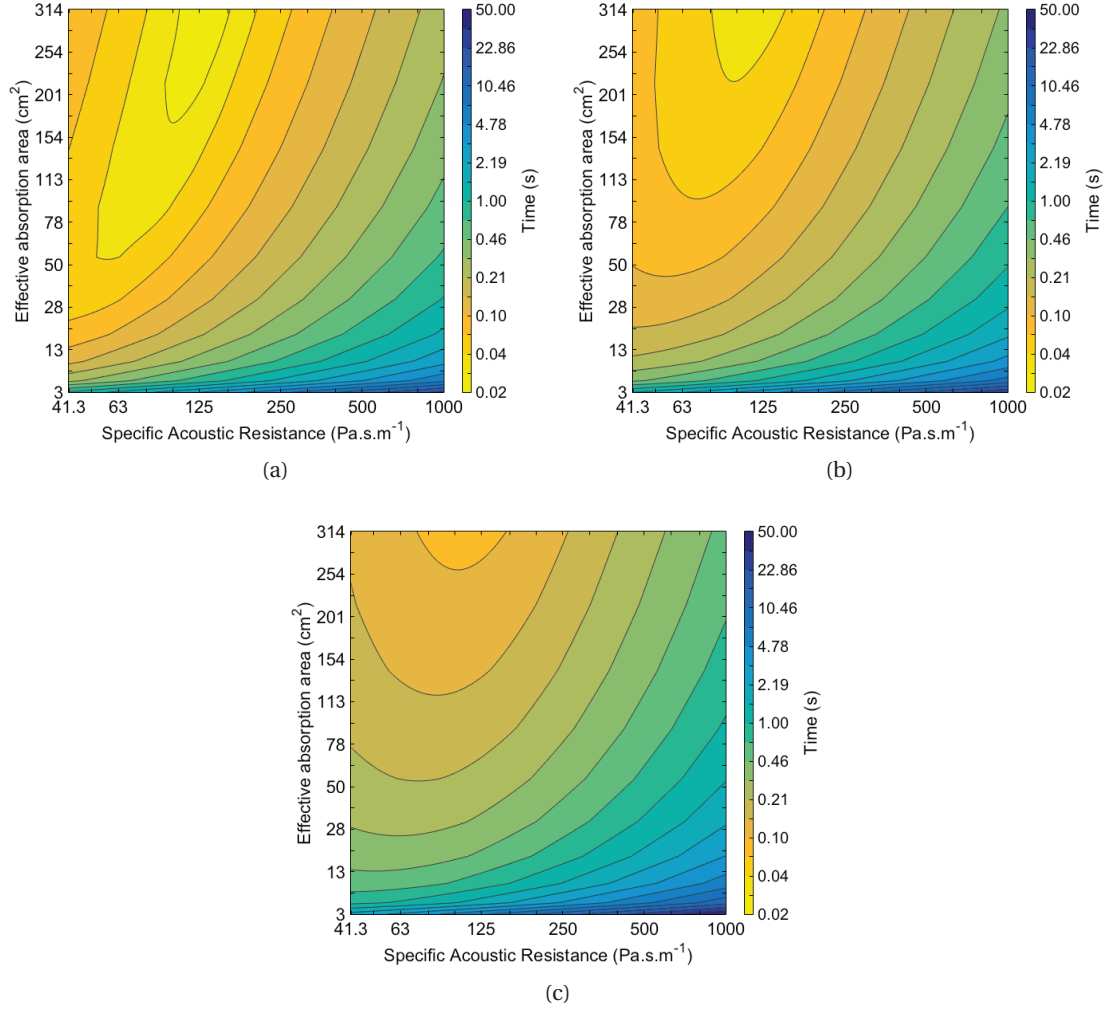
Figure 5.5 – Specific acoustic resistance – effective absorption area maps of the modal decay times of the (a) mode 1, (b) mode 2, and (c) mode 3 computed for an absorber under grazing incidence in a 1D waveguide.

each in an individual closed box, were placed in the four bottom corners of the room, as illustrated in Fig. 5.7. The diaphragms (in blue) were vertical and faced the corner at 45° from each wall, as suggested in [160, 230]. The specific acoustic impedance R_s of the absorbers varied from $0.1\rho c$ to $2.5\rho c$, and the diaphragm radius varied from 8 cm to 17 cm, which was equivalent to a variation of the total effective absorption area from 804 cm^2 to 3632 cm^2. The dimensions of each box was 0.35 m × 0.37 m × 0.35 m and its surface impedance was the same as that of the wall surface areas. The meshing and computation conditions were the same as in the previous 1D cases, but here with a larger number of elements.

The results for the six first modes are presented in Fig. 5.5. The following modes can be found in Figs A.1 and A.2 in Appendix A. Figs 5.8a and 5.8c show the maps of modal decay times
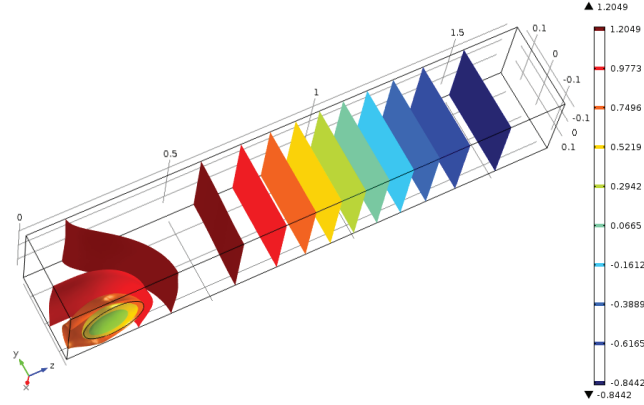
Figure 5.6 – Sound pressure isosurfaces for the first mode in the 1D waveguide with the absorber under grazing incidence (rear view), whose specific acoustic resitance is $R_s = \rho c / 4$ and effective absorption area is $S_{abs} = 314 \, \text{cm}^2$.
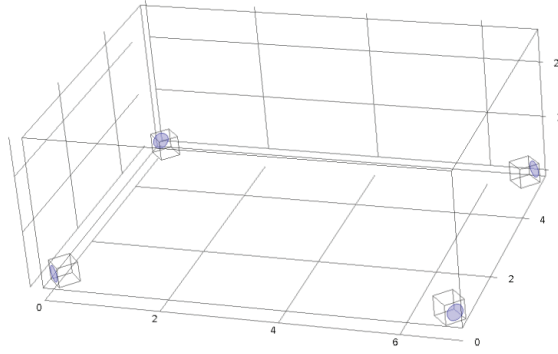
Figure 5.7 – Geometry of the finite element model of the room with 4 absorbers located in the bottom corners.

MT_{60} for two low order modes, namely (1,0,0) at 24.4 Hz and (1,1,0) at 41.7 Hz respectively, for which the absorbers are quite efficient. The modal decay times are reduced to 1 s when the target specific acoustic resistance R_s is low and the total effective absorption area S_{abs} is large enough. Because the wave vector is normal to the absorber diaphragms, the absorbers are the most efficient for the mode (1,1,0). For the two modes (0,1,0) at 33.6 Hz and (2,1,0) at 59.5 Hz illustrated in Figs 5.8b and 5.8e respectively, the modal decay times are well controlled thanks to the absorbers. Even though the mode (2,0,0) at 48.9 Hz illustrated in Fig. 5.8d is the second axial mode over the length of the room, the absorbers are less efficient than for the first axial mode (see Fig. 5.8a). The modal decay time cannot be below 2.2 s for this mode with any value of specific acoustic resistance R_s. However, the value of the optimal resistance has approximately doubled compared to the first mode. Lastly, the first vertical mode (0,0,1) at 63.6 Hz illustrated in Fig. 5.8f is less affected by the presence of the absorbers compared to the five previous modes. The absorbers are not enough efficient to damp this mode, even if
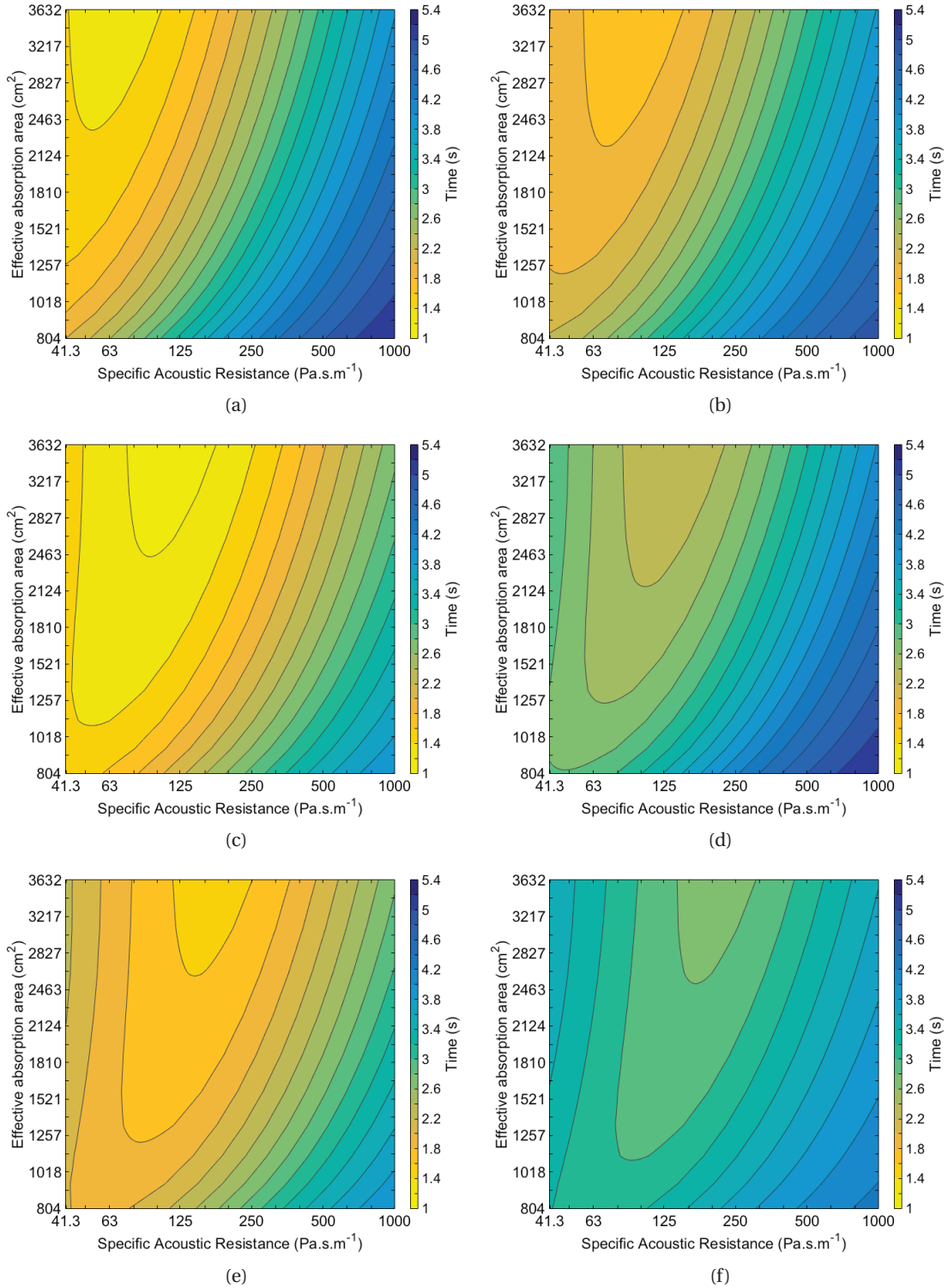
Figure 5.8 – Specific acoustic resistance – total effective absorption area maps of the modal decay times of the modes (a) 1,0,0 - 24.4 Hz, (b) 0,1,0 - 33.6 Hz, (c) 1,1,0 - 41.7 Hz, (d) 2,0,0 - 48.9 Hz, (e) 2,1,0 - 59.5 Hz, and (f) 0,0,1 - 63.6 Hz computed for 4 absorbers located in bottom corners of the medium room M1.

good performance is expected following the results of the 1D case under grazing incidence (see Fig. 5.5c).

As in the previous 1D cases, the larger the effective absorption area, the lower the modal decay times. Nevertheless, even with four large diaphragms in a reverberant room, no mode can have a modal decay time below 1 s, which remains too high to be turned into a good listening room. Moreover, the optimal value of specific acoustic resistance R_s is different for each mode. The higher the central frequency of the mode, the larger the value of the optimal resistance. This remark also applies to the modes illustrated in Figs. A.1 and A.2. As each mode has its own centre frequency, optimal absorbers would thus have a frequency-dependent specific acoustic resistance that matches these different values.

5.3 Target impedance versus room dimensions

From the previous results in Section 5.2, the modal decay times are dependent on the effective absorption area, whatever the location of the absorbers in 1D and 3D cases. Given a total effective absorption area, there exists an optimal specific acoustic resistance for each mode, which minimises the corresponding modal decay time. To study the effect of the room dimensions on the performance of modal equalisation, the total effective absorption area of the absorbers in the room as well as their orientation are arbitrarily fixed. As the hybrid sensor-/shunt-based impedance control described in Chapter 4 has provided the best absorption performance and flexibility in the choice of the target specific acoustic resistance, the value of the effective absorption area of one absorber is chosen equal to that of the loudspeaker used for the control. To get a significant effective absorption area in the room, 16 absorbers are used for every configuration resulting in a total effective absorption area $S_{abs} = 2416\,\text{cm}^2$. Moreover, the results of the previous simulations have shown that the absorber is more efficient when it is under normal incidence rather than under grazing incidence. As the vertical axis generally contributes less to the low-frequency modes, the diaphragms are oriented normal to the axial modes along the horizontal axes.

Four boxes, each constituted of four absorbers located on two adjacent sides, are placed in the four bottom corners of the three studied rooms, as illustrated for the room S in Fig. 5.9. In the simulation in Section 5.2.3, the absorbers were closer to the corners and oriented towards them. However, when the acoustic load impedance seen by the absorbers is very large, especially in a lightly damped room [101, 231], it can result in instabilities in actual cases with the impedance control. With this second configuration, it is intended to simulate a more realistic case where the absorbers would be controlled, hence the orientation towards the centre of the room. The dimensions of every box was $0.3\,\text{m} \times 0.3\,\text{m} \times 0.62\,\text{m}$ corresponding to a global volume of around $40\,\text{dm}^3$. This layout might correspond to an actual implementation of electroacoustic absorbers (see Chapter 6).
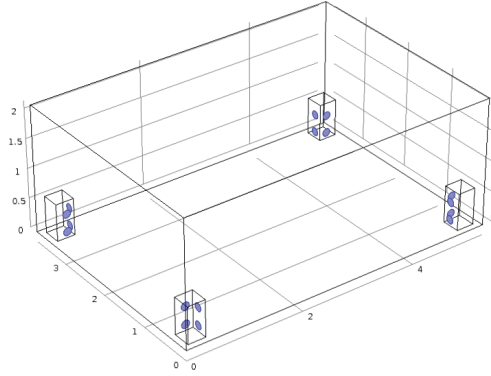
Figure 5.9 – Geometry of the finite element model of the room S with 16 absorbers located in the bottom corners.

5.3.1 Target impedance from modal decay time

The optimal specific acoustic resistance values of the modes should be different depending on the room dimensions. To study the variation of the modal decay times for every mode up to 120 Hz, one small and two medium rooms denoted S, M1 and M2 respectively, whose dimensions are summarised in Table 5.1, were simulated. Unlike the previous study in Section 5.2.3, the performance of the absorbers was evaluated in rooms with a substantial acoustic treatment at mid and high frequencies. A same specific acoustic resistance $R_{S_{wall}}$ was imposed for all the wall surface areas. To reproduce the actual behaviour of listening rooms, this resistance was assumed frequency-dependent and interpolated from three values equal to: $78\rho c$ at 10 Hz, $38\rho c$ at 100 Hz, and $18\rho c$ at 200 Hz, corresponding to sound absorption coefficients (under normal incidence) $\alpha = 0.05$, $\alpha = 0.10$, and $\alpha = 0.20$ respectively. The surface impedance of the boxes was arbitrary set at $18\rho c$. The specific acoustic impedance R_s of the absorbers varied from $0.1\rho c$ to $2.5\rho c$, and the meshing and computation conditions were the same as in the previous 3D case.

The results for the rooms S, M1, and M2 are presented in Figs. 5.10a, 5.10c, and 5.10e respectively. The modal decay times MT_{60} are displayed as a function of the specific acoustic resistance R_s. These modal decay times increase with the size of the room. In the medium room M1, the modal decay times of the first modes are particularly different from those in the two other rooms S and M2. Because of the diaphragms orientation being different from the previous simulation, these resistance values are larger than those obtained in Fig. 5.8, probably because the diaphragms are farther from corners.

For each modal decay time, there exists an optimal specific acoustic resistance for the absorbers. This optimal resistance should be below $0.01\rho c$ for the first modes below 40 Hz. The ideal target frequency-dependent resistance to assign at the diaphragms should be chosen to match the optimal value of every mode at best. The results have shown that the absorbers are
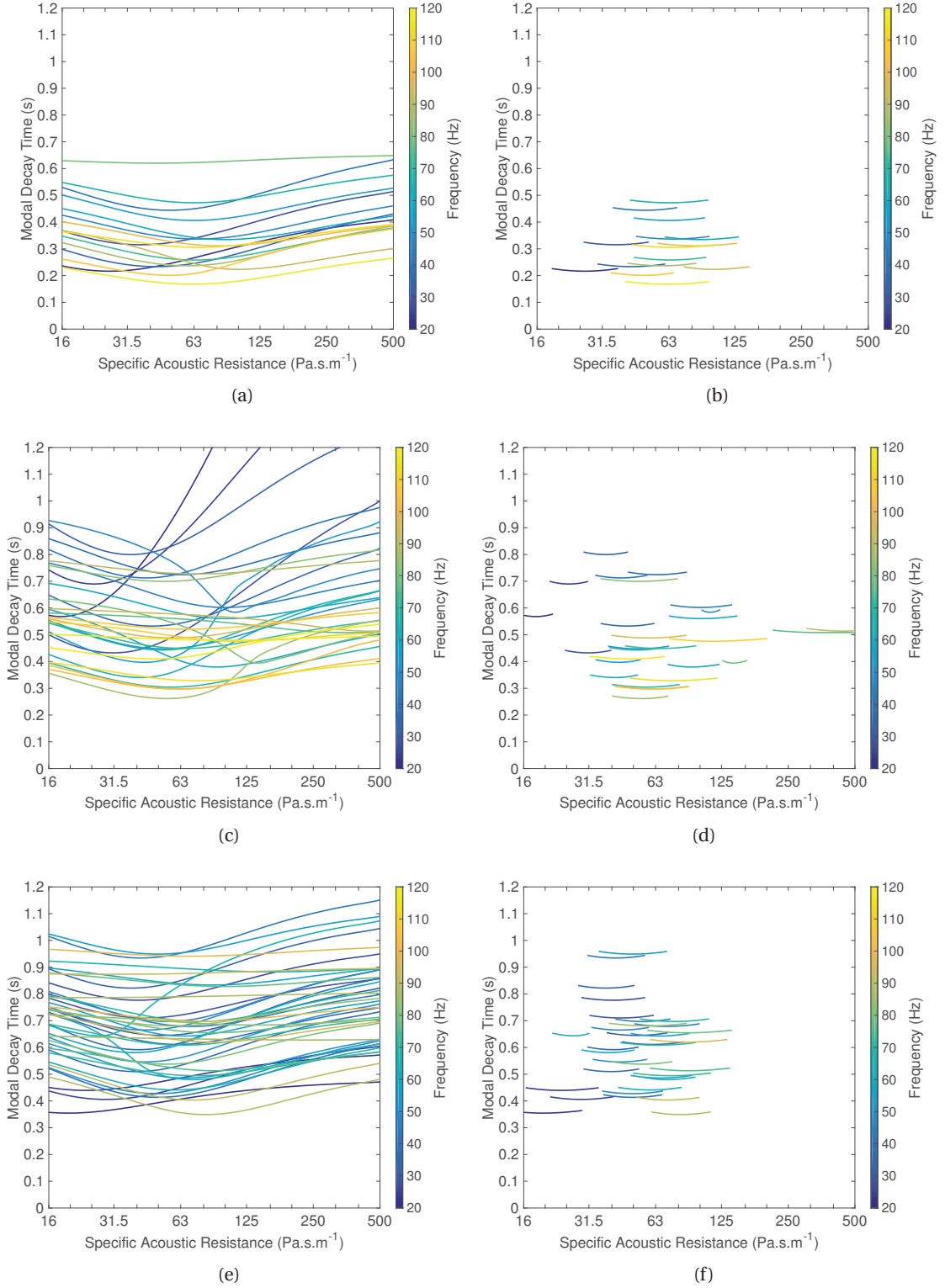
Figure 5.10 – (a), (c), & (e) Modal decay times and (b), (d), & (f) after sorting of the modes between 20 and 120 Hz depending on the specific acoustic resistance computed for 16 absorbers located in bottom corners of the (a) & (b) small room S, (c) & (d) medium room M1, and (e) & (f) medium room M2.
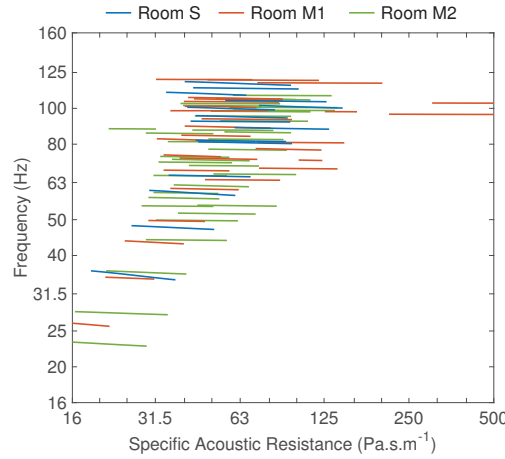
Figure 5.11 – Corresponding modal decay times after sorting computed for 16 absorbers located in bottom corners of the small room S, and medium rooms M1 and M2.

quite inefficient to lower some modal decay times, whatever the specific acoustic resistance value at the diaphragms. From these results, all the modes, whose modal decay time (between 16 and 500 Pa·s·m^{-1}) varies less than a threshold arbitrary set at 66 ms, are removed. Then, for every remaining mode, only the values between the bounds [min(MT_{60}) min(MT_{60})+0.01 s] are kept. The results of this selection are given in Figs. 5.10b, 5.10d, and 5.10f for the rooms S, M1, and M2 respectively; they are summarised in Fig. 5.11, where the eigenfrequencies are displayed as a function of the specific acoustic resistance R_s. Unlike what was assumed, few differences can be observed between the three rooms. Although the optimal specific acoustic resistance increases with the frequency of the mode, the profile of this resistance is the same whatever the room. This suggests that once the target resistance is chosen, the impedance control would be suitable for any room at equivalent wall impedance.

5.3.2 Target impedance from sound power

When properly designed, the absorber can significantly lower the modal decay times, thanks to the active sound power dissipated into its mechanical and electrical parts, as discussed in Section 4.5. This power is obtained from the integration of the normal component of the active sound intensity $\vec{I}(\omega)$ over a closed surface volume $\mathcal{P}_s(\omega) = \int_S \vec{I}(\omega)\,d\vec{S}$ [232]. Since it is the power per area, the sound intensity that gives the direction of the energy flow follows the inverse square law for a free field propagation, and the active sound power radiated is the same whatever the distance. The active sound power is derived from the sound intensity integrated on the surface areas of 4 cubes of 1 m^3 surrounding the four boxes of absorbers in the bottom corners of rooms. A point source delivers a volume flow rate of 1 mm^3·s^{-1} at the arbitrary position (2 m, 1.5 m, 0.3 m) in Cartesian coordinates.

The results of the active sound power are presented for the room S in Fig. 5.12, depending on 16 specific acoustic resistances for the four first modes between 25 and 75 Hz. For the two
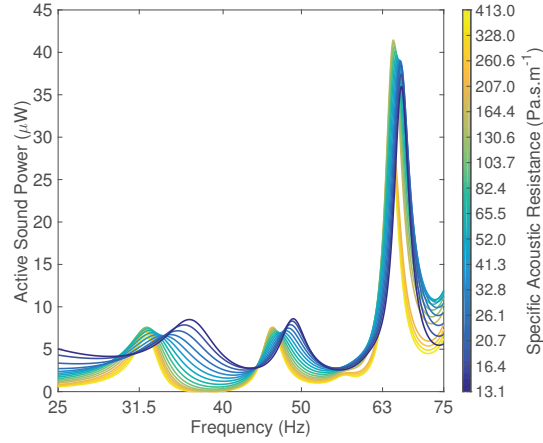
Figure 5.12 – Active sound power between 25 and 75 Hz depending on the specific acoustic resistance computed for 16 absorbers located in bottom corners of the small room S.

first modes at 32 Hz and 48 Hz, the optimal acoustic resistance, for which the active sound power is maximal, is very low (below 13 Pa·s·m^{-1}). However, the maximal local value of the active sound power for the third mode at around 59 Hz cannot be determined, because this mode is affected by the fourth mode at 66 Hz. The optimal acoustic resistance for the fourth mode is around 164 Pa·s·m^{-1}. These values of optimal acoustic resistance are different from those found from the modal decay times (see Fig. 5.10b). Equalising the sound field in the room is thus not equivalent to maximising the absorbed sound power. Moreover, these results show the difficulty of finding the profile of optimal acoustic resistances from the active sound power, and confirm the choice of the modal equalisation through the minimisation of the modal decay times.

5.4 Target impedance versus wall impedance

In Section 5.3.1, it was found out that the optimal resistances followed the same profile whatever the room for a given wall impedance. The effect of the value of this impedance on the modal decay times is also studied. Two other wall impedances were simulated for the room S to study the variation of the modal decay times for every mode up to 120 Hz. For the two configurations, the specific acoustic resistance $R_{s_{wall}}$, whose value was assumed constant and equal to $78\rho c$ labelled Z_{w1}, then $398\rho c$ corresponding to a sound absorption coefficient under normal incidence $\alpha = 0.01$, labelled Z_{w2}, was imposed for every wall surface area.

The results are given in Figs. 5.13a, and 5.13c respectively. To highlight the modes where the absorbers are efficient, the results are selected according to the method described in Section 5.3.1. These results are compared to those obtained with the frequency-dependent impedance in Fig. 5.10b (here labelled Z_{w1}); they are summarised in Fig. 5.14. Surprisingly, the frequency of modes and optimal specific acoustic resistances are perfectly superimposed, pointing out that the variation of the value of the wall impedance has no effect on the target

(a)

(b)

(c)

(d)
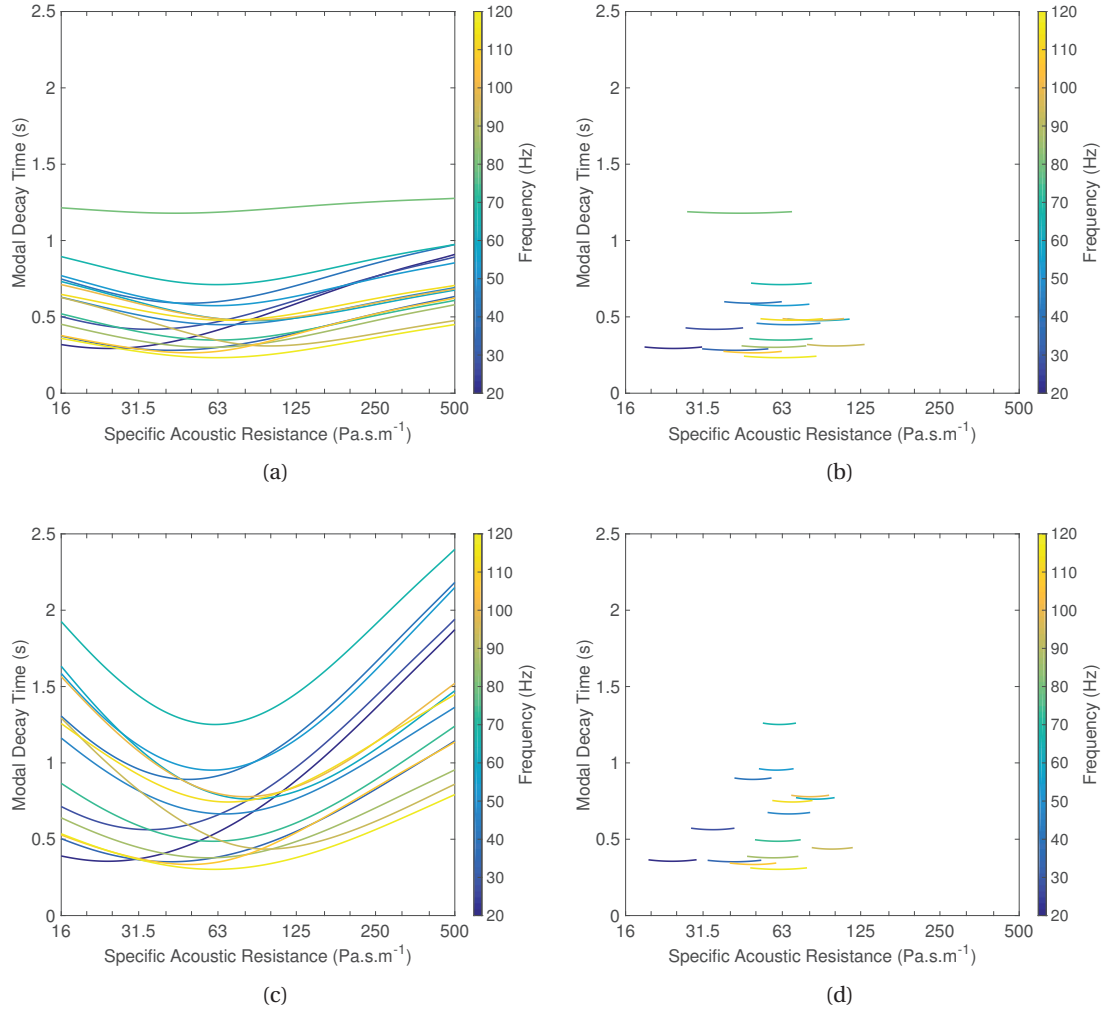
Figure 5.13 – (a) & (c) Modal decay times and (b) & (d) after sorting of the modes between 20 and 120 Hz depending on the specific acoustic resistance computed for 16 absorbers located in bottom corners of the small room S with two values of wall impedance (a) & (b) Z_{w2} and (c) & (d) Z_{w3}.
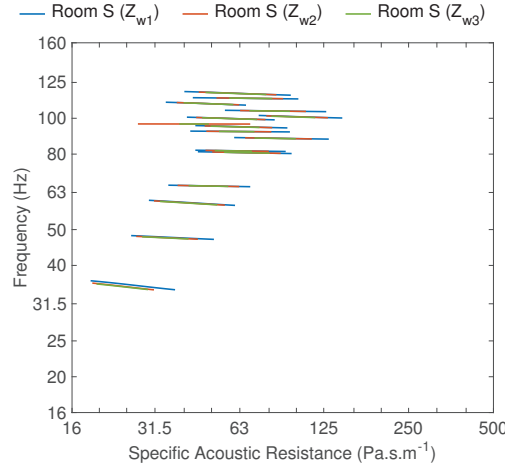
Figure 5.14 – Corresponding modal decay times after sorting computed for 16 absorbers located in bottom corners of the small room S for three values of wall impedances.

impedance according to to the simulations.

5.5 Optimisation of multiple degree-of-freedom target impedance

5.5.1 Design

Multiple degree-of-freedom target impedance

From the results of the preceding simulations, the target specific acoustic impedance $Z_{st}(\omega)$ at the diaphragms is now optimised to minimise the modal decay times in rooms. Following a strategy similar to that in [174], the target specific acoustic impedance $Z_{st}(\omega)$ should be chosen to reach a compromise, so as to approach at best the optimal resistance value of every mode, while keeping the reactive part very small relative to the resistive part. In Section 3.2.4, a general target specific acoustic impedance $Z_{st}(\omega)$ has been introduced, parametrised with one (or two) reduction factor(s) μ (or μ_M and μ_C), and a target specific acoustic resistance R_{st}. Although it is possible to modify the centre frequency f_0' of the electroacoustic absorber, only one value of resistance can be assigned to the diaphragm. In addition, the bandwidth of efficient absorption BW is dependent on the target resistance R_{st}: the lower the target resistance value, the smaller the bandwidth. There is a compromise between bandwidth and target resistance, which should minimise the modal decay times over the targeted bandwidth.

Following the idea of multiple degree-of-freedom resonators designed in Chapter 2, the resistance can vary thanks to a more complex impedance, as it was the case for the electroacoustic absorber coupled to additional resonators. Thus, a multiple degree-of-freedom target specific acoustic impedance is defined from n one degree-of-freedom impedances in parallel, and is

expressed as

$$Z_{st_{n-DOF}}(\omega) = \cfrac{1}{\displaystyle\sum_{k=1}^{n} \cfrac{1}{Z_{st_k}(\omega, v_{2k-1}, R_{st_{2k-1}}, v_{2k})}} \tag{5.4}$$

where $n \in \mathbb{N}^*$ and

$$Z_{st_k}(\omega, v_{2k-1}, R_{st}, v_{2k}) = j\omega \frac{M_{ms}}{S_d v_{2k-1}} + R_{st} + \frac{1}{j\omega S_d v_{2k} C_{mc}} \tag{5.5}$$

corresponding to the one degree-of-freedom impedance. To keep both the asymptotes of the n degree-of-freedom target impedance equal to those of the one degree-of-freedom target impedance $Z_{st_{1-DOF}}(\omega) = j\omega M_{ms}/(S_d v_{M_1}) + R_{st} + 1/(j\omega S_d v_{C_1} C_{mc})$ [1], the conditions are

$$v_1 = v_{M_1} - \sum_{k=2}^{n} v_{2k-1} \tag{5.6}$$

$$v_{2n} = v_{C_1} - \sum_{k=1}^{n-1} v_{2k} \tag{5.7}$$

From the results obtained in Sections 5.2.2 and 5.3.2, the particle velocity is locally almost normal to the absorber diaphragm. Thus, it is hypothesised that the waves are only under normal incidence in front of the diaphragms for the optimisation. To evaluate the performance of the electroacoustic absorber, a modified sound absorption coefficient $\tilde{\alpha}$ is defined, with respect to the specific acoustic resistance R_s under normal incidence, as

$$\tilde{\alpha}(R_s, f) = 1 - \left| \frac{Z_s(f) - R_s}{Z_s(f) + R_s} \right|^2 \tag{5.8}$$

This way, the absorption capabilities can be determined in relation to the frequency for any specific acoustic resistance value.

Weighting function of optimal resistances

To take into account the results found in Section 5.3.1 for the optimisation of the target impedance expressed in Eq. (5.4), a profile $R_{s_p}(f)$ is estimated from a polynomial of second order to fit the optimal values of the specific acoustic resistances of every mode at best, between 16 Hz and 100 Hz. Above 100 Hz, the profile $R_{s_p}(f)$ is constant and equal to the value at 100 Hz. Then, a weighting function is adapted for the optimisation from the profile $R_{s_p}(f)$ of the optimal specific acoustic resistances and defined through a Gaussian function as

$$R_{s_{opt}}(R_s, f) = (a_1 f + b_1) \exp\left[-\frac{(R_s - g R_{s_p}(f))^2}{2(a_2 f + b_2)} \right] \tag{5.9}$$

---

[1] for the special case $n = 1$, $v_1 = v_{M_1}$ and $v_2 = v_{C_1}$

Table 5.2 – Parameters used for the weighting function of optimal specific acoustic resistances.

Parameter	a_1	b_1	a_2	b_2	g
Value	-0.02	5.33	-0.10	26.67	0.75
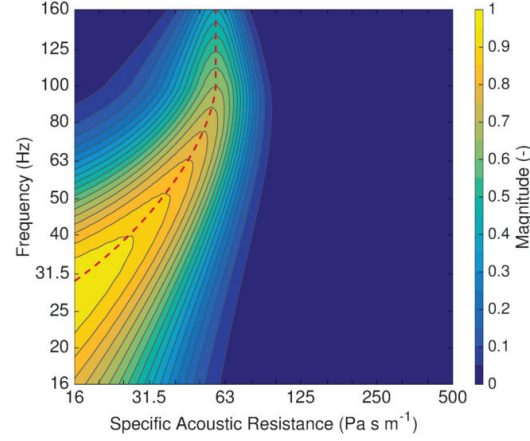
Figure 5.15 – Specific acoustic resistance – frequency map of the weighting function for the optimisation of the target specific acoustic resistance.

where a_1 and a_2 are coefficients of the frequency f and b_1 and b_2 are the constant terms of two linear functions respectively, and g is an overall coefficient of the profile $R_{s_p}(f)$. This way, the maximal magnitude and standard deviation of the Gaussian function vary according to both linear functions. The parameter values of the weighting function $R_{s_{opt}}(R_s, f)$ are summarised in Table 5.2. Figure 5.15 illustrates the specific acoustic resistance – frequency map of the weighting function of optimal specific acoustic resistances. The red dotted line depicts the profile $R_{s_p}(f)$. The parameter values were chosen to give more importance to the first modes between 20 Hz and 40 Hz, and give less importance to the modes higher than around 80 Hz. The coefficient g was also chosen below 1, so that the normalised sound absorption coefficient, expressed in Eq. (5.8), covers the minimal values of optimal resistance of all the modes depicted in Fig. 5.11.

Strategy

From the weighting function of optimal resistances, a parametric optimisation is carried out to take advantage of the system through one of both objective functions proposed in Chapter 2. As the main motivation is to damp the modes as much as possible, the objective function $\mathcal{A}$ (area over threshold) is preferred. This function is defined according to the modified sound absorption coefficient $\tilde{\alpha}(R_s, f)$ and weighting function expressed in Eqs. (5.8) and (5.9) respectively; it is expressed as

$$\mathcal{A}_2 = \int \int \max\left(\tilde{\alpha}(R_s, f) - \alpha_{th}, 0\right) R_{s_{opt}}(R_s, f)\, \mathrm{d}R_s\, \mathrm{d}f \tag{5.10}$$

Table 5.3 – Parameter values of the optimised one, two, and three degree-of-freedom target specific acoustic impedances relative to the basic configuration of the open circuit electroacoustic absorber.

Case	Z_{st_1}			Z_{st_2}			Z_{st_3}		
	ν_1	R_{st_1}	ν_2	ν_3	R_{st_3}	ν_4	ν_5	R_{st_5}	ν_6
	(-)	(Pa·s·m^{-1})	(-)	(-)	(Pa·s·m^{-1})	(-)	(-)	(Pa·s·m^{-1})	(-)
C0	1.00	R_{ms}/S_d	1.00	-	-	-	-	-	-
C1	6.25	52.20	25.00	-	-	-	-	-	-
C2	2.16	67.01	2.36	4.09	55.24	22.64	-	-	-
C3	1.86	85.99	2.86	1.32	54.81	1.11	3.07	57.32	21.03

It corresponds to the weighted bandwidth wBW minus the bandwidth of efficient absorption BW, weighted by the threshold of efficient absorption α_{th} according to every value of specific acoustic resistance R_s. This difference is multiplied by the weighting function $R_{s_{opt}}(R_s, f)$. This way, instead of favouring a large bandwidth of efficient absorption with a "low" maximal value of sound absorption coefficient, this objective function enables the absorption coefficient to be maximised (that is near a perfect absorption) depending on the weighting function, over a frequency range as large as possible. The optimisation is limited to finding the factors ν_{2k-1} and ν_{2k} and specific acoustic resistances $R_{st_{2k-1}}$ depending on the imposed values ν_{M_1} and ν_{C_1} expressed in Eqs. (5.6) and (5.7) respectively.

5.5.2 Performance analysis

The performance of the electroacoustic absorber is estimated by computing the equations presented in Section 5.5.1, considering the Peerless SDS-P830657 loudspeaker mounted in a closed-box of volume $V_b = 10\,\text{dm}^3$, whose parameters are summarised in Table 4.1. Table 5.3 presents the parameter values optimised for three configurations of target specific acoustic impedance, as well as the corresponding centre frequency f_0'. The baseline configuration C0 corresponds to the passive electroacoustic absorber, which is equivalent to the case A in Chapter 4. Cases C1, C2, and C3 correspond to the one, two, and three degree-of-freedom target impedances respectively. Table 5.4 presents the corresponding performance indicators for the objective function $\mathcal{A}_2$, such as the centre frequency f_0', the bounds BW^- and BW^+ of the maximal bandwith of efficient absorption at the corresponding specific acoustic resistance $R_{s_{BW\,max}}$.

Figures 5.16a and 5.16b illustrate the optimisation results of the two- and three degree-of-freedom target impedances constituted of the one degree-of-freedom impedances. Thanks to the one degree-of-freedom impedances in parallel, the phase of the target impedances in cases C2 and C3 is close to zero over a narrow frequency band. Figures 5.17a and 5.17b illustrate the bode plots and real and imaginary parts of the specific acoustic impedance

Table 5.4 – Absorption performance indicators of the optimised one, two, and three degree-of-freedom target specific acoustic impedances relative to the basic configuration of the open circuit electroacoustic absorber.

Case	f_0' (Hz)	BW^- (Hz)	BW^+ (Hz)	$R_{s_{BW_{max}}}$ (Pa·s·m^{-1})	$\mathcal{A}_2$ (Pa·s·m^{-1}·Hz)
C0	84.4	77.7	91.7	109.13	106.73
C1	42.2	23.3	76.6	70.90	569.82
C2	42.2	23.6	88.8	54.35	890.13
C3	42.2	23.1	95.2	50.93	1037.97
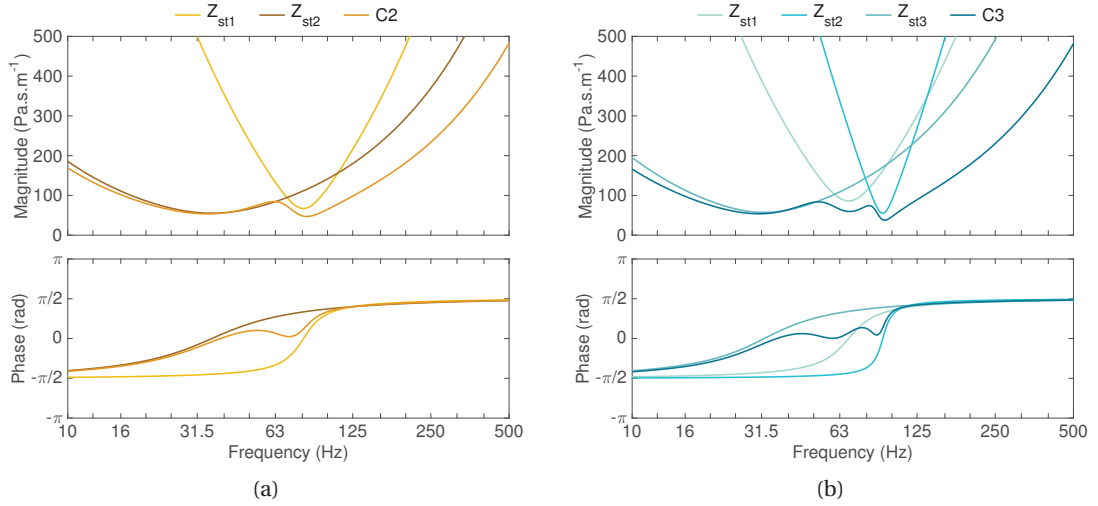
Figure 5.16 – Bode plots of the specific acoustic impedances of the electroacoustic absorber computed for the (a) two- and (b) three degree-of-freedom target impedances optimised from the objective function of area over threshold.

of the electroacoustic absorber computed in cases C1, C2, and C3, relative to the baseline configuration C0. Although the target specific acoustic resistance is constant in case C1 and is equal to 52.47 Pa·s·m^{-1}, it varies between 30.23 Pa·s·m^{-1} and 82.65 Pa·s·m^{-1} in case C2, and between 21.35 Pa·s·m^{-1} and 83.33 Pa·s·m^{-1} in case C3. The higher the degree-of-freedom of the target impedance, the larger the dynamics of the resistance value. While the expression of the multiple degree-of-freedom impedance in Eq. (5.4) differs from those expressed with the additional resonators in Eqs. (2.12), (2.21), and (2.23), the real and imaginary parts are similar at equivalent degree-of-freedom (see Fig. 2.11). Note that the largest bandwidth of efficient absorpion is obtained in case C3. Also, the value of the resistances from 100 Hz seems too low in cases C2 and C3 compared to those of optimal resistance illustrated in Fig. 5.11.

To go further in the analysis of the absorption capabilities of the diaphragm, the modified sound absorption coefficient $\tilde{\alpha}$ defined in Eq. (5.8) is computed for every case summarised in

113
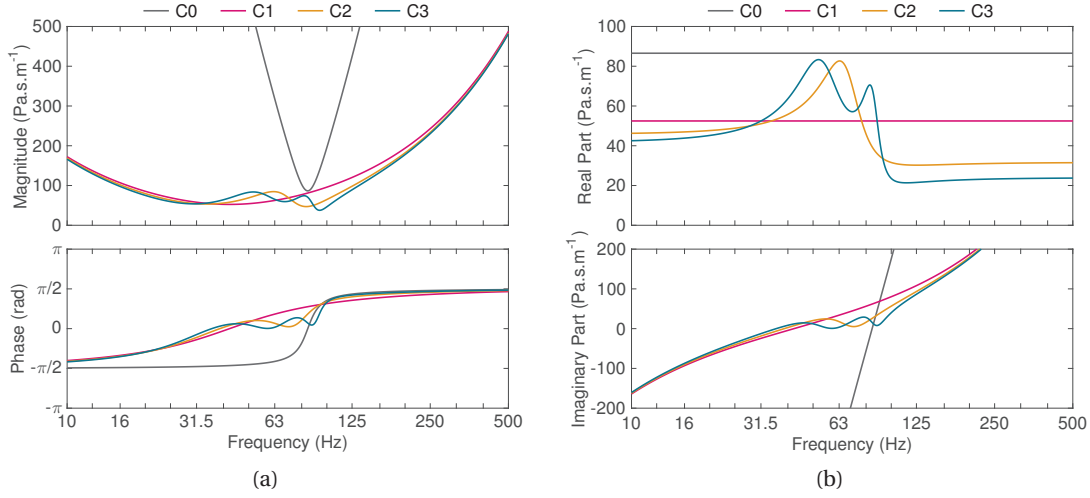
Figure 5.17 – (a) Bode plots and (b) real and imaginary parts of the specific acoustic impedance of the electroacoustic absorber, computed for the one-, two- and, three-degree-of-freedom target impedances optimised from the objective function of area over threshold, relative to the baseline configuration.

Table 5.3. The results are given in Fig. 5.18. The violet line highlights the threshold inside which the absorption is considered as efficient. Thanks to the impedance control, the absorption capabilities increase considerably at low frequencies, relative to the baseline configuration. The case C1, C2, and C3 cause a larger area of efficient absorption. However, because of the lower values of specific acoustic resistances, the cases C2 and C3 absorb less than the case C1 from around 100 Hz, even if the imaginary part of the impedances $Z_{st_{2-DOF}}(\omega)$ and $Z_{st_{3-DOF}}(\omega)$ are lower than that of the impedance $Z_{st_{1-DOF}}(\omega)$.

To compare the performance between the four cases, the threshold of efficient absorption are displayed together in Fig. 5.19, as well as the modal decay times after sorting, computed for 16 absorbers located in bottom corners of the small room S and medium rooms M1 and M2, illustrated in Fig. 5.11. As expected, the best performance is expected in case C3. Although the thresholds of efficient absorption include the optimal resistances for the first modes in the three cases, the upper bound of the bandwidth is higher in case C2 relative to the case C1, and even more in case C3. Note that the coefficient g expressed in Eq. (5.9) enables the modified sound absorption coefficient $\tilde{\alpha}(R_s, f)$ to include the minimal values of optimal resistance of the first modes.

In the case of the use of the hybrid-/shunt-based impedance control described in Chapter 4, the bode plots of the transfer function $\Theta(s)$ of order two, four, and six, computed for the cases C1, C2, and C3 respectively, are given in Fig. 5.20. Because of the low value of effective stiffness needed in the three cases, the maximal magnitude of the electrical current, at equivalent sound pressure level, is larger than that in cases B and C in Chapter 4. Decreasing the centre frequency f_0' of the electroacoustic absorber relative to the resonance frequency f_0 of the
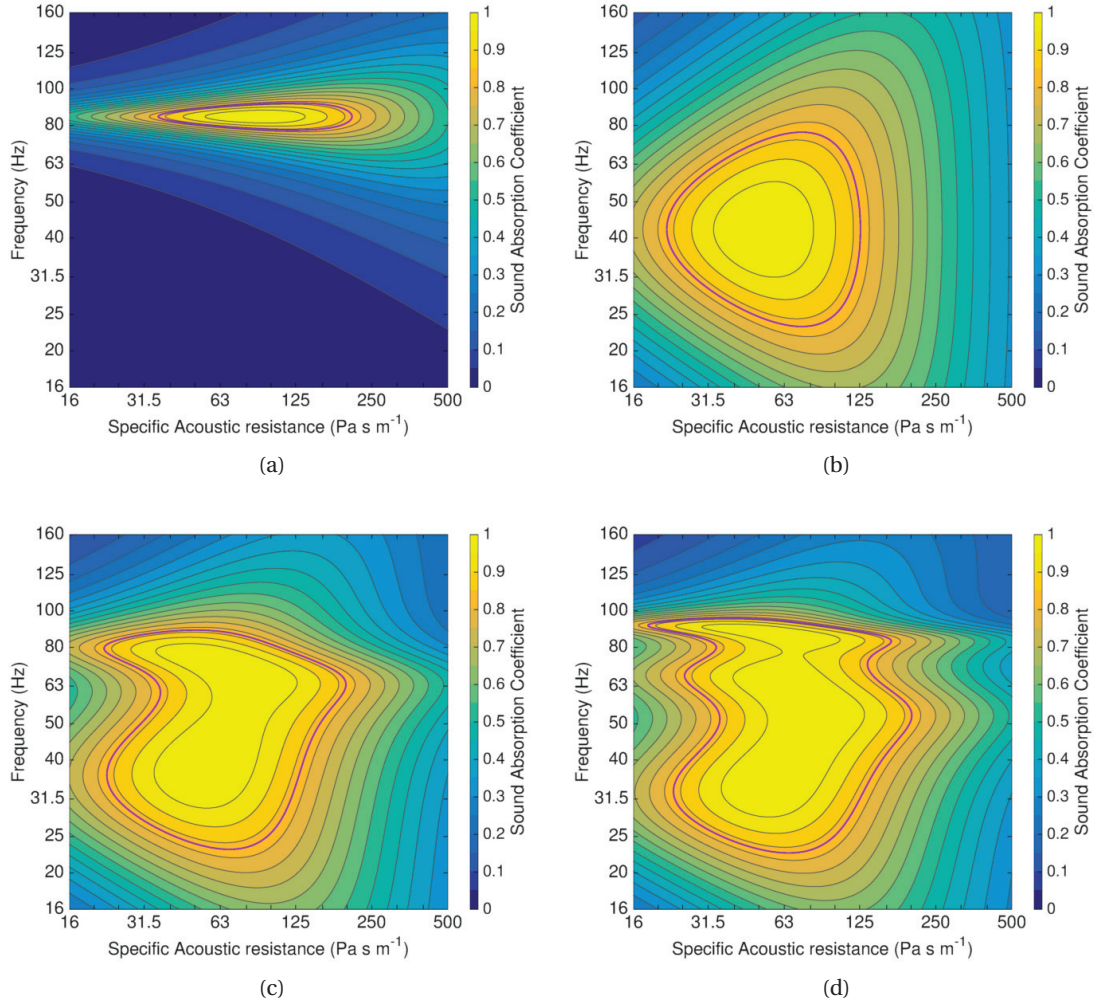
Figure 5.18 – Specific acoustic impedance – frequency maps of the normalised sound absorption coefficient for the electroacoustic absorber (a) in case C0, and optimised target specific acoustic impedances in cases (b) C1, (c) C2, and (d) C3. The violet line highlights the threshold inside which the absorption is considered as efficient.

loudspeaker system thus requires larger values of electrical power.

5.5.3   Sound absorption measurements

The absorption capabilities of the electroacoustic absorber were experimentally evaluated by measuring the frequency response function of the specific acoustic impedance at the diaphragm in a waveguide, according to the ISO 10534-2 standard [197]. The experimental setup was the same as the one described in Section 3.3.1, but the controller was different. The transfer functions $\Theta(s)$ given by Eqs. (4.1) and (5.4) were implemented onto an Analog Devices digital signal processor (Sharc processor) and discretised at $50\,\mathrm{kHz}$, whose time delay was
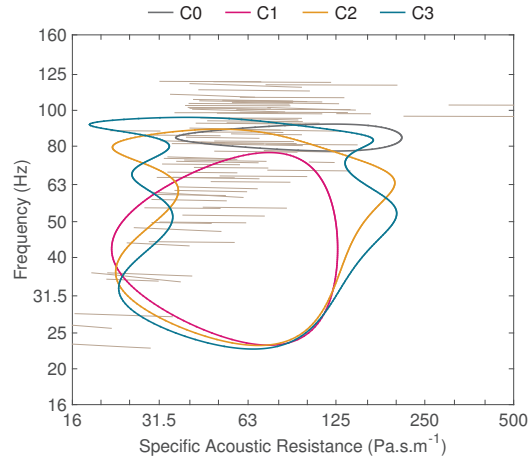
Figure 5.19 – Thresholds of efficient absorption for cases C0, C1, C2, and C3 with the modal decay times after sorting computed for 16 absorbers located in bottom corners of the small room S and medium rooms M1 and M2.
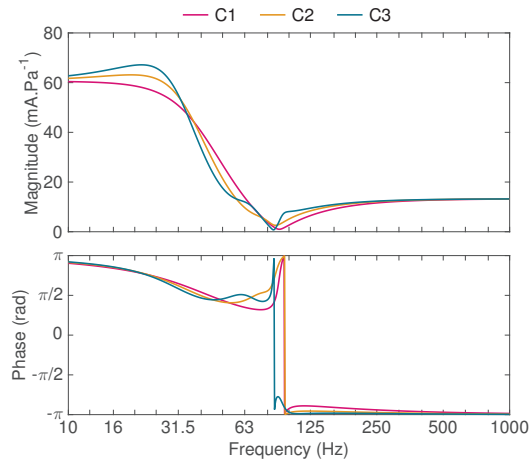
Figure 5.20 – Bode plots of the transfer function from the total sound pressure at the diaphragm to the current flowing through the voice coil computed for the cases C1, C2, and C3.

equal to 18.1 μs. The signals were converted thanks to Analog Devices analog-to-digital and digital-to-analog converters.

The results are illustrated in Fig. 5.21. The Bode plot of the measured specific acoustic impedance in case C1 is not displayed because it is similar to that displayed in Fig. 4.25a. The control modified both the acoustic resistance and reactance of the diaphragm to reach as close as possible the target specific acoustic impedances $Z_{st_{2-DOF}}(\omega)$ and $Z_{st_{3-DOF}}(\omega)$. As for the measurements in Section 4.6.2, the first modes of the electroacoustic absorber enclosure caused the resonances at 587 Hz and 655 Hz. In cases C2 and C3, the magnitude is kept below one fifth of the characteristic impedance of the air and the phase is close to zero over a broader frequency band than when the control is switched off in case C0.
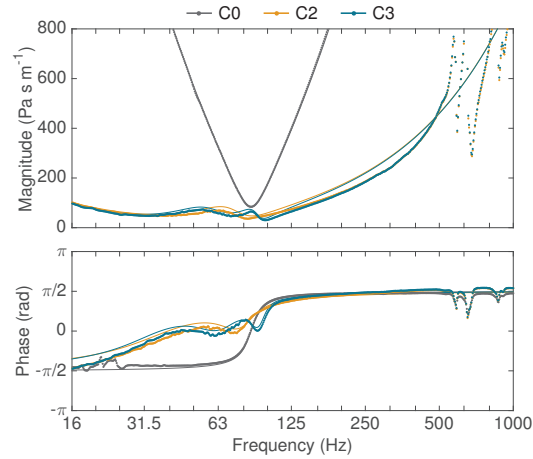
Figure 5.21 – Bode plot of the specific acoustic impedance of the electroacoustic absorber computed (solid lines) and measured (dotted lines) in cases C0, C2, and C3.

5.6 Conclusion

In this chapter, the effect of electroacoustic absorbers on the damping of modes in cavities has been investigated. In a first step, the absorbers were modelled by flat disks representing the diaphragms, where a purely resistive acoustic impedance was assigned to the effective area. Two numerical studies on unidimensional cavities were computed by varying the effective absorption surface and specific acoustic resistance at the diaphragm. The absorber causes a decrease of the modal decay times, whether its diaphragm is oriented normal to the propagation dimension (that is normal incidence) or parallel to it (that is grazing incidence), though slightly favouring the first configuration. A third numerical study on a 3D cavity, corresponding to a medium room with hard boundary conditions, has also shown the efficiency of four electroacoustic absorbers, which were located in the bottom corners, to provide an additional damping to the low-frequency modes, as shown in Sections 4.3.2 and 4.6.3. For every mode, the optimal specific acoustic resistance is dependent on the mode and total effective absorption area of absorbers: the larger the area, the lower the modal decay times. Moreover, a lightly damped room may not be turned into a good listening room with only a few perfect absorbers.

Then, the effect of the room dimensions has been studied from the simulation of three rectangular rooms of different dimensions. A given layout of a possible actual implementation of electroacoustic absorbers, with a fixed effective absorption area, was proposed for these simulations. Whatever the room dimensions for a given wall impedance value, the optimal resistances of the modes have the same profile of optimal resistances for minimising the modal decay times. The sound power dissipated in the absorbers has also been investigated from the same simulations. The results have pointed out the difficulty of finding the optimal resistance values from the absorbed sound power, and have confirmed the choice of minimising the modal decay times for the modal equalisation. Moreover, for a same room, no effect of the

variation of the wall impedance value on the optimal resistances of the modes has been found. Although this parametric study could have been done through an experimental design, it is not easy to choose only one output variable characterising the effect of the absorbers on the decrease of modal decay times. As the reactive part of the specific acoustic impedance of the absorbers is dominant at very low and high frequencies, further work should include this frequency dependence in the modelling.

Finally, taking into account the results of the simulations with the given layout of absorbers in the bottom corners, the target specific acoustic impedance at the diaphragms was optimised to minimise the modal decay times. Thanks to the optimisation of multiple degree-of-freedom target impedances, a compromise has been reached to approach at best the optimal resistance value of every mode, while keeping the reactive part very small relative to the resistive part. Then, the performance of the electroacoustic absorber has been experimentally evaluated in a waveguide, by measuring the frequency response functions of the specific acoustic impedance, for the optimised one, two, and three degree-of-freedom target impedances. The best performance is obtained for the higher degree-of-freedom impedance, causing the largest area of efficient absorption. Although higher degree-of-freedom target impedances could also be optimised, the performance is limited by the bandwidth of efficient absorption and target resistance values. To validate the results found in simulation, the performance of the electroacoustic absorbers in actual rooms will be evaluated in Chapter 6.

6 Evaluation of modal equalisation in actual listening rooms

6.1 Introduction

Modal equalisation aims at flattening the frequency response at every location and reducing the modal decay times. Preliminary experimental studies were carried out in lightly damped rooms with shunted loudspeakers [233] and sensorless electroacoustic absorbers [6]. It was shown that the control of the acoustic impedance of a few surfaces at discrete locations contributed to balance the distributions in space and frequency of the sound field, by dissipating the sound power into the electroacoustic absorber components. However, since the target specific acoustic impedance at the diaphragms were set to match the characteristic impedance of the air in these cases, the performance for modal equalisation was limited. Taking into account the investigation of an optimal value for the acoustic impedance as described in Chapter 5, better performance was obtained again in lightly damped rooms [234, 235], which are not detailed in the thesis.

The last objective of this thesis is to prove that the electroacoustic absorbers can actually improve the sound quality in the low-frequency range in any room. To do this, this chapter investigates what can be seen as the worst case to highlight the potential of the electroacoustic absorber concept for the modal equalisation, that is in actual listening rooms that are well damped at mid and high frequencies. Neither the optimal room ratio nor optimal configuration of sound sources is considered here. The electroacoustic absorbers are just set up in existing rooms intended for the sound reproduction. As it was difficult to find listening rooms, which are locally reacting (that is the waves propagating in or behind the walls do not interact with the sound field inside the room) and available for measurements, only two rooms were investigated: a showroom and a home cinema. In addition, it is not intended to characterise the studied rooms to match as best as possible the simulation with the measurements. The idea was to set up electroacoustic absorbers, whose acoustic impedance at the transducer diaphragms has been optimised, in these rooms to evaluate their performance for the low-frequency modal equalisation. In the first part, the performance of the electroacoustic absorbers is evaluated in each room through the frequency response measurements at
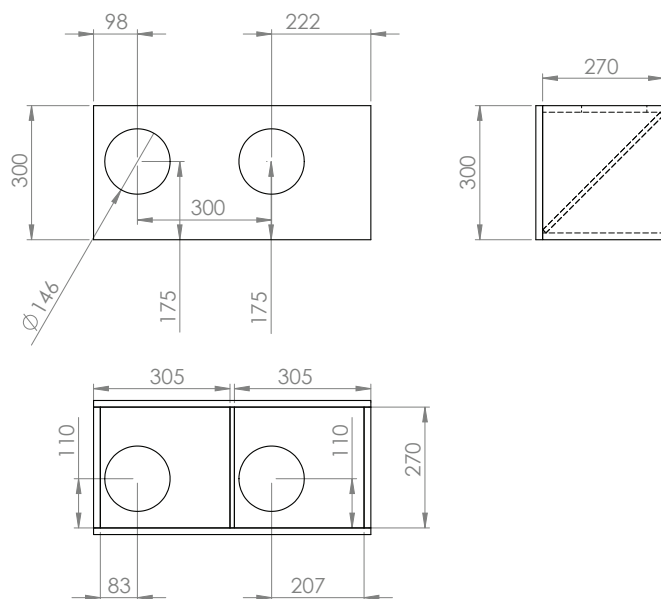
Figure 6.1 – Layout of the prototype.

different locations as well as the corresponding modal decay times. Different configurations of absorbers with the control switched on or off are compared to each other. In the second part, their effect is subjectively evaluated from a psychoacoustic perspective, and the results are compared with previous studies, which were summarised in Section 1.4.

6.2 Objective evaluation

6.2.1 Experimental setup

Prototypes of electroacoustic absorbers

Four prototypes of electroacoustic absorbers have been designed for the study. The aim was to get a large enough effective absorption area with few electronic components. Every prototype consists of four Peerless SDS-P830657 loudspeakers (used in Chapters 4 and 5) in individual boxes, which are located on two adjacent sides of a wooden cabinet (0.3 m × 0.3 m × 0.62 m), with a total effective absorption area of 0.24 m^2 as illustrated in Fig. 6.1. Only one microphone is used for the control and the four loudspeakers are connected in series because of technological constraints, such as the required electrical power. As the acoustic coupling coefficient is independent of the microphone – loudspeaker arrangement, no optimal position of the receiver exists [236]. For the first eigenfrequencies of any mode type (axial, tangential, or oblique), the sound pressure at the four diaphragms of one prototype may be considered uniform. The microphone is thus located at the edge of the cabinet between the four diaphragms, so as to limit the distance between the microphone and extremities of the diaphragms, even though the diffraction caused by the enclosure shape could alter

the specific acoustic impedance at the diaphragms above the frequency band of absorption. First, the electrical signal from the microphone is digitally converted via an Analog Devices analog-to-digital converter, then modified by the filter, which is implemented on an Analog Devices digital signal processor and whose transfer function $\Theta(s)$ is given in Eq. (4.1). The target specific acoustic impedance that is assigned to the transducer diaphragms corresponds to the impedance $Z_{st_{3-DOF}}(\omega)$ found in Section 5.5 (case C3). Lastly, the current proportional to the output voltage delivered by an Analog Devices digital-to-analog converter drives the series voice coils of the loudspeakers with the help of a voltage controlled current source, which has been described in Section 3.3.1. When the control is switched on, the sound pressure level at 1 m from one prototype in an anechoic room is 18 dB(A).

Listening rooms

To evaluate the performance of the electroacoustic absorbers, measurements were performed in two actual listening rooms. The layouts and pictures of the setup of the small and medium rooms are illustrated in Figs. 6.2 and 6.3 respectively. The small room, whose dimensions are summarised in Table 5.1 (denoted small room S), is usually used as home cinema with an arrangement of two rows of three seats. The second row of seats is raised thanks to a stage represented on Fig. 6.2a. The medium room, whose dimensions are summarised in Table 5.1 as well (denoted medium room M2), is usually used as a listening room; it has a floated floor and a false ceiling. Both rooms meet the standards set out in ITU-R BS.1116-3 [1] and IEC 60268-13 [67]. The reverberation times RT_{60} were measured according to the standard ISO 3382-2:2008 [36] (12 measurements: 2 sources, 3 microphone locations with 2 measurements for every location). The results in the medium room are shown in Fig. 6.4. Only the reverberation times at 200 Hz and 250 Hz in the medium room are just above the tolerance limits (0.04 s and 0.01 s higher respectively) required by the standards. Given these values, the listening conditions should not be disturbed for the psychoacoustic tests. For logistical reasons, the reverberation times could not be measured in the small room. Nevertheless, the tolerance limits should be [0.139 s 0.239 s] between 200 Hz and 4 kHz and the estimated modal decay times presented in Section 6.2.2 suggest that the reverberation times are between these limits. In every room, the four prototypes were located on the ground in the room corners, assuming an ideal sound pressure distribution in the room. Because of the floor layout in the small room, the prototypes were stacked up by two at two corners.

For the frequency response measurements, the usual sound diffusion system in each room was not used. Instead, a low-frequency closed box sound source, whose acoustic volume flow could be measured, was used. This sound source, represented in Figs. 6.2a and 6.3a, delivered a pink noise with the help of a Brüel and Kjaer power amplifier 2706. Frequency responses from the diaphragm velocity of the sound source to the sound pressure level at random locations were measured with a Polytec OFV-525 vibrometer sensor head and its OFV-5000 controller, with PCB 130D20 microphones, and with a Brüel and Kjaer 3160 Pulse multichannel analyser. The measurement locations are represented by black dots in Figs. 6.2a
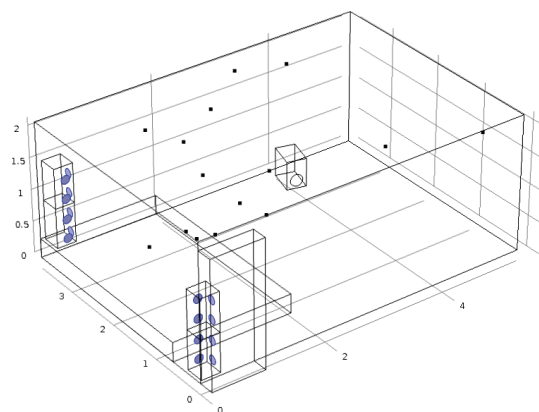
(a)

(b)
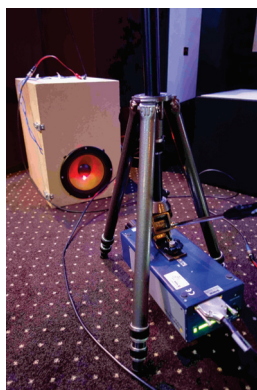
(c)   (d)

Figure 6.2 – (a) Representation of the small room with the 4 electroacoustic absorbers, the sound source used for the transfer functions and 15 measurement points ; (b), (c), and (d) Pictures of the setup (the sound source used for the transfer functions was located between the left loudspeaker and the left seat).

(a)

(b)

(c)

(d)
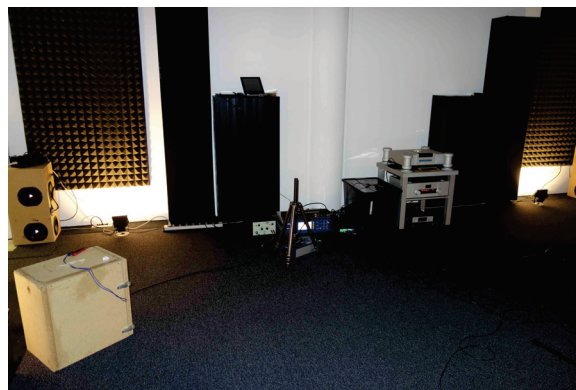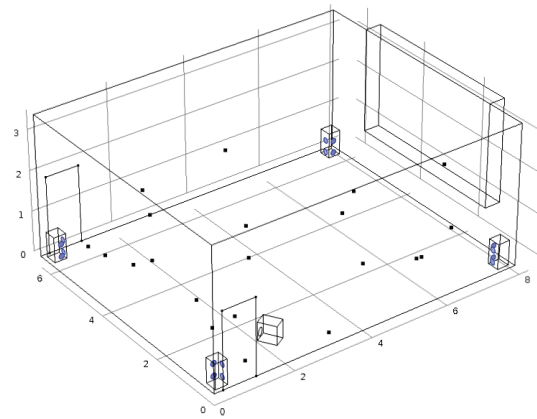
Figure 6.3 – (a) Representation of the medium room with the 4 electroacoustic absorbers, the sound source used for the transfer functions and 21 measurement points ; (b), (c), and (d) Pictures of the setup.
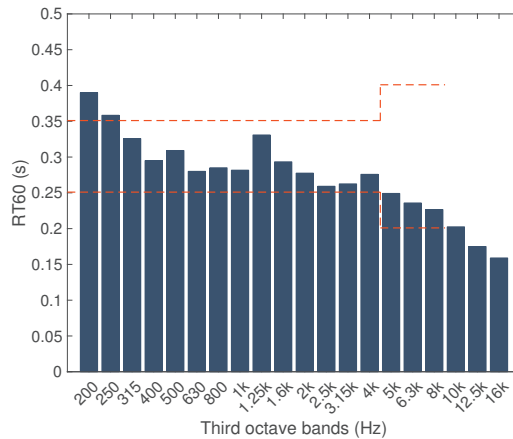
Figure 6.4 – Measurement of the reverberation time RT_{60} in the medium room with the tolerance limits (in orange) required by the standard [1].

and 6.3a (15 points for the small room and 21 points for the medium room) and summarised in Table A.1.

6.2.2 Performance evaluation

Modal equalisation

The distributions in space and frequency of the sound field were evaluated for every room through the measured frequency responses for three configurations:

- The control was switched on for the four prototypes,

- The control was switched on for two prototypes (two bottom prototypes in the small room and two rear prototypes in the medium room), and the control switched off for the two others (that is all the loudspeakers of the prototypes were in open circuit),

- The control was switched off for the four prototypes.

The last configuration was preferred in the empty room configuration to highlight the performance of the active impedance control relative to that of the passive system (that is the open circuit case). Table A.1 summarises the different locations of the measurement microphones in both rooms (see Appendix A).

The frequency responses from the diaphragm velocity of the sound source to the sound pressure level measured in the small and medium rooms are illustrated in Figs. 6.5 and 6.6 respectively. The frequency responses measured at the other microphone locations can be found in Figs. A.3, A.4, A.5, A.6, and A.7 in Appendix A. The results show that the dynamics of the sound pressure level are globally reduced, suggesting a better modal equalisation with the
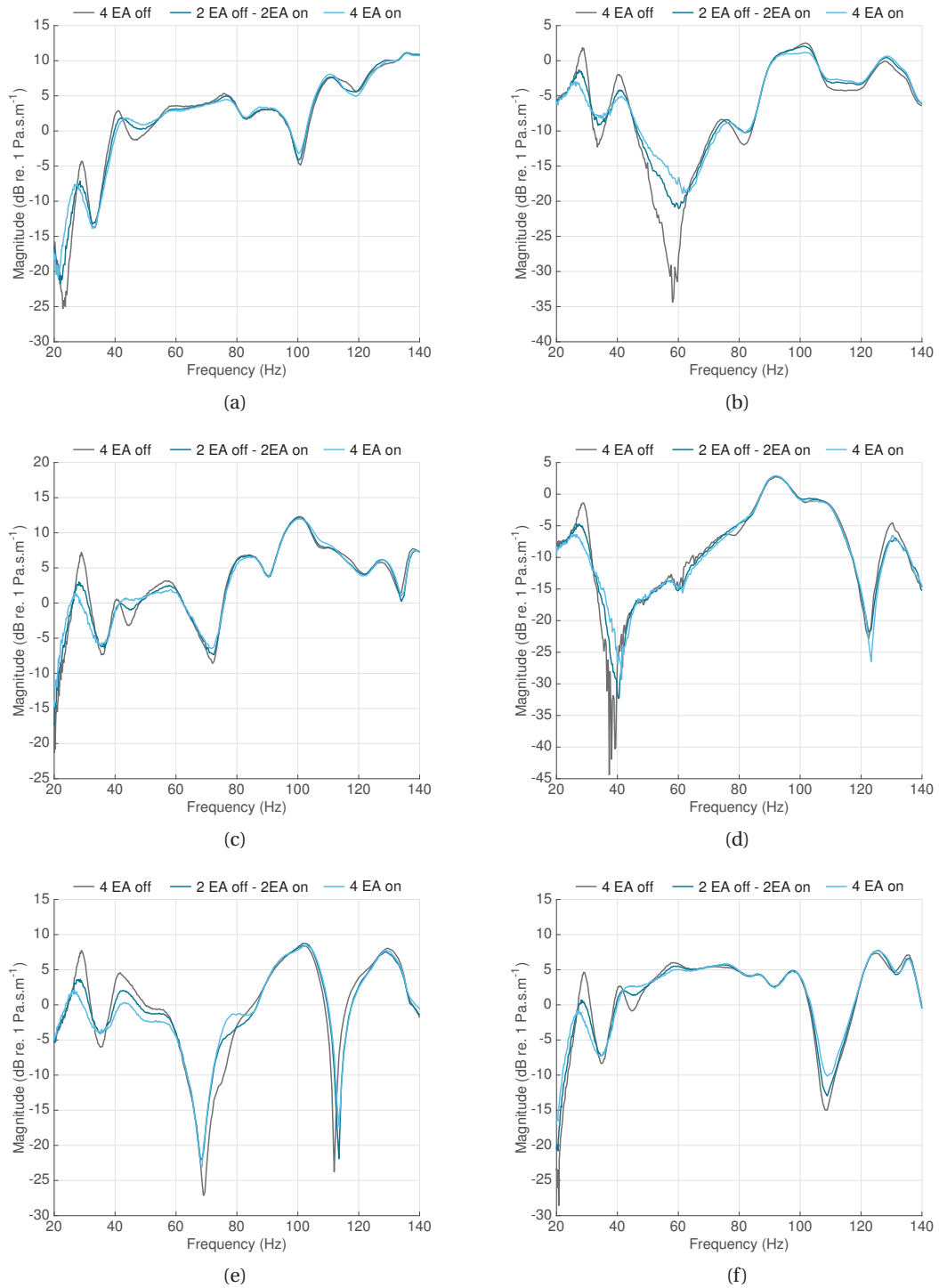
Figure 6.5 – Measured frequency responses from the diaphragm velocity of the sound source to the sound pressure level in the small room for microphone locations (a) C, (b) E, (c) F, (d) I, (e) K and (f) M.
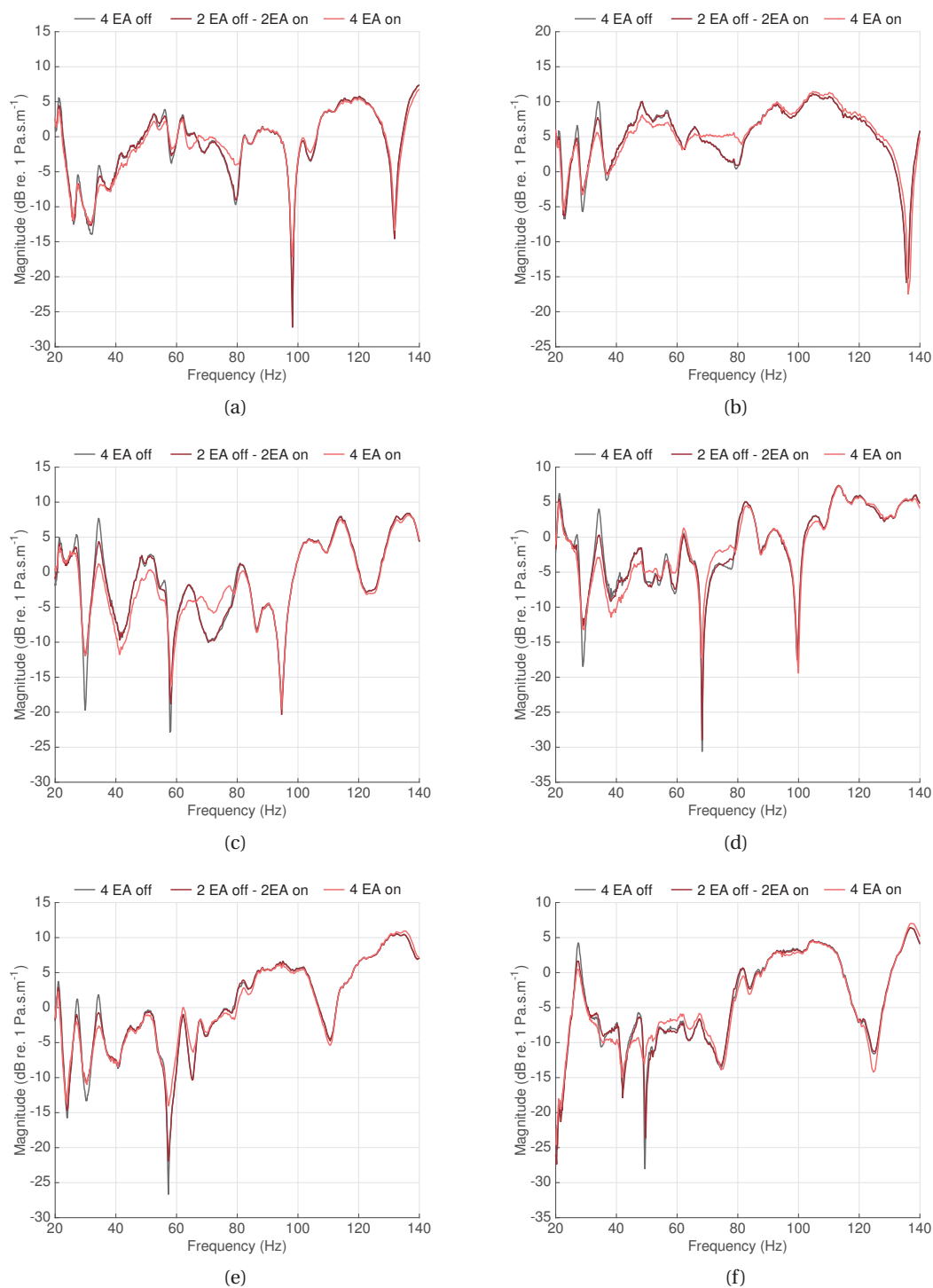
Figure 6.6 – Measured frequency responses from the diaphragm velocity of the sound source to the sound pressure level in the medium room for microphone locations (a) B, (b) G, (c) J, (d) P, (e) R and (f) T.

active impedance control. For most of the measured frequency responses, the sound pressure level dynamics between the peaks and dips are reduced. Nevertheless, a few measured frequency responses show larger dips with the control switched on relative to the control switched off (see Figs. 6.6d, A.3c, A.3d,A.5e, A.6b, A.6d, A.6e, A.6f, and A.7c). Because of the modification of certain mode shapes caused by the electroacoustic absorbers, minima and maxima of sound pressure may have shifted by a few centimetres. Thus, it is not realistic to compare the gains of sound pressure levels between two configurations for every microphone location. A more accurate evaluation of the performance for the modal equalisation would be to measure several frequency responses at different positions very close to each other, so as to observe the increase in local minima of the sound pressure level. As this method would require numerous measurements, the modal decay times may also give a representative overview of the performance for modal equalisation.

Decrease of modal decay times

The effect in terms of temporal behaviour was evaluated through the estimation of the modal decay times MT_{60} (that is the time needed for a decrease of 60 dB of the magnitude of the sound pressure level during the free response of a given mode). The modal decay time of each mode is related to its centre frequency f_{0_n} and quality factor Q_n as

$$MT_{60_n} = \frac{3\ln(10)\, Q_n}{\pi\, f_{0_n}} \tag{6.1}$$

Modal decay times can be estimated from different techniques, which were described in Section 1.2.2. However, these techniques suffer from a lack of precision and are highly sensitive to the positions at which the frequency response is measured (when the microphone is located in a minimum of sound pressure for a given mode for example). Thus, a global curve fitting technique based on rational fraction polynomials [237, 238] was preferred to estimate the modal decay times from multiple-point frequency response measurements. It was assumed that the frequency response measurements are linear and represented as a ratio of two polynomials, where the denominator is the same for all the frequency responses as long as the the waves propagating behind the walls do not interact with those inside the room. First, the coefficients of the denominator (or characteristic) polynomial, whose roots are the eigenfrequencies and corresponding damping (or quality factor), were estimated by curve fitting simultaneously all the frequency response measurements. Then, the numerator polynomial coefficients were estimated by curve fitting each frequency response by itself. Last, these coefficients were used in a numerical partial fraction expansion to yield the residue (mode shape component) for each mode and each frequency response. Figure 6.7 illustrates the curve fitting applied to the whole frequency response measurements in the small room with the control switched on for the four prototypes. This way, even for small values of modal decay times, this method is more accurate and more robust than single-point measurement estimates: the higher the number of frequency response measurements, the more accurate the parameter estimates. Nevertheless, since the measurements include some noise, this method
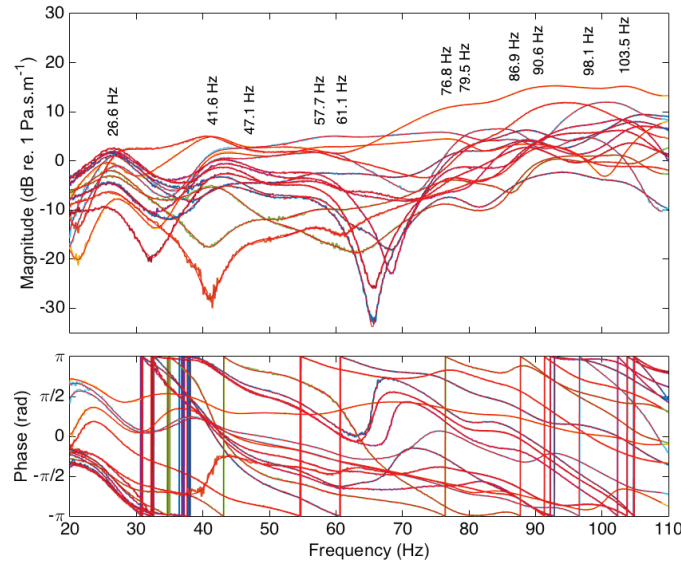
Figure 6.7 – Curve fitting (red solid lines) of the measured frequency responses (other coloured solid lines) in the small room with the control switched on for the four prototypes.

is not fully automatic and must be performed by varying frequency spans by hand.

The estimated modal decay times between 20 Hz and 100 Hz are displayed in Figs. 6.8 and 6.9 comparing the three configurations described in Section 6.2.2. The results are also summarised in box plots. On each box, the central mark is the median; the edges of the box are the 25th and 75th percentiles; the whiskers extend to the 10th and 90th percentiles; the outliers are plotted individually. The mean value of modal decay times for the small room is reduced from 296 ms (standard deviation $\sigma = 136$ ms) to 215 ms ($\sigma = 60$ ms). For the medium room, the mean value of modal decay times is reduced from 866 ms ($\sigma = 394$ ms) to 696 ms ($\sigma = 296$ ms).

Thanks to the active impedance control, the temporal acoustic response is improved. Even with a small ratio of the effective absorption area to the surface area of the walls (0.3 % in the small room and 0.12 % in the medium room), the modal decay times reduce significantly thanks to the four prototypes, except for the first mode in the medium room. The variance of the decay times among the different modes is smaller when the control is switched on, relative to that switched off in each room. The decrease is also clearly visible through the results in the small room: there is no more dominant modal decay time after switching the control on. However, adding two active supplementary electroacoustic absorbers relative to the second configuration do not significantly lower the modal decay times in the small room. As two prototypes were arranged on top of the two others, they were potentially located in minima of sound pressure for a few modes, making the absorption almost inefficient. Better results could be expected with supplementary electroacoustic absorbers in the room, which would be located in the top corners for example. Moreover, even if the impedance control is efficient, this method is limited by the ratio of the active absorption surface to the surface of the walls. The smaller this ratio is, the less audible the effect is.
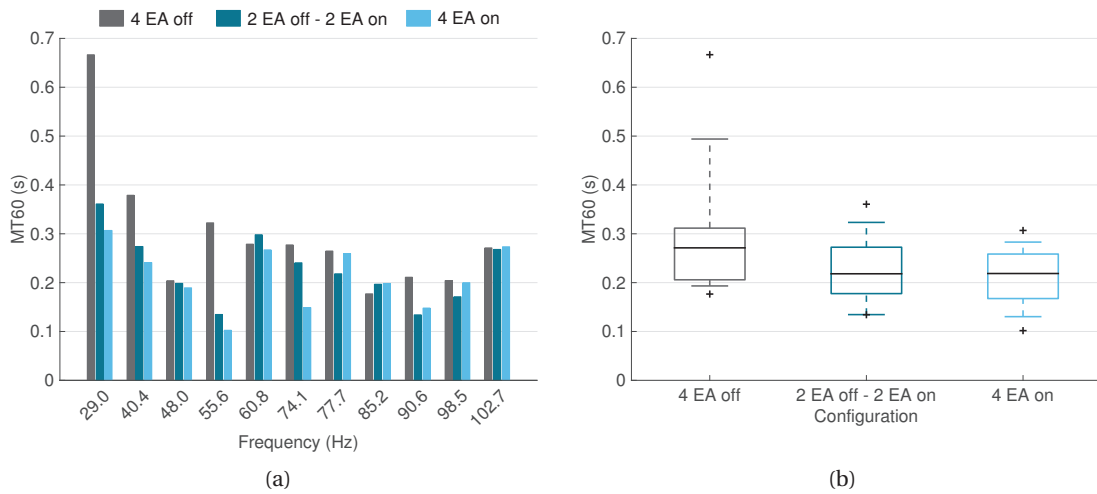
Figure 6.8 – Estimated modal decay times of the small room represented with (a) bar graphs and (b) box plots.
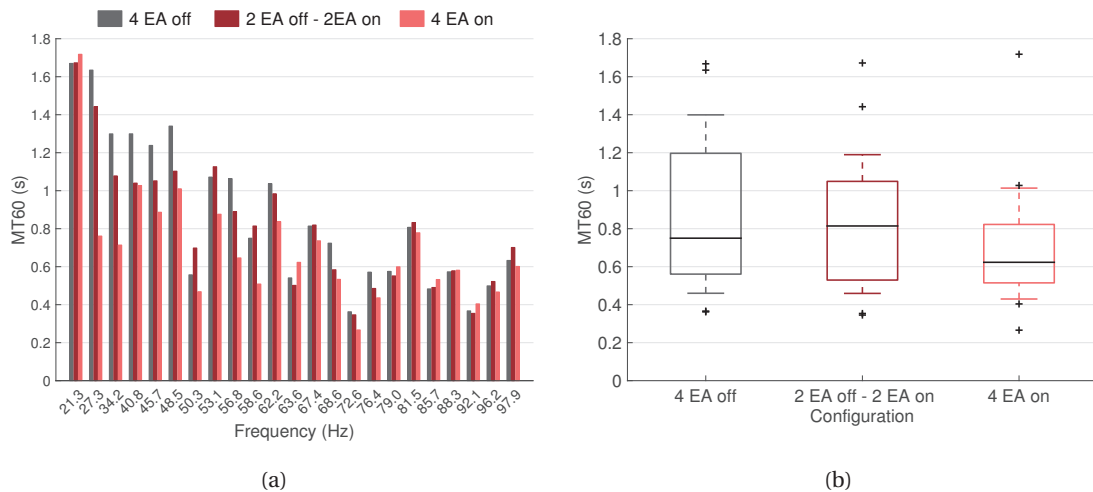
Figure 6.9 – Estimated modal decay times of the medium room represented with (a) bar graphs and (b) box plots.

6.3 Subjective evaluation

6.3.1 Problem statement

In this second part, the effect of the electroacoustic absorbers on the sound reproduction is evaluated. The rooms have been previously described in Section 6.2.1 and meet the standards set out in ITU-R BS.1116 [1] and IEC 268-13 [67]. Because these rooms were only available for a very short period, it was not possible to carry out long-lasting psychoacoustic tests in both rooms. It has then been decided to present the recorded audio samples over headphones. As

discussed in Section 1.4, the modal decay time is an important criterion in the discomfort perceived by the listener. It might be difficult to know in which specific audible attribute(s) two configurations of electroacoustic absorbers differ. In addition, the subjective preference about the low-frequency content can differ between listeners. In [239], there were significant variations in the preferred bass levels caused by differences in individual taste and listener training. The forced-choice methods requiring the nature of difference, that is asking to select the sample with the strongest or weakest characteristic, were not appropriate for this discrimination test (that is 2-/3-/4-alternative force choice, specified tetrad, specified "M + N", A-Not A). Thus, the purpose here is the evaluation of the audible perception of the impedance control of the electroacoustic absorbers relative to the case when the control is switched off. The secondary point is to know if the number of electroacoustic absorbers in the room has a significant effect on the audible perception.

6.3.2 Methodology

Variables

To avoid numerous variables, only two music samples were used for the listening test:

- Track 1: Bruno Coulais – Norbu (24 s – 30 s). It is almost 7 s in length and contains naturally long decay times between 20 Hz and 63 Hz, which can easily be audible.

- Track 2: Massive Attack – Paradise Circus (129 s – 136 s). It is around 7 s in length as well and contains a number of sparse bass notes with short decay times; it is likely to excite room modes between 50 Hz and 125 Hz.

Figs. 6.10 and 6.11 show the spectrograms of both original music samples. The audio samples were played from the original sound diffusion system in both rooms (stereo reproduction with two sets of Goldmund Logos 1N-2N-3N system for the small room and two Goldmund Apologue Anniversary system for the medium room). Because the distribution in frequency of the sound field and the temporal acoustic response were preferred to the distribution in space for this study, only one listening position was studied for each room to avoid numerous variables. The listening positions were voluntarily chosen away from the nodal surfaces of each room. A Schoeps KFM6 sphere microphone was used to record the acoustic signals with the help of a M-Audio M-Track Eight sound card as illustrated in Fig. 6.12. In the small room, it was located at the position 1.82 m × 0.97 m × 1.54 m, corresponding approximately to a listener seated in the second row of seats to the right. In the medium room, it was located at the position 1.82 m × 1.32 m × 1.65 m, corresponding to a standing listener. The audio waveforms recorded in the small room are illustrated in Fig. 6.13 (right microphone) when the control was switched off and on, as well as the original soundtrack sample waveform.

The three configurations were the same as those used in Section 6.2. Figs. 6.14 and 6.15 show the measured frequency responses from the original pink noise delivered by the sound
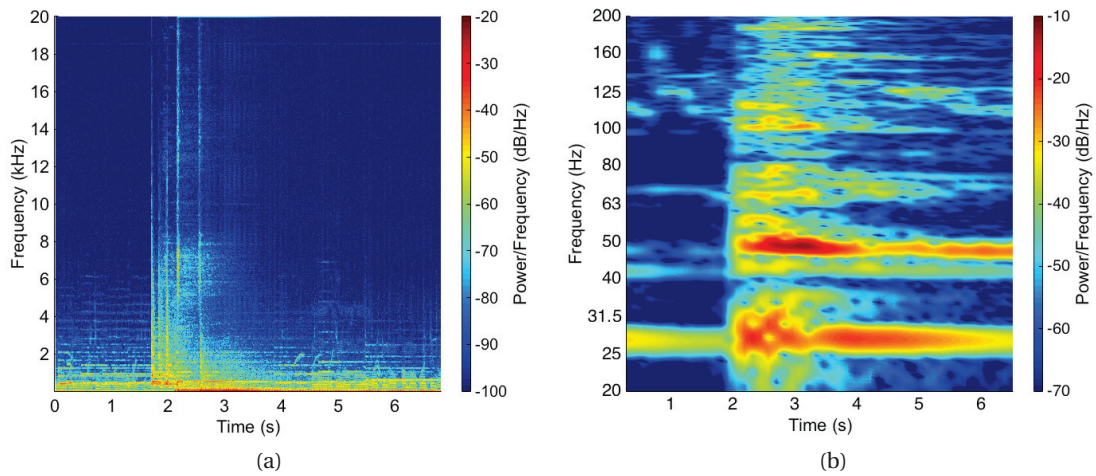
Figure 6.10 – Spectrograms of the audio sample *Track 1* (left channel) (a) from 20 Hz to 20 kHz and (b) zoom from 20 Hz to 200 Hz.
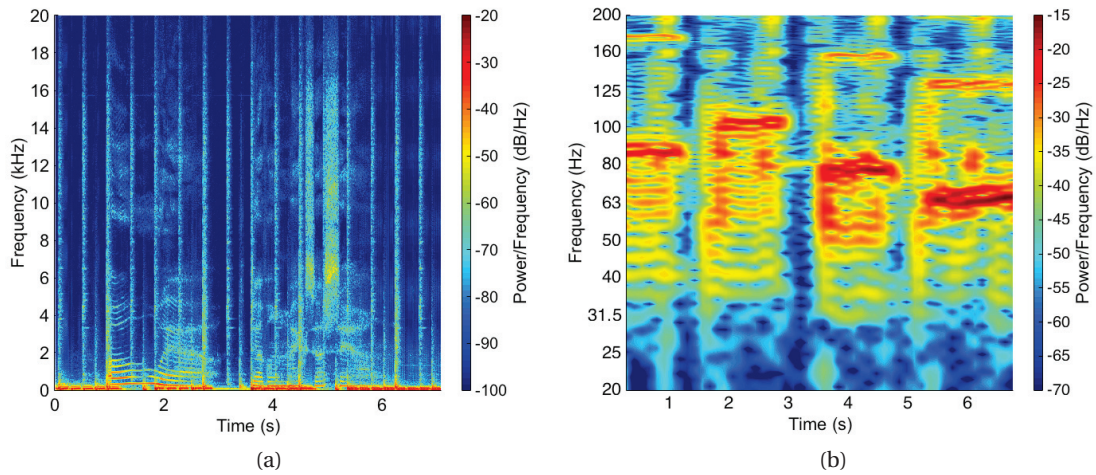
Figure 6.11 – Spectrograms of the audio sample *Track 2* (left channel) (a) from 20 Hz to 20 kHz and (b) zoom from 20 Hz to 200 Hz.

diffusion system to the sphere microphone in the small and medium rooms respectively, for the three configurations of the electroacoustic absorbers. Note that the frequency response measurements are different for the left and right channels. In addition, these frequency response measurements are almost identical between the "4 EA off" and "2 EA off & 2 EA on" configurations in the medium room.

(a)   (b)
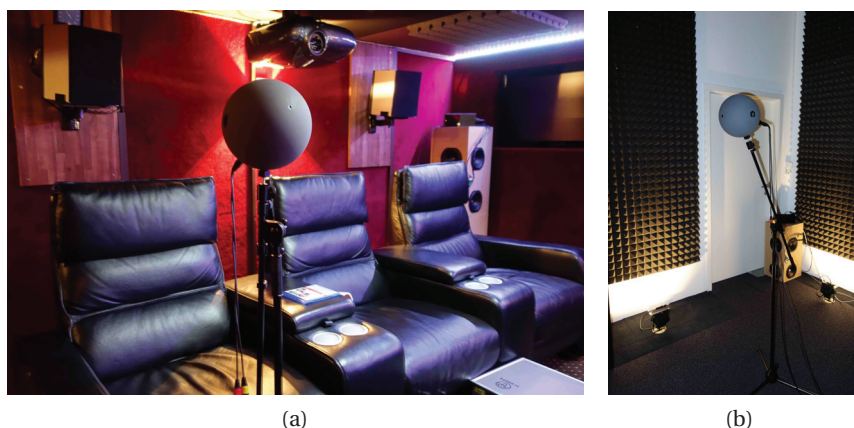
Figure 6.12 – Pictures of the setup in (a) the small room and (b) medium room for the recording of audio samples with a sphere microphone.
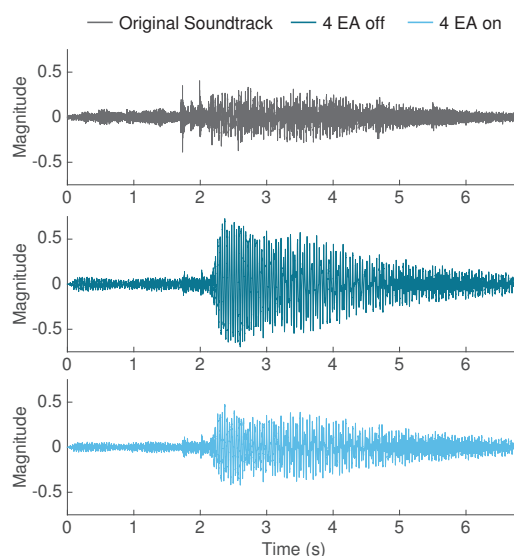
Figure 6.13 – Audio waveforms recorded in the small room as well as the original soundtrack sample waveform.

Protocol

The double constant-reference duo-trio discrimination method has been chosen for the listening tests. The double discrimination methods have lower guessing probabilities and higher test powers than the traditional discrimination methods for a given number of panelists [240]. Moreover, the duo–trio with a constant-reference has generally been found to be superior to the balanced-reference caused by the memory advantage and stability of discriminative dimension [241] (comparisons for different duo-trio methods can be found in [242–244]). It was assumed that all panellists had the same probability of giving a correct response and that all responses were independent of one another. For each comparison, three audio samples
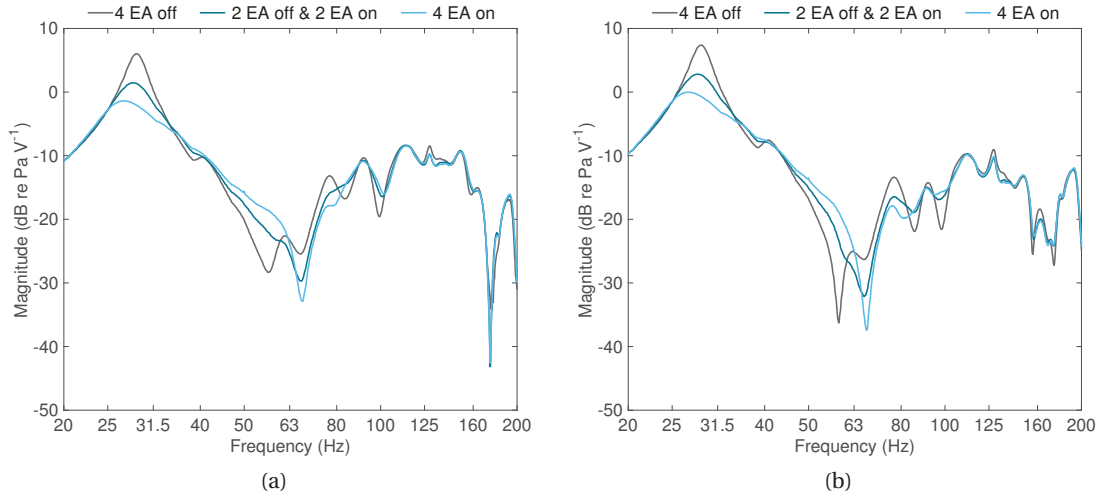
Figure 6.14 – Measured frequency responses from the original pink noise delivered by the sound diffusion system to the sphere microphone in the small room for (a) the left microphone and (b) right microphone, for the three configurations of the electroacoustic absorbers.
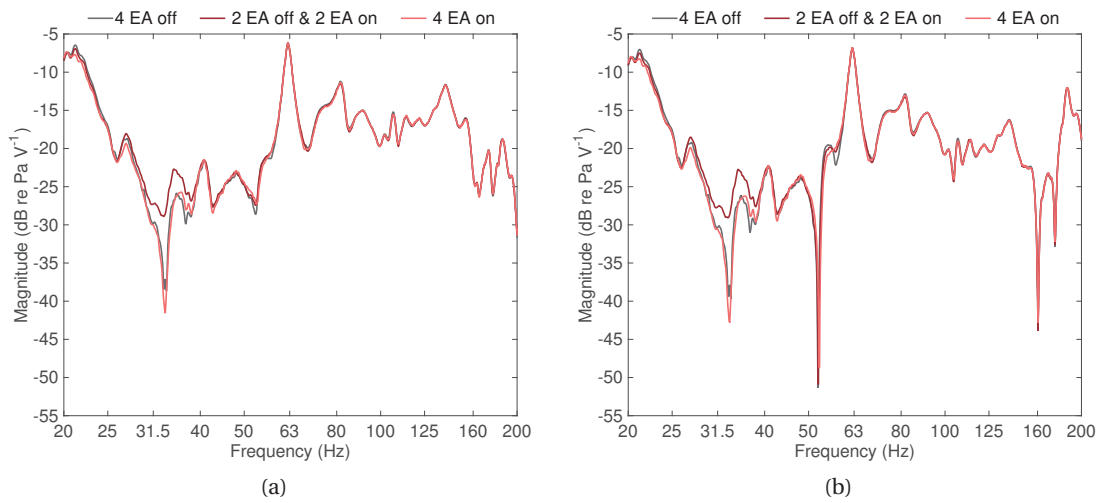
Figure 6.15 – Measured frequency responses from the original pink noise delivered by the sound diffusion system to the sphere microphone in the medium room for (a) the left microphone and (b) right microphone, for the three configurations of the electroacoustic absorbers.

were presented to the participants

- A reference always corresponding to the configuration where the control was switched off for every prototype,

- Two other samples, one corresponding to the same sample as the reference (4 EA off) and the other one corresponding to one of the two other configurations, that is where the

133

control was switched on for every prototype (4 EA on), or switched on for two prototypes and switched off for the two others (2 EA off - 2 EA on).

The participants were asked to determine which sample was the same as the reference presented first. They were able to listen several times every comparison and to take breaks. To verify that a participant could really judge the difference, they had to answer correctly two times, reducing the probability of the subject guessing to 25 %. A total of 24 comparisons were presented for every participant, including 8 comparisons for the training, so as to get accustomed with the audio samples and requested task. All the tests were randomised between participants so as to avoid presentation bias. A user interface recorded the answers of the participants.

Equipment

The reproduction system consisted of the test computer, the sound card that was used for the audio recording in both rooms, and the equalised headphones. The test took place in the listening room at Ecole polytechnique fédérale de Lausanne, which meet the standards set out in ITU-R BS.1116 [1]. Audio samples were delivered in stereo through a pair of Beyerdynamic DT770 Pro 250 Ω. Headphones equalisation consisted of a 2000 tap finite impulse response filter corresponding to the inverse of the frequency response of both channels measured on the sphere microphone via the sound card. The target response was a flat magnitude response up to 16 kHz, to maintain the overall original balance of the music recording in every room. Fade-in and fade-out with window length of 10 ms were added to the audio samples to prevent audible artefact effects, which could not be related to the recorded samples. These fade-in/-out window times were well below the modal decay times estimated from the measurements.

After compensating the headphones, the loudness of each audio sample was normalised with the help of an algorithm provided by Genesis according to ANSI S3.4-2007 [245]. The presentation level to participants was set to 85 phons, which was considered to be a suitable realistic level for music reproduction in room, and without introducing acoustical distortion from the headphones. This audition level was also chosen so as to compare the results with those of previous studies, which have showed the possible difficulty to compare two different samples at lower audition levels [2]. In order to calibrate the loudness level of the audio samples, a standard 1 kHz sine tone was used as a reference (at 1 kHz, 1 dB SPL = 1 phon). The tone was played through the headphones on a Brüel and Kjaer 4157 ear simulator. The level was measured with a 01dB NetdB sound analyser and the output from the sound card was adjusted until reaching the desired level. This tone was then passed through the loudness algorithm to obtain a reference loudness value for the 1 kHz tone appearing at the ears at 85 dB SPL. The music samples were then passed through the algorithm and adjusted by the appropriate gain factor such that the overall sample loudness was considered perceptually similar to the 1 kHz tone.

Panel

There were 17 participants (1 female, 16 males), ranging from 19 to 62 years old. As pointed out in the study in [246], the trained listeners are the most discriminating and reliable listeners. Thus, the participants were musicians playing bass guitar or double bass (professional or amateur), sound engineers (former or current), or people who were used to this type of exercise (and sensitive to small perceptual differences). No participant reported any serious hearing impairment. The overall test duration varied among participants (including the training session), with an average duration of 34 min. As the listener had the option of taking breaks, the effect of fatigue on the reliability of subjective evaluations was considered to be negligible. The study was approved by the Human Research Ethics Committee of the Ecole polytechnique fédérale de Lausanne, to ensure that it was designed in compliance with fundamental ethical principles.

6.3.3 Results

Test statistic

The test statistic, which follows approximately a standard normal distribution, is used to conclude, through the p-value, if there is a significant audible perception between two configurations of the electroacoustic absorbers for each comparison. The significant level α_I is equal to 0.05, the null hypothesis H_0 is $p_c = p_0 = 1/4$, and the alternative hypothesis H_1 is $p_c \neq p_0 = 1/4$. Two types of errors can be made in discrimination testing: type I error α_I and type II error β. The probability $1 - \beta$, called the power of discrimination testing, defines if the null hypothesis is correctly rejected when it is false. This probability therefore depends on the specified alternative hypothesis. The tests generally are required to reach at least 0.8 for the testing power [247]. For every comparison, the proportion of discriminators p_d for the configurations (also called the proportion of correct responses above chance) is also estimated, which exclude the guessing effect contrary to the proportion of correct responses p_c ($p_c = p_d + p_0(1 - p_d)$). However, note that this proportion is still dependent on the method used, and is therefore not a pure index of discrimination. The efficiency of a given method is mainly based on the Thurstonian δ, which is a good index of discriminability, because it is independent of the chosen method, contrary to the proportion of correct responses for example [247]. As the true δ cannot be observed, the estimate d' is generally used and its precision is expressed by its variance or 95 % confidence interval (denoted C.I.). This estimate is computed from the proportion of correct responses p_c and chosen discrimination method.

Considering all the comparisons together, the proportion of correct responses p_c is 0.493 and the proportion of discriminators p_d is 0.459 with a 95 % confidence interval [0.205 0.712]. The estimate d' is 1.715 with a 95 % confidence interval [0.708 2.722], the Z-value is 2.030, and the corresponding p-value is 0.021. As the corrected tested power for the test is equal to 0.51 < 0.8, the test is not considered significant despite the result of the test statistic. Table 6.1 presents the results for each comparison for the discrimination testing. R1 refers to the medium room

Table 6.1 – Results of comparisons for the discriminating testing.

Test	p_c	p_d (95 % C.I.)	d' (95 % C.I.)	Pow.*[a]	Z-val.	p-val.
R1 T1 A02	0.471	0.435 (0.182 0.688)	1.630 (0.611 2.649)	0.428	1.820	0.034
R1 T1 A04	**0.706**	**0.686 (0.455 0.917)**	**2.686 (1.600 3.771)**	**0.977**	**4.061**	**0.000**
R1 T2 A02	0.176	0.122 (0.000 0.315)	[b]	0.000	-0.980	0.837
R1 T2 A04	0.235	0.184 (0.000 0.399)	[b]	0.000	-0.420	0.663
R2 T1 A02	**0.706**	**0.686 (0.455 0.917)**	**2.686 (1.600 3.771)**	**0.977**	**4.061**	**<0.001**
R2 T1 A04	**0.941**	**0.937 (0.818 1.000)**	**4.609 (2.602 6.616)**	**1.000**	**6.301**	**<0.0001**
R2 T2 A02	0.412	0.373 (0.123 0.622)	1.363 (0.274 2.452)	0.230	1.260	0.104
R2 T2 A04	0.294	0.247 (0.016 0.478)	0.663 (0.000 2.474)	0.000	0.140	0.444

[a]Pow.* corresponds to the corrected testing power.
[b]There is no value of d' because $p_c < p_0 = 1/4$.

and R2 refers to the small room. T1 refers to Bruno Coulais – Norbu and T2 refers to Massive Attack – Paradise Circus. A02 corresponds to the comparison between 4 EA off and 2 EA off - 2 EA on, and A04 corresponds to the comparison between 4 EA off and 4 EA on. This table reports, for every test, the proportion of correct responses p_c, the proportion of discriminators p_d, the estimate d', the corrected testing power Pow.* that takes into account the correction factor of the sample size, the Z-value and its associated p-value. From these results, three configurations are considered significantly different: *R1 T1 A04*, *R2 T1 A02* and *R2 T1 A04*. As the corrected tested power for the first configuration is equal to 0.43 < 0.8, this configuration is not considered significant despite the result of the test statistic. Although the sample size of the test is small, the three configurations, which are considered significantly different, have high values of corrected testing power. These results could be compared with other difference tests (2-/ 3-/4-alternative force choice methods or triangular methods for example) thanks to the estimate d' of the Thurstonian δ for a same significance level α_I [247].

Effects of variables

A binomial logistic regression is also performed to ascertain the effects of room, track and absorber on the likelihood that participants can perceive audible differences. The criterion of statistical significance is kept at 0.05. The logistic regression model is statistically significant, $\chi_2(3) = 33.572$, p < 0.0005. The model explains 29.2 % (Nagelkerke R^2) of the variance in audible perception and correctly classifies 71.3 % of cases. The sensitivity, which is the percentage of cases that had the observed characteristic correctly predicted by the model (that is true positives), is 71.6 %. The specificity, which is the percentage of cases that had not the observed characteristic correctly predicted by the model (that is true negatives), is 71.0 %. The positive predictive value, which is the percentage of correctly predictive cases with the observed characteristic compared to the total number of cases predicted as having the characteristic,

Table 6.2 – Logistic regression predicting likelihood of audible perception based on room, track, and absorber.

	B	$S.E.$	Wald	df	p-val.	exp(B) (95 % C.I.)
Constant	-1.324	0.683	3.760	1	0.052	0.266
Room	**-0.977**	**0.400**	**5.964**	**1**	**0.015**	**0.377 (0.172 0.825)**
Track	**1.953**	**0.402**	**23.608**	**1**	**0.000**	**7.048 (3.206 15.494)**
Absorber	-0.532	0.393	1.828	1	0.176	1.702 (0.787 3.680)

is 70.6 %. The negative predictive value, which is the percentage of correctly predictive cases without the observed characteristic compared to the total number of cases predicted as not having the characteristic, is 72.1 %.

Of the three predictor variables, two are statistically significant: room and track, as shown in Table 6.2. The regression coefficient B, which give the linear combination of the explanatory variables that best predict the log odds, the odds ratio indicated as exp(B), the standard error $S.E.$ around the coefficient for the constant, the Wald statistic to test the statistical significance, the degree of freedom df of each variable, and the associated p-value are reported in this table. In the psychoacoustic test, the first audio sample has 7 times higher odds than the second one and the small room has 2.6 times higher odds than the medium one to perceive audible differences between two different configurations of electroacoustic absorbers. Even if the modal decay times are shorter in the small room, decreasing the volume of the room is associated with an increased likelihood of audible perception. However, no prediction can be done about the different configurations of the electroacoustic absorbers in rooms.

Interaction effects between variables

A second binomial logistic regression is performed to ascertain the interaction effects between room, track and absorber on the likelihood that participants can perceive audible differences. The variables Room × Track, Room × Absorber, and Track × Absorber are added to the model. One standardised residual with a value of standard deviation equal to -3.089 is kept in the analysis. The logistic regression model is statistically significant, $\chi_2(6) = 37.100$, p < 0.0005. The model explains 31.8 % (Nagelkerke R^2) of the variance in audible perception and correctly classifies 72.1 % of cases. The sensitivity is 59.7 %, the specificity is 84.1 %, the positive predictive value is 78.4 %, and the negative predictive value is 68.2 %. Of the three predictor variables, none is statistically significant as shown in Table 6.3. Note that the interaction between the variables track and absorber is the most important.

Table 6.3 – Logistic regression predicting likelihood of audible perception based on room, track, absorber, and their first interaction effects.

	B	*S.E.*	Wald	df	p-val.	exp(B) (95 % C.I.)
Constant	-0.308	1.028	0.090	1	0.765	0.735
Room	-0.921	1.351	0.465	1	0.495	0.398 (0.028 5.621)
Track	0.164	1.282	0.016	1	0.898	1.178 (0.095 14.533)
Absorber	-.200	0.649	0.095	1	0.758	0.819 (0.230 2.919)
Room × Track	-0.517	0.821	0.397	1	0.529	0.596 (0.119 2.979)
Room × Absorber	0.119	0.828	0.021	1	0.886	1.126 (0.222 5.710)
Track × Absorber	1.400	0.830	2.846	1	0.092	4.055 (0.797 20.624)

6.3.4 Discussion

The results show that the effect of the electroacoustic absorbers can be perceptibly audible, mainly depending on the given listening room and chosen music sample. The number of absorbers for modal equalisation seems less important. Obviously, the higher the number of absorbers, the more perceptible the effect. But doubling the number of electroacoustic absorbers with the control switched on does not make much difference: it is less perceptible than listening another music track for example. Note that the sound reproduction could also be done from recordings with natural sounds, such as musical instruments for example.

Although the purpose was different in the studies [2, 33, 186] summarised in Section 1.4, which have investigated perceptual thresholds, some comparisons can be made with the present results. While the modal decay times in the medium room are too high to be compared to the thresholds, those obtained in the small room are more interesting for the comparison. As the playback levels were the same, the modal decay times in the small room are superimposed in Fig. 6.16 with the map of perceptual regions for modal decay time proposed in [2]. The threshold in dashed line was obtained with artificial samples reproduced at 85 dB SPL. The "modal threshold" line corresponds to the shortest audible modal decay time, which has been derived from the lower 2.5 % confidence interval of the data with artificial samples. The highest threshold was obtained from the average of tests with music samples for the two replay levels tested (75 dB SPL and 85 dB SPL). As highlighted in Fig. 6.16, the modal decay times in the small room, which have been estimated from the frequency response measurements, are shorter than the lowest threshold below 63 Hz and similar to the threshold obtained with artificial samples in the previous study above this frequency. Note that the audible perception was found significant for one of the two music samples proposed in this study, even though the modal decay times are below the threshold values of decay acceptable for music. According to the remarks of listeners for the comparisons involving the Track 1 in the small room (tests R2 T1 A0X in Table 6.1), their decision during the test was mainly caused by the difference of the modal decay time of the first mode between the three configurations. As noticed in [2],
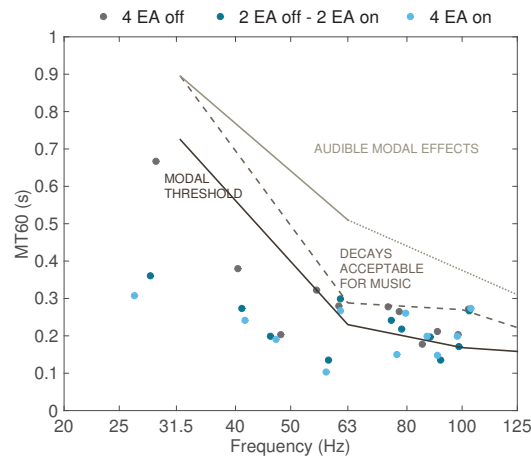
Figure 6.16 – Estimated modal decay times of the small room with the modal thresholds obtained in [2] with artificial (dashed line) and music (dotted line) samples.

the characteristics of music, that is its tonal, transient, and temporal contents, play a part in revealing modal problems in rooms. This remark is confirmed in this study, where the natural long decay time in the Track 1 at around 28 Hz (see Fig. 6.10b) corresponded exactly to the first mode in the small room, highlighting the modal problem caused by the coupling with the room. Nevertheless, the small differences above 63 Hz (and even above 100 Hz) might have helped influence the decision of the participants.

The proportions of correct responses for comparisons involving the Track 2 are too low to be significantly perceptible whatever the room. As can be seen in Fig. 6.11b, the dominant frequencies in the low-frequency spectrum of Track 2 are between 63 Hz and 100 Hz. The threshold of efficient absorption for the control switched off (case C0) is between 75 Hz and 95 Hz, while that for the control switched on (case C3) is between 23 Hz and 100 Hz (see Fig. 5.19). It partly explains why the effect of the electroacoustic absorbers might therefore be difficult to be highlighted with the Track 2. However, it might be significantly perceptible relative to the empty room configuration. It is worth noticing that the audible perception from the sound diffusion system in the listening room or over equalised headphones might be different. Headphones can only reproduce the information given by the listener's ears and not by the listener's body like the vibrations for example. It would be interesting to carry out similar psychoacoustic tests in real conditions in the listening rooms.

Moreover, the impedance control does not change the acoustics of the room at higher frequencies, contrary to a correction with passive absorbers. These devices are efficient even without specifically optimising the target specific acoustic impedance at the diaphragm for a given room. At some frequencies, the sound pressure at the diaphragms may actually be different (for frequencies between two modes for example). For better performance, some microphones could be added to the prototypes, so as to obtain more precise values of the sound pressure in front of every transducer diaphragm. Another improvement in the performance of the

electroacoustic absorber would be to add multi-layered elements, like in [248] for example, so as to absorb at mid and high frequencies as well.

6.4 Conclusions

The effect of electroacoustic absorbers on modal equalisation of two actual well damped listening rooms was investigated. Four prototypes, each constituted of four 6" loudspeakers, were set up in the bottom room corners, whose target impedance found in the Chapter 5 was assigned to the transducer diaphragms. The results showed a decrease in the dynamics of the frequency responses at different locations, improving the sound reproduction without lowering the performance of the sound diffusion system. The temporal behaviour was also improved with an overall decrease of the modal decay times in both rooms. The first advantage of this technique is that the electroacoustic absorbers can be easily moved from one room to another, relative to some active equalisation-based systems. Even if the furniture is moved in the room or a door is slammed, the control remains stable and is not deteriorated.

To evaluate the audible effect of the electroacoustic absorbers, a preliminary psychoacoustic test has been carried out from two audio samples recorded in every room. Two configurations of electroacoustic absorbers were compared (half of them switched off and others switched on for the one, and all switched on for the other) relative to the case where all were switched off. Results showed that the audible perception was independent on the number of electroacoustic absorbers, but significant effects were found depending on the given room and selected music samples. That is to say, the effect of the electroacoustic absorbers on the sound reproduction might not be perceived in every case: it mainly depends on the chosen audio sample and the given listening room.

Conclusion

The work reported in this thesis intended to validate the use of a limited number of active absorbers for the modal equalisation in listening rooms, paving the way to a wide range of possible applications and future studies on low-frequency perception in music. Despite the great academic and industrial interest on the topic, still few actual applications make use of such a technology to improve the listening conditions at low frequencies. In the frame of an industrial project, different specifications were imposed for the absorber design, such as the necessity of a silent and "plug-and-play" device, and the ability of the control to perform in any room. Moreover, the definition of new performance metrics were required to evaluate and optimise their performance. A psychoacoustic study was also required to evaluate the audible effect of the electroacoustic absorbers in actual listening rooms. The original contributions and further work of research are presented hereafter.

Original contributions

Design guidelines for setting electroacoustic absorbers

• Impedance control through multiple degree-of-freedom resonators
Guidelines have been provided to design different electroacoustic absorber systems through electrical and mechanical resonators constituted of conventional components. From the shunt-based methods and a judicious arrangement of several loudspeakers in an enclosure, this may result in two or three degree-of-freedom resonators. Nevertheless, this approach might be limited in the case where the target specific acoustic resistance value is low, as it is the case in rooms. The absorption performance may be improved by designing high degree-of-freedom resonators, but to the price of a more complex implementation.

• Impedance control through sensorless velocity feedback
The design based on self-sensing methods with a dual coil electrodynamic loudspeaker has then been investigated. Using a linear relationship of the voltages at the primary and secondary coils combined with a current driving method, the diaphragm velocity can be derived, so as to assign a target specific acoustic impedance at the diaphragm. However, because of the use of the transducer both as an actuator and a sensor, the absorption performance is limited by

transducer model uncertainties and control stability.

• **Hybrid sensor-/shunt-based impedance control**

A hybrid impedance control merging sensor- and shunt-based methods has thus been developed. From a functional relationship between the measurement of the sound pressure at the transducer diaphragm (or diaphragm velocity) and the electrical current flowing through the voice coil, the target specific acoustic impedance can be assigned as in the previous approach. Stability and absorption performance have been studied in the presence of uncertainties in the transducer model and possible control limitations, and the power balance of the electroacoustic absorber has been investigated as well. This third control strategy presents a much broader and stable low-frequency electroacoustic absorber.

Performance optimisation

• **Definition of new performance metrics**

To maximise the absorption performance of the electroacoustic absorber, different optimisations have been carried out from the definition of some performance indicators, such as the bandwidth of efficient absorption and corresponding threshold of sound absorption coefficient, and a derived absorption coefficient relative to the frequency and specific acoustic resistance. As it might be difficult to find the optimal values for the parameters of the developed multiple degree-of-freedom resonators, two strategies have been proposed to maximise the bandwidth of efficient absorption or the absorption capabilities relative to a minimal efficiency criterion.

• **Methodology for performance improvement**

In the cases where the absorption surface is much smaller than the wall surface area, relationships between implementation and performance of the absorbers have been established through simulations for different configurations. For each eigenfrequency, the optimal specific acoustic resistance is dependent on the mode shape, the geometry of the room, the effective absorption area, and the location of absorbers, but independent on the wall impedance. For the control strategies where a target acoustic impedance can be directly assigned, a multiple degree-of-freedom specific target acoustic impedance has thus been optimised to lower the modal decay times.

Performance evaluation for modal equalisation

• **Development of demonstration prototypes**

Prototypes of electroacoustic absorber, whose multiple degree-of-freedom target specific acoustic impedance has been optimised, have been implemented. These devices can be easily moved from one room to another, are "plug-and-play", and do not make any audible sound.

Even if the furniture is moved into the room or a door is slammed, the control remains stable and is not deteriorated. The other advantage of the impedance control is that this technology does not affect the room acoustics at mid and high frequencies, contrary to a low-frequency correction with passive absorbers. The demonstration prototypes are also a pedagogical tool to highlight the audible effect of room modes at low frequencies, thanks to the control switch in real time.

• **Objective evaluation**

The electroacoustic absorber concept has first been validated in a waveguide, showing the feasibility for damping the resonances at low frequencies. The performance of the prototypes has then been investigated in actual listening rooms that are well damped at mid and high frequencies. To highlight the potential of the proposed concept in the worst conditions, frequency response functions have been measured and modal decay times have been estimated through a global curve fitting technique from these measurements. The results have shown a decrease in the dynamics of the sound pressure level at different locations, improving the sound reproduction without lowering the performance of the sound diffusion system. The temporal behaviour has also been improved with an overall decrease of the modal decay times. Even if the frequency response functions are still far from being flat, such active absorption through electroacoustic absorbers may be adequate to achieve a good listening experience.

• **Subjective evaluation**

The audible perception has been subjectively evaluated through a psychoacoustic study over headphones. The effect of the electroacoustic absorbers on the sound reproduction might not be perceived in every case: it mainly depends on the chosen audio sample and given listening room. As a result, the main drawback might be the inefficiency of this correction procedure, if the ratio of the absorption area to the wall surface area is very small. Nevertheless, a listening over headphones might not give as much information as in real conditions in the room to evaluate this effect accurately. This preliminary study paves the way for other psychoacoustic tests, where the modal decay times of any room may be lowered in real time thanks to the absorbers, in contrary to other studies based on samples filtered by a frequency response function of a modelled room.

Further work

• **Absorber design**

In the frame of an industrial project with specific constraints, the different strategies proposed in this thesis have been based on commercial electrodynamic loudspeakers, which are not intended for this application. As pointed out in Section 2.2.2, the higher the ratio S_d/M_{ms}, the wider the bandwidth of efficient absorption. Ideally, the loudspeaker should be the lightest and the least stiff to avoid consuming a lot of electrical power, while the acoustic resistance is

already in the range of optimal values. On the other hand, the loudspeaker could be replaced with a plate controlled by another type of electrodynamic actuator, so as to increase the effective absorption area for example.

• Development of electroacoustic absorber-speaker systems

Another direction of research would be the investigation of possible electroacoustic absorber-speaker systems, so as to emit sound and damp the low frequency modes at the same time. To merge the sound generation function with the sound absorption capability (through the hybrid impedance control) in a unique system, the driving electrical currents related to each function must be combined, as illustrated in Fig. 5a. Experiments in a waveguide have validated the concept in 1D case. Figure 5b shows the measured frequency response functions from the source signal emitted by the electroacoustic absorber-speaker system located at the left end of the waveguide used in Chapter 4 to the sound pressure level. At the right end, a hard-wall termination or an electroacoustic absorber in case C (see Section 4.3.1) was imposed. Note that for the configuration with the hard wall termination, the peaks have decreased without modifying the dips, because of the reflection of sound waves at the right end. The sound pressure level is almost flat at low frequencies with a second absorber at the other end. Nevertheless, as the acoustic radiation impedance in 3D case is different from the 1D case, the experiment was not convincing in 3D case, and further work is required.

(a)

(b)
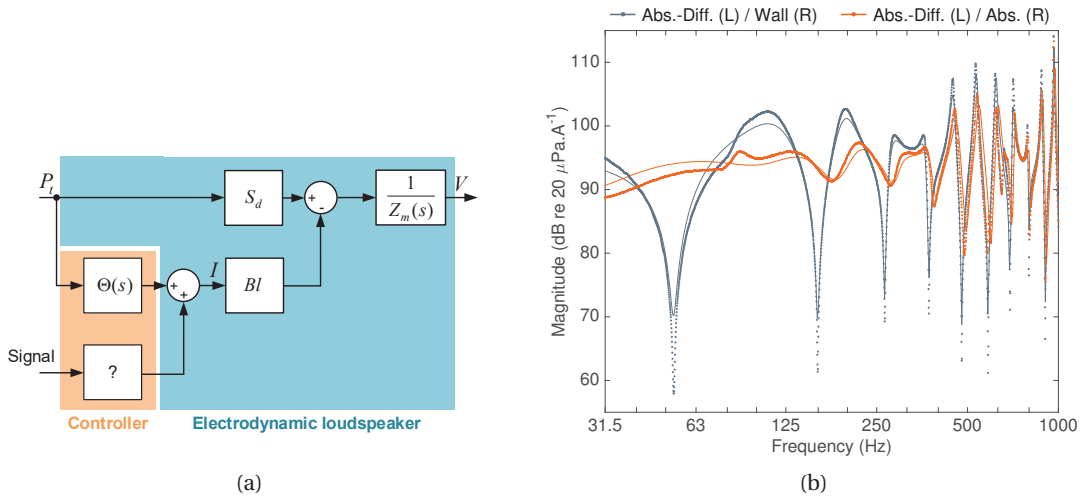
Figure 5 – (a) Block diagram of the electroacoustic absorption-diffusion system; (b) Frequency response functions from the electroacoustic absorption-diffusion system of the sound source located at the left end of the waveguide to the sound pressure level, measured (points) and simulated (solid lines), at location $x_1 = 1.02\,\text{m}$ from the sound source. At the right end, a hard-wall termination or an electroacoustic absorber in case C (see Section 4.3.1) was imposed.

• **Performance optimisation**

Despite the different methods for the characterisation of the sound field, it may be difficult to assess in a simple way the acoustic properties of any actual listening room (with furniture inside), such as the distributions in space and frequency of the sound field, as well as the modal decay times. The simulations performed in Chapter 5 for the optimisation of the target specific acoustic impedance could be improved, by adding reactive terms in the expression of the absorber and wall impedances. The target impedance could even directly be optimised in the room from one or several microphones located in the room. The modal decay times could be estimated from the frequency response function measurements (as seen in Chapter 6) at the same time as the target impedance that is assigned at the absorber diaphragms is varied, to evaluate the best configuration of absorbers that lowers the modal decay times optimally. This approach would require firstly to improve the global curve fitting technique, which is currently not fully automated. On the other hand, a compressive sensing technique could be developed from those described in Section 1.2.2 to reconstruct the sound field in actual rooms. Analysing the spatial distribution could then be useful for the optimisation of the location of absorbers. Lastly, in addition to the simulations performed in Section 5.3.2, the sound power absorbed by the prototypes could also be measured through a simple experimental protocol (with sound intensity probes for example), so as to establish some relationship between the absorbed sound power and modal decay times.

A Additional figures and tables

Table A.1 – Locations of microphones in the small and medium rooms.

Location	Small room			Medium room		
	x (m)	y (m)	z (m)	x (m)	y (m)	z (m)
A	2.27	2.91	1.94	3.11	3.17	1.19
B	4.62	0.01	2.10	0.10	2.91	1.51
C	3.17	3.60	1.94	7.76	1.98	0.01
D	1.70	3.75	1.40	1.95	1.99	0.01
E	1.93	1.19	1.23	3.14	0.35	0.01
F	5.32	2.90	0.30	5.32	1.99	0.01
G	2.03	2.78	1.05	1.17	0.56	0.01
H	0.69	1.26	1.40	5.27	0.01	1.20
I	2.00	1.88	1.05	4.00	5.13	1.80
J	3.88	3.75	0.01	6.36	1.46	0.01
K	1.28	2.13	2.12	7.01	4.46	0.01
L	0.27	0.01	2.12	1.91	5.24	1.50
M	4.19	3.75	1.65	1.80	4.78	0.01
N	0.01	1.10	1.50	5.24	2.84	1.03
O	1.70	2.46	0.30	0.57	4.70	0.65
P	-	-	-	0.01	4.46	1.20
Q	-	-	-	0.01	0.04	1.55
R	-	-	-	2.39	2.09	1.22
S	-	-	-	1.10	2.14	0.67
T	-	-	-	4.32	1.45	1.90
U	-	-	-	1.30	4.06	1.69
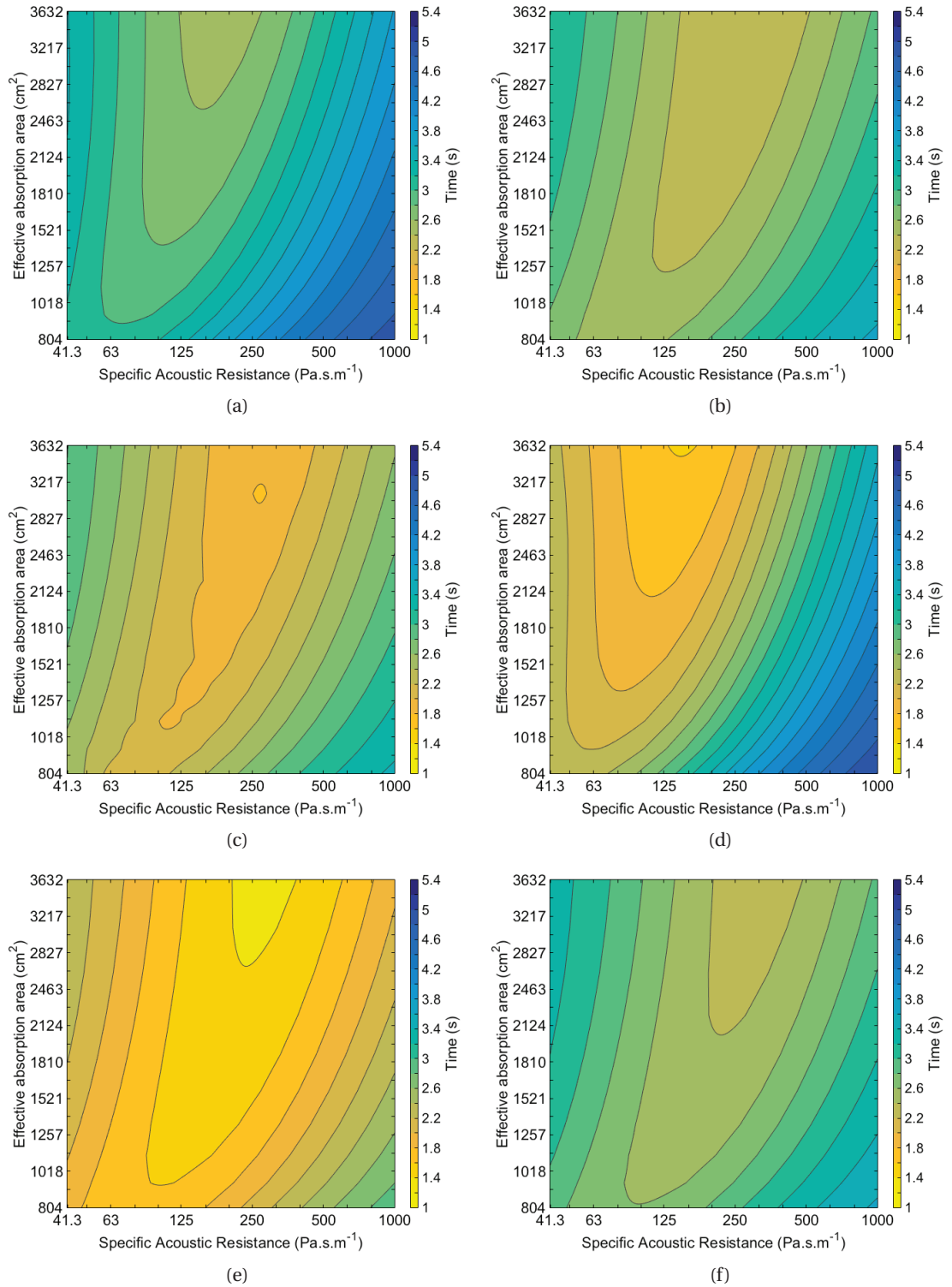
Figure A.1 – Specific acoustic resistance – effective absorption area maps of the modal decay times of the modes (a) 0,2,0 - 67.3 Hz, (b) 1,0,1 - 68.2 Hz, (c) 0,1,1 - 72.1 Hz, (d) 3,0,0 - 73.4 Hz, (e) 1,1,1 - 76.3 Hz, and (f) 2,0,1 - 80.3 Hz for 4 absorbers located in bottom corners of the medium room M1.

Figure A.2 – Specific acoustic resistance – effective absorption area maps of the modal decay times of the modes (a) 3,1,0 - 80.8 Hz, (b) 2,2,0 - 83.3 Hz, (c) 2,1,1 - 87.4 Hz, (d) 0,2,1 - 92.7 Hz, and (e) 1,2,1 - 96.0 Hz for 4 absorbers located in bottom corners of the medium room M1.
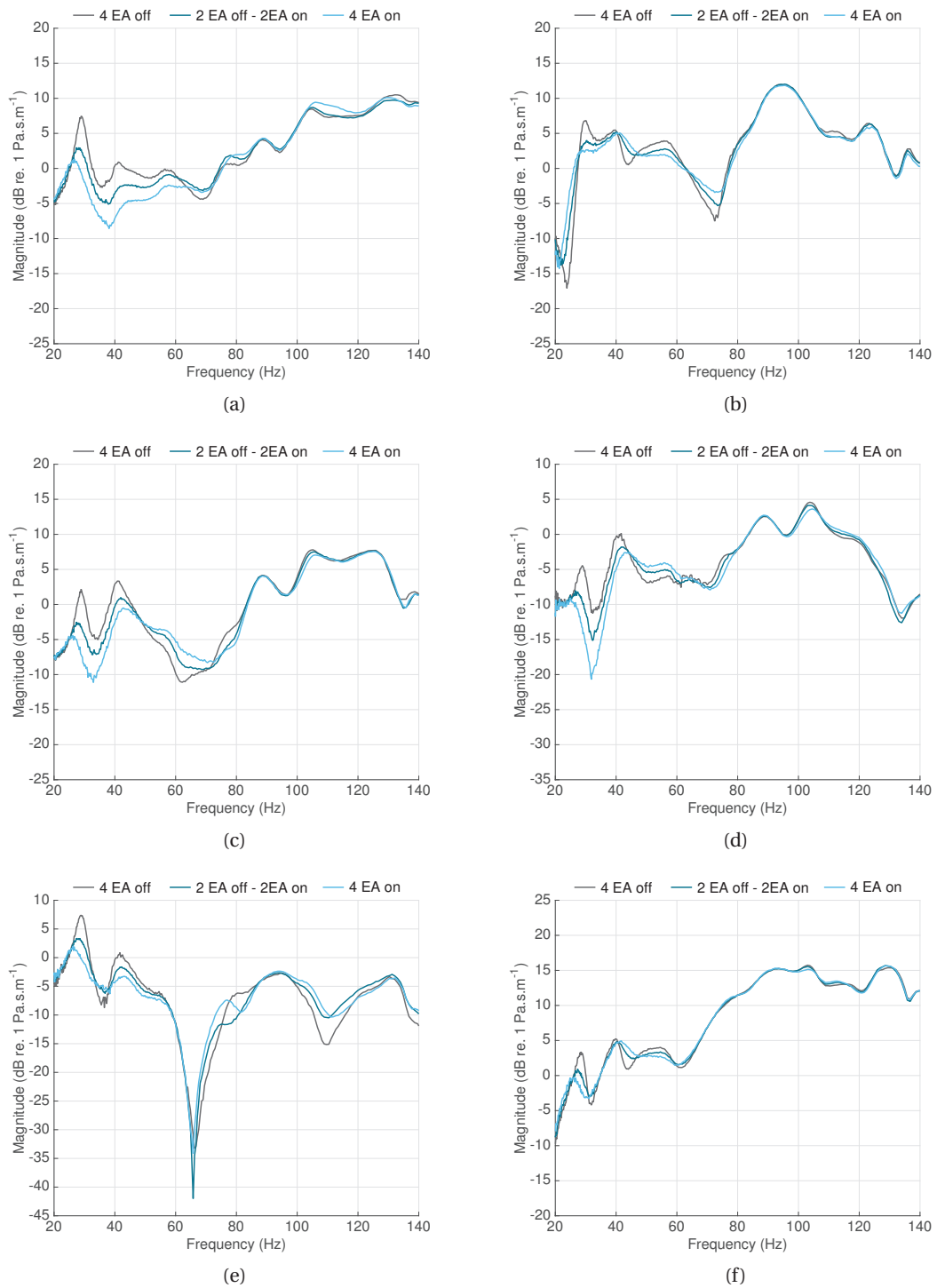
Figure A.3 – Measured frequency responses from the diaphragm velocity of the sound source to the sound pressure level in the small room for microphone locations (a) A, (b) B, (c) D, (d) G, (e) H, and (f) J.

Appendix A. Additional figures and tables

(a)

(b)

(c)
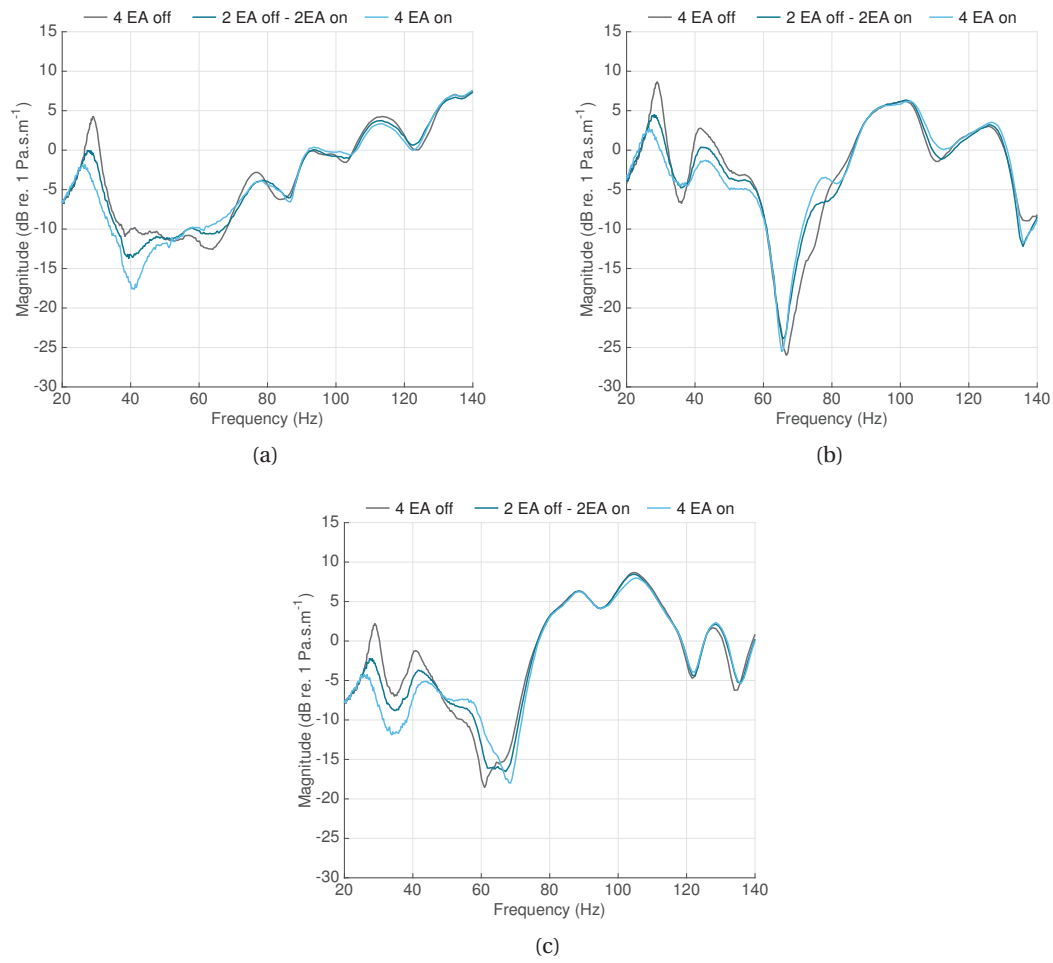
Figure A.4 – Measured frequency responses from the diaphragm velocity of the sound source to the sound pressure level in the small room for microphone locations (a) L, (b) N, and (c) O.
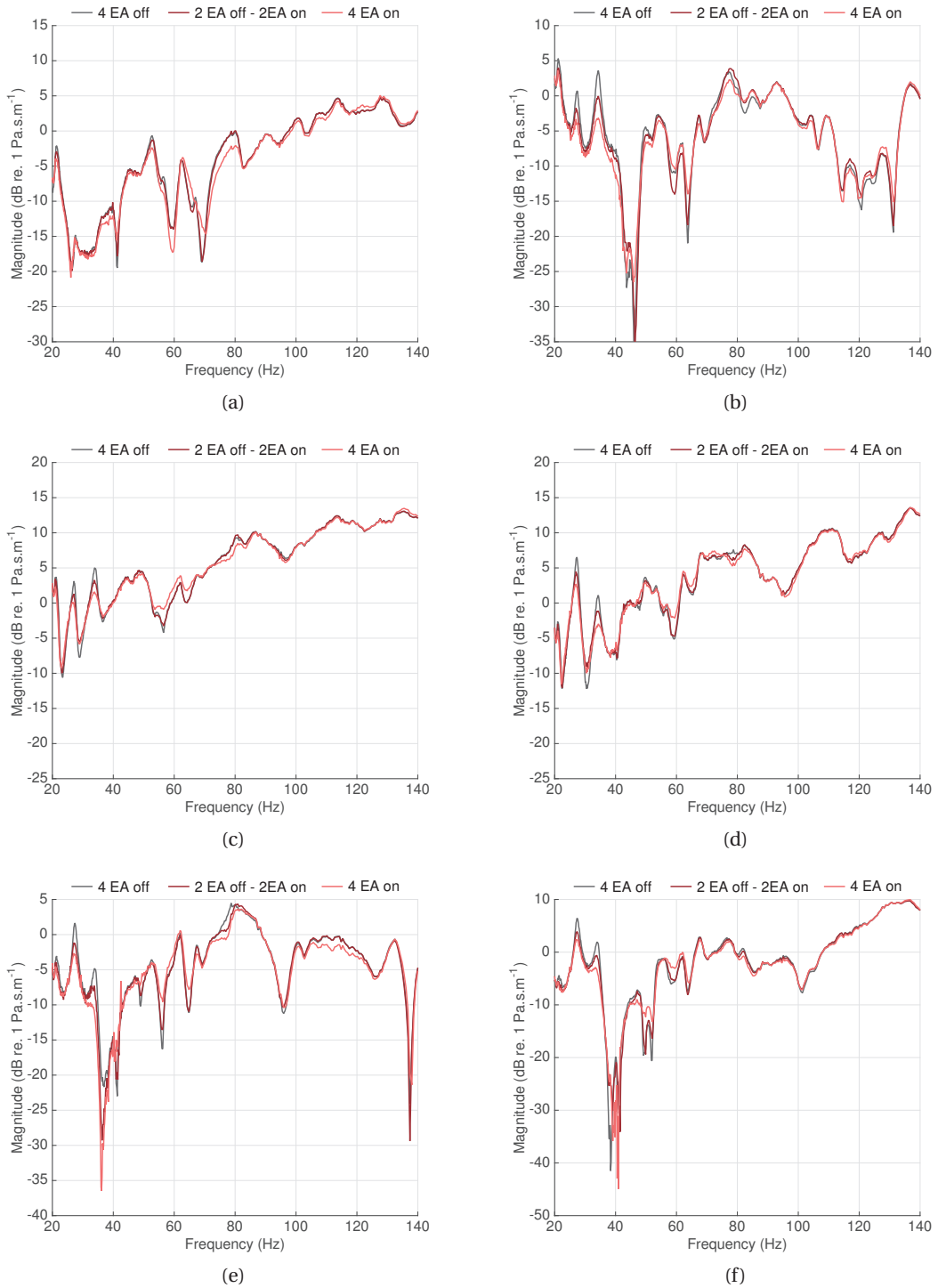
Figure A.5 – Measured frequency responses from the diaphragm velocity of the sound source to the sound pressure level in the medium room for microphone locations (a) A, (b) C, (c) D, (d) E, (e) F, and (f) H.
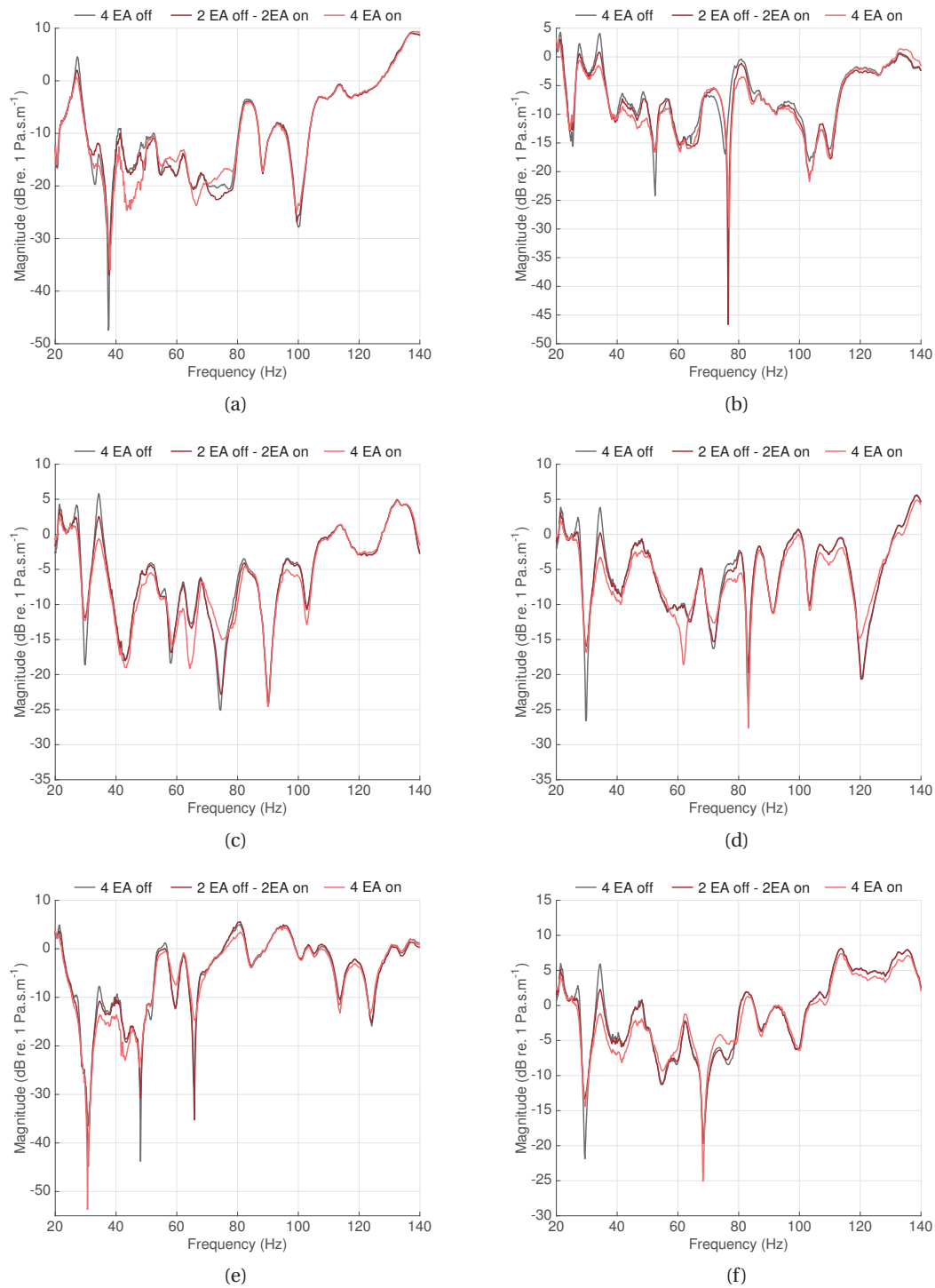
Figure A.6 – Measured frequency responses from the diaphragm velocity of the sound source to the sound pressure level in the medium room for microphone locations (a) I, (b) K, (c) L, (d) M, (e) N, and (f) O.
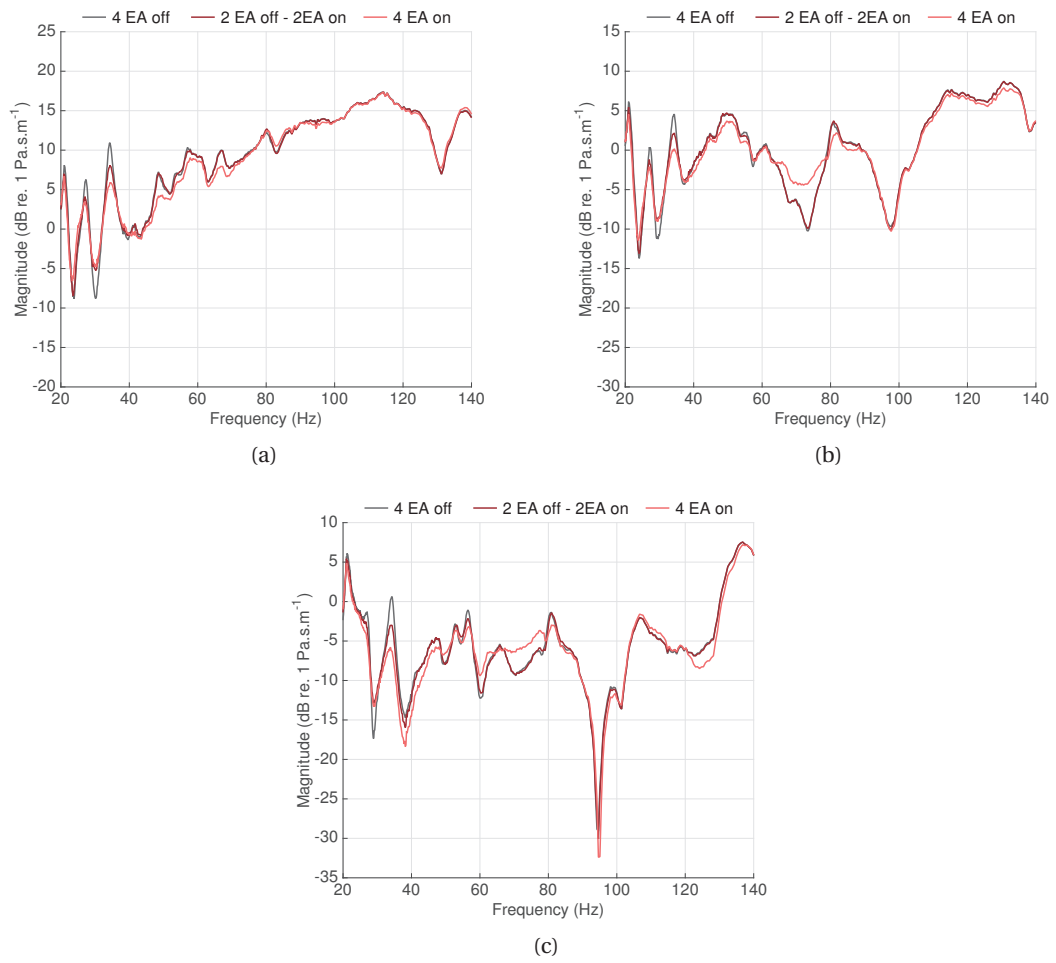
Figure A.7 – Measured frequency responses from the diaphragm velocity of the sound source to the sound pressure level in the medium room for microphone locations (a) Q, (b) S, and (c) U.

Bibliography

[1] ITU-R BS.1116-3. Methods for the subjective assessment of small impairments in audio systems. Technical report, Geneva, Switzerland, 2015.

[2] Bruno M Fazenda, Matthew Stephenson, and Andrew Goldberg. Perceptual thresholds for the effects of room modes as a function of modal decay. *The Journal of the Acoustical Society of America*, 137(3):1088–1098, 2015.

[3] Mendel Kleiner and Jiri Tichy. *Acoustics of small rooms*. CRC Press, 2014.

[4] Trevor J. Cox and Peter D'Antonio. *Acoustic absorbers and diffusers: Theory, design and application*. Taylor and Francis, 2nd edition, 2009.

[5] P. A. Nelson and Stephen J. Elliott. *Active Control of Sound*. Academic Press Inc, 1993.

[6] Romain Boulandet. *Tunable electroacoustic resonators through active impedance control of loudspeakers*. PhD thesis, Ecole Polytechnique Fédérale de Lausanne (EPFL), 2012.

[7] Heinrich Kuttruff. *Room acoustics*. Spon Press, 5th edition, 2009.

[8] Jie Pan and David Alan Bies. The effect of fluid–structural coupling on sound waves in an enclosure—theoretical part. *The Journal of the Acoustical Society of America*, 87(2):691–707, 1990.

[9] Jason E Summers. Accounting for delay of energy transfer between coupled rooms in statistical-acoustics models of reverberant-energy decay. *The Journal of the Acoustical Society of America*, 132(2):EL129–EL134, 2012.

[10] Ning Xiang, Yun Jing, and Alexander C Bockman. Investigation of acoustically coupled enclosures using a diffusion-equation model. *The Journal of the Acoustical Society of America*, 126(3):1187–1198, 2009.

[11] Jason E Summers, Rendell R Torres, Y Shimizu, and Bengt-Inge L Dalenbäck. Adapting a randomized beam-axis-tracing algorithm to modeling of coupled rooms via late-part ray tracing. *The Journal of the Acoustical Society of America*, 118(3):1491–1502, 2005.

[12] N. G. Kanev. Sound decay in a rectangular room with impedance walls. *Acoustical Physics*, 58(5):603–609, 2012.

Bibliography

[13] Eric A Lehmann and Anders M Johansson. Prediction of energy decay in room impulse responses simulated with an image-source model. *The Journal of the Acoustical Society of America*, 124(1):269–277, 2008.

[14] Nick Stefanakis, John Sarris, and George Cambourakis. Source placement for equalization in small enclosures. *Journal of the Audio Engineering Society*, 56(5):357–371, 2008.

[15] Renato Cipriano, Robi Hersberger, Gabriel Hauser, Dirk Noy, and John Storyk. Low frequency behavior of small rooms. In *Audio Engineering Society Convention 139*. Audio Engineering Society, 2015.

[16] V Easwaran and A Craggs. An application of acoustic finite element models to finding the reverberation times of irregular rooms. *Acta Acustica united with Acustica*, 82(1):54–64, 1996.

[17] Christos I Papadopoulos. Redistribution of the low frequency acoustic modes of a room: a finite element-based optimisation method. *Applied Acoustics*, 62(11):1267–1285, 2001.

[18] Christos Sevastiadis, George Kalliris, and George Papanikolaou. Analysis tool development for the investigation of low frequency room acoustics by means of finite element method. In *Audio Engineering Society Convention 128*. Audio Engineering Society, 2010.

[19] Mezhlum A Sumbatyan, Michael Yu Lannie, and Vittorio Zampoli. A fast galerkin-based method for eigenfrequencies in acoustics of small rooms with slanted boundary planes. *Journal of Sound and Vibration*, 367:101–113, 2016.

[20] Dick Botteldooren. Finite-difference time-domain simulation of low-frequency room acoustic problems. *The Journal of the Acoustical Society of America*, 98(6):3302–3308, 1995.

[21] Sofus Birkedal Nielsen and Adrian Celestinos. Optimizing placement and equalization of multiple low frequency loudspeakers in rooms. In *Audio Engineering Society Convention 119*. Audio Engineering Society, 2005.

[22] Philip M Morse and Richard H Bolt. Sound waves in rooms. *Reviews of modern physics*, 16(2):69, 1944.

[23] EH Dowell, GF Gorman, and DA Smith. Acoustoelasticity: general theory, acoustic natural modes and forced response to sinusoidal excitation, including comparisons with experiment. *Journal of Sound and vibration*, 52(4):519–542, 1977.

[24] Linda P Franzoni and Earl H Dowell. On the accuracy of modal analysis in reverberant acoustical systems with damping. *The Journal of the Acoustical Society of America*, 97(1):687–690, 1995.

[25] Sylvio R Bistafa and John W Morrissey. Numerical solutions of the acoustic eigenvalue equation in the rectangular room with arbitrary (uniform) wall impedances. *Journal of Sound and Vibration*, 263(1):205–218, 2003.

[26] Stephen M Dance and Gil Van Buuren. Effects of damping on the low-frequency acoustics of listening rooms based on an analytical model. *Journal of Sound and Vibration*, 332(25):6891–6904, 2013.

[27] Buye Xu and Scott D Sommerfeldt. A hybrid modal analysis for enclosed sound fields. *The Journal of the Acoustical Society of America*, 128(5):2857–2867, 2010.

[28] F Jacobsen. A note on instantaneous and time-averaged active and reactive sound intensity. *Journal of Sound and Vibration*, 147(3):489–496, 1991.

[29] Finn Jacobsen and Alfonso Rodríguez Molares. Ensemble statistics of active and reactive sound intensity in reverberation rooms. *The Journal of the Acoustical Society of America*, 129(1):211–218, 2011.

[30] Mirosław Meissner. Acoustic energy density distribution and sound intensity vector field inside coupled spaces. *The Journal of the Acoustical Society of America*, 132(1):228–238, 2012.

[31] Mirosław Meissner. Analytical and numerical study of acoustic intensity field in irregularly shaped room. *Applied Acoustics*, 74(5):661 – 668, 2013.

[32] Mirosław Meissner. Numerical investigation of acoustic field in enclosures: Evaluation of active and reactive components of sound intensity. *Journal of Sound and Vibration*, 338:154 – 168, 2015.

[33] M.R. Avis, B.M. Fazenda, and W.J. Davies. Thresholds of detection for changes to the q factor of low-frequency modes in listening environments. *J. Audio Eng. Soc.*, 55(7/8), 2007.

[34] Jens Holger Rindel. A note on modal reverberation times in rectangular rooms. *Acta Acustica united with Acustica*, 102(3):600–603, 2016.

[35] Mirosław Meissner. Influence of wall absorption on low-frequency dependence of reverberation time in room of irregular shape. *Applied Acoustics*, 69(7):583–590, 2008.

[36] ISO 3382-2-2008. Acoustics - measurement of room acoustic parameters - part 2 : reverberation time in ordinary rooms. Technical report, International Organization for Standardization, Geneva, Switzerland, 2008.

[37] Mirosław Meissner. Evaluation of decay times from noisy room responses with pure-tone excitation. *Archives of Acoustics*, 38(1):47–54, 2013.

[38] M. R. Schroeder. Integrated-impulse method measuring sound decay without using impulses. *J. Acoust. Soc. Am.*, 66(2), 1979.

Bibliography

[39] Matti Karjalainen, Poju Ansalo, Aki Mäkivirta, Timo Peltonen, and Vesa Välimäki. Estimation of modal decay parameters from noisy response measurements. *Journal of the Audio Engineering Society*, 50(11):867–878, 2002.

[40] Andrea Prato, Federico Casassa, and Alessandro Schiavi. Reverberation time measurements in non-diffuse acoustic field by the modal reverberation time. *Applied Acoustics*, 110:160–169, 2016.

[41] Thibaut Ajdler, Luciano Sbaiz, and Martin Vetterli. The plenacoustic function and its sampling. *IEEE transactions on Signal Processing*, 54(10):3790–3804, 2006.

[42] Yoichi Haneda, Yutaka Kaneda, and Nobuhiko Kitawaki. Common-acoustical-pole and residue model and its application to spatial interpolation and extrapolation of a room transfer function. *IEEE Transactions on Speech and Audio Processing*, 7(6):709–717, 1999.

[43] Claire Masterson, Gavin Kearney, and Frank Boland. Acoustic impulse response interpolation for multichannel systems using dynamic time warping. In *Audio Engineering Society Conference: 35th International Conference: Audio for Games*. Audio Engineering Society, 2009.

[44] Remi Mignot, Gilles Chardon, and Laurent Daudet. Low frequency interpolation of room impulse responses using compressed sensing. *IEEE/ACM Transactions on Audio, Speech, and Language Processing*, 22(1):205–216, 2014.

[45] Jan Voetmann and John Klinkby. Review of the low-frequency absorber and its application to small room acoustics. In *Audio Engineering Society Convention 94*. Audio Engineering Society, 1993.

[46] W Frommhold, HV Fuchs, and S Sheng. Acoustic performance of membrane absorbers. *Journal of Sound and Vibration*, 170(5):621–636, 1994.

[47] Ganghua Yu, Deyu Li, and Li Cheng. Effect of internal resistance of a helmholtz resonator on acoustic energy reduction in enclosure. *J. Acoust. Soc. Am.*, 124(6), 2008.

[48] FJ Fahy and C Schofield. A note on the interaction between a helmholtz resonator and an acoustic mode of an enclosure. *Journal of Sound and Vibration*, 72(3):365–378, 1980.

[49] Sylvio R Bistafa, Mark P Hodgkin, William S Morita, Bruno O Köhn, and João J Neto. Adaptive control of low-frequency acoustic modes in small rooms. *Open. Acoust. J*, 5:16–22, 2012.

[50] A Doria. Control of acoustic vibrations of an enclosure by means of multiple resonators. *Journal of Sound and Vibration*, 181(4):673–685, 1995.

[51] MB Xu, A Selamet, and H Kim. Dual helmholtz resonator. *Applied Acoustics*, 71(9):822–829, 2010.

[52] Changbin Guan and Zongxia Jiao. Modeling and optimal design of 3 degrees of freedom helmholtz resonator in hydraulic system. *Chinese Journal of Aeronautics*, 25(5):776–783, 2012.

[53] A Cummings. The effects of a resonator array on the sound field in a cavity. *Journal of Sound and Vibration*, 154(1):25–44, 1992.

[54] Deyu Li and Li Cheng. Acoustically coupled model of an enclosure and a helmholtz resonator array. *Journal of Sound and Vibration*, 305(1):272–288, 2007.

[55] Daa-You Maa. Potentials of micro perforated absorbers. *J. Acoust. Soc. Am.*, 104(5), 1975.

[56] Dah-You Maa. Potential of microperforated panel absorber. *the Journal of the Acoustical Society of America*, 104(5):2861–2866, 1998.

[57] Xiao-Ling Gai, Tuo Xing, Xian-Hui Li, Bin Zhang, and Wen-Jiang Wang. Sound absorption of microperforated panel mounted with helmholtz resonators. *Applied Acoustics*, 114:260–265, 2016.

[58] Y. Y. Lee, E. W. M. Lee, and C. F. Ng. Sound absorption of a finite flexible micro-perforated panel backed by an air cavity. *Journal of Sound and Vibration*, 287(1):227–243, 2005.

[59] Masahiro Toyoda, Seiji Kobatake, and Kimihiro Sakagami. Numerical analyses of the sound absorption of three-dimensional mpp space sound absorbers. *Applied Acoustics*, 79:69–74, 2014.

[60] Kimihiro Sakagami, Masakazu Kiyama, Masayuki Morimoto, and Daiji Takahashi. Sound absorption of a cavity-backed membrane: a step towards design method for membrane-type absorbers. *Applied Acoustics*, 49(3):237–247, 1996.

[61] Dengke Li, Daoqing Chang, and Bilong Liu. Enhancing the low frequency sound absorption of a perforated panel by parallel-arranged extended tubes. *Applied Acoustics*, 102:126–132, 2016.

[62] Richard H Bolt. Note on normal frequency statistics for rectangular rooms. *The Journal of the Acoustical Society of America*, 18(1):130–133, 1946.

[63] MM Louden. Dimension-ratios of rectangular rooms with good distribution of eigentones. *Acta Acustica united with Acustica*, 24(2):101–104, 1971.

[64] CLS Gilford. The acoustic design of talks studios and listening rooms. *Journal of the Audio Engineering Society*, 27(1/2):17–31, 1979.

[65] Oscar J Bonello. A new criterion for the distribution of normal room modes. *Journal of the Audio Engineering Society*, 29(9):597–606, 1981.

[66] R Walker. Optimum dimension ratios for small rooms. In *Audio Engineering Society Convention 100*. Audio Engineering Society, 1996.

Bibliography

[67] IEC.60268-13. Sound system equipment - part 13: Listening tests on loudspeakers. Technical report, Geneva, Switzerland, 1998.

[68] Todd Welti. Investigation of bonello criteria for use in small room acoustics. In *Audio Engineering Society Convention 127*. Audio Engineering Society, 2009.

[69] Trevor J Cox, Peter D'Antonio, and Mark R Avis. Room sizing and optimization at low frequencies. *Journal of the Audio Engineering Society*, 52(6):640–651, 2004.

[70] Roy F Allison. The influence of room boundaries on loudspeaker power output. *Journal of the Audio Engineering Society*, 22(5):314–320, 1974.

[71] Allen R Groh. High-fidelity sound system equalization by analysis of standing waves. *Journal of the Audio Engineering Society*, 22(10):795–799, 1974.

[72] Keith O Ballagh. Optimum loudspeaker placement near reflecting planes. *Journal of the Audio Engineering Society*, 31(12):931–935, 1983.

[73] Xiaoxiang Shen, Yong Shen, and Jinglei Zhou. Optimization of the locations of the loudspeaker and absorption material in a small room. *Applied acoustics*, 65(8):791–806, 2004.

[74] Todd Welti and Allan Devantier. Low-frequency optimization using multiple subwoofers. *Journal of the Audio Engineering Society*, 54(5):347–364, 2006.

[75] Todd Welti. Optimal configurations for subwoofers in rooms considering seat to seat variation and low frequency efficiency. In *Audio Engineering Society Convention 133*, Oct 2012.

[76] Adam J. Hill and Malcolm O. J. Hawksford. Wide-area psychoacoustic correction for problematic room-modes using nonlinear bass synthesis. *J. Audio Eng. Soc*, 59(11):825–834, 2011.

[77] Paul Lueg. Process of silencing sound oscillations. *U.S. Patent no US2043416*, 1936.

[78] John Mourjopoulos, P Clarkson, and J Hammond. A comparative study of least-squares and homomorphic techniques for the inversion of mixed phase signals. In *Acoustics, Speech, and Signal Processing, IEEE International Conference on ICASSP'82.*, volume 7, pages 1858–1861. IEEE, 1982.

[79] John N Mourjopoulos, Efstathios D Kyriakis-Bitzaros, and Costas E Goutis. Theory and real-time implementation of time-varying digital audio filters. *Journal of the Audio Engineering Society*, 38(7/8):523–536, 1990.

[80] German Ramos and Jose J Lopez. Filter design method for loudspeaker equalization based on iir parametric filters. *Journal of the Audio Engineering Society*, 54(12):1162–1178, 2006.

[81] Matti Karjalainen and Tuomas Paatero. Equalization of loudspeaker and room responses using kautz filters: Direct least squares design. *EURASIP Journal on Applied Signal Processing*, 2007(1):185–185, 2007.

[82] Balázs Bank. Warped iir filter design with custom warping profiles and its application to room response modeling and equalization. In *Audio Engineering Society Convention 130*, May 2011.

[83] Jack Oclee-Brown. Pole-zero analysis of the soundfield in small rooms at low frequencies. In *Audio Engineering Society Convention 121*. Audio Engineering Society, 2006.

[84] Yoichi Haneda, Shoji Makino, and Yutaka Kaneda. Multiple-point equalization of room transfer functions by using common acoustical poles. *IEEE transactions on speech and audio processing*, 5(4):325–333, 1997.

[85] Jan Abildgaard Pedersen and Kasper Thomsen. Fully automatic loudspeaker-room adaptation - the room perfect system. In *Audio Engineering Society Conference: 32nd International Conference: DSP For Loudspeakers*, Sep 2007.

[86] M. Miyoshi and Y. Kaneda. Inverse filtering of room acoustics. *IEEE Transactions on Acoustics, Speech, and Signal Processing*, 36(2):145–152, 1988.

[87] Stephen J Elliott and Philip A Nelson. Multiple-point equalization in a room using adaptive digital filters. *Journal of the Audio Engineering Society*, 37(11):899–907, 1989.

[88] ARD Curtis, PA Nelson, SJ Elliott, and AJ Bullmore. Active suppression of acoustic resonance. *The Journal of the Acoustical Society of America*, 81(3):624–631, 1987.

[89] F. Asano and D.C. Swanson. Sound equalization in enclosures using modal reconstruction. *Journal of the Acoustical Society of America*, 98(4):2062–2069, 1995.

[90] Balázs Bank. Full room equalization at low frequencies with asymmetric loudspeaker arrangements. In *Audio Engineering Society Convention 132*. Audio Engineering Society, 2012.

[91] Lars-Johan Brännmark, Adrian Bahne, and Anders Ahlén. Improved loudspeaker-room equalization using multiple loudspeakers and mimo feedforward control. In *2012 IEEE International Conference on Acoustics, Speech and Signal Processing (ICASSP)*, pages 237–240. IEEE, 2012.

[92] Gabriel Weinreich and Eric B Arnold. Method for measuring acoustic radiation fields. *The Journal of the Acoustical Society of America*, 68(2):404–411, 1980.

[93] Manuel Melon, Christophe Langrenne, Philippe Herzog, and Alexandre Garcia. Evaluation of a method for the measurement of subwoofers in usual rooms. *J. Acoust. Soc. Am.*, 127(1):256–263, 2010.

[94] Philippe Herzog, Emmanuel Friot, Dominique Habault, Cédric Pinhede, Alexandre Gintz, Pierre Leroy, and Marc Pachebat. Toward an active anechoic room. In *7th Forum Acusticum*, number R01-3, 2014.

[95] Dieter Guicking. Active control of sound and vibration: History–fundamentals–state of the art. *Oscillations, Waves and Interactions–60 Years Drittes Physikalisches Institute*, pages 107–138, 2007.

[96] Arturo O. Santillán. Spatially extended sound equalization in rectangular rooms. *The Journal of the Acoustical Society of America*, 110(4):1989, 2001.

[97] John C. Sarris, Nick J. Stefanakis, and George E. Cambourakis. Signal processing techniques for robust multichannel sound equalisation. In *Audio Engineering Society Convention 116*, May 2004.

[98] Arturo O Santillán, Christian S Pedersen, and Morten Lydolf. Experimental implementation of a low-frequency global sound equalization method based on free field propagation. *Applied Acoustics*, 68(10):1063–1085, 2007.

[99] Christian Sejer Pedersen and Henrik Møller. Sound field control for a low-frequency test facility. In *Audio Engineering Society Conference: 52nd International Conference: Sound Field Control-Engineering and Perception*. Audio Engineering Society, 2013.

[100] Adrian Celestinos and Sofus Birkedal Nielsen. Controlled acoustic bass system (cabs) a method to achieve uniform sound field distribution at low frequencies in rectangular rooms. *Journal of the Audio Engineering Society*, 56(11):915–931, 2008.

[101] Pierre-Jean René. *Contributions aux études sur le couplage électroacoustique dans les espaces clos en vue du contrôle actif.* PhD thesis, Ecole Polytechnique Fédérale de Lausanne (EPFL), 2006.

[102] John Vanderkooy. Multi-source room equalization: Reducing room resonances. In *Audio Engineering Society Convention 123*. Audio Engineering Society, 2007.

[103] Stephen J. Elliott, P. Joseph, P. A. Nelson, and M. E. Johnson. Power output minimization and power absorption in the active control of sound. *J. Acoust. Soc. Am.*, 90(5), 1991.

[104] P Darlington. Suppressing room modes using active absorbers. *Proceedings of Institute of Acoustics*, 16:389–402, 1994.

[105] Philippe Herzog, Alberto Soto-Nicolás, and Franck Guéry. Passive and active control of the low-frequency modes in a small room. In *Audio Engineering Society Convention 98*. Audio Engineering Society, 1995.

[106] P Darlington and MR Avis. Time/frequency response of a room with active acoustic absorption. In *Audio Engineering Society Convention 100*. Audio Engineering Society, 1996.

[107] MR Avis. *The active control of low frequency room modes*. PhD thesis, University of Salford, 2000.

[108] Aki Mäkivirta, Poju Antsalo, Matti Karjalainen, and Vesa Välimäki. Modal equalization of loudspeaker-room responses at low frequencies. *Journal of the Audio Engineering Society*, 51(5):324–343, 2003.

[109] Jyunji Hagio, Akihiro Kakiuchi, and Akira Omoto. Sound field equalization by active acoustic impedance control. In *Audio Engineering Society Conference: 40th International Conference: Spatial Audio: Sense the Sound of Space*, Oct 2010.

[110] Reza Kashani and James Wischmeyer. Electronic bass trap. In *Audio Engineering Society Convention 117*. Audio Engineering Society, 2004.

[111] Harry F. Olson and E. G. May. Electronic sound absorber. *J. Acoust. Soc. Am.*, 25(6), 1953.

[112] R. L. Clark and D. G. Cole. Active damping of enclosed sound fields through direct rate feedback control. *J. Acoust. Soc. Am.*, 93(3), 1995.

[113] Dieter Guicking and K. Karcher. Active impedance control for one-dimensional sound. *J. of Vibration, Acoustics, Stress and Reliability in Design*, 106, 1984.

[114] Felipe Orduña-Bustamente and P. A. Nelson. An adaptive controller for the active absorption of sound. *J. Acoust. Soc. Am.*, 91(5), 1992.

[115] Jing Yuan. Causal impedance matching for broadband hybrid noise absorption. *The Journal of the Acoustical Society of America*, 113(6):3226–3232, 2003.

[116] Claude J Mazzola. *Active sound absorption*. Namlak, 1993.

[117] Guy Charles Nicholson. *The active control of acoustic impedance*. PhD thesis, University of Salford, 1994.

[118] D Thenail, O Lacour, MA Galland, and M Furstoss. The active control of wall impedance. *Acta Acustica united with Acustica*, 83(6):1039–1044, 1997.

[119] Marc Furstoss, Denis Thenail, and Marie-Annick Galland. Surface impedance control for sound absorption: direct and hybrid passive/active strategies. *J. Sound and Vibration*, 203(2), 1997.

[120] Hervé Lissek. Les matériaux actifs à propriétés acoustiques variables. Technical report, Université du Maine, 2002.

[121] E Bazin, P Filippi, and G Dumery. Control of reflection coefficient of surfaces using piezoelectric materials. *Smart Materials and Structures*, 3(1):1, 1994.

[122] Mateus de Freitas Virgilio Pereira, Alexander Mattioli Pasqual, and Guilherme de Souza Papini. Numerical and theoretical analysis of sound absorption by an actively controlled electrodynamic loudspeaker. *Journal of the Brazilian Society of Mechanical Sciences and Engineering*, pages 1–7, 2016.

Bibliography

[123] R. L. Clark, K. D. Frampton, and D. G. Cole. Phase compensation for feedback control of enclosed sound field. *J. Sound and Vibration*, 195(5), 1996.

[124] R. Boulandet and H. Lissek. Toward broadband electroacoustic resonators through optimized feedback control strategies. *J. Sound and Vibration*, 333(20):4810 – 4825, 2014.

[125] N. G. Kanev and M. A. Mironov. Active resonators for sound control in narrow pipes. *Acoustical Physics*, 54(3):437–443, 2008.

[126] M. Collet, P. David, and M. Berthillier. Active acoustical impedance using distributed electrodynamical transducers. *J. Acoust. Soc. Am.*, 125(2), 2009.

[127] Petr David, Manuel Collet, and Jean-Marc Cote. Experimental implementation of acoustic impedance control by a 2d network of distributed smart cells. *Smart Materials and Structures*, 19(3):035028, 2010.

[128] N. W. Hagood and A. von Flotow. Damping of structural vibration with piezoelectric materials and passive electrical networks. *J. Sound and Vibration*, 146(2), 1991.

[129] Giovanni Caruso. A critical analysis of electric shunt circuits employed in piezoelectric passive vibration damping. *Smart Materials and Structures*, 10(5):1059, 2001.

[130] Andrew J Fleming, Sam Behrens, and SO Reza Moheimani. Optimization and implementation of multimode piezoelectric shunt damping systems. *IEEE/ASME Transactions on mechatronics*, 7(1):87–94, 2002.

[131] CH Park. Dynamics modelling of beams with shunted piezoelectric elements. *Journal of Sound and Vibration*, 268(1):115–129, 2003.

[132] Jaehwan Kim and Young-Chae Jung. Broadband noise reduction of piezoelectric smart panel featuring negative-capacitive-converter shunt circuit. *The Journal of the Acoustical Society of America*, 120(4):2017–2025, 2006.

[133] Andrew J. Fleming and *et al*. Control of resonant acoustic sound fields by electrical shunting of a loudspeaker. *IEEE Transaction on Control System Technology*, 15(4):689–703, 2007.

[134] Hervé Lissek, Romain Boulandet, and Romain Fleury. Electroacoustic absorbers: bridging the gap between shunt loudspeakers and active sound absorption. *J. Acoust. Soc. Am.*, 129(5), 2011.

[135] Robert J. Bobber. An active transducer as a characteristic impedance of an acoustic transmission line. *J. Acoust. Soc. Am.*, 48(126), 1970.

[136] M Černík and Pavel Mokrỳ. Sound reflection in an acoustic impedance tube terminated with a loudspeaker shunted by a negative impedance converter. *Smart Materials and Structures*, 21(11):115016, 2012.

[137] Jiancheng Tao, Ruixiang Jing, and Xiaojun Qiu. Sound absorption of a finite micro-perforated panel backed by a shunted loudspeaker. *J. Acoust. Soc. Am.*, 135(1):231–238, 2013.

[138] Yumin Zhang, Yum-Ji Chan, and Lixi Huang. Thin broadband noise absorption through acoustic reactance control by electro-mechanical coupling without sensor. *The Journal of the Acoustical Society of America*, 135(5):2738–2745, 2014.

[139] Fei Liu, Stephen Horowitz, Toshikazu Nishida, Louis Cattafesta, and Mark Sheplak. A multiple degree of freedom electromechanical helmholtz resonator. *J. Acoust. Soc. Am.*, 122(1), 2007.

[140] Daoqing Chang, Bilong Liu, and Xiaodong Li. An electromechanical low frequency panel sound absorber. *The Journal of the Acoustical Society of America*, 128(2):639–645, 2010.

[141] Jeffrey J Dosch, Daniel J Inman, and Ephrahim Garcia. A self-sensing piezoelectric actuator for collocated control. *Journal of Intelligent Material Systems and Structures*, 3(1):166–185, 1992.

[142] Ben Hanson and Martin Levesley. Self-sensing applications for electromagnetic actuators. *Sensors and Actuators A: Physical*, 116(2):345–351, 2004.

[143] Andrew J. Fleming, S. O. Reza Moheimani, and Sam Behrens. Synthesis and implementation of sensor-less active shunt controllers for electromagnetically actuated systems. *IEEE Transaction on Control System Technology*, 13(2), 2005.

[144] C Paulitsch, P Gardonio, and SJ Elliott. Active vibration damping using self-sensing, electrodynamic actuators. *Smart materials and structures*, 15(2):499, 2006.

[145] Sang-Myeong Kim, Semyung Wang, and Michael J Brennan. Dynamic analysis and optimal design of a passive and an active piezo-electrical dynamic vibration absorber. *Journal of sound and vibration*, 330(4):603–614, 2011.

[146] Romain Boulandet, Marc Michau, Philippe Micheau, and Alain Berry. Aircraft panel with sensorless active sound power reduction capabilities through virtual mechanical impedances. *Journal of Sound and Vibration*, 361:2–19, 2016.

[147] Steven A. Lane and Robert L. Clark. Improving loudspeaker performance for active control applications. *J. Audio Eng. Soc.*, 46(6):508–519, 1998.

[148] Egbert De Boer. Theory of motional feedback. *IRE Transactions on Audio*, 9(1), 1961.

[149] Steven A. Lane and Robert L. Clark. Dissipative feedback control of a reverberant enclosure using a constant volume velocity source. *ASME J. Vibr. Acous.*, 120, 1998.

[150] Yaoyu Li and GT-C Chiu. Control of loudspeakers using disturbance-observer-type velocity estimation. *IEEE/ASME Transactions on Mechatronics*, 10(1):111–117, 2005.

Bibliography

[151] Youngeun Cho, Semyung Wang, and Kyihwan Park. Electroacoustic absorber using disturbance-observer-type velocity estimator. *IEEE/ASME Transactions on Mechatronics*, pages 1–1, 2015.

[152] D. J. Leo and D. Limpert. A self-sensing technique for active acoustic attenuation. *J. Sound and Vibration*, 235(5), 2000.

[153] R. Boulandet, E. Rivet, and H. Lissek. Sensorless electroacoustic absorbers through synthesized impedance control for damping low-frequency modes in cavities. *Acta Acustica united with Acustica*, 102(4):pp. 696–704(9), 2016.

[154] Toshiya Samejima. A state feedback electro-acoustic transducer for active control of acoustic impedance. *J. Acoust. Soc. Am.*, 113(3), 2003.

[155] MR Bai and HH Lin. Comparison of active noise control structures in the presence of acoustical feedback by using the hinf synthesis technique. *Journal of Sound and Vibration*, 206(4):453–471, 1997.

[156] Mingsian R Bai and Hsinping Wu. Robust control of a sensorless bass-enhanced moving-coil loudspeaker system. *The Journal of the Acoustical Society of America*, 105(6):3283–3289, 1999.

[157] Yaoyu Li, GT-C Chiu, and Luc G Mongeau. Dual-driver standing wave tube: acoustic impedance matching with robust repetitive control. *IEEE transactions on control systems technology*, 12(6):869–880, 2004.

[158] D Guicking and E Lorenz. An active sound absorber with porous plate. *Journal of vibration, acoustics, stress, and reliability in design*, 106(3):389–392, 1984.

[159] Samson Beyene and Ricardo A Burdisso. A new hybrid passive–active noise absorption system. *the Journal of the Acoustical Society of America*, 101(3):1512–1515, 1997.

[160] O Lacour, MA Galland, and D Thenail. Preliminary experiments on noise reduction in cavities using active impedance changes. *Journal of sound and vibration*, 230(1):69–99, 2000.

[161] Jerome P Smith, Brody D Johnson, and Ricardo A Burdisso. A broadband passive–active sound absorption system. *The Journal of the Acoustical Society of America*, 106(5):2646–2652, 1999.

[162] Pedro Cobo, Alejandro Fernández, and Olivier Doutres. Low-frequency absorption using a two-layer system with active control of input impedance. *J. Acoust. Soc. Am.*, 114(6), 2003.

[163] C. Guigou and C. R. Fuller. Adaptive feedforward and feedback methods for active/passive sound radiation control using smart foam. *J. Acoust. Soc. Am.*, 104(1), 1998.

[164] Pedro Cobo, Jaime Pfretzschner, Maria Cuesta, and David K. Anthony. Hybrid passive–active absorption using microperforated panels. *J. Acoust. Soc. Am.*, 116(4), 2004.

[165] Pedro Cobo and María Cuesta. Hybrid passive-active absorption of a microperforated panel in free field conditions. *the Journal of the Acoustical Society of America*, 121(6):EL251–EL255, 2007.

[166] Maria Cuesta, Pedro Cobo, Alejandro Fernández, and Jaime Pfretzschner. Using a thin actuator as secondary source for hybrid passive/active absorption in an impedance tube. *Applied Acoustics*, 67, 2006.

[167] Tao Wu, Trevor J Cox, and YW Lam. A profiled structure with improved low frequency absorption. *The Journal of the Acoustical Society of America*, 110(6):3064–3070, 2001.

[168] Lejun Xiao, Trevor J. Cox, and Mark R. Avis. Active diffusers: some prototypes and 2d measurements. *Journal of Sound and Vibration*, 285(1–2):321–339, 7 2005.

[169] Trevor J. Cox, Mark R. Avis, and Lejun Xiao. Maximum length sequence an bessel diffusers using active technologies. *J. Sound and Vibration*, 289:807–829, 2006.

[170] Marie-Annick Galland, Benoit Mazeaud, and Nadine Sellen. Hybrid passive/active absorbers for flow ducts. *Applied acoustics*, 66(6):691–708, 2005.

[171] Nadine Sellen, Maria Cuesta, and M-A Galland. Noise reduction in a flow duct: Implementation of a hybrid passive/active solution. *Journal of sound and vibration*, 297(3):492–511, 2006.

[172] Benjamin Betgen and Marie-Annick Galland. A new hybrid active/passive sound absorber with variable surface impedance. *Mechanical Systems and Signal Processing*, 25(5):1715–1726, 2011.

[173] Benjamin Betgen, Marie-Annick Galland, Estelle Piot, and Frank Simon. Implementation and non-intrusive characterization of a hybrid active–passive liner with grazing flow. *Applied Acoustics*, 73(6):624–638, 2012.

[174] Jean-Baptiste Dupont and Marie-Annick Galland. Active absorption to reduce the noise transmitted out of an enclosure. *Applied Acoustics*, 70(1):142–152, 2009.

[175] Manuel Melon, Philippe Herzog, Azzedine Sitel, and Marie-Annick Galland. Onde dimensional study of a module for active/passive control of both absorption and transmission. *Applied Acoustics*, 73(234-242), 2012.

[176] Roland Bücklein. The audibility of frequency response irregularities. *Journal of the Audio Engineering Society*, 29(3):126–131, 1981.

[177] Peter A Fryer. Intermodulation distortion listening tests. In *Audio Engineering Society Convention 50*. Audio Engineering Society, 1975.

Bibliography

[178] Floyd E Toole and Sean E Olive. The modification of timbre by resonances: Perception and measurement. *Journal of the Audio Engineering Society*, 36(3):122–142, 1988.

[179] Sean E Olive, Peter L Schuck, James G Ryan, Sharon L Sally, and Marc E Bonneville. The detection thresholds of resonances at low frequencies. *Journal of the Audio Engineering Society*, 45(3):116–128, 1997.

[180] Bruno M Fazenda, Mark R Avis, and William J Davies. Perception of modal distribution metrics in critical listening spaces—dependence on room aspect ratios. *Journal of the Audio Engineering Society*, 53(12):1128–1141, 2005.

[181] Tomas Salava. Imperfections at low frequencies-how much are they audible or annoying? In *Audio Engineering Society Convention 116*. Audio Engineering Society, 2004.

[182] Bruno Fazenda and Matthew Wankling. Optimal modal spacing and density for critical listening. In *Audio Engineering Society Convention 125*. Audio Engineering Society, 2008.

[183] Sean E Olive, Peter L Schuck, Sharon L Sally, and Marc E Bonneville. The effects of loudspeaker placement on listener preference ratings. *Journal of the Audio Engineering Society*, 42(9):651–669, 1994.

[184] Eric Benjamin and Benjamin Gannon. The effect of room acoustics on subwoofer performance and level setting. In *Audio Engineering Society Convention 109*. Audio Engineering Society, 2000.

[185] Matthew Wankling, Bruno Fazenda, and William J Davies. The assessment of low-frequency room acoustic parameters using descriptive analysis. *Journal of the Audio Engineering Society*, 60(5):325–337, 2012.

[186] Poju Antsalo, Matti Karjalainen, Aki Makivirta, and Vesa Valimaki. Perception of temporal decay of low-frequency room modes. In *Audio Engineering Society Convention 116*, May 2004.

[187] Andrew Goldberg. Measuring the threshold of audibility of temporal decays. In *Audio Engineering Society Convention 120*. Audio Engineering Society, 2006.

[188] Andrew Goldberg. Windowed sine bursts: In search of optimal test signals for detecting the threshold of audibility of temporal decays. In *Audio Engineering Society Convention 126*. Audio Engineering Society, 2009.

[189] Matti Karjalainen, Esa Piirilä, Antti Järvinen, and Jyri Huopaniemi. Comparison of loudspeaker equalization methods based on dsp techniques. *Journal of the Audio Engineering Society*, 47(1/2):14–31, 1999.

[190] Poju Antsalo, Matti Karjalainen, Aki Makivirta, and Vesa Valimaki. Comparison of modal equalizer design methods. In *Audio Engineering Society Convention 114*. Audio Engineering Society, 2003.

[191] Andrew Goldberg and Aki Makivirta. Performance comparison of graphic equalisation and active loudspeaker room response controls. In *Audio Engineering Society Convention 116*. Audio Engineering Society, 2004.

[192] Sean Olive, John Jackson, Allan Devantier, and David Hunt. The subjective and objective evaluation of room correction products. In *Audio Engineering Society Convention 127*. Audio Engineering Society, 2009.

[193] Bruno Fazenda, Matthew Wankling, Jonathan Hargreaves, Lucy Elmer, and Jonathan Hirst. Subjective preference of modal control methods in listening rooms. *Journal of the Audio Engineering Society*, 60(5):338–349, 2012.

[194] Juha Backman. Subwoofers in rooms: stereophonic reproduction. In *Audio Engineering Society Convention 138*. Audio Engineering Society, 2015.

[195] Todd S Welti. Subjective comparison of single channel versus two channel subwoofer reproduction. In *Audio Engineering Society Convention 117*. Audio Engineering Society, 2004.

[196] Leo L. Beranek and Tim J. Mellow. *Acoustics: Sound Fields and Transducers*. Academic Press, 2012.

[197] ISO 10534-2-1998. Acoustics - determination of sound absorption coefficient and impedance in impedance tubes - part 2 : Transfer-function method. Technical report, Internation Standard Organization, Geneva, Switzerland, 1998.

[198] Andrew J. Fleming and S. O. Reza Moheimani. Adaptive piezoelectric shunt damping. *Journal of Smart Materials and Structures*, 12, 2003.

[199] William Marshall Leach. Loudspeaker voice-coil inductance losses: circuit models, parameter estimation, and effect on frequency response. *J. Audio Eng. Soc.*, 50(6), 2002.

[200] Knud Thorborg and Andrew D. Unruh. Electrical equivalent circuit model for dynamic moving-coil transducers incorporating a semi-inductor. *J. Audio Eng. Soc*, 56(9):696–709, 2008.

[201] Knud Thorborg and Claus Futtrup. Electrodynamic transducer model incorporating semi-inductance and means for shorting ac magnetization. *J. Audio Eng. Soc.*, 59(9), 2011.

[202] Boaz Elieli. The application of an inductively coupled shorted turn and the dual-coil loudspeaker system. In *Audio Engineering Society Convention 83*. Audio Engineering Society, 1987.

[203] Clark J Radcliffe and Sachin D Gogate. Velocity feedback compensation of electromechanical speakers for acoustic applications. In *International Federation of Automatic Control, Triennial World Congress, July*, 1996.

Bibliography

[204] Cheng-Yi Chen, G TC Chiu, CC Cheng, and H Peng. Passive voice coil feedback control of closed-box subwoofer systems. *Proceedings of the Institution of Mechanical Engineers, Part C: Journal of Mechanical Engineering Science*, 214(7):995–1005, 2000.

[205] Ching-Wen Liao and Jong-Yih Lin. Mfxrls-based adaptive feed-forward controller implemented with velocity sensor identified by frequency response to improve actuator speaker performance in anc systems. *Journal of the Chinese Institute of Engineers*, 29(5):883–891, 2006.

[206] H Song, HJ Lim, and H Sohn. Electromechanical impedance measurement from large structures using a dual piezoelectric transducer. *Journal of Sound and Vibration*, 332(25):6580–6595, 2013.

[207] Ulf Seidel and wolfgang Klippel. Fast and accurate measurement of the linear transducer parameters. In *Audio Engineering Society Convention 110*, May 2001.

[208] Richard Hastings-James and George W Holbrook. Multi-filar moving coil loudspeaker, November 10 1981. US Patent 4,300,022.

[209] Robert A Pease. A comprehensive study of the howland current pump. *National Semiconductor. January*, 29, 2008.

[210] Jerry Steele and Tim Green. Tame those versatile current-source circuits. *feedback*, 2:H5, 1992.

[211] Mark Dodd, Wolfgang Klippel, and Jack Oclee-Brown. Voice coil impedance as a function of frequency and displacement. In *Audio Engineering Society Convention 117*. Audio Engineering Society, 2004.

[212] Knud Thorborg, Carsten Tinggaard, Finn Agerkvist, and Claus Futtrup. Frequency dependence of damping and compliance in loudspeaker suspensions. *Journal of the Audio Engineering Society*, 58(6):472–486, 2010.

[213] Shaolin Wei, Tony Xie, and Hunter Huang. Low frequency nonlinear model for loudspeaker transducers. In *Audio Engineering Society Convention 138*. Audio Engineering Society, 2015.

[214] John Vanderkooy. A model of loudspeaker driver impedance incorporating eddy current in the pole structure. *J. Audio Eng. Soc.*, 37(3), 1989.

[215] Xiao-Peng Kong, Finn Agerkvist, and Xin-Wu Zeng. Modeling of lossy inductance in moving-coil loudspeakers. *Acta Acustica united with Acustica*, 101(3):650–656, 2015.

[216] Michael J. Turner and David A. Wilson. The use of negative source impedance with moving coil loudspeaker drive units: an analysis and review. In *122th Convention, paper 7072, Vienna, Austria*, 2007.

[217] V Pagneux, N Amir, and J Kergomard. A study of wave propagation in varying cross-section waveguides by modal decomposition. part i. theory and validation. *The Journal of the Acoustical Society of America*, 100(4):2034–2048, 1996.

[218] Antoine Chaigne and Jean Kergomard. Acoustique des instruments de musique. 2008.

[219] N. G. Kanev. The stabilizing effect of feedback on the operation of an active noise control system. *Acoustical Physics*, 58(2):262–263, 2012.

[220] George Ellis. *Control system design guide: using your computer to understand and diagnose feedback controllers*. Butterworth-Heinemann, 2012.

[221] William Cardenas and Wolfgang Klippel. Loudspeaker rocking modes (part 1: Modeling). In *Audio Engineering Society Convention 139*. Audio Engineering Society, 2015.

[222] William Cardenas and Wolfgang Klippel. Rocking modes (part 2: Diagnostics). In *Audio Engineering Society Convention 140*. Audio Engineering Society, 2016.

[223] SJ Loutridis. Resonance identification in loudspeaker driver units: A comparison of techniques. *Applied acoustics*, 66(12):1399–1426, 2005.

[224] Jason D Sagers, Timothy W Leishman, and Jonathan D Blotter. An extended lumped-element model and parameter estimation technique to predict loudspeaker responses with possible surround-dip effects. *The Journal of the Acoustical Society of America*, 134(5):3580–3593, 2013.

[225] Stephen J Elliott and Michele Zilletti. Scaling of electromagnetic transducers for shunt damping and energy harvesting. *Journal of Sound and Vibration*, 333(8):2185–2195, 2014.

[226] Dimitri Torregrossa, Sami Karkar, Etienne Rivet, Hervé Lissek, and Mario Paolone. Acoustic energy harvesting using electrochemical double layer capacitors: technical feasibility and performance assessment. In *Industrial Electronics Society, IECON 2016-42st Annual Conference of the IEEE*. IEEE, 2016.

[227] V Martin and A Bodrero. An introduction to the control of sound fields by optimising impedance locations on the wall of an acoustic cavity. *Journal of sound and vibration*, 204(2):331–357, 1997.

[228] Luís MBC Campos and João MGS Oliveira. On sound generation in cylindrical flow ducts with non-uniform wall impedance. *International Journal of Aeroacoustics*, 12(4):309–347, 2013.

[229] Lothar Gremer. Theorie der luftschall-dämpfung im rechteckkanal mit schluckender wand und das sich dabei ergebende höchste dämpfungsmaβ. *Acta Acustica united with Acustica*, 3(Supplement 2):249–263, 1953.

Bibliography

[230] Etienne Rivet, Romain Boulandet, Hervé Lissek, and Iris Rigas. Study on room modal equalization at low frequencies with electroacoustic absorbers. In *Acoustics 2012, Nantes, France*, 2012.

[231] Tomas Salava. Acoustic load and transfer functions in rooms at low frequencies. *Journal of the Audio Engineering Society*, 36(10):763–775, 1988.

[232] Frank Fahy. *Sound intensity*. CRC Press, 2002.

[233] Hervé Lissek, Romain Boulandet, and Pierre-Jean René. Shunt loudspeakers for modal control in rooms. In *Proc. 16th International Congress on Sound and Vibration*, 2009.

[234] Etienne Rivet, Sami Karkar, and Hervé Lissek. Egalisation modale des salles avec des absorbeurs électroacoustiques. In *Journées des Jeunes Chercheurs en vibrations, Acoustique et Bruit*, 2014.

[235] Hervé Lissek, Sami Karkar, Etienne Rivet, Véronique Adam, Torje Thorse, Quentin Berthet, Antoine Pittet, David Strobino, Alain Roux, and Christian Martin. Experimental assessment of active electroacoustic absorbers for broadband room modes damping. In *Proceedings of INTERNOISE 2015*, 2015.

[236] NG Kanev. Effect of errors on the efficiency of local active sound absorbers. *Acoustical Physics*, 52(5):571–575, 2006.

[237] Mark H Richardson and David L Formenti. Parameter estimation from frequency response measurements using rational fraction polynomials. In *Proceedings of the 1st international modal analysis conference*, volume 1, pages 167–186. Union College Schenectady, NY, 1982.

[238] Mark H Richardson and David L Formenti. Global curve fitting of frequency response measurements using the rational fraction polynomial method. In *Proceedings of the Third International Modal Analysis Conference*, pages 390–397, 1985.

[239] Sean Olive, Todd Welti, and Elisabeth McMullin. Listener preferences for in-room loudspeaker and headphone target responses. In *Audio Engineering Society Convention 135*, Oct 2013.

[240] Jian Bi. The double discrimination methods. *Food quality and preference*, 12(8):507–513, 2001.

[241] Min-A Kim, Ji-Eun Chae, Danielle van Hout, and Hye-Seong Lee. Higher performance of constant-reference duo–trio test incorporating affective reference framing in comparison with triangle test. *Food Quality and Preference*, 32:113–125, 2014.

[242] Min-A Kim, Young-Mi Lee, and Hye-Seong Lee. Comparison of d estimates produced by three versions of a duo-trio test for discriminating tomato juices with varying salt concentrations: The effects of the number and position of the reference stimulus. *Food quality and preference*, 21(5):504–511, 2010.

[243] Jian Bi, Michael O'Mahony, and Hye-Seong Lee. The performance of the dual reference duo-trio (drdt) method using a balanced-reference mode. *Food Quality and Preference*, 48:303–313, 2016.

[244] Hyun-Kyung Shin, Michael J Hautus, and Hye-Seong Lee. Unspecified duo–trio tests can be as powerful as the specified 2-afc: Effects of instructions and familiarization procedures on cognitive decision strategies. *Food Research International*, 79:114–125, 2016.

[245] ANSI.S3.4. Procedure for the computation of loudness of steady sounds. Technical report, American National Standards Institute, New-York City, USA, 2007.

[246] Sean E Olive. Differences in performance and preference of trained versus untrained listeners in loudspeaker tests: A case study. *Journal of the Audio Engineering Society*, 51(9):806–825, 2003.

[247] Jian Bi. *Sensory discrimination tests and measurements: Statistical principles, procedures and tables*. John Wiley & Sons, 2008.

[248] Yonghua Wang, Chengchun Zhang, Luquan Ren, Mohamed Ichchou, Marie-Annick Galland, and Olivier Bareille. Sound absorption of a new bionic multi-layer absorber. *Composite Structures*, 108:400–408, 2014.

Curriculum Vitae

Etienne Rivet was born in Angers, France. He received the Dipl. Ing. degree in Electronics, Telecommunications and Computer Science at École Supérieure de Chimie Physique Électronique de Lyon, Lyon, France, in 2011. In March 2011, he joined the Electromagnetics and Acoustics Laboratory (LEMA) of the École polytechnique fédérale de Lausanne (EPFL), Lausanne, Switzerland, as a research assistant where he has been responsible for several projects. In September 2012, he enrolled the PhD studies at the LEMA and then the Signal Processing Laboratory 2 (LTS2) of the EPFL. As a teaching assistant, he has been involved in the exercises and teaching of classes on Electroacoustics and Audio Engineering. He also supervised several semester and master projects. He is a member of the Swiss Acoustical Society, the French Acoustical Society, and the Audio Engineering Society.

List of publications

Journal papers

E. Rivet, S. Karkar, and H. Lissek. Broadband low-frequency electroacoustic absorbers through hybrid sensor-/shunt-based impedance control. *IEEE Transactions on Control Systems Technology*, 2016.

R. Boulandet, E. Rivet, and H. Lissek. Sensorless electroacoustic absorbers through synthesized impedance control for damping low-frequency modes in cavities. *Acta Acustica united with Acustica*, 102(4):pp. 696–704(9), 2016.

Conference papers

Dimitri Torregrossa, Sami Karkar, Etienne Rivet, Hervé Lissek, and Mario Paolone. Acoustic energy harvesting using electrochemical double layer capacitors: technical feasibility and performance assessment. In *Industrial Electronics Society, IECON 2016-42st Annual Conference of the IEEE*, 2016.

Etienne Rivet, Sami Karkar, Hervé Lissek, Torje Nikolai Thorsen, and Véronique Adam. Experimental assessment of low-frequency electroacoustic absorbers for modal equalization in actual listening rooms. In *Audio Engineering Society Convention 140*, May 2016.

Etienne Rivet, Sami Karkar, and Hervé Lissek. Egalisation modale des salles avec des absorbeurs électroacoustiques. In *Actes du Actes du 13ème Congrès Français d'Acoustique*, Le Mans, France, 2016.

Hervé Lissek, Sami Karkar, Etienne Rivet, Véronique Adam, Torje Thorse, Quentin Berthet, Antoine Pittet, David Strobino, Alain Roux, and Christian Martin. Experimental assessment of active electroacoustic absorbers for broadband room modes damping. In *Proceedings of*

Bibliography

Internoise 2015, 2015.

Etienne Rivet, Sami Karkar, and Hervé Lissek. Egalisation modale des salles avec des absorbeurs électroacoustiques. In *Journées des Jeunes Chercheurs en vibrations, Acoustique et Bruit*, 2014.

Sami Karkar, Etienne Rivet, Hervé Lissek, David Strobino, Antoine Pittet, Véronique Adam, and Alain Roux. Electroacoustic absorbers for the low-frequency modal equalization of a room: what is the optimal target impedance for maximum modal damping, depending on the total area of absorbers? In *Proceedings of Forum Acusticum 2014*, Krakow, Poland, September 7-12, 2014.

Etienne Rivet, Sami Karkar, and Hervé Lissek. Absorbeurs électroacoustiques pour l'égalisation modale des salles: une nouvelle approche avec des haut-parleurs à double bobine. In *Actes du 12e Congrès Français d" Acoustique*, 2014.

Hervé Lissek, Etienne Rivet, and Victor Desarnaulds. Development of electroacoustic absorbers as soundproofing solutions for industrial ventilation systems. In *Proceedings of Internoise 2013*, Innsbruck, Austria, 2013

Etienne Rivet and Hervé Lissek. Optimization of electroacoustic resonators for semi-active room equalization in the low-frequency range. In *Proceedings of Meetings on Acoustics*, volume 19, page 015056. Acoustical Society of America, 2013.

Romain Boulandet, Etienne Rivet, and Hervé Lissek. Design of a built-in electroacoustic resonator for active noise reduction. In *Proceedings of Meetings on Acoustics*, volume 19, page 030017. Acoustical Society of America, 2013.

Etienne Rivet, Romain Boulandet, and Hervé Lissek. Practical realization of «smart acoustic materials» by controlling a loudspeaker with the help of a cRIO platform. In *NIDays 2012 Conference*, Zürich, Switzerland, 2012.

Hervé Lissek, Romain Boulandet, Etienne Rivet, and Iris Rigas. Assessment of active electroacoustic absorbers as low-frequency modal dampers in rooms. In *Proc. of Internoise*, pages 19–22, New-York City, USA, 2012.

Hervé Lissek, Romain Boulandet, Etienne Rivet, and Iris Rigas. On the damping of room resonances with electroacoustic absorbers in the low frequency range. In *Euronoise 2012*, Prague, Czech Republic, 2012.

Etienne Rivet, Romain Boulandet, Hervé Lissek, and Iris Rigas. Study on room modal equalization at low frequencies with electroacoustic absorbers. In *Acoustics 2012*, Nantes, France, 2012.

Hervé Lissek, Romain Boulandet, and Etienne Rivet. Optimization of electric shunt resonant circuits for electroacoustic absorbers. In *Acoustics 2012*, Nantes, France, 2012.

Romain Boulandet, Hervé Lissek, and Etienne Rivet. Advanced control for modifying the acoustic impedance at the diaphragm of a loudspeaker. In *Acoustics 2012*, Nantes, France, 2012.

Romain Boulandet, Etienne Rivet, and Hervé Lissek. Conception de matériaux electroacoustiques intelligents par contrôle d'un haut-parleur à l'aide de filtres numériques. In *Journées Jeunes Chercheurs en VibroAcoustique et Bruit*, Nevers, France, 2011.

Romain Boulandet, Etienne Rivet, and Hervé Lissek. Electroacoustic absorbers II: implementation of a digital synthetic admittance for controlling the dynamics of electroacoustic absorbers. In *Proc. 18th International Congress on Sound and Vibration*, 2011.

Technical papers

Etienne Rivet, Romain Boulandet, Hervé Lissek, and Iris Rigas. Étude expérimentale d'égalisation modale d'une salle aux basses fréquences à l'aide d'absorbeurs électroacoustiques actifs. *Acoustique & Techniques*, 68:38–45, 2012.

Patents

Etienne Rivet, Sami Karkar, and Hervé Lissek. Versatile Electroacoustic Diffuser-Absorber. Patent PCT/IB2015/059028, pending.

Romain Boulandet, Etienne Rivet, and Hervé Lissek. Baffle Electroacoustique. Patent WO 2014/053994, 2014.

Workshops

Hervé Lissek, Etienne Rivet, and Sami Karkar. All about that bass! Montreux Jazz Workshops, Montreux, Switzerland, 2015.